EXPERIMENTAL INVESTIGATION FOR PERFORMANCE ENHANCEMENT OF WIRE ELECTROCHEMICAL MACHINING (WECM) DURING MICROMACHINING OF SHAPE MEMORY ALLOY

THESIS SUBMITTED BY

BESEKAR NARESH WALMIK

DOCTOR OF PHILOSOPHY (ENGINEERING)

DEPARTMENT OF PRODUCTION ENGINEERING

FACULTY COUNCIL OF ENGINEERING & TECHNOLOGY

JADAVPUR UNIVERSITY

KOLKATA-700 032

INDIA

2024

JADAVPUR UNIVERSITY

KOLKATA-700032, INDIA

Index No. 287/21/E

Registration No. 1012116001

TITLE OF THE PHD (ENGG.) THESIS:

EXPERIMENTAL INVESTIGATION FOR PERFORMANCE ENHANCEMENT OF WIRE ELECTROCHEMICAL MACHINING (WECM) DURING MICROMACHINING OF SHAPE MEMORY ALLOY

NAME, DESIGNATION & INSTITUTION OF SUPERVISOR:

Dr. BIJOY BHATTACHARYYA

Professor, Production Engineering Department

Jadavpur University,

Kolkata-700032, India

LIST OF PUBLICATIONS

Journals

(a) International Journals

1. Naresh Besekar, B. Bhattacharyya, "Vibration-assisted axial nozzle jet flow wire electrochemical machining for micromachining", Journal of Micro and Nano Manufacturing, Transactions of ASME, Vol.9, (2021) pp. 044501–7.

2. Naresh Besekar, B. Bhattacharyya, "Experimental Investigation and Characterization of Nitinol Shape Memory Alloy during Wire Electrochemical Machining", Journal of Manufacturing Processes, Vol.81, (2022) pp. 346–361.

3. Naresh Besekar, B. Bhattacharyya, "Wire electrode insulation method for stray current and overcut reduction during WECM- a novel approach", International Journal of Advanced Manufacturing Technology, Vol.123, (2022) pp. 3917–3942.

4. Naresh Besekar, B. Bhattacharyya, "Influence of energy input parameters on wire feed rate and surface characteristics during WECM of Nitinol SMA", Journal of Micromanufacturing, Vol.7, (2023), pp.5-16, DOI: 10.1177/25165984231151303.

5. Naresh Besekar, B. Bhattacharyya, "Electrochemical characterization and micromachining of Nitinol SMA by WECM using citric acid mixed H_2SO_4 electrolyte ", ECS Advances, Vol.2 (2023) pp.032501.

6. Naresh Besekar, B. Bhattacharyya, "Wire electrochemical machining of nitinol shape memory alloy using different electrolytes", Journal of solid state electrochemistry, (2024). https://doi.org/10.1007/s10008-024-05917-3.

(b) National Journals

1. Naresh Besekar, B. Bhattacharyya, "Investigation into energy interaction behavior of Nitinol SMA during WECM", Manufacturing Technology Today, 22(5), (2023), pp. 1-6.

Book Chapters

1. Naresh Besekar., Bhattacharyya B., "Experimental investigation into wire electrochemical micro- machining for reduction of micro-sparks and overcut", Lecture Notes in Mechanical Engineering, Journal of Micro, Nano Manufacturing and Surface Engineering, Springer Natures, Chapter 5, (2022), pp.222-232.

List of Papers Presented in International Conference

1. Naresh Besekar, B. Bhattacharyya, "Experimental investigation into wire electrochemical micro- machining for reduction of micro-sparks and overcut", 8th International & 29th All India Manufacturing Technology, Design and Research Conference (AIMTDR 2021), 9th–12th Dec., 2021, PSG college of Technology and Applied Research, Coimbatore, India.

2. Naresh Besekar, B. Bhattacharyya, "Investigation into energy interaction behavior of Nitinol SMA during WECM", 12th International Conference on Precision, Meso, Micro and Nano Engineering (COPEN 2022), 9th-11th Dec., 2022, IIT Kanpur, Uttar Pradesh, India.

3. Naresh Besekar, B. Bhattacharyya, "Investigation into WECM of Nitinol SMA using ozonated $NaNO_3$ electrolyte", 9th International & 30th All India Manufacturing Technology, Design and Research Conference (AIMTDR 2023), 8th–10th Dec., 2023, PSG IIT-BHU, Varanasi, India.

Patents: Nil

Awards:

Best paper award at, 8th International & 29th All India Manufacturing Technology, Design and Research Conference (AIMTDR 2021), 9th–12th Dec., 2021, PSG College of Technology and PSG Institute of Technology and Applied Research, Coimbatore, India.

Besekar

02/01/2024

Bhattacharyya 02/01/2024

Ex Professor
Production Engineering Department
Jadavpur University
Kolkata - 700 032

PROFORMA – 1

"Statement of Originality"

I Besekar Naresh Walmik registered on 30th July 2021 do hereby declare that this thesis entitled "EXPERIMENTAL INVESTIGATION FOR PERFORMANCE ENHANCEMENT OF WIRE ELECTROCHEMICAL MACHINING (WECM) DURING MICROMACHINING OF SHAPE MEMORY ALLOY" contains literature survey and original research work done by the undersigned candidate as part of Doctoral studies.

All information in this thesis have been obtained and presented in accordance with existing academic rules and ethical conduct. I declare that, as required by these rules and conduct, I have fully cited and referred all materials and results that are not original to this work.

I also declare that I have checked this thesis as per the "Policy on Anti Plagiarism, Jadavpur University, 2019", and the level of similarity as checked by iThenticate software is **9** %.

Signature of Candidate:

Date: 02/01/2024

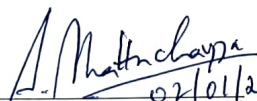Certified by Supervisor(s):
(Signature with date, seal)

1.

02/01/2024

Er. Professor
Production Engineering Department
Jadavpur University
Kolkata - 700 032

JADAVPUR UNIVERSITY
FACULTY OF ENGINEERING & TECHNOLOGY
DEPARTMENT OF PRODUCTION ENGINEERING

CERTIFICATE FROM THE SUPERVISOR

This is to certify that the thesis entitled "EXPERIMENTAL
INVESTIGATION FOR PERFORMANCE ENHANCEMENT OF
WIRE ELECTROCHEMICAL MACHINING (WECM) DURING
MICROMACHINING OF SHAPE MEMORY ALLOY" submitted by
Mr. BESEKAR NARESH WALMIK, who got his name registered on
30th July 2021 for the award of Ph.D. (Engg.) degree of Jadavpur
University, is absolutely based upon his own work under the supervision of
PROF. BIJOY BHATTACHARYYA and that neither his thesis nor any
part of the thesis has been submitted for any degree/diploma or any other
academic award anywhere before.

02/01/2024

Signature of the Supervisor

With

Date and Office Seal

Ex. Professor
Production Engineering Department
Jadavpur University
Kolkata - 700 032

ACKNOWLEDGEMENT

PREFACE

Electrochemical machining has turned into widely accepted process with the recent advancements and requirements in the fabrication of macro and micro components. Wire electrochemical machining (WECM) is a promising method for the fabrication of high aspect ratio complex microfeatures for fulfilling the requirements of micromachining for recent industrial and medical applications without affecting any properties of materials. The various researchers across the globe made several approaches in improvement of quality with wire electrochemical machining processes by proper setting of control parameters, developing experimental setups and achieving different outcomes. With rapid development in industrial and biomedical fields, this process finds more application in the manufacturing of titanium and titanium alloy, and other hard to cut super alloys which pose many challenges in machining with other conventional and nonconventional processes without affecting original properties of metal. This process provides additional opportunity in the machining of complex microfeatures without heat affected zone (HAZ), thermal stress, burr formation and tool wear. It can be implemented on metals regardless of their hardness which facilitates it to execute with higher machining accuracy. Therefore, this research work has been focused on WECM due to its potential applications and requirements in demanding situations especially in areas of micro fabrication.

Till the date, no work was found in literature for understanding the anodic dissolution mechanisms for unique nitinol shape memory alloy during WECM. As nitinol is widely used shape memory alloy for number of advanced aerospace, automobile and biomedical applications due to its strength and magical super elastic properties, hence, in this research work, experimental investigation for performance enhancement of WECM during micromachining of nitinol shape memory alloy by developing novel experimental setups and planning with diversified advanced industrial applications in the fabrication of microfeatures is proposed by considering the needs of the modern micromachining applications. The objectives of the present research work have been stated below:

(i)   To develop in-house WECM setup utilizing different procured, customized and in house fabricated components and subsystems for details experimental investigation during micromachining of stainless steel and shape memory alloy (SMA).

(ii)   To develop vibration assisted axial nozzle jet flow system and to investigate the effect of different diameter nozzles at varying stand-off distances and comparing

vibration assisted axial nozzle jet flow system with other existing flow systems for performance enhancement of WECM during machining of nitinol SMA.

(iii)   To develop wire insulation method and investigate the effect of wire coating and insulation on machining accuracy, surface quality in the region near machined zone using developed WECM setup for experiments with controlled process parameters for reduction of micros-parks, stray current and overcut etc.

(iv)   To investigate the use of different types of electrolytes e.g. neutral, acidic as well as mixed and ozonated mixed electrolyte with suitable eco-friendly complexing agents (ex. Citric acid, EDTA) for improvement in surface quality and homogeneity during micromachining of nitinol shape memory alloy during WECM.

(v)   To investigate the effect of different parameters and characterization of nitinol shape memory alloy using developed experimental setup with various processing conditions as well as to explore influence of energy input process parameters on maximum achievable wire feed rate for overall performance enhancement of WECM.

The thesis has been structured and described all the investigations and research work in a well organized manner into seven chapters in details as follows:

Chapter 1 deals with the introductory part i.e. history and progress of WECM process considering its working principle, classifications, process parameters and other influencing factors, process capabilities, limitations, importance and applications. Also, the overview of types of SMA, machining of SMA, properties and uses of nitinol SMA, need and challenges of nitinol SMA micromachining, review of past literatures showing various attempts in the relevant topic as well as research gaps and problematic areas in available research works and prospective direction of approach in merging that existing gap which forms the base for the framing of the objectives of the present thesis..

Chapter 2 focuses on the development of WECM experimental setup for the fabrication of microfeatures of different geometries and the detailed experimental procedure for preparation of the stainless steel SS304 and nitinol SMA samples required during the experimentation for the enhancement of machining performance. The basic components of WECM system includes mechanical machining unit, motion control unit, power supply unit, machining chamber, ozone generator and accessory units. It is a step by step development process. Hence, corresponding to specific development stage, axial flow system, vibration system and nozzle jet system has been used for the flushing, the details of which have been incorporated. The different wire electrode insulators also used. The components include procured ones, the specification, and capability of which have been

selected according to setup configurations requirements, machining conditions and needs; while others have been developed indigenously in house for fulfilling the experimental requirements. The modifications and improvements on the base setup have been conducted repeatedly based on the research needs and to facilitate performance enhancement in machining process. All these have also been described throughout in the concerned chapter.

Chapter 3 highlights the investigation on vibration assisted axial nozzle jet flow machining for performance enhancement of WECM. It contains development of mathematical model with working principle and selection of electrolyte, wire electrode, and workpiece. The performance enhancement in WECM has been carried out by comparing vibration-assisted axial nozzle jet flow system with other flushing methods considering the effect of pulse voltage, duty ratio and wire feed rate on slit width and accuracy. Also, the investigation has been carried out for the effect of nozzle diameter and workpiece nozzle stand-off distance on slit width and accuracy and finally fabricated the microslits of nitinol shape memory alloy.

Chapter 4 highlights fundamental experimentations utilizing the developed experimental setup for analyzing the influences of the predominant WECM process parameters during the fabrication of microslits and also study its effect on the dimensional uniformity and surface characteristics of the generated microfeatures on SS304 for reduction of stray current effect, overcut and micro sparks during WECM. Further, it incorporates the experimental investigations carried out for the reduction of overcut and stray current attack using different wire coating and insulation methods during WECM. The effect of novel PTFE tube insulation coating and synthetic enamel coating have been studied experimentally during WECM considering exposed wire angle and distance of coating from the upper surface of the workpiece for reduction of stray current and overcut. This chapter also includes the comparison between these wire coating methods with uncoated wire for microslits generated by WECM. Finally, the microslits array of nitinol shape memory alloy has been fabricated.

Chapter 5 deals with the effect of different aqueous neutral electrolytes, mixed neutral electrolytes and mixed ozonated electrolytes in addition with EDTA as complexing agents. The influence of pulse voltage and different concentrations of electrolytes have been investigated for machining accuracy and surface finish during nitinol SMA microgrooves fabrications and results are discussed in details and confirmed the best possible combination of electrolytes and the microfeatures have been fabricated on nitinol shape

memory alloy. It also incorporates the use of mixed acidic electrolyte and the effect of pulse voltage and electrolyte concentration on dimensional characteristics and surface finish has been found out during the machining of nitinol shape memory alloy. Also, the electrochemical impedance spectroscopy (EIS) and potentiodynamic electrochemistry (PDE) tests for polarization behaviour of nitinol SMA have been conducted for electrochemical characterization.

Chapter 6 overviews the experimentation carried out for investigating the effect of most of the prominent process parameters for micromachining of nitinol shape memory alloy during WECM. It includes in-depth study of dissolution behaviour of nitinol SMA in 0.1 M H_2SO_4 acidic electrolyte solution and characterization of nitinol SMA before and after machining. It also incorporates the effect of energy input parameters i.e. pulse voltage, pulse frequency and duty ratio on wire feed rate and machining accuracy during fabrication of microslits on nitinol shape memory alloy and finally complex curved microfeatures of nitinol shape memory alloy has been fabricated.

Lastly, **Chapter 7** consolidates the outcomes of the present research work along with the future scope of the research in the area of WECM during micromachining of SS304 and difficult to cut nitinol shape memory alloy used in advanced industrial and biomedical applications for improvement in the machining performance.

The researcher has attempted to justify the uniqueness of the present research work by exploring the possibilities of micromachining of various microfeatures on stainless steel SS304 and nitinol shape memory alloy material utilizing wire electrochemical machining process. The most salient and unique research finding that has been observed in the present research includes development of the vibration-assisted axial nozzle jet flow wire electrochemical machining experimental system setup for fabrication of various microfeatures on SS304 and difficult to cut nitinol SMA and also has tried to justify the distinctiveness and originality of the present work by incorporating various novel methodologies and investigations. The analysis of fabricated microfeatures of nitinol SMA utilizing vibration-assisted axial nozzle jet flushing based on critical examination of various SEM micrographs to determine the influence of significant WECM parameters on machining accuracy and surface roughness during micromachining is another significant outcome. This research study also contribute by setting up most suitable WECM process parameters and operating conditions for machining of various microfeatures on nitinol SMA. The investigation in the new field of wire electrochemical machining can be of

enormous support to the present manufacturing industries because of its expected superiority of machining characteristics with respect to other machining processes. The extensive research work move towards closing the existing research and knowledge gap by contribution of a cost effective machining system for fabricating microfeatures on difficult to machine nitinol shape memory alloy and by providing a appropriate platform for commercialization of this emerging anodic dissolution process at the end. Hence, the study presented in this research work through the in-depth experimental investigations on wire electrochemical machining of nitinol SMA may be useful for effective utilization of WECM process for various practical engineering applications.

VITA

The author, Mr. Besekar Naresh Walmik, son of Mrs. Sevanti & Mr. Besekar Walmik Raoji was born on 04th August 1981 in a town, Wani in the district of Yavatmal, Maharashtra. Author passed both the S.S.C as well as H.S.C from S.P.M. High School and Jr. College, Wani, District-Yavatmal, Maharashtra under the State Board of Secondary and Higher Secondary Education in the year 1996 and 1998 respectively.

The author earned B.E. in Production (S/W) Engineering in the year 2003 from College of Engineering, Pune (COEP) under Pune University with first class (62.82%). He completed his M.Tech. in Production Engineering with specialization in Manufacturing Engineering & Automation from College of Engineering, Pune under Pune University in 2006 with first class with distinction with a CGPA of 7.58.

The author is working as Lecturer in Mechanical Engineering Department, Government Polytechnic, Gondia from February 2011. The author has joined as a Research Scholar in December 2020 at the Production Engineering Department, Jadavpur University, Kolkata, under All India Council of Technical Education's scheme of the Quality Improvement Programme (QIP Poly). The author has been working in the area of wire electrochemical machining especially micromachining of nitinol shape memory alloy. In July 2021; he got his name registered for Ph.D. (Engg.) in the Department of Production Engineering. He continued to pursue his research activities in the Department for completion of Ph.D. (Engg.).

Author is engaged in research work from 2020 onwards. He has published six research papers in reputed international journals, one research paper in national journal and one book chapter. Author presented his research work in three international conferences during his research tenure and also received best paper award in AIMTDR-21 conference held at PSG college of Engineering and Technology, Coimbatore on 8th-10th December 2021. His research interests include micromachining and advanced manufacturing processes.

Dedicated to my Family & Teachers ….

My pillar of strength and source of

inspiration for their faith in education,

endless support and love

TABLE OF CONTENTS

LIST OF FIGURES

LIST OF TABLES

LIST OF ABBREVIATIONS AND SYMBOLS

Symbol & Abbreviation	Description
U_0	Machining Voltage
A	Ampere
μm	Micrometer
Ω	Ohm
m	mass material removal
Q	Electric charge passed through the substance in coulombs
F	$96.485\,C\,mol^{-1}$ is the Faraday constant
z	Valancy number of ions of the substance
I	Constant current (Amp)
Δb	Inter-electrode frontal gap
ɳ	Current efficiency
ɯ	volumetric electrochemical equivalent
k	Electrolyte conductivity
v, f_w	Wire feed rate
n	number of measurements taken
S_i	Each measurement value
S_{mean}	mean of S_i
U_c	Charging voltage
U_0	Steady-state potential
ꞓ	Time constant of an equivalent circuit of a double layer
t	Charging time
R_{eq}	Equivalent resistance of the circuit
α_e	Volumetric electrochemical equivalent
C_d	Double-layer capacitance
D_r	Duty cycle
f	Applied frequency
V	Applied pulse voltage
l	Initial inter-electrode gap
L	distance from the centre of the wire electrode
j	Current density
E	Electric field strength
K_0	Initial electrolyte conductivity
α	Temperature coefficient
ΔT	Temperature difference
α_v	void fraction of bubbles
α_s	void fraction of dissolution hydroxide sludge
k_d	Dispersed medium electrical conductivity

β_1	Volume ratio of hydrogen
β_2	Hydroxide volume ratio in electrolyte mixture
A	Atomic weight
t	Machining time
e_a	Electrochemical equivalent
R	Resistance for current flow
k_e	Electrolyte and electrolysis product mixture conductivity
a_r	Area of the wire in the machining zone
q_1	Hydrogen volume flow
q_2	Hydroxide volume flow
q_g	Total volume flow through IEG
q_p	pump output electrolyte volume flow
k_1	Overflow coefficient
k_2	Leakage coefficient
f	processing surface complexity coefficient
a_p	Cross-sectional area of the flow in pump output mouth
v_p	Average electrolyte velocity
q_n	Flow rate of nozzle jet flow
r_1	Radius of pump output mouth
r_2	Radius of nozzle
ρ_a	Anode material density
t_a	Anode thickness
ω	Anode electrochemical equivalency
δV	Electrode potential difference
R_S	Active electrolyte resistance
R_P	Polarization resistance
ρ_s	Specific resistivity (Ω-cm)
ΔS	Inter-electrode gap
V_m	Valence of metal dissolution
a	Molecular weight of the metal
f	Applied frequency in Hertz
d_W, D_w	diameter of wire electrode
θ	Exposed wire angle
WOC	Width overcut
LOC	Length overcut
W_s, S_w	Slit width
EIS	Electrochemical impedance spectroscopy
PDP	Potentiodynamic polarization
EDS,EDX	Energy dispersive X-ray spectrum
XRD	X-ray diffraction

PTFE	Polytetrafluroethylene
EDTA	Ethylenediamine tetraacetic acid
NaCl	Sodium chloride
NaBr	Sodium bromide
$NaNO_3$	Sodium nitrate
H_2SO_4	Sulphuric acid
ECM	Electrochemical machining
EMM	Electrochemical micromachining
WECM	Wire electrochemical machining
MEMS	Electromechanical systems
IEG	Inter electrode gap
MRR	Material removal rate
SMA	Shape memory alloy
PZT	Piezoelectric transducer
SEM	Scanning electron microscope
CCI	Coherent correlation interferometer
OCP	Open circuit potential

Chapter1. INTRODUCTION

1.1 Introduction

The importance of various machining technologies by existing fabricators is a result of modern technical improvement and more requirements. Many of the processes used today are quite well-established, with some having a significant impact and others, which are more recent developments, having a small but much focused influence on contemporary manufacturing industries. However, substantial research is still being done to better explore and determine the process potential as well as applicability for both established and emerging machining technologies in order to fully satisfy the vast and constantly increasing demand. Of course, each of these machining techniques has distinct metal removal characteristics, differs from the others entirely or in part, and has advantages and limitations of its own. The advantages which ECM anodic dissolution technique offers are quite phenomenal, as it can machine metals regardless of their hardness. This allows the process to generate different complex features easily, even on various difficult to machine materials such as titanium, nitinol shape memory alloys etc, which pose several challenges for conventional machining techniques. In contrast to the thermal induced material removal processes, ECM can machine features without generating thermal stress which can deteriorate surface quality and integrity, without the formation of a heat affected zone (HAZ) where surface property changes due to the modification of the grain structure, without formation of burrs which are detrimental to product homogeneity, and without wearing out of the tool leading to its premature failure. Further, the electrolytes i.e. salt solutions combined with water and tools used for electrochemical processes are very cost effective, eco-friendly and easily available as compared to other machining processes. As such, to readily generate high aspect ratio microfeatures as well as other complex 3D microstructures with ease, a new variety of electrochemical machining has recently been introduced. This new process, called wire electrochemical machining (WECM), entails changes in anode type and shape as well as machining parameters and conditions and works on the same principle of anodic dissolution of EMM and ECM.

The development of high strength materials and shape memory alloys (SMA) like nitinol was made possible by advances in the science of metallurgy and the demand for high strength materials across a variety of sectors. The conventional methods are quite difficult to use when machining these alloys. When these alloys are machined using conventional tools, both the workpiece and the tool suffer damage. The main distinction between

conventional and unconventional machining techniques is that traditional techniques involve physically removing the material with a sharp cutting tool. However, unconventional procedures work by using chemical, thermal, electrical, or a mix of these energies to remove material. The process of creativity proceeds by way of research, design and development. The research work concerned with creation of new system, process, and equipment for the benefit of mankind is engineering. The new system emerging from innovation may be constituted by mechanical, electro mechanical, hydraulic, thermal, or other such elements. One of these machining methods that leverage Faraday's law of electrolysis as a process fundamental is electrochemical machining (ECM), which was invented by W. Gusseff and patented in 1929. By using anodic dissolution, the process removes the workpiece's material. The high velocity electrolyte flows through the inter electrode gap (IEG) between the pre-shaped cathode tool and anode workpiece, and when DC voltage is applied across the gap, the tool's appearance on the workpiece is roughly mirrored. The process's basics, important components, and applications are reasonably well established and commercialised; therefore a lengthy description is not necessary. Electrochemical micromachining (EMM) has made a remarkable impact in the area of advanced micro manufacturing through fabrication of various microproducts that are successfully utilized in various micro engineering applications. Over the years through research and development in this area, EMM has diversified and its operational capabilities have been increased by the introduction of different features to exploit its potential in the area of submicron and nano range fabrication. Different variants of EMM such as wire EMM, solid-state EMM (SSEM), surface structuring by EMM, micro patterning and stamping by EMM, and nanofabrication by applying EMM have been established [1]. The ability to easily produce different complex features from harder metals like stainless steel, super alloys, titanium, and titanium alloys with softer tools, removal of substrate material without heating or altering grain structure, generation of thermal stress and subsequent surface as well as subsurface cracking, modification of surface property, degradation of product homogeneity by forming burrs, and wearing out of the tool are some of its main advantages. Many micromachining technologies have recently been adopted by modern manufacturers as a result of the extremely high demand for miniaturised products or features; however, only a few of these technologies are specifically designed for the micro- and even nano scale. As a result of increasing shop floor and space compression, improved mobility, higher efficiency, lower operating costs, lower energy consumption,

etc., miniaturisation has become the only viable solution. It's important to note that component downscaling has already beyond the micro regime with current production capabilities in the few nanometer regions. Electrochemical micromachining (EMM), a variation of electrochemical machining (ECM) that has been modified to be used in the manufacturing of microfeatures and components, has made significant and noteworthy contributions in this domain. EMM incorporates and modifies new operating characteristics like frequency and duty ratio in order to produce accurate results by using pulsed DC power as opposed to constant DC power for the involved operating parameters. As a result of the improved electrolyte flushing condition in the narrow IEG and the increased localization of anodic dissolution, which is necessary to get feature resolution in micro ranges, these incorporation and improvements enable extremely accurate machining with greater process stability **[2].** In addition, unlike ECM, EMM frequently necessitates significant and necessary changes in operating conditions, such as the use of a stagnant electrolyte rather than a flowing one to reduce potential vibration of the introduced micro tool as well as disturbances and achieve necessary stability. With the advancement of technology and the requirement of high aspect ratio structures, a new kind of EMM has been introduced. One of these techniques, widely familiar as wire electrochemical machining (WECM) has added advantages and eradicates the weakness of machining high aspect ratio microstructure through combining with the idea of wire cutting and it is thoroughly discussed in details in next sections.

1.2 Wire Electrochemical Machining (WECM): Overview

Wire electrochemical machining is a relatively recent technique that uses cathode wire and anode workpiece soaked in an appropriate electrolyte solution and separated by a small inter-electrode gap (IEG) to dissolve materials through the necessary electrochemical processes. Without experiencing any heat stress, burr formation, or tool wear, WECM can effortlessly produce complex 3D high aspect ratio microfeatures on a variety of difficult-to-machine materials such stainless steel, titanium and titanium alloys, other super alloys, etc **[3].** In order to meet the demands of micromachining for current industrial and medical applications without altering the characteristics of materials, wire electrochemical machining is a promising technology for the manufacture of high aspect ratio complex and 3D microfeatures.

1.2.1 History and Progress of WECM

Wire Electrochemical Machining (WECM) got patented in 1977 by Chikamori and modelling of WECM using finite element method was done by Jain in 1980. By carefully

establishing control settings, creating experimental setups, and attaining varying results, numerous researchers from across the world have taken several ways to improving quality with wire electrochemical machining process. It is an electrolysis-based anodic dissolution process, and Michael Faraday invented the laws governing it in 1834. By introducing wire electrode of suitable dimensions and by applying electrolyte of suitable concentration between the tool and workpiece, this process removes material by electrochemical reactions that occur during the machining. The chronological improvement in WECM process with year wise progress has been shown in **figure1.1.**
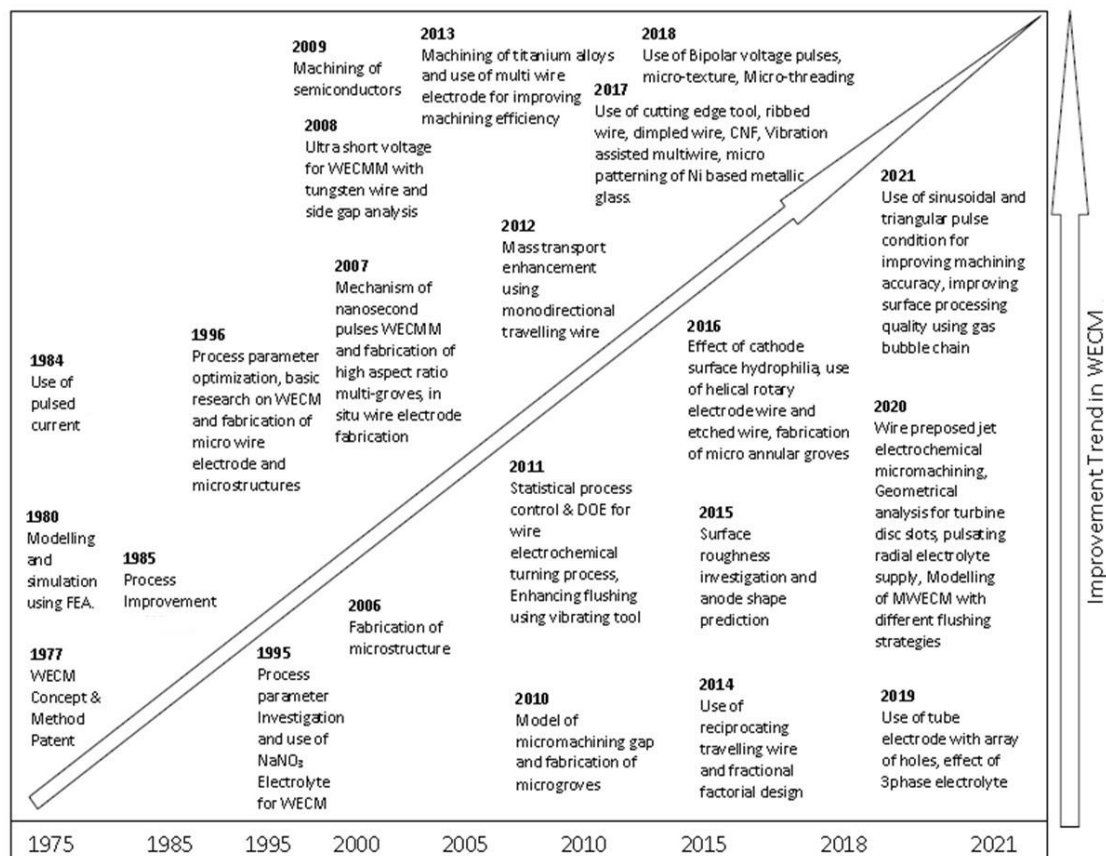
Figure1.1 Chronological Improvement in WECM

The various researchers across the globe made several approaches in improvement of quality with wire electrochemical machining processes by proper setting of control parameters, developing experimental setups and achieving different outcomes. Chikamori and Jain conceptualize the process, Meada et al. worked on process improvement, Bejar et al. on analysis and optimization, Zhu et al. & Shin et al. on improvement in machining accuracy, Wang et al, Zeng et al, Ninsong et al, Xu et al, Volgin et al, Debnath et al. investigated on enhancement of mass transport, improvement in machining efficiency and surface quality, Taweel et al & Sharma et al. worked on turning and threading operations using WECM, Fang et al, Zou et al, Meng et al, He et al. worked on use of novel tool

4

profiles, Gao et al. found use of bipolar pulses during WECM but still process is under investigation and not commercialized. However, the process has been able to fabricate various types of laboratory grade microfeatures required for different end use purposes and numerous other micro components without formation of heat-affected zones, recast layer, spatters and micro cracks on the machined surface **[4].** The detailed literature review for various investigations and analysis in wire electrochemical machining for fabrication of microfeatures has been explained in next section.

1.2.2 Working Principle and Classifications of WECM

As implied by the name, WECM maintains the same core idea of ECM/EMM while introducing solid metallic wire as a tool for machining operations and working principle is shown in **figure1.2.** Similar to EMM, WECM employs pulsed dc power to localise dissolution in the micron or submicron ranges, improve the cleaning of electrolysis by-products and the regeneration of fresh electrolyte in the IEG during pulse off times, and improve microfeatures resolution and accuracy. Contrary to EMM, WECM also uses pulsed dc voltage, but in order to get the desired effects, it also needs to include specific flushing processes. Electrolytes act as electrical conductors in WECM, and wire serves as the tool electrode. When compared to other electrochemical processes, WECM has a number of benefits. A wire attached to a DC pulsed power source's negative terminal (cathode) is referred to as a tool in WECM.
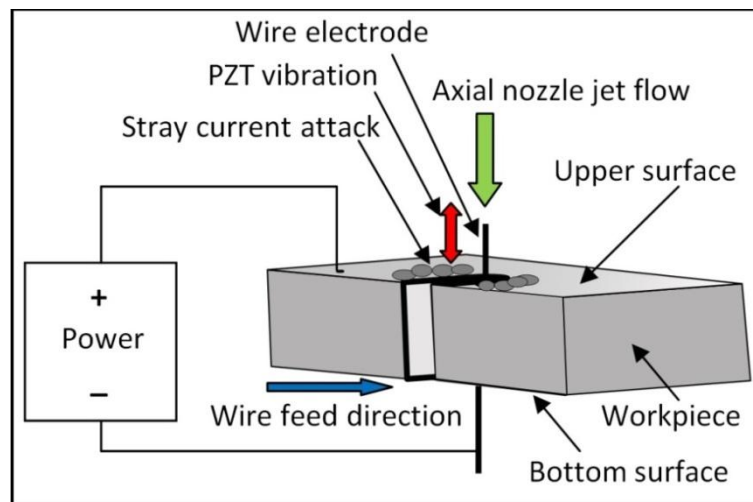
Figure1.2 Working principle of WECM

This wire follows a predetermined path inside a workpiece that is connected to the anode, or positive terminal. A microfeatures with the desired form is machined while an electrically conducting fluid (electrolyte) is provided between the two electrodes at IEG in the machining zone. No material dissolves from the wire electrode. As a result,

machining can be done repeatedly using the same wire. For instance, tungsten metal is the most commonly used tool material in WECM because it can withstand attacks from oxygen, acids, and alkalis. Mechanical (hardness, toughness) characteristics of the workpiece have no effect on the machining properties of this method, such as precision, efficiency, and surface quality. The machined by-products i.e. sludge, gas and dissolved products are removed from the electrode gap by electrolyte circulation and efficient flushing. The wire electrode gap must be maintained by moving the tool at the necessary feed rate for continuing the process.
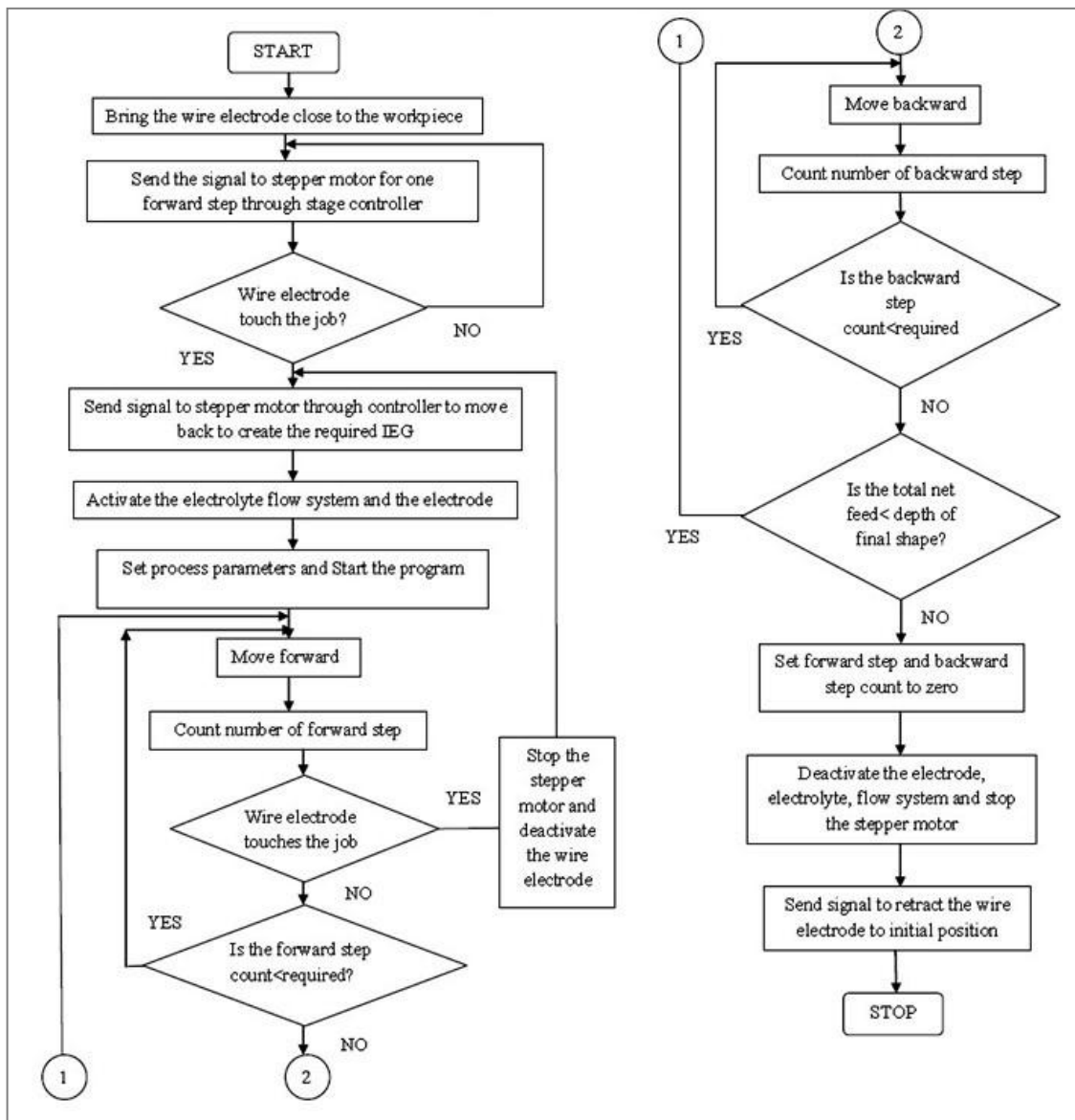
Figure1.3 Operations of WECM

If the relevant operating parameters are maintained properly, this leads to the generation of smaller machining products with easier gas bubble expulsion as opposed to the direction of gravity where fewer amounts of leftover reaction products do not get enough

time to clog the IEG for machining shallower microfeatures. On the other hand, disintegration occurs along the length of the wire in WECM because the wire is tightly tension and fixed in the direction of gravity. The thickness of the specimen is typically more than the wire diameter employed because it generates a larger area that can be machined than the circular cross section of a micro wire with the micron level diameter. As a result, there are more reaction products in the restricted IEG, and the problem gets worse when producing features with greater aspect ratios.This makes the use of a specialised flushing process in WECM vital for effectively cleaning the machining gap and obvious for achieving a higher aspect ratio. In this case, the wire tension gives WECM the advantage because the wire stays fixed, stretched, and stable during operations. Additionally, since the feed forward direction in WECM is perpendicular to gravity, it is simpler to reproduce the machining gap during operations. The flowchart for the operation of WECM shown in **figure1.3** covers complete process from its start to end for fabricating various microfeatures. WECM is an effective method for fabricating higher aspect ratio features because of all these fair advantages that have been carried over from the parent EMM process, as well as its various attributes and properties. It may also introduce new and improved applications in the fields of micro fluidics, biomedical, and other cutting-edge scientific and advanced industrial fields, such as producing precise micro parts for micro electromechanical systems (MEMS). The process is classified into five different areas in order to understand the range of active research in WECM. These are based on type of machining, the number of wires, the geometry of the workpiece, the electrolyte flow system, and the dynamics between the tools and the workpiece. The classification of WECM has been depicted in **figure1.4.**
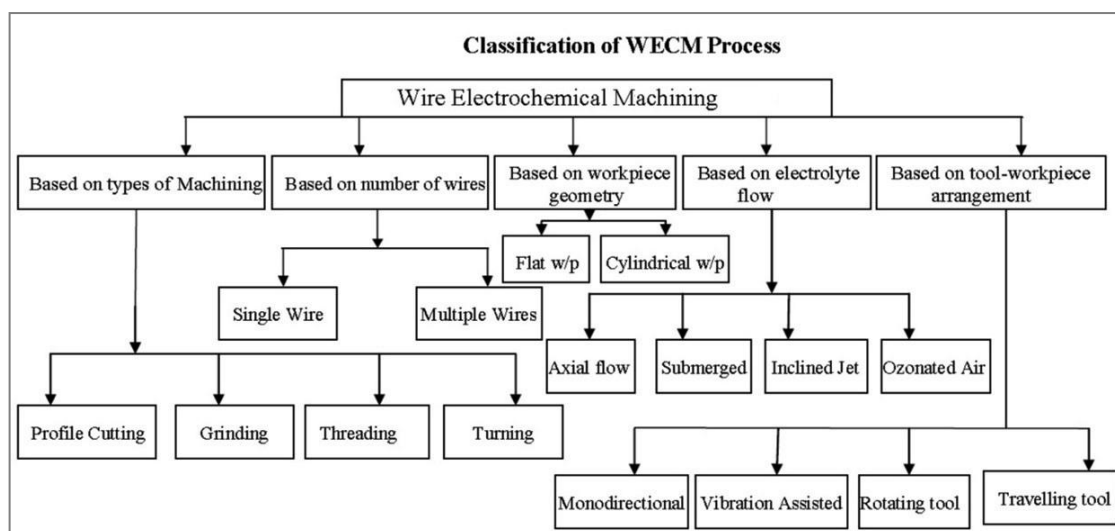
Figure1.4 Classifications of WECM

The next session will cover the process parameters and, for better understanding, the influence of different process parameters and other factors that occurs during WECM for fabricating different simple and high aspect ratio 3D complex microfeatures.

1.2.3 Process parameters and influencing factors of WECM

Setting, maintaining, and managing the process parameters in the inter electrode gap (IEG) determines the accuracy of the fabricated microfeatures as well as the stability of the WECM process. The cause-and-effect (fish-bone) diagram in **figure1.5** depicts the influencing process parameters of the WECM on the machining accuracy. However, the following primary process factors of the WECM system will need to be ideally regulated in order to achieve the efficient and high precision machining in the order of microns. The distance between the wire and the workpiece (inter electrode gap), temperature, electrolytic concentration, flow rate, and wire feed rate and other energy input parameters i.e. pulse voltage, pulse frequency, pulse width and duty ratio are major influencing factors which have to be investigated in depth for machining of shape memory alloy. The effectiveness of the process can be assessed based on the quality, precision, and efficiency of the machining. The greatest tool/workpiece feed rate (µm) that is attainable for a particular set of working parameters is used to measure the efficiency of machining.
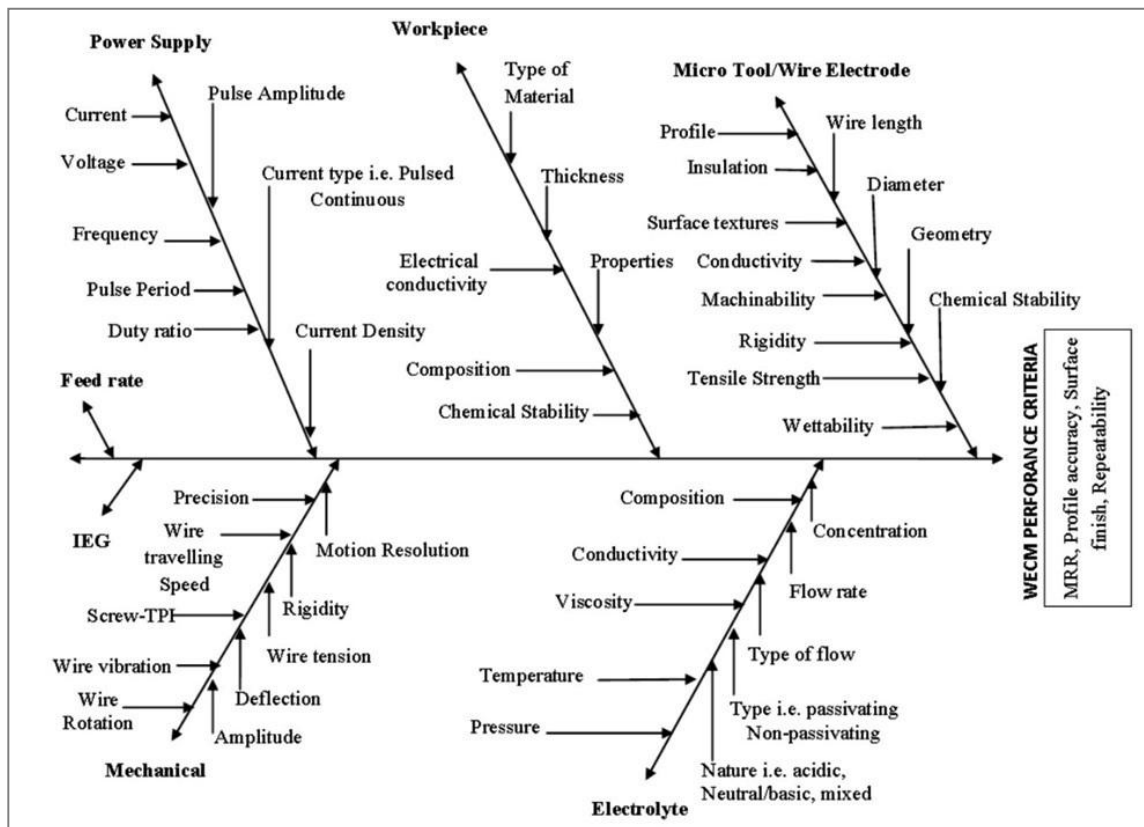
Figure1.5 Process parameters of WECM

The side inter electrode gap width produced during machining is used to measure machining accuracy. The surface roughness produced after machining is used to analyze the quality of the machining process. Other than these, several variables depend on a combination of other input parameters and the electrochemistry of the process is not directly under the operator's control. These factors have a considerable impact on the stability and quality of the machining. The frontal and side inter electrode gaps that define the machining region are typical. A layer of ionic species known as the electric double layer (EDL), which forms during electrolysis and functions as a capacitor with a capacitance, is formed close to the two electrodes. The production of an oxide film over the workpiece surface, which serves as a barrier between the surface and electrolyte, depends on the metal and electrolyte combination. Because of its low ionic conductivity, this oxide coating slows the pace of anodic dissolution. The passivation is the phrase for the occurrence, which may also result in the termination of machining. Sparks can be produced when hydrogen and oxygen gas generated during electrolysis become ionised in the presence of an electric field.

Electrolytes of WECM

In addition to completing the electrical circuit between the tool and the workpiece, the electrolyte also enables the desired machining reactions. The formation of anodic films is typically permitted on workpiece surfaces, which aids in anodic smoothing; nevertheless, occasionally, smaller IEG can result in short circuiting during WECM. Although the precipitate has no direct effect on the process, it obviously raises the risk that a short circuit will cause damage to electrode. Therefore, it is advised to utilize new, clean electrolyte rather than re-circulating it while micromachining. The machining zone's heat and reaction products are removed by the electrolyte. Low throwing power, strong chemical stability, high electrical conductivity, and minimal variation in conductivity and viscosity due to temperature rise during machining, and other features are required for an electrolyte. It should be cheap and non-corrosive to improve the accuracy of the machining, safe, non-toxic, and less damaging to the machine body, prevent the creation of a passive layer on the anodic surface. During machining, maintain the product's steady components and pH level **[5].** The various types of electrolytes and their characteristics are shown in **Figure1.6.** Based on their pH, the electrolytes used in WECM can be categorized as acidic, neutral, or basic. Both non-passivating and passivating types of electrolytes exist. Based on the types of anions present, non-passivating electrolytes and passivating electrolytes are distinguished from one another. Passivating electrolytes

contain anions like nitrates and chlorates, but non-passivating electrolytes have aggressive anions like chlorides and bromides. Aggressive anions are known to hinder passive film development and encourage breakdown from the metal or alloy surface.
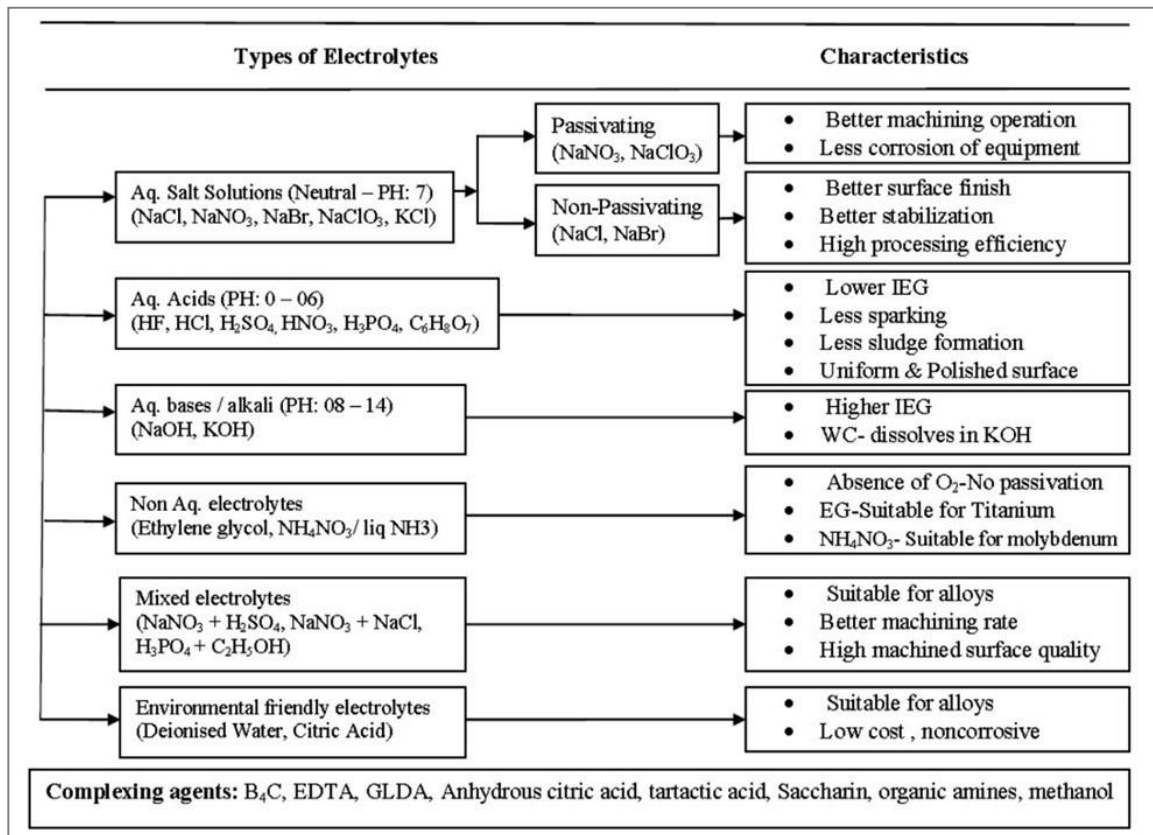
Figure1.6 Electrolytes of WECM

A neutral electrolyte with the advantages of high processing efficiency, improved stabilization, and low cost, aqueous sodium chloride solution has the drawbacks of poor machining precision and increased equipment corrosion. The complexing agents can be used to improve the surface finish as well as dissolution process. In practice, the composition of the electrolyte starts to alter as the machining process advances. The electrolyte's pH can rise and its electrical conductivity can decrease as a result of hydrogen loss. The removal of water from a solution is through evaporation or by hydrogen gas evolution, which could raise the concentration of the solution and impact its viscosity and electrical conductivity. The precipitate formation will lower the electrolyte's concentration and could have an impact on its electrical conductivity. It is possible for metal ions from the anode to enter the solution and then deposit themselves on the cathode and the electrical conductivity must be kept essentially constant in order to enable process management and guarantee machining accuracy. Avoiding too much precipitation is necessary. All types of electrolytes with combination of different

complexing agents must take into account for fabrication of microfeatures during wire electrochemical of machining of shape memory alloy which has to be further investigated for the performance improvement of WECM.

Wire electrodes of WECM

One of the key elements in the WECM process is the wire electrode, which has a direct impact on the dimensional accuracy, precision, and surface quality of the machined microfeatures. As a result, choosing the right wire electrodes with a good surface polish is essential for the machining of microfeatures. The strong chemical stability, wettability and etch ability, low electrical resistivity, and good tensile strength are all desirable in tool material for WECM. Wire made of tungsten, stainless steel 304, molybdenum, copper; carbon nanotubes, platinum, brass, and tungsten carbide are mostly used. The mobility of ionic species in the IEG may be hampered by a tool composed of chemically stable material since it does not produce any precipitates during machining. Although copper has a low electrical resistivity, it cannot be used as a tool material due to its poor strength. The usage of carbon nanotube (CNT) as a tool material has received very little attention despite its great tensile strength and wettability. Perhaps this results from its weak electrical conductivity. Additionally, the wire is maintained in a tightened posture to stop it from swinging radially as a result of the momentum of the electrolyte jet and the force of the gas bubbles. Due to its excellent chemical stability and great tensile strength, tungsten is the most commonly used wire electrode material. With neutral, basic, and acidic electrolytes, tungsten wire can be employed. Commercially available wires with a diameter of up to 4 μm are made of it. It is crucial to remember that handling a wire with a small diameter is challenging. Such wires are challenging to place on a machining fixture and are easily bent. Each of these materials has certain desired qualities, and the application determines which material to use. When evaluating the content solely in terms of its qualities, it would be reasonable to assume that choosing the property with the highest rating would be the right decision. Such electrodes provide a high anodic dissolution potential, low hydrogen overvoltage, and extremely favorable electron transfer kinetics. Platinum is a soft metal, but it becomes harder when alloyed with iridium and rhodium. The long segments of tungsten wire are offered for sale on the marketplace. Due to the annealing process, tungsten wire can occasionally become contaminated with carbon, necessitating additional processing to clean the surface. The small-scale flaws in or on the electrode surface will have an impact on the finished machined surface. To achieve high machining accuracy, those wire electrode surfaces that

do not participate in WECM action should be isolated. Lack of adequate tool insulation will result in unintended workpiece machining and lost accuracy in the working profile. Spraying a layer of synthetic rubber, tapping, or dipping can be used to achieve the insulation. The in-depth investigation is needed on the insulation methods for reduction of stray current and overcut during WECM. Further, the performance of WECM process has been improved employing multiple wires for increasing machining efficiency **[6].**

Nature of power supply

There are two different forms of applied power supplies, such as pulsed and D.C. full wave rectified. Low voltages in the order of 1 to 10V are required for the WCEM process' micromachining requirements. The workpiece material may no longer dissolve uniformly due to an accumulation of contaminants on the wire electrode. Additionally, the accuracy may suffer from changes in the electrolyte composition, temperature increases, and electrical resistance. By using pulsed voltage instead of continuous, these issues can be mostly avoided. The gap can be almost fully swept clean during the current intervals, leading to a regular WECM process, when the pulse duration and the intervals between the pulses are suitably matched to current density. The pulse off-time needs to be long enough to guarantee that the electrolyte in the narrow IEG is completely flushed. When pulsed voltage is utilized instead of continuous voltage, the current efficiency is considerably more reliant on the current density. Without the use of a complex electrolyte pumping system or a rigid machine frame, one can apply exceptionally high instantaneous current densities to a workpiece by employing pulsing current. This is made possible by the fact that each current pulse is followed by a relaxation period of zero current, allowing reaction products and heat to be removed from the inter electrode gap. Therefore, high precision micromachining of sensitive workpiece where high electrolyte flow rate cannot be allowed is a particularly good use for pulsating current. It is ideal to have a shorter pulse period for greater accuracy.

Inter electrode gap (IEG)

In WECM process, the distance between the workpiece (anode) and wire electrode (cathode) called as inter electrode gap (IEG) is crucial to ensuring reliable metal removal. The IEG can be configured as shown in **figure 1.7**. The setting has to be carried out by positioning wire electrode to specific and moving it by giving specific feed rate to see the increase in current and check for any touch with continuity tester and finalize the IEG. The accuracy of the machined microfeatures will improve if the inter electrode gap is preserved at a very low value. By reducing the machining voltage and the electrolyte

concentration in WECM, the electrode gap was reduced to few micrometers.
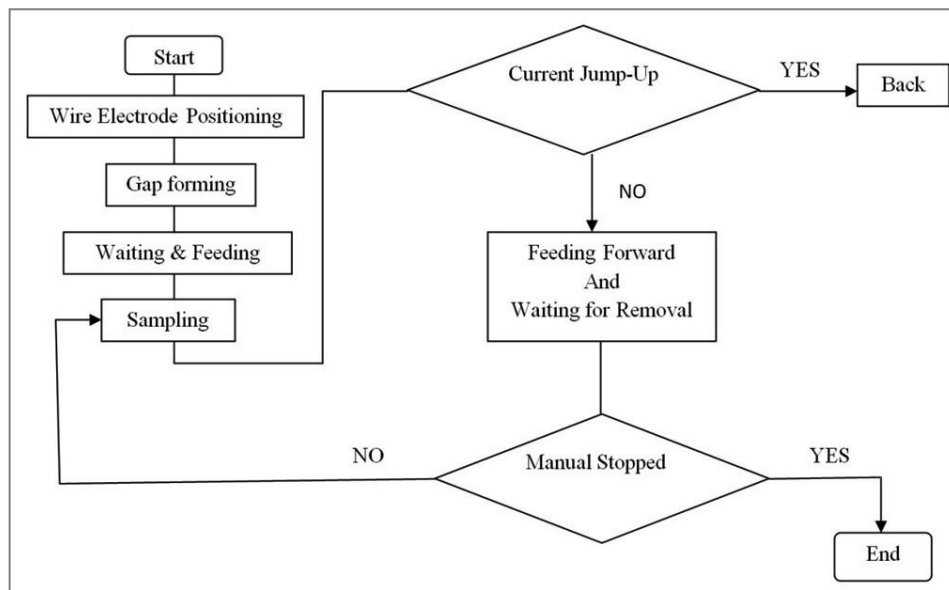
Figure1.7 Setting of IEG

Electrolyte concentration, temperature, and flow

The workpiece surface should slightly passivate and the electrolyte in the IEG needs to be a strong electrical conductor. The types of electrolyte and its concentrations are selected to guarantee effective workpiece material dissolution during the WECM process without damaging the electrode. An important factor is the variation in electrolyte temperatures between the entrance and exit of the IEG. When an electrolyte's temperature rises, this could reduce its specific resistance. The increase in variations in the current and voltage are likely to appear once temperature rises to a high level. The flow rate and pressure properties of the electrolyte would undoubtedly alter as a result of these modifications. Since the bubbles create a non-conducting zone, the presence of cavitations bubbles within the inter electrode gap may force the termination of machining. The cavitation has been proposed as the cause of the ECM's extremely rough, striated finish. Low current flow resistance is provided by a concentrated electrolyte. For a particular working voltage, a higher current density is made possible. In situations where the surface finish is crucial, diluted electrolytes are employed. When the machining voltage is high, dilute electrolyte and a narrow gap should be used. The electrolyte is pumped from an electrolyte chamber to the machining gap, for example, through a hose pipe, via a pressure controller and a filter. The electrolyte travels to the machining chamber after passing through the gap, where anodic dissolution causes the sludge to dissolve and be removed. The complexing agents can be added to lower the concentration of dissolved contaminants. Therefore, the system needs to be capable of circulating and purifying

13

electrolytes. The detailed investigations for machining shape memory alloy have to be investigated using different electrolyte in variation in concentrations.

1.2.4 Process capabilities and limitations of WECM

The process capabilities of WECM in terms of machining accuracy, roughness, power consumption, and volumetric material removal rate (MRR) are comparable to those of the ECM processes. In terms of machining tolerance, the electrochemical machining processes are superior to WJM and AWJM but inferior to EDM, EBM, and LBM. WECM can be used to fabricate microfeatures with precise dimensional tolerance. It has become a popular choice for micromachining. In general, WECM produces surfaces with less roughness than other non conventional machining processes. As a result, ECM and its variations are the best choice for operations demanding a high level of surface polish. ECM requires less power to remove a unit volume of material per unit time than EBM, AJM, LBM, AWJM, and WJM. This shows that employing the WECM technique for machining has an economic benefit.

Table.1.1 Process capabilities, investigated workpiece material and research opportunities

Process capabilities	Workpiece material investigated
Cutting	Stainless steel SS304, Pure tungsten, cobalt, nickel, Ni-based metallic glass, Copper Titanium alloys, TiAl alloys, Inconel718, Tungsten carbide, $Ni_{72}Cr_{19}Si_7B_2$, Aluminium, $Ti_{42}Al_6V_1Cr$, $Ti_2Al_{1.5}Mn$, AA6061-TiB2 composite, 3J21 alloy, metallic glass Ni82Cr7Si5Fe3B3
Turning	Copper, Stainless steel SS304, Aluminium alloy, Mild steel,
Grinding	Tungsten micro rod
Drilling	high aspect ratio cylindrical micro tools for deep hole drilling in turbine blades,
Grooving	Stainless steel SS304,
3D micro structuring	Ni-based metallic glass, Stainless steel SS304,cobalt based super alloys
Micro channels	Ni-based metallic glass
Micro Threading	Stainless steel SS304,
Micro tool arrays	Ni-based metallic glass, cobalt
Slicing	Silicon
Terahertz hollow core metal for rectangular waveguide	Nickel foil

The material removal rate is influenced by elements such as material type, power input, machining current, and area processed for the majority of advanced machining methods

but WECM metal removal is influenced by the type of material and machining current. Because the toughness or hardness of the workpiece material has no effect on the mechanism of material removal in ECM, WECM has been utilized to machine high hardness conductive alloys. These processes have been used to fabricate microfeatures on different materials as shown in **table1.1.**

The various wire electrochemical processes with different hybrid variants in the process have been developed and varieties of materials are investigated which has proven the capabilities of WECM process in variety of advanced industrial applications. However, the microfeatures fabrication on shape memory alloys need to be investigated for in depth analysis and improvement in WECM performance. WECM is used to precisely fabricate various microfeatures on different materials. Advanced micromachining necessitates performing a variety of extremely accurate jobs on incredibly small and thin workpiece **[7].** The high precision 3D complex microfeatures are crucial to machine having applications in the aerospace, automotive, electronic, robotic, and bio-medical industries**.** The advantages of wire electrochemical machining (WECM) include higher machining accuracy, homogeneity, and surface integrity; better precision and control; the ability to machine a variety of conductive materials; cost effectiveness; environmental friendliness; the absence of heat affected zones and spatters; and independence from material properties. Using the WECM technique, it is possible to manufacture challenging-to-cut materials i.e. shape memory alloy that conduct electricity without the requirement for surface distortion. In this process, no tool wear is produced. Furthermore, no residual stress is produced during machining because no direct force is applied to the work piece. Instead, anodic dissolution is used to remove the material. As a result, no heat is generated during the machining operation. Due to its qualities and capacities, which enable the processing of difficult-to-cut materials without altering their physical properties, the WECM technology is advantageous in a variety of industries. Usually, it provides submicron resolution. As WECM is still not commercialized, fabricating 3D complex micro features for regular advanced industrial applications is challenging task of research and investigations. To keep the inter electrode gap (IEG) between the two electrodes constant, the wire electrode is directed towards the work piece. Electrode movement will either be too high or insufficient if the tool feed is not coordinated with the machining. Either anode and cathode contact or an excessively large IEG will arise from this. Both situations will result in the early cessation of the machining operation. In order to achieve the necessary machining, a constant IEG must be maintained. In WECM,

flushing the precipitate is essential. In the absence of this, the machining debris would collect and cause a short circuit between the wire electrode and the workpiece. A protective coating with an insulating material is put on the non-machining zone of the wire in order to ensure that material removal only occurs at the frontal IEG of the wire electrode, maintaining the quality of the machining process. Due to this, it has a limited scope in industrial sector but advancement of WECM through continuous performance improvement in the process will get it towards commercialization in near future.

Electrochemistry of WECM

The electrolysis principle of Faraday's law is the foundation for many industrial processes. One of them is ECM. It is regarded as the electroplating process in reverse. The primary distinction between the ECM process and other electrolytic processes is that the work item is controlled to change in size and shape in addition to having material removed from it. Phase boundaries are when two or more distinct phases, such as liquid and solid, converge. When ions and electrons cross these borders, reactions occur at both the cathode and the anode. Understanding the energy distribution during the ECM process requires an understanding of the potential difference.
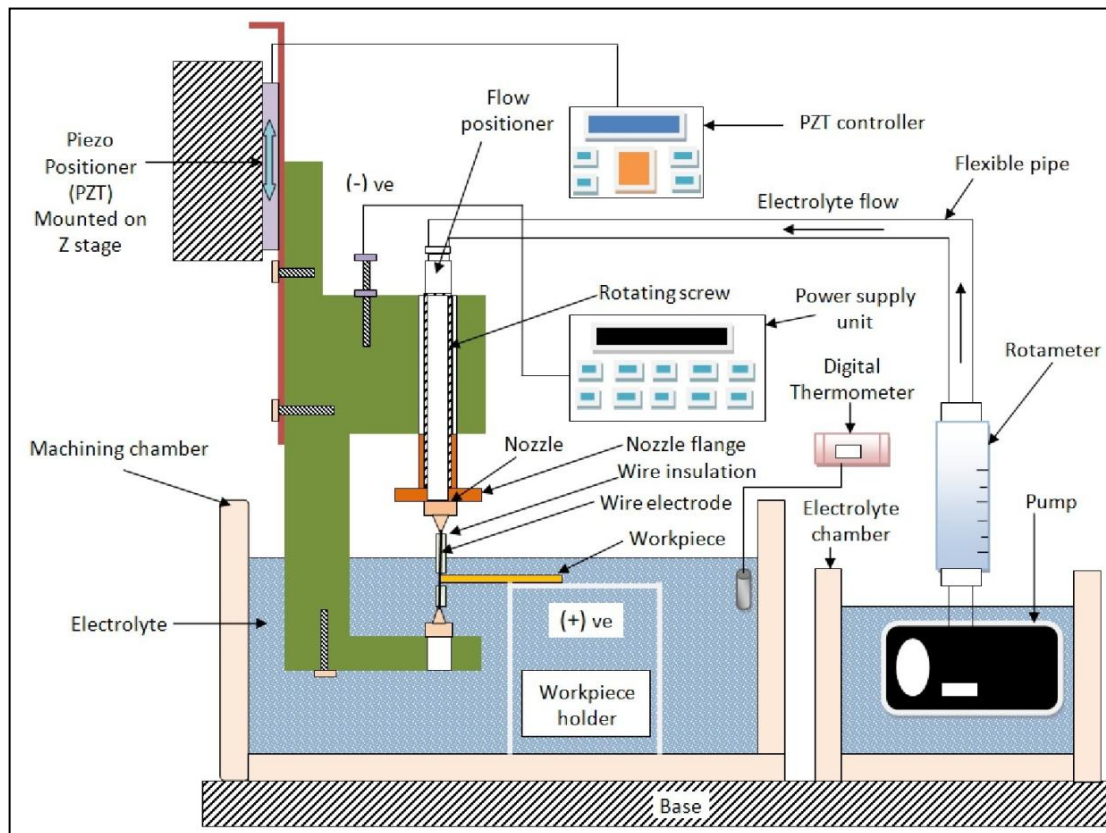
Figure1.8 Schematic diagram of basic WECM setup

As was already mentioned, EMM and ECM share a foundation with WECM. **Figure 1.8**

depicts a schematic representation of a simple WECM configuration. It is an anodic dissolution technique where the workpiece serves as the anode and the wire serves as the cathode. When the responding section of the wire and the workpiece are submerged in an appropriate electrolyte solution, metal is removed via electrochemical reactions from the necessary anode site. The cathode and anode are set before machining by preserving a small initial IEG of a few microns. A precise XYZ stage with three axes of motion is needed to perform machining operations, with the wire staying mounted in an additional configuration on the Z axis and maintained straight, stretched, and stable. Additionally, a special arrangement is used to generate and maintain the tension based on the diameter, shape, and type of the wire because generating too much tension on the wire can cause it to break, while maintaining a lower tension can cause the wire to deform and impair the stability and quality of the machining process. When machining begins, the tool wire is fed forward by maintaining an IEG inside the workpiece along the predesigned path. The transport of electrons between ions and electrodes happens as a result of applying the necessary DC voltage across the cathode and the anode. The circuit is kept in working order by removing electrons from metal atoms' outer orbits, or by creating metallic ions. As a result of the applied potential difference, the current runs in the opposite direction to the movement of the electrons, and metal begins to dissolve into metallic ions through associated electrochemical processes. When stainless steel is electrochemically reacted with diluted sulphuric acid during WECM, iron is anodically dissolved at the anode and hydrogen bubbles are produced at the cathode. The cathode and anodic reactions can be summarized as

Reaction at anode: $\qquad Fe \rightarrow Fe^{3+} + 3e^-$ $\qquad\qquad\qquad\qquad$ (1.1)

$\qquad\qquad\qquad\quad Cr \rightarrow Cr^{3+} + 3e^-$ $\qquad\qquad\qquad\qquad$ (1.2)

Reaction at cathode: $\quad 2H^+ + 2e^- \rightarrow H_2 \uparrow$ $\qquad\qquad\qquad$ (1.3)

Reaction at electrolyte: $H_2SO_4 \rightarrow 2H^* + (SO_4)^{2-}$ $\qquad\qquad\qquad$ (1.4)

$\qquad\qquad\qquad\quad 2Fe^{3+} + 3(SO_4)^{2-} \rightarrow Fe_2(SO_4)_3 \ (yellow)$ $\qquad$ (1.5)

$\qquad\qquad\qquad\quad 2Cr^{3+} + 3(SO_4)^{2-} \rightarrow Cr_2(SO_4)_3 \ (reddish \ brown)$ $\qquad$ (1.6)
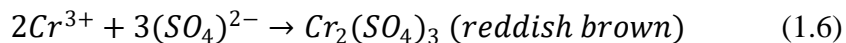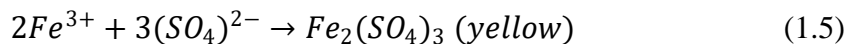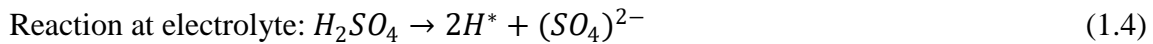
The reactions product ferric sulphate is soluble salt and chromic sulphate is insoluble. Hence, the solution becomes saturated after machining and turns slightly yellowish due to presence of these compounds. This shows the ions depletion and need of fresh electrolyte. The workpiece takes on the desired shape as a result of anodic dissolution, which occurs

during the entire machining process and varies with the position of the wire electrode on the workpiece. To prevent short-circuiting or sparking and to maintain the necessary machining stability, the wire electrode's feed rate must be balanced with the rate of workpiece disintegration throughout the machining process. In order to keep the dissolving process within micron or sub-micron ranges, improve machining precision, and shrink the IEG to a few microns, DC pulsed power is supplied across the IEG throughout the machining process. The use of a DC pulse power source also guarantees improved cleaning and regeneration of new electrolyte during operations in the IEG. This is because machining only occurs during the pulse-on time.

1.2.5   Importance and Applications of WECM

The creation of manufacturing processes capable of carrying out micro manufacturing operations is required by the miniaturization of various ultra-precise parts needed for the manufacture of high precision machinery and equipment **[8].** More and more micro-parts must be included into diverse industrial goods as a result of recent social changes. Micromachining of difficult-to-machine materials is also possible using standard machining techniques, but there are still issues that must be addressed, such as excessive tool wear, tool stiffness issues, and heat generation at the tool-workpiece interface, etc. Due to their adaptability and control over the process parameters, non-traditional machining techniques, particularly WECM, are becoming more and more important. The majority of non-traditional machining methods, such as electro discharge machining (EDM), wire electro discharge machining (WEDM), laser beam machining (LBM), electron beam machining (EBM), etc., are thermally orientated. The machined surface may experience thermal distortion as a result of these processes. Due to WECM's benefits, which include improved precision and control, greater machining accuracy, homogeneity, integrity, and surface quality, as well as its environmental friendliness, it seems to be a very promising micromachining technique. The Chemically resistant materials, such as titanium, copper alloys, super alloys, and stainless steel, which are frequently utilized in biomedical, electrical, and MEMS applications, can also be machined using WECM. The WECM technique can be used to form hard metals, and the rate of machining is independent of the metal's hardness. Contrary to traditional machining methods, the wire electrode utilized in the process does not wear, allowing soft material wire to be employed as tools to shape harder work parts. It is possible to create the desired shape on the workpiece regardless of the material's hardness, which is extremely challenging in traditional machining because the tool needs to be harder than

the workpiece. Therefore, with the right choice of process parameters, "difficult-to-machine materials" as well as any hard alloys can be machined with WECM. Wire that is used for machining in WECM has a diameter of only a few microns (5μm). Therefore, different high aspect ratio micro-features with complicated shapes can be easily manufactured utilizing WECM employing this very small diameter wire. In contrast to WEDM, there is no wire tool wear here since the process is anodic, which prevents cathode erosion. As a result, it is possible to reuse the same tools repeatedly, which indirectly lowers the cost of machining. There are no induced mechanical or thermal stresses because, as in the case of WECM, there is no direct contact between the tool and the workpiece. Because there is no heat affected zone (HAZ), there is no surface degradation brought on by thermal damage. Due to this benefit, WECM continues to be a step above other non-traditional machining methods. In WECM, improved surface quality is attained since material is removed atom by atom, negating the need for post processing (finishing operations). MRR is essentially unaffected by the kind of material. Alloys that are hard and durable can be machined simultaneously. Electrolyte regeneration (micro filtration) has made it possible to purify the electrolyte to a ppm (parts per million) level, making it possible for unlimited re-use. Depending on its composition, the resulting sludge can frequently be recycled and is therefore suitable for the environment.

Applications of WECM

It is still needed further research to fully understand the enormous potential of WECM, which is still a laboratory procedure. However, up till a certain point, this method has demonstrated its capacity in laboratory grade microfeatures for research purposes. This procedure is effectively utilized for the machining of high strength alloys and chemically resistant materials like nickel, stainless steels, etc. due to a variety of its advantages. To create the intricate shapes needed in the electronics and medical industries, micromachining is widely employed. Additionally, WECM is a promising and affordable option for a variety of industrial applications. In WECM, when the wire electrode advances into the workpiece, a constant space known as the Inter Electrode Gap (IEG) is kept between it and the workpiece. The electrolyte flow is uniform across the workpiece, in contrast to other techniques. This technology is mostly employed in the electronics and medical industries to produce intricately formed microstructure components. Additionally, it is frequently used to shape highly precise components for the aerospace sector. According to the information shown in **Table 1.2**, the manufacturing of various

products and microfeatures has been one of the main uses of WECM to date.

Table1.2 Potential application areas of wire electrochemical machining

Application sectors	Products / features
Aerospace Industry	Micro tenon tooth structure, Micro cam, Micro rectangular cantilever, Structures on TC1, micro propeller blade
Automotive Industry	micro cams, micro gear structure, micro keys and key grooves, square and circular spiral springs
Manufacturing industry	Fir tree like turbine disk tenon, micro curved channel , small crankshafts, micro curved flow channel, micro spline, maple leaf structure, pointer components, sealing rings in flanges, very thin turned parts (turning, threading, grooving, indexed cutting), ,Grinding, fingerprint like coil spring, machining of thin walled tubes, Micro-annular grooves, micro beam, Turbine disc slots
Medical / biomedical industry	comb structure in micro-actuators, multi slits in X-ray phase contrast imaging systems, micro cantilever beams for weighing of micro species, Micro textures on body implants, grooving on hypodermic needles, micro threads on dental implants, surgical instruments, surgical blades
Chemical industry	Micro heat exchangers
Tooling	Multiple pins, micro tool arrays, high aspect ratio cylindrical micro tools for deep hole drilling in turbine blades, High aspect ratio micro tools for EDM/ECDM with tight tolerance. Multilayered 3D microelectrodes,
Energy sector	Slicing of thin wafers from silicon ingots for making solar panels
Communication industry	Terahertz hollow core metal for rectangular waveguide
General applications	micro-channels, micro-slots, micro-cavities, spiral microgrooves, complex internal and external shapes, square micro pillar shaped surface textures, 3D hollow & tree like microstructures, square micro holes, square micro helix, micro triangular shapes etc,

1.3. Shape Memory Alloy (SMA): Overview

Arne Olander a Swedish researcher, made the initial discovery of shape memory alloy, also called a smart alloy, in 1932, but Vernon first used the term "shape memory" for polymer dental material in 1941 **[9].** A smart material is one whose properties alter in response to particular environmental factors such temperature, pH, stress, electric current, and moisture. Piezoelectric materials, magnetic form memory alloys, pH-sensitive

polymers, and shape memory alloys are examples of smart materials that have been produced. When Dr. William Buehler's and Frederick Wang with their team at the US Naval Ordnance Laboratory identified the existence of the unusual shape memory effect (SME) of equiatomic nickel and titanium alloy in 1963, they gave the alloy name as "NITINOL" **[10].** Shape memory alloy (SMA), one of those intelligent materials, has a unique property known as the shape memory effect (SME), which is the subject of ongoing research. SME is the process of returning a deformed alloy to its original state by applying heat or stress to the alloy. Nitinol SMAs may be categorized as a subset of a large collection of smart materials, where the SRA is connected to the micro structural changes that occur in response to non-mechanical external stimuli, such as changes in temperature or magnetic field **[11].** Shape memory alloys were first used in commercial items and machinery in the 1970s. The field has advanced significantly since that time. With the development of smart materials, non-traditional machining techniques have been investigated for smart materials, including laser machining, ER/MR fluid machining, and electrochemical machining (ECM). Shape memory alloys (SMAs) are new substances that, when heated, can assume a specified shape again. An SMA has extremely low yield strength when cold, or below its transformation temperature, and is easily bent into any new shape that it will hold. When a force greater than their elasticity restoration stress is applied, metals that experience plastic deformation typically cannot be returned to their original shape. However, even if the applied force exceeds the elasticity restoration stress, a SMA can be returned to a particular memorized shape when a certain stress or temperature is applied.
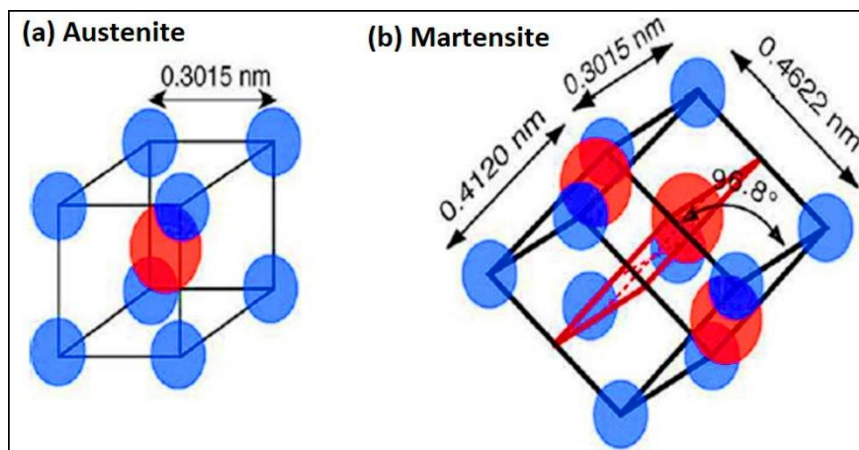
Figure1.9 Nitinol SMA austenite and martensite structures

According to reports, SME is negatively impacted by machining heat and the physiological tension that follows. As a result, there is a lot of study being done on the

use of unconventional machining techniques on nitinol SMA. The SMA has austenite in cubic crystal structure, whereas martensite is known for having a monoclinic crystalline formation. The crystal structure of nitinol SMA depicted in **figure1.9** shows austenite and martensite which has a phase transformation phenomenon **[12].** Practically, SMAs can go through four different transformations (transition temperatures: M_f, M_s, A_s, and A_f) and exist in two separate phases with three different crystal structures. The phase transformation of SMA is shown in **figure1.10.** The SMA starts to transition from the martensite phase into the austenite phase as it heats. A_s-austenite-start-temperature, where the transformation begins, and A_f- austenite-finish-temperature," where it terminates, are the two temperature points during this process. When a SMA is heated past a certain point, it starts to contract and change into an austenite structure, or to return to its previous shape. Due to the fact that this change can occur even with heavy applied loads, it produces high actuation energy densities. The transformation begins to revert to the martensite during the cooling phase at the martensite-start temperature (M_s), and it is finished when it reaches the martensite-finish temperature (M_f). Above Mf, the temperature at which martensite can no longer be stressed; the SMA becomes permanently distorted like any other common metallic material **[13].**
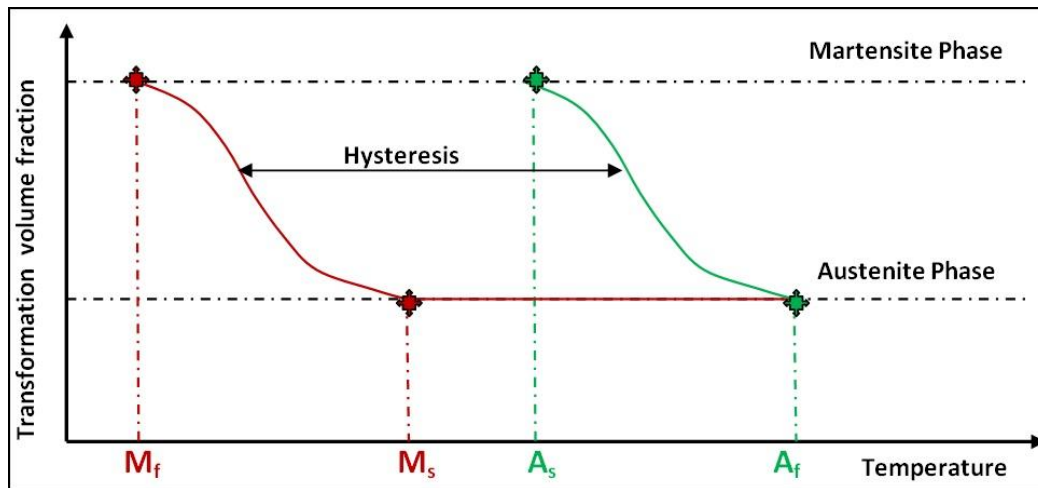
Figure1.10 SMA phase transformation

Depending on the shape memory alloy property, repeating the main and reverse transformation processes may cause a change in temperature where the transformation process begins and stops. Functional stress refers to these phenomena, which affects both the material's operational characteristics and fine structure **[14].** When the applied deformation stress is removed, the SMA returns to its original shape because of pseudo elasticity (also known as super elasticity) which is accomplished by recovering the

deformation strain after the stress has been released. When an external force is removed, the one-way shape memory effect keeps the distorted state afterward and returns it to its normal shape when heated. Although the two-way or reversible shape memory effect can retain its shape both at high and low temperatures, it is less frequently used in commercial settings. Shape memory effect, pseudo elasticity, and thermal phase change are special properties of SMA. After a given number of cycles, the thermo-mechanical analysis cycle can result in permanent deformation under the imposed loading condition, which is referred to as premature fatigue of SMA. This depends on a number of variables, including different fabrication techniques (such as welding, powder metallurgy, heat treatment, forming, and casting), ambient conditions (such as humidity and temperature), microstructural changes during transformation, and working conditions (such as stress and strain, etc.). Given the mechanical and thermal changes, the microstructural changes are anticipated with cyclic loading. The shape memory behavior subsequently suffers as a result of this mechanical and thermally induced microstructural alteration **[15].** The fatigue life of SMAs is also influenced by the crystallographic orientation of the grains and the production of precipitates in the microstructure. Furthermore, oxidation and corrosion cause quick crystal degradation, which in turn affects fatigue life. The fatigue life of SMAs can also be changed using heat treatment procedures. The primary shape is maintained inside the SMAs while mechanical stress deforms the twinned martensite to a detwinned structure. It must take an additional two steps to return to its former state. The outer load must first be lifted before the austenite transforms when heated. This period of high temperatures starts at A_s and progresses till A_f. The strain recovery is dependent on the process region because all of these events start a cycle. One-way SMAs are the components that establish these stages. The final strategy, which has a special quality, is known as a two-way SME. At a higher temperature, one-way SMAs only have one starting shape. For two-way SMAs, two recoverable conditions might be created, one in the austenite state and the other in the martensite state **[16].**

1.3.1   Types and Applications of SMA

Numerous metals, polymers, ceramics, and other materials are available that exhibit shape memory effects. There is a large variety of shape memory alloys (metals) available, as follows [13, 15]:

(i) Iron-based alloy Fe–Mn–Si;

(ii) Copper-based SMAs such as Cu–Zn–Al; Cu–Al–Ni, Cu–Al–Ni–Mn, and Cu–Sn;

(iii) Nickel–Titanium based alloys such as NiTi, NiTiCu, NiTiPd, NiTiFe, NiTiNb, NiFeGa, and NiTiCo;

(iv) Kovar (29% Ni, 17% Co, 0.3% Si, 0.1% C and Fe balance);

(v) Hi-temperature shape memory alloys such as TiNiPd, TiNiPt, NiTiHf, NiTiZr, ZrRh, ZrCu, ZrCuNiCo, ZrCuNiCoTi, TiMo, TiNb, TiTa, TiAu, UNb, TaRu, NbRu, and FeMnSi;

(vi) Magnetic shape memory alloys, namely, NiMnGa, FePd, NiMnAl, FePt, Dy, Tb, LaSrCuO, ReCu, NiMnIn, and CoNiGa.

In 1960, the CdAgAu alloy was used to create a temperature switch for the first time using the shape memory effect. The use of SMAs in practical applications increased as it was learned that nitinol have good shape memory capabilities. The field has advanced significantly. SMAs have been in demand for applications including micro-electromechanical systems (MEMS), robotics, consumer and industrial products, automotive, aerospace, and biomedical areas because of the aforementioned special qualities. However, among all these above shape memory alloys, nitinol has been widely used in the industries for many advanced engineering applications. In general, four groups can be made up of SMA applications based on how the shape memory effect works (1990; Duerig):

(i) Motion generation: A SMA in the martensite phase is what is being deformed. Then, by heating above A_s melting point, it takes on its native form. A nitinol wire, for instance, might be cooled to a temperature of M_f, bent into a different shape, and then heated to it's A_s temperature to return to its original shape.

(ii) Force generation: A tension is produced after heating if a SMA that is deformed in its martensite condition is restricted in a way that prevents it from assuming its original shape. The primary purpose of this function is to create a mechanical junction, such as a fastener, pipe coupling, connector, or sealing.

(iii) Work production: When there is motion against a stress, the SMAs can operate. This feature can be used to create an extremely effective actuator that combines sensing and actuation. SMA actuators have a small size, a straightforward mechanism, and a high displacement/work output.

(iv) Superelasticity: This application, which is thermal in nature and involves storing potential energy, produces stress that is nearly constant despite a significant variation in strain. The surgical hook, orthodontic arch, and eyeglass frame are a few examples of applications. The superelasticity is now being used much more frequently in the medical

sector. The stents produced by nitinol SMAs are among the most intriguing medicinal applications. A novel approach to preventing strokes called stenting is as effective as surgery but less stressful. The biocompatibility of nitinol alloys, improvements in the micromachining process, and tendencies towards less invasive surgical procedures are the justifications for their use.

Further, SMA's offer a number of benefits, including safety, pressure sensitivity, and ideal working conditions, including cleanliness, quietness, and spark-free operation. They can even function in zero-gravity environments. As a result, they are currently used in a variety of reciprocating applications across a range of industries, including clamping tools, fire detection systems, and refrigerant circuit valves, which are perpetually stopping and operating. These miniature electrically powered motors are only one illustration of how these reciprocating applications are available in small sizes. Braces, orthodontics, and medical guide wire are just a few of the uses it has in the medical industry. Additionally, SMAs were used in the wires (strings) that operate the hinge-less ailerons in fixed-wing aircraft and the aerospace sector. Shape memory alloys are also being used in structural connectors, vibration dampers, manipulators, and certain pathfinder applications in aerospace in addition to actuators. SMAs have also been employed successfully in artificial muscles for robotic applications as well as micro- and macro-actuators for robotic fingers and hands. Flying robots have been managed by SMA-based actuators. A leading choice for biomedical applications, nitinol SMA is used to create surgical instruments, dental implants, bone implants, stents, and other medical devices **[17, 18].** The micromachining of nitinol without affecting material properties is the major issue in this field therefore in depth experimental investigations are still needed.

1.3.2 Machining of SMA

The term "machining" refers to the use of cutting tools to remove undesirable elements from the specimen in order to give it the desired appearance. The high ductility, typical stress-strain behavior, low thermal conductivity, and high degree of work hardening of these alloys cause poor chip breaking, burr formation, and progressive tool wear while machining, the occurrence of weld defects and low joint strength during their welding and joining, non-uniform melting, and difficult fabrication processes, so despite the aforementioned characteristics and significant applications of SMAs, they are considered difficult-to-fabricate and process materials. Consequences of all of them include poor work surface integrity, high energy and resource consumption, rising fabrication and processing costs, and huge environmental footprints. Regarding the production and

processing of SMAs, major efforts have been made to improve part quality, lower costs, and increase safety and sustainability. These efforts have taken the form of inventions, research, and development. The traditional and nontraditional machining methods can be employed for machining of shape memory materials by exploring the effects of engineering various process parameters on the machining accuracy and surface finish of SMAs.

The knowledge provided revolves around nitinol as they are used extensively in traditional machining of SMAs. High dynamic loads, specimen distortions, and shortened tool life are caused by titanium's reactivity with low heat conductivity, shaping tools, significant strength at elevated temperatures, and soft elastic modulus effect in prolonged temperatures. Similar to titanium, nickel-based metals and super alloys display high strength and due to their austenitic pattern, nickel super alloys perform badly during machining and result in linked chips that are difficult to control **[19].** Fast flank wear, notching, and cratering are the results of the aforementioned qualities, and they vary depending on the tool component and the specific operation conditions. In addition, important shape memory alloy characteristics like the pseudoplasticity, and high ductility of titanium and nickel alloys present additional challenges when machining these materials, leading not only to rapid tool failure but also to lower specimen quality due to extreme burr generation, adhesions on the surface of the shaped part, and changes in the sample substance's microstructure. High stress, high strain rates, and high temperatures during SMA operation can result in surface and sub-surface defects such the development of a white layer and the enlargement of micro cracks **[20].** SMA implementation in various industries necessitates great dimensional accuracy with precise tolerance and affordable machining. The shortcomings of conventional machining include a lengthy procedure, significant tool wear, and poor dimensional accuracy. The variety of traditional machining processes i.e. turning; milling, drilling, grinding etc have been used for machining of shape memory alloy. The use of conventional machining came with numerous challenges. Additionally, traditional machining has unfavorable outcomes such as excessive tool wear, decreased dimensional precision, and a lengthy procedure.

 The SMAs are machined using non-traditional machining techniques gives better results in terms of accuracy as well as surface finish. When it comes to cutting complex shapes, the methods of electrochemical machining (ECM), laser machining, and water jet machining (WJM) have some restrictions. To better machine complicated components with high dimensional accuracy, use electrical discharge machining (EDM) or wire

electrical discharge machining (WEDM). These days, SMAs are frequently machined using laser cutting and electrical discharge machining. **[21]**. Tool wear is thereby drastically decreased or completely avoided, although high temperatures produced during the process has poor integrity surface due to formation of heat affected zone(HAZ) on the machined surface. However, these processes are widely used in 3D complex high aspect ratio microfeatures fabrication.

1.3.3 Nitinol SMA: Properties and Usage

Nitinol is extensively utilized in micro-electromechanical system (MEMS) devices, and a variety of other advanced applications in the robotics, electronics, aerospace, biomedical, automotive areas, among others. However, it is a hard-to-cut metal because of its diverse particular features and properties. There are numerous obstacles to machining nitinol SMA with traditional machining. Noncontact operation between the wire electrode (cathode) and workpiece (anode) of the wire electrochemical machining (WECM) process removes many of the issues associated with traditional machining techniques. Further, the working principle of WECM is well known for the outstanding property of an unaffected rim in terms of residual stresses and HAZ.

Table1.3 Physical and mechanical properties of nitinol SMA and stainless steel SS304

Properties	Nitinol Martensite (M) /Austenite (A)	Stainless Steel SS304
Melting point (°C)	1240-1310	1400-1450
Density (kg/m3)	6450	7850
Electrical resistivity ($\mu\Omega$-cm)	76(M) / 82(A)	72
Thermal expansion (10-6/ °C)	6.6(M) / 11(A)	17.2
Thermal conductivity (W/m- °C)	18	16.2
Elastic modulus (GPa)	40(M) / 75(A)	193
Recovered elongation	8%	0.8%
Tensile Strength (MPa)	1450	540-750
Elongation thickness (%)	60	45
Hardness (HRA)	65-68	70
Torqueability	Excellent	Fair
Wear and corrosion resistance	Excellent	Fair
shape memory effect	Yes	No
superelasticity	Yes	No
Biocompatibility	Excellent	Fair

Table.1.3 illustrates the physical and mechanical properties of nitinol SMA compared

with properties of stainless steel SS304 to establish the uniqueness of this material. Making biomedical devices like cardiovascular stents, catheter tubes, guide wires, stone retrieval baskets, filters, needles, dental files, and arch wires as well as other surgical instruments, aerospace and automotive industry applications, nitinol SMA is an expensive but highly intelligent material of choice.

Nitinol alloys are a suitable option for lightweight actuators because they have a high specific actuation stress when used as wires or springs. In the emerging topic of soft robotics, robotic actuators and micromanipulators based on nitinol are utilized to simulate the fluid motion of human muscles. This reversible deformation is aided by the phase changes brought on by loading and the return to the unstable phase once loading is ceased. Despite its widespread use in a variety of sectors, the majority of research focuses on finding alternatives to conventional biomaterials like titanium and stainless steel in the biomedical industry. For instance, bone implants are implanted to support the bones and assist in the healing of complex fractures. Nitinol SMA is particularly appealing due to its resistance to corrosion and has mechanical properties that are equal to those of human bone **[22].**

1.3.4 Need of nitinol SMA micromachining

The controlled input parameter settings for machining are necessary to produce nitinol microfeatures of higher quality, and additional study is required to determine the impact of novel machining techniques on the enhancement of machining accuracy and surface quality. In contrast to silicon and other conventional semiconductor materials, the potential application of nitinol is growing in the field of micro engineering and Micro Electro Mechanical Systems (MEMS). Due to its improved biocompatibility and high fracture toughness, nitinol micromachining provides a comprehensive solution to the limitations of the standard micro machined materials. Nitinol offers the potential for better device safety. Compared to traditional materials made of Si or glass, which is prone to catastrophic failure because of their inherent brittle qualities, these variables can boost safety and reliability. In addition, nitinol has a long history of use in orthopaedic and dental implants, demonstrating its greater physiological compatibility with cutting-edge biomedical micro devices. For instance, thin-foil devices for bio molecule separation and characterization, large area thermal ground planes for electronics cooling, and rationally nanopatterned substrates for enhanced cellular response are a few examples of such devices. Micro needles for transdermal drug delivery are another. However, attempts at micromachining nitinol have been less successful than those of ordinary silicon or other

micro machined materials. Due to the lack of application-specific technologies currently available and the potential to develop devices with improved safety, reliability, and performance, researchers are looking into the development of flexible micromachining processes and techniques that can guarantee accurate nitinol shape memory alloy micromachining without affecting its properties to fulfil all the requirements in biomedical and advanced industrial applications **[23].**

1.3.5 Challenges in nitinol SMA machining

Nitinol SMA is an intermetallic mixture that accelerates the transition between the martensite and austenite phases when combined in equiatomic proportion. The surface state has a significant impact on the functionality of manufactured nitinol microfeatures. At the moment, laser machining or WEDM for micromachining of nitinol are frequently used in the fabrication of complex biomedical components. These machining processes, however, cause heat damage to the surfaces of machined micro-features, forming HAZ and recast layers, which leads to a very poor surface quality and reduces the functionality of the microfeatures. In order to maintain the characteristics of machined microfeatures for biomedical applications, surface quality enhancement is crucial **[24].** It is well known that the WECM process is used to manufacture electrically conductive materials. It is found that it is quite difficult to machine nitinol without changing its original properties because to the unique material attributes. SMAs are new intelligent elements that may remember their initial form and return to it by modifying their environment. Other distinctive and adaptive characteristics of shape memory alloys are their intelligent nature, biocompatibility, pseudo-elasticity, strong corrosion resistance, and wear resistance. These elements have gained a lot of attention and interest in a variety of implementations over the past few years due to their intriguing features. These materials must be machined in order to be used in diverse applications. It is possible to carry out this machining in both conventional and non-conventional ways. However, conventional SMA operation is difficult due to extreme strain hardening, high toughness, and high cutting pressures, whereas with unconventional operation the surface integrity and the accuracy of dimensions are considerably improved as well as the machining time was lowered. Every machining technique, in general, has obstacles that produce favorable or unfavorable outcomes. The fact that heat created during milling in nitinol does not discharge smoothly when using conventional machining techniques is one of its downsides since nitinol more closely resembles titanium than nickel. Numerous unconventional machining techniques, such as non-contact machining, have been

researched for use with nitinol in an effort to solve this challenge. Despite its benefits, typical machining techniques like milling, drilling, and turning are very difficult to use on nitinol. As a result, it creates internal stress and is unable to emit machining heat. According to a previous literature review, no attempts have been made on nitinol micromachining for the production of intricate microfeatures utilizing WECM. When compared to other electrochemical machining methods, the WECM process differs in the machining kinematics and the exposed side crosssection of the wire. The in-depth literature review for wire electrochemical machining on nitinol shape memory alloy has been described in the following section.

1.4 Literature review

In many manufacturing sectors, including aerospace, biomedical, electrical and electronics, automotive, thermal and nuclear power plants, etc., where difficult-to-cut materials are employed; WECM is a crucial machining technique. By investigating the influence of process parameters on the machining process, several studies have tried to enhance the performance characteristics of the WECM method. But the WECM approach has yet to be used to its full potential. This is because there are many different variables to investigate, which is complex and chaotic. The literature review undertaken for this research work found that the investigations on WECM has been related to current WECM trends and the influence of process factors on different microfeatures mostly on common conductive materials. In order to meet the demands of micromachining for current industrial and biomedical applications without altering the characteristics of materials, wire electrochemical machining (WECM) is a promising technology for the manufacture of high aspect ratio complex and 3D micro features. Further investigations in the area of nitinol shape memory alloy micromachining employing WECM encompassing a variety of process parameters as well. Micromachining using WECM has gained more attention in recent years, particularly for the fabrication of intricately shaped micro and nano-microfeatures. Because most of the works devoted to wire electrochemical machining are experimental, the influence of electrochemical machining process parameters for the difficult to cut nitinol shape memory alloys have not yet been sufficiently investigated. The development and related research activities that have taken place on WECM as well as few investigations on shape memory alloy are reported in this section. This discussion has been presented to highlight the improvements and technological advancements chronologically to get an idea of the current scenario of the WECM process since it is a relatively new process in the field of machining technologies and very few researches has

been carried out for investigating the effect of electrochemical processes on nitinol shape memory alloy. The literature that is available can be categorized into various categories, including;

(i)   Fundamentals and process improvement,

(ii)   Mathematical modelling and simulations,

(iii)   Influence of process parameters and other factors,

(iv)   Enhancement of mass transport, machining accuracy and efficiency, and

(v)   Investigations on nitinol shape memory alloy etc.

(i)   Fundamentals and Process improvement

Many attempts have been made to create a functioning setup in this novel field of micro/macro machining in order to comprehend various phenomena encountered during machining as well as to investigate the capability and potential. Regarding fundamentals and process capabilities here, managing the same yield towards advantageous manipulation and the attainment of desired results is crucial. Additionally, the results are dependent on the accurate machining conditions, which might again add flexibility in meeting specific output requirements. The following describes the research endeavours that address the aforementioned;

Maeda et al. **[25]** introduced pulsed DC voltage and axial electrolyte flushing techniques in 1984 and investigated the effect of a number of operating parameters on the feed rate of wire electrode, including applied voltage, electrolyte pressure with varying wire diameter, wire tension, nozzle diameter and length of wire span, thickness of workpiece, and pulse period under various duty factors. Additionally, an effort has been made to develop and validated feed rate equations that take into account the values of reaction product concentration and temperature rise under instantaneous changes caused by varying pulse period and duty ratios. With the use of pulse periods that are shorter than the electrolyte's residence time, or the amount of time needed for the electrolyte to move between electrodes, feed rate has improved. But the negative effects of wire vibration above the feed rate at critical electrolyte pressure are particularly pronounced, which is why methods like using nozzles with smaller diameters, shorter wire spans with higher wire tension, as well as increasing applied voltage, have been suggested**.**

Bejar et al. **[26]** analyzed the effects of machining current under various applied current values, workpiece thickness, wire diameter, and electrolyte concentration on corresponding feed rate. Additionally, efforts have been made to determine the impact of side gap and material removal rate under various workpiece thicknesses, electrolyte

concentrations, and wire diameters on feed rate as well as influence of side gap and material removal rate on machining current. It is seen that the research involves both machining with constant and pulsed DC power supplies, it has been hypothesized that using pulsed DC produces larger applied feed and lower side gap values**.**

Zhu et al. **[27]** introduced in-situ micro-tool fabrication technique for the improvement in machining accuracy and created a wire electrode in situ via reverse electrochemical etching by maintaining the anode wire stationary in a cathode stainless steel barrel. By measuring the fluctuations in resistance, the reduction in wire diameter has been mathematically estimated in order to determine the final etching time necessary to reach the desired wire diameter. Additionally, efforts have been made to look into the effects of applied feed rate, pulse voltage, pulse duration under various voltage values on the corresponding side gap of micro feature, which is the determining factor for machining accuracy. Further, varieties of intricate nonlinear microfeatures as well as a pattern of linear microslits have been fabricated using anode vibration for improved flushing effectiveness**.**

Shin et al. **[28]** used ultra short voltage pulsed and performed WECM operations using tungsten wire rather than weaker platinum wire. However, potential control of both the tool and work electrode has been examined using potentiostat in order to avoid the potential creation of a passive oxide layer and to achieve transpassive dissolution. It has also been investigated how the electrolyte concentration, applied voltage, pulse on time, and pulse period affect the side gap of a micro-feature. Additionally, investigations have been conducted for producing regular and uniform machined surfaces influenced by various pulse conditions as well as pulse period, which also determines the bubble size, which, if higher, can distort the wire due to surface tension. Complex micro-features, such as various types of micro grooves, micro triangular shapes, and micro gear, have also been machined**.**

Zou et al. **[29]** in-situ fabricated a ribbed tool referred as a ribbed wire from a 500 μm stainless steel rod and utilized to carry out research work on wire electrochemical micromachining. A cathode molybdenum wire with a diameter of 100 μm is fed into the rod while it is rotating and kept still in the perpendicular Z direction, where it dissolves electrochemically to produce a rib. The creation of a sequence of ribs has been secured by the upward and downward motion in the Z direction, where the rotation also improved flushing and increased mass movement. Additionally, the influence of changing pulse frequency, duty cycle, and electrolyte concentration on rib width has been studied. With

the right parameter settings, the rod with the promised high L/D ratio has been fabricated. WECM has been performed using ribbed electrodes with the best parameter values, where the reciprocating and synchronous rotation of the ribbed electrode ensured stirring and improved product expulsion. Furthermore, using rotary motion to fabricate ribbed wire is actually exceedingly difficult, and no definitive feedback has been provided in the work. The experiment has been discussed, nevertheless, to elicit ideas for potential future ribbed wire fabrications and to outline the potential benefits of using ribbed wire**.**

Gao et al. **[30]** reduced the diameter of tungsten wire from 12.8 µm to 8.5 µm by utilizing electrochemical dissolution in a non-aqueous electrolyte solution comprising an ionic liquid made of a mixture of calcium chloride and ethylene glycol,. After being cleaned with anhydrous calcium chloride and further pre-processing, the electrolyte has been uniformly combined with an additive, such as ethanol solution of sodium hydroxide. The wire has been securely held during fabrication by a stationary steel counter electrode with a cylindrical form. An effort has been made to define the electrochemical behaviour of tungsten in the aforementioned non-aqueous solution, and under various voltage levels, changes in surface morphology and micro structural analyzes have been studied. It has been claimed that the electrochemical behaviour of tungsten differs from the specimen in aqueous solution and that no oxidation or passive layer generation has been seen as a result of the application of ionic liquid**.**

Fang et al. **[31] [32]** fabricated rotary helical wire electrode. In place of helical wire, a helical drill has been employed. The simultaneous use of rotation, reciprocation in the Z axis, and cathode feed in the X direction, however, can also result in helical formations if ribbed wire can be produced using the same method**.** As a result, research involving machining with a helical drill has not been covered in this area due to lack of viability or because it would only be possible to obtain it after fabricating ribbed wire using the same method, further, the large amplitude vibration of wire electrode tool is introduced to enhance electrolyte renewal and bubble removal process in both its upward duration and downward because of its specific structure during wire electrochemical machining**.**

He et al. **[33]** used a low alkaline (KOH) electrolyte and a smaller pulse time to achieve stable machining and evaluated the effects of operating factors including feed rate and applied voltage on side gap. Using tungsten wire with a diameter of 10 µm, microfeatures with dimensions of 5µm side gap, 20 µm widths, and a 15:1 aspect ratio were created on pure tungsten under ideal parametric conditions. To machine quasi-periodic multi-slit micro features with slit widths of 24 µm, the multi wire (3 wires) has also been added.

Low magnitude piezoelectric vibration has also been introduced. Another example of this is the production of tungsten-based quasi-periodic or periodic micro features for anticipated end uses in gratings to be used in X-ray absorption contrast imaging systems. This illustrates the fact that using multiple wires can increase efficiency during WECM.

Meng et al. **[34]** used the WECM technique for machining of Ni-based metallic glass (Ni72Cr19Si7B2). The dissolution behaviour of Ni-based metallic glass has been described in light of passive and transpassive regime. The effects of various electrolyte solutions have been studied, and a non-aqueous solution of H_2SO_4 and methanol has been employed to inhibit the development of passive film. Since using a shorter rise time can ensure rapid rise of machining current in transpassive regime and limit the loss owing to passive film growth, the effect of pulse rise time on corresponding standard deviation and slit width has been investigated. By applying a bias potential that is close to the onset potential of transpassivity, the workpiece can be kept polarized in the transition between the passive and transpassive regime during pulse off time without causing passive film growth. This shortens the duration of the following pulse, which decreases capacitive losses. Therefore, research has been done to determine how pulse voltage affects slit width and standard deviation. Additionally, by adding an oxidizing agent to bring the workpiece potential close to the onset potential of transpassivity, redox processes that arise in the presence of a semi-conducting passive layer and affect the open circuit voltage can be reduced. The effect of the aforementioned machining circumstances on the surface's quality of microfeature has been separately investigated. Finally, it has been found that using oxidizing agents like H_2O_2 with H_2SO_4 instead of methanol results in the highest maximum feed rate that can be used for machining complex non-linear micro features. This is followed by using H_2SO_4 in methanol and water. When H_2O_2 was added, the transpassivity potential dropped to 2V. However, it has also been determined that redox reactions that result in polishing can improve surface quality and uniformity when it happens in the very low potential semiconducting passive regime, whereas complex surfaces with pits and isolated islands have been seen as the dissolution rate varies with surface elements when H_2O_2 has been added.

Again, **Meng** et al. **[35]** studied that how different process parameters, such as pulse period, pulse on time, feed rate, voltage, and electrolyte concentration, affect slit width and homogeneity when fabricating various complex micro features on Ni-based metallic glass with the best parameter settings. In order to optimise the flow condition in the IEG, cathodes travelling as well as anode vibration have been applied along with analysis and

simulation of the impact of bubble density and size on current distribution in the machining gap**.**

In another research study, **Meng** et al. **[36]** employed CNF wire as electrode while machining Ni-based metallic glass and compared it to smooth tungsten wire. To help with electrolyte cleansing, the reciprocating travelling cathode has been used, and PZT on the anode has supplied micro vibration. Utilizing spiral CNF wire, which is naturally hydrophilic, improves mass transfer in addition to upward and downward motion. Flow field simulation, hydrophilicity analysis, and experimental studies have all supported this improvement in mass transfer efficiency. A carbon nanotube array was used to spin CNF like yarn. After that, the fibres were made denser in an ethanol bath and repeatedly rinsed in deionised water to remove any silicon that had become stuck to the surface during the pre-processing step of chemical vapour deposition on the silicon wafer. Hydrogen bubbles can easily escape when wetting agent $C_{12}H_{25}OSO_3Na$ is added, significantly lowering the interfacial tension at the liquid-solid-air interface. However, due to the existence of amorphous carbon and other impurities that produce in high contact resistances, the electrical conductivity of CNF is significantly lower than that of defect-free carbon nanotubes. Because of this, a thin Ni coating was electrodeposited on the CNF surface before use to raise the conductivity to a useful level. It has been determined that the presence of a passive film in a stable passivation regime, which has contributed to electrochemical polishing, makes the use of diluted H_2SO_4 electrolyte during machining result in superior surface quality and localization of anodic dissolution. Contrarily, use of HCl results in chloride-induced pitting corrosion, when passive coating cracks as a result of chloride ions' adsorptive action. While doing so, the surface quality degrades and machining effectiveness rises. The use of CNF wire also improves machining stability, increases machining efficiency by two times, and increases homogeneity of the micro slits by more than five times when compared to smooth tungsten wire**.**

Klocke et al. **[37]** used twisted brass wires to create a double helix structure and to fabricate micro features in Inconel718 using the WECM technique. On a 200 mm span, 12 twists have been made in the wire, which has a diameter of 0.25 mm. Two rotating units have been used throughout the machining process, and the wire has also been clamped and tightened by a spring. Axial electrolyte flow has been used in conjunction with the rotating motion on the wires to promote flushing, which has now been optimized. The effects of voltage, electrolyte pressure, and nozzle diameter on cutting kerfs, surface roughness, and cutting rate during WECM of micro features have also been

investigated. It has been determined that surface roughness is affected by electrolyte pressure, with too low of a flow rate being deleterious and too high of a flow rate again increasing it by creating flow grooves in the flank of the cut. Roughness increases as a result of incorrect flushing and widening flow grooves caused by an excessive increase in feed rate. On the other hand, roughness is unaffected by nozzle diameter. Roughness reduces with higher voltage values because of adequate dissolving. However, it grows once more with an excessive increase in voltage values because of the uneven dissolving of the various phases present in the workpiece, and it gets worse when flow grooves start to form because of the addition of a very high electrolyte pressure. Additionally, it has been mentioned that in addition to axial flushing, additional bottom flushing may be necessary as workpiece thickness increases. Additionally, non-symmetrical edge rounding during entry has been caused by the helical wire's rotational direction. However, the research has also suggested that by modifying settings and employing wire with various geometries, the material removal rate in WECM might be increased in comparison to that of other machining techniques, such as wire electro discharge machining**.**

Gao et al. **[38]** introduced negative voltage in appropriate ranges in addition to positive voltage values as an in situ dressing approach for removing blackened precipitates on wire In order to improve machining stability and accomplish isotropic dissolving. This improved surface morphology and achieved isotropic dissolution. Flushing techniques, such as the combination of wire reciprocating motion and low amplitude workpiece vibration, have been used during machining. Single pulsed and double pulsed WECM have been compared in terms of electrical flow field uniformity, product homogeneity, feed rate, and machining stability. 10 µm diameter tungsten wire, SS 304 stainless steel, and 0.1 M HCl were used as the cathode, anode, and electrolyte during positive voltage machining. When negative voltage is applied, the situation is reversed. According to the EDX analysis, the black precipitates are primarily composed of iron, chromium, and nickel with a little amount of trace elements including chlorine and oxygen. With the exception of less deposits of iron that have been flushed away due to its higher weight and a higher percentage of chromium, the weight percentages of elements like iron, chromium, and nickel are essentially identical to those of stainless steel type 304. For this optimization, negative voltage is required, which, if lower, results in the presence of black precipitate and, if greater, in the precipitate's removal and the reverse etching of the wire. it should be noted that the reverse etching can only take place when the electrochemical

series is met, which is possible in this instance because both tungsten and SS 304 dissolve in acid solution. However, because it offers better control over dissolution, alkaline solution is typically used in the manufacturing of tungsten wire. When using two pulses, the feed rate is lower than when using one. A portion of the charge from the positive pulse is needed to balance off the charge that was kept in the double layer during the negative pulse as the pulse changes from negative to positive. In order to recharge the double layer in a timely manner, additional charge is needed. This charge loss, when combined with the same pulse period and amplitude, reduces feed rate and workpiece dissolution**.**

(ii)   Mathematical modelling and simulations

Another crucial topic is the modelling and simulation of WECM process in different conditions. Researchers can forecast the data produced from actual tests as well as analyze it by using various mathematical models and simulating the outcomes. This aids in creating a framework with the right understanding of what will happen when a regular process is repeated or modified without leading to further experiments. Here are some examples of mathematical modelling and simulations that are commonly used and analyzed during WECM:

Volgin et al. **[39]** proposed a mathematical model and numerical simulation for forecasting workpiece topology, geometry, and repeatability of machining during WECM with travelling wire. The potential distribution along the IEG is approximated linearly in the model. However, the distribution of current density has been estimated for better validation because there is a slightly greater IEG in a WECM with travelling wire. Additionally, the topological changes were taken into account while using the boundary element method to solve the model with different shaped rotating or static travelling wire electrodes moving along a random path**.**

Zeng et al. **[40]** introduced reciprocating travelling of wire for better flushing and better insulation strategies, such as implementation of hollow insulating tubes covering the wire at either side of work surface as well as shielding box for the wire portions that are wrapped in pulleys in order to reduce the effect of stray corrosion during WECM. Without insulation, the machining zone's current density distribution was uneven, and the effect of stray current was particularly strong at the workpiece's top surface, where it led to the formation of pits. Due to the combined action of gravity and downward drag force, the electrolysis products gravitate towards the bottom portion of the machining zone as the wire descends. At the base of the machining zone, stray corrosion and conductivity

both decline. However, a small amount of larger size debris moves towards the bottom due to gravity during upward movement. Insulating glass tubes with an inner diameter of 0.35mm have been utilised to insulate molybdenum wire measuring 100 μm in diameter. The pattern of current density distribution during upward/downward movement and on either side of the workpiece, which has also been analyzed and simulated by COMSOL software by taking the process in an equilibrium state, is greatly influenced by the distance of the insulating tube from the work surface as well as from the wire surface. The trials' findings were in strong agreement with the insulation approach that was put into place because the dissolution was more uniform, localized, and less affected by stray corrosion, which enhanced the surface quality.

Wang et al. **[41]** used the WECM method to create an array of micro annular grooves on aluminium alloys with a high strength to weight ratio. The mechanism is comparable to that used with the fabrication method for ribbed wire that was previously disclosed. In this instance, neutral sodium nitrate solution was used as the electrolyte and tungsten wire with a diameter of 20 μm was used as the cathode. Use of sodium nitrate leads in the creation of a passive layer on the surface of the aluminium that can only be eliminated by raising the current density, unlike acid electrolyte where no passive film occurs. Since sodium nitrate creates a passive film, it reduces machining stability and accuracy. However, when machining is taking place in the transpassive regime, it significantly lessens the effect of stray corrosion and increases anodic dissolution. As a result, using an acid electrolyte causes severe stray corrosion even at low current density values. Due to the dynamic nature of the development of micro annular grooves in cylindrical surfaces, a 3D electrical model was also created, and simulation using the COMSOL programme was conducted to examine the current distribution in the machining gap. Additionally, the effects of the workpiece's rotational speed, applied voltage, and pulse frequency on the formation of passive films, surface quality, and groove width have been investigated. It has been observed that using very high rotational speeds can again grow passive layers due to a lack of electrolyte in the area of the machining zone caused by centrifugal force, and using excessive voltage can also cause stray corrosion as passive layer grows even in non-machining areas.

He et al. **[42]** used multiwires electrode for performance enhancement during WECM. To improve mass transportation, multiwire reciprocating motion using the Z stage during machining has been used. To simulate the electrolyte flow in the machining gap during wire passage, a flow field model has been created and developed, followed by analysis

using ANSYS and Fluent. The impact of various operating parameters, such as duty ratio, the number of wire electrodes, and the pulse frequency on the microslit width and total machining current, the number of wire electrodes on maximum feed rates, the total rate of material removal, and the average current for each wire, as well as the amplitude of wire travel on maximum feed rate, slit width, and total rate of material removal, have all been studied. Last but not least, utilizing the best parameter settings, a multi-slit with an aspect ratio of 20 has been fabricated using 15 wire electrodes, and an array of complex microfeatures has been machined with good consistency and great surface quality using 7 wire electrodes. Further, H. He et al. **[43]** have used laser direct scanning on wire to create micro patterns that can improve mass transmission, boost machining efficiency, and improve homogeneity by reducing cohesive force and increasing hydrophilicity.

Xu et al. **[44]** employed dynamic liquid membrane to electrochemically etch a tungsten wire. Due to surface tension, the electrolyte droplets stay suspended in the tungsten ring. The 300μm diameter un-etched tungsten rod was clamped securely in the centre of the aforementioned ring while reciprocating motion was applied perpendicularly to periodically machine within the amplitude regime. In order to reduce the adhesion of the electrolysis products on the anode surface and to improve the renewal of the electrolyte inside the droplet, PZT has also been used to create low frequency and small amplitude vibrations during the manufacture of wire. The electrolyte droplet was absorbed with filter paper after etching using the best parametric settings, and the tungsten ring was severed so that the manufactured wire could be used for further machining operations. A mathematical model has also been put forth to forecast the wire's final diameter in relation to the length of the etching process. Tungsten wire has a reduced diameter of 14 μm and stretches to a length of 200 μm while maintaining a uniform cylindrical shape.

He et al. **[45]** experimentally verified that using coupling axial and intermittent feed-direction vibrations is capable in enhancing the maximum feed rate, resulting in the increase of machining rate. In addition, using low feed rate beside a small feed length in the process is suitable for getting better the homogeneity of machined slit width and the machined surface roughness and same has been confirmed through simulation that could force the electrolyte to flow with a high velocity in both axial and feeding directions, which flushed out the sludge and dissolved electrolysis products away and out from the machining gap.

Yang et al. **[46]** used a tube with an array of holes as the cathode and a reciprocating workpiece was utilized to enhance the machining efficiency and potential of WECM for

thick workpiece. When the amplitude of the reciprocating motion is greater than the spacing between the holes, the machining efficiency and accuracy are enhanced obviously, relative to WECM with a tube electrode and no reciprocating motion of workpiece. It has been confirmed through the simulation that the use of tube electrode promotes removal of electrolysis products and the reciprocating motion of the workpiece is supportive to increase the uniformity and consistency of the flow field.

Debnath et al [47] carried out further research work on modelling and the effect of voltage and duty ratio on wire feed in WECM considering potential alternative for WEDM. The experimental analysis based on a specific experimental setup and settings highlights the influence of key elements like applied voltage and duty ratio on the corresponding maximum wire feed rate during the machining of microslits. A table for the maximum wire feed rate has also been provided, together with the corresponding voltage and duty ratio values. In addition, a mathematical model that links maximum feed to voltage and duty ratio has been created and afterwards verified by experiments. Microslits that were created using various voltage, duty ratio, and maximum wire feed values demonstrated very good and controlled dissolving, with the created slits being homogeneous and having the appropriate range of widths and lengths of 700–800 μm. This finding unequivocally supports the notion of raising the matching voltage and duty ratio values in order to increase wire feed rate. Given that the model's viability has been confirmed, it may be utilised to determine the maximum feed rate at specific parameter values and operating conditions**.**

Debnath et al. [48] researched on the effect of high duty ratio and frequency in WECM using an in-situ constructed ribbed wire,. The tungsten wire, which is used for machining, has undergone in situ etching to reduce its initial diameter of 50μm to 23.43μm and also attained a diameter of 5.85μm, however it was exceedingly challenging to fabricate. Along with adding PZT vibration to the tool, an axial electrolyte flow system has been designed. They noticed that the slit width grew to a maximum width of 183.02μm when high duty ratio was applied. But when a 30% duty ratio was used with wire that had a diameter of 23.43μm, a microslits with a slit width of 51.29μm was produced. Other machining parameters, such as frequency, applied voltage, and electrolyte medium, were also maintained at 1MHz, 5V, and 0.1M, respectively. The minimum and maximum widths were discovered to be 46.09μm and 56.09μm, respectively, when high frequency was introduced, while a declining tendency in width was also seen. They also created a mathematical model that establishes a relationship between the duty ratio, pulse

frequency, and machined slit width. The model was evaluated using the experimental results as well, and a very small discrepancy was discovered. In order to further select the appropriate duty ratio and pulse frequency ranges for a desired slit width using WECM, the model can be employed. Additionally, using a tungsten wire with a diameter of 43.12 µm and a 25% duty ratio, a complex stepwise micro-feature was produced.

Jing et al **[49]** presented an experimental investigation on wire preposed jet electrochemical machining (WPJet-ECM) in order to fulfil the machining requirement of microstructure with higher aspect ratio and better inner surface quality. An electric field simulation model was established to simulate the distribution of current density. The COMSOL multiphysics software was used to calculate the distributions of current density and simulate the machining processes of these proposed methods, WPJetECM and IWPJet-ECM. WPJetECM technology has been proposed based on Jet-ECM, and it can be named IWPJet-ECM when the lateral surface of the wire is insulated. The simulation results show that these two techniques can achieve the current density distribution more concentrated which is useful to enhance the machining localization According to the experimental findings, WPJet-ECM, when compared to Jet-ECM, can increase the aspect ratio of the concave, while the IWPJet-ECM approach can considerably minimize the lateral size of the microfeatures in order to further raise the aspect ratio. Due to the use of wire electrode, WPJet-ECM and IWPJet-ECM are able to efficiently manage the machining gap during the processing, allowing for the maintenance of a higher and more concentrated level of current density in the processing region. Therefore, even though the machining concave is deeper, higher inner surface quality of the concave can still be attained.

(iii)   Influence of process parameters and other factors

Even now, WECM is a lab-scale machining process. Therefore, from a commercialization perspective, learning about the applications and conducting research on this process are quite important. In this regard, WECM has been applied by a number of researchers for the fabrication of various micro/macro components and features, which can once more confirm to its viability and promise for achieving better results compared to other processes in many aspects. Additionally, numerous attempts have been made to find out how different process parameters affect the geometry, dimension, and surface quality of the microfeatures in order to develop them with consistency, accuracy, and efficiency using a process with predefined parameter settings. These research initiatives are described below.

Lee et al. **[50]** employed wire electrochemical machining to cut single crystalline Si wafers and polycrystalline Si blocks without the application of cutting forces using aqueous HF solution and platinum wire as electrode. For both n-type and p-type Si wafers, research has been done to determine the effects of voltage and HF concentration on the grooving rate and surface morphology of groove walls. Additionally, it has been investigated how the integrated gravity feed mechanism's pressure on the wire holder affects the pace of grooving and current flow. The block's grooving rate and applied pressure were substantially below those in the actual world and significantly lower than those for wafers, which indicate the creation of more useful machine mechanisms for boosted pressure and solution replacement in the created grooves. The method produces smaller kerfs than the widely used conventional sawing method**.**

Liu et al. **[51]** created intricately formed metal micro tools using WECM. A tungsten rod of 300 μm and a wire measuring 20 μm were utilized in the process. By using a DC pulsed power source, tungsten wire was fed into a cylindrical rod that was positioned perpendicularly. By coupling linear motion in the Z axis, rotation around the Z axis, and wire feed in the X direction, fabrication of a variety of micro tool shapes, including semi-cylindrical, thinly sliced, triangular prismic, etc., was made possible. Additionally, research has been done to determine the effects of operating voltage, pulse duration, wire feed rate, and electrolyte concentration on overcut and machining stability**.**

Xu et al. **[52]** used multiple wires instead of a single wire to increase productivity while milling comb structures or arrayed micro features. Contrary to single wire electrochemical machining, double layer charging efficiency depends on the number of wires linked to a single power source, and the influence of operating parameters in multiwire WECM are non linear phenomena. The wires are parallel and have the same length and, for the most part, the same diameter. As a result, the double layer's resistance and capacitance likewise remain parallel. The quantity of wires enhances double layer capacitance while lowering cell impedance. Therefore, when the charging time constant increases, the power loss also increases and the rising time of the double layer potential increases. As a result, when the pulse on time is shorter, the potential might not increase to the necessary level. As a result, the feed rate drops when the duty ratio is fixed. Additionally, higher voltage values are desirable since the actual applied voltage and machining current decrease. In addition to the aforementioned parametric analysis, attempts have been undertaken to create complex and nonlinear microfeatures using three wire electrodes on an elastic alloy sheet that is 80 mm thick**.**

Again, **Xu** et al. **[53]** fabricated rectangular and square micro tool arrays using single as well as multiple WECM incorporating reciprocating travel by Z stage on 10μm tungsten wire and micro vibrations by PZT on cobalt-based workpiece. After analyzing the effects of various parameters on fillet radius and standard deviation during the fabrication of micro slits, such as reciprocating travel speed and amplitude, anode vibration frequency and amplitude, voltage, pulse period, electrolyte concentration, and pulse duration, the best parametric setting has been identified. Additionally, electric field modelling has been done to determine the impact of bubble behaviour on the homogeneity, breadth, and edge radius of the slit. The method demonstrates its viability because EMM has once more employed the manufactured arranged square micro tool to create a micro dimple array. Furthermore, it has been found that the use of low voltage, low duty ratio, and high feed rates improves stability, homogeneity, and decreases edge radius, whereas the use of higher concentrations, such as 0.07 M HCl, improves homogeneity but causes edge radius to increase**.**

Wu et al. **[54]** adopted WECM as a sequential process in order to get rid of the recast layer and enhance the surface quality of the micro features produced by WEDM. The deionised water utilized as a dielectric and but permits weak electrochemical reactions. When material is removed from a surface by a wire discharge, fractures, craters, and recast layers are left behind. Given that the input rate is lower than the rate at which metals are being removed by electric discharge, the spark gap widens until no discharge occurs at all; instead, anodic dissolution occurs, removing the recast layer and smoothing the surface. Metal removal keeps going when the operation is repeated over and over. The feed rate has also been optimized through experimental research, and it has been indicated that using repeated feeds may be a likely strategy to further lower the surface roughness achieved using WECM**.**

Bi, et al. **[55]** focused on several machining indicators and found that employing 0.1 mol/L HCl as an electrolyte improved machining uniformity during machining high-quality pure-nickel microstructures,. Under the effect of various machining parameters, the best results for each machining conditions vary, although variations in machining homogeneity and surface roughness are often stable and the variation in machining rounded edge radius follows a linear trend. As a result, no one set of process parameter combinations can produce the best machining results for all machining combinations. The best parameter combinations for thick workpiece have to be selected with an emphasis on good surface roughness and small machining rounded edges**.**

According to research by **A. Tyagi** et al. **[56]**, the pH of the electrolyte solution and working potential are the key variables that influence the kind of anodic dissolution. When the working voltage and electrolyte pH encourage corrosion, a higher rate of material removal can be achieved. When the passivation phenomenon is prominent, higher surface polish can be attained**.**

Rajkumar et al. **[57]** conducted experimental investigations on the wire electrochemical micro machining (WECM) integrity of an AA6061-TiB$_2$ composite, and they looked at the effects of different WECM parameters like voltage, electrolyte concentration, and flow rate on the rate of material removal, surface roughness, and kerfs width. Surface roughness and material removal rate are positively correlated, with an increase in voltage and electrolyte concentration resulting in higher dissolution rates and rougher surfaces. Higher material removal rate and narrower kerfs width are produced as a result of increased flow rate, which also renews the electrolyte at the machining zone and flushes away electrochemical sludge and dissolved products**.**

Debnath et al. **[58]** investigated the influence of wire electrochemical machining parameters during the fabrication of microfeatures. It emphasises the significance of including axial electrolyte flow, which becomes much more effective when combined with the use of small vibrations by PZT to achieve regulated and uniform machining. Fabricating intricate microfeatures has become a significant problem, and the WECM technique might be crucial for producing desired microfeatures with the necessary accuracy and dimensions. To improve the process capability by identifying appropriate machining conditions and its efficacy, however, in-depth research is still required. As a result, the future direction of this work will focus on reducing the width of the created microslits utilizing wire with a lower diameter and examining the impact of various flow rates**.**

Debnath et al. **[59]** investigated the effect of wire feed rate on the width of microslits produced by the wire ECM process in more detail, and they found that this parameter like tool wire feed rate has a significant impact on the related micromachining criterion. Increasing the feed values in one experiment led to the creation of microslits that gradually shrank in width regardless of voltage variations. By altering the corresponding feed values, complex miroslit with various cross-sections have been created. Axial electrolyte flow is very important and becomes even more effective when combined with the use of tiny vibrations by PZT for achieving controlled and homogenous machining. This type of microfeatures may opt towards greater importance in the fields of micro

fluidics and other advanced engineering applications.

(iv)   Enhancement of mass transport, machining accuracy and efficiency

The flow system for electrolyte flushing plays an important role in WECM. As a result, determining the effect of the same is crucial to attaining effective dissolution. Several researchers have used a variety of flushing strategies depending on the applicability and usage requirements, ranging from simple and highly effective methods to different flushing strategies that are easy to use. As a result, several research initiatives, including the flushing approach used, the justification for its usage, and the impact of those strategies on possible outcomes, have been stated as follows:

Zeng et al. **[60]** looked into the effects of different flushing techniques to fabricate various complex micro features,, such as axial electrolyte flushing with the best flow entrance angle, flushing by wire travelling in a single direction, introducing micro vibration on wire, and combining wire and workpiece vibration. According to certain theories, flushing with axial and mono-directional wire travel can produce features with extremely high aspect ratios, but flushing with micro vibration can increase machining accuracy and precision.

Wang et al. **[61]** used a solo axial electrolyte flow system. Investigations have been conducted to determine how the flow rate of the electrolyte affects the maximum feed rate that can be achieved as well as the stability of the machining process, or the reduction in short circuits during machining. Additionally, the effects of applied voltage, electrolyte concentration, and initial IEG on stray current attack at the entry point of the micro features have been investigated. Machining accuracy is defined as a reduction in side gap. It has been proposed that using a higher, yet ideal, electrolyte flow and implementing a lower starting IEG can prevent stray corrosion and enhance machining stability and efficiency. The fabrication of various microfeatures, including micro curved flow channels and micro splines, has also been done with the best process parameter settings.

Qu et al. **[62]** designed a stream of electrolyte coaxially enclosing the wire with a flow entry angle of $0°$ to remove the sludge and dissolved products from the IEG and achieve stable machining on titanium alloy (TCI). A study on the effect of changing nozzle diameter on the side gap of the generated micro slit came to the conclusion that, when using a nozzle with a larger diameter and maintaining a constant flow flux, the side gap was increased by scattered corrosion, a decrease in electrolyte pressure as well as flow rate, loose encasement, and the scattering of electrolyte from wire over the work surface. Additionally, Taguchi approach has been used to determine the combination of optimized

parameters to produce microfeatures with lower side gap under stable machining conditions. Efforts have also been made to fabricate an array of microfeatures with enhanced productivity by employing multiple wires as an electrode.

Further, **Qu** et al. **[63]** once more proposed the flushing technique, which entails combining a low-frequency anode vibration with the reciprocating motion of the cathode wire to replenish fresh electrolyte in the IEG, improve uniformity, and decrease side gap. Additionally, by investigating their effects on pertinent output criteria like side gap and homogeneity, efforts have been made to determine the best flushing parameters for anode vibration frequency as well as amplitude and cathode travelling amplitude as well as frequency. Additionally, research has been done to determine the effects of other operating factors, such as pulse period and voltage, on the side gap of the produced microslits. Finally, a variety of complicated linear and nonlinear micro features have been fabricated with the right parameter values.

In another research work, **Qu** et al. **[64]** employed reciprocating wire electrode movement to flush electrolysis products during WECM. Investigations have been conducted to determine the effects of operating parameters on corresponding slit width and standard deviation of the width of the produced microfeatures. These operating parameters include wire travelling velocity, concentration of electrolyte, applied voltage, duty cycle, pulse frequency, and feed rate. Using this flushing method, a microfeature with a very high aspect ratio of 113 was created using 100 μm molybdenum wires on a substrate made of 20 mm of stainless steel (SS 304). The usage of pulsed DC, reciprocating moving wire, low applied voltage, duty ratio, and electrolyte concentration, along with a high feed rate, have all been found to improve machining stability, homogeneity and accuracy.

Zeng et al. **[65]** introduced mono-directional travelling wire to flush the electrolysis products from the IEG during WECM. Additionally, a comparison of the effects of utilizing reciprocating and mono-directional travelling wire has been done. Although the flow field model of the electrolyte produced for the IEG has recommended increasing the wire travelling velocity to raise the flow velocity to increase the electrolyte renewal rate, the operational parameters must also be optimized. For this, it has been observed that using low voltage, higher electrolyte concentration, but not excessive increase in travelling velocity and feed rate, as well as flushing parameters like wire travel flow rate would improve machining accuracy.

Xu et al. **[66]** designed a combined flushing technique to prevent the frictional loss of electrolyte pressure in IEG, which included low frequency anode vibration and cathode

movement in an axial direction. This strategy was especially effective for coaxially flushing very low resolution microfeatures. For the purpose of removing cathode travelling later on, the low amplitude anode vibration disturbs the flow field, speeds up diffusion, and evenly distributes machining products across the machining zone. Further research has been done into the effects of several parameters on the corresponding roughness of the microfeatures sidewall, including cathode travelling speed, anode vibration amplitude and frequency, pulse period, duty ratio, and voltage. Surface roughness increases again when too high parametric values are included, which may result in improper flushing, while it decreases when process parameters are implemented at extremely low ranges, but which may gives improper and inhomogeneous dissolution as well as short circuiting. Increases in cathode speed, anode vibration frequency, and amplitude have also been claimed to reduce surface roughness; however, excessive anode vibration frequency and cathode travelling speed have been shown to be harmful, and anode vibration amplitude has very little impact on the flow field. Finally, by using the best parametric settings, complicated micro components like micro cams with controlled side walls and surface quality have been fabricated**.**

In a different approach, **Xu** et al. **[67]** improved the mass transport by making the wire hydrophilic and rougher in addition to the reciprocating travelling of wire during machining. According to the theoretical research, surface hydrophilia has a major role in both the thickness of the boundary layer and the viscosity of the electrolyte. Using wire with a high hydrophilic surface produces thick boundary layer, increases its viscosity, and boosts mass transfer. The tungsten wire was chemically etched with a 0.5M KOH solution to make it hydrophilic, and the surface roughness was managed through pilot experiments that looked at how wire diameter and etching time were affected by changes in surface roughness. According to a comparative study and set of investigations, using hydrophilic wire improved process stability, homogeneity, and surface quality on a variety of linear and nonlinear microfeatures when the best feed rate were used**.**

According to **Kalaimathi** et al. **[68]**, the TWECM process settings and the ozonated aqueous NaCl electrolyte both affect the machining performances for Monel400 alloys, namely the material removal rate (MRR) and surface roughness (Ra). The removal of oxide and sludge deposits from the specimen surface is what causes the MRR in the ozonated aqueous NaCl electrolyte to increase by 3 to 90%. In addition to the impact of ozonation, the variance in MRR rise is caused by the influence of other factors, such as voltage and electrolyte flow rate. The largest reduction in surface roughness (Ra) is 32%.

Secondary oxidants like the extremely reactive hydroxyl and peroxyl radicals are formed when ozone breaks down. These radicals are among the most reactive oxidising elements and react with dissolved substances like oxides and metal hydroxides in quick, non-selective free radical reactions. The fresh surface of the specimen is exposed during these processes, increasing the MRR and decreasing Ra for improved machining. SEM and energy dispersive X-ray spectrum images demonstrate the superior surface created by the ozonated aqueous NaCl electrolyte**.**

Qu et al. **[69]** investigated the use of gas bubble chains in wire electrochemical micromachining to assist the emission of insoluble products out of the machining gap. The discharge of electrolytic products from the machining area is facilitated by the gas bubble chain, which significantly contributes to the remarkable improvement in surface processing quality. Gas bubble chains in WECM are used to create ultra-smooth machined surfaces. The 3J21 alloy sheet's machined average surface roughness is Ra=0.032 μm and Ra of 0.025 μm on 304 SS sheet, respectively. The technique is a promising substitute for creating microfeatures with excellent surface processing**.**

Jiang et al. **[70]** suggested vibration-assisted wire electrochemical micromachining with B_4C particles suspended in the electrolyte. Based on the findings of the experiment, B_4C particles were suspended in the $NaNO_3$ electrolyte, and the electrolytic products that had accumulated on the wire cathode's surface were successfully removed by the low-frequency vibration of the wire cathode. In addition, the electrolyte's B_4C particles reduced the generation of huge bubbles, which improved the uniform distribution of the current density on the machining surface. Using WECM, this technique helped to achieve stable and effective machining**.**

Li et al. **[71]** fabricated microgrooves on a cobalt-based alloy in an H_3PO_4 solution to carry out cutting and polishing operations simultaneously using WECMM. To increase the electrolyte's fluidity, ethanol was added. By measuring the polarisation curve of the 3J21 in phosphoric acid, it was possible to analyze the dissolving behaviour of the material and the electrochemical machining principle in the H_3PO_4 solution. Ethanol was added to the electrolyte; however this had no effect on the electrochemical properties of phosphoric acid. In a low concentration H_3PO_4 solution, electrolytic products might be transported more easily due to the solution's low viscosity. Mass transportation was accelerated by the addition of ethanol. Better flatness resulted from consistent electrolyte conductivity along the wire electrode's axial direction. The electrolyte's conductivity was influenced by the water content. There must be a specific amount of water in the

electrolyte to ensure machining effectiveness.

Tak et al. **[72]** discovered that adding EDTA to electrolyte solution minimizes the production of titanium oxides on the machined surface of the holes during pulse-ECMM of titanium alloys, which in turn tends to reduce stray currents. Improved titanium alloy machining results in less overcut of holes when electrolyte solutions with EDTA are used. In conclusion, the dimensional properties of the micro-holes produced in the pulse-electrochemical micro-drilling are improved by the addition of EDTA to the electrolyte solutions.

Maity et al. **[73]** devised a multi wire electrochemical machining (MWECM) system with three distinct flushing techniques to increase efficiency when machining arrayed microfeatures,. Additionally, a mathematical model for determining slit width has been created and verified. Three 50 µm diameter tungsten wire electrodes fitted with a 1 mm inter-electrode spacing have successfully been used in a multi-wire electrochemical micromachining setup that can produce multiple microslits on SS304 specimens with great accuracy. To forecast slit width, a mathematical model for MWECM that takes into account the double layer charging theory has been created. The combined technique has been regarded significant as ideal flushing when the maximum feasible feed rate is still in the high range, thereby validating the established model.

Ryu [74] investigated eco-friendly electrochemical machining (ECM) characteristics for drilling and milling stainless steel utilizing microwire and microfoil electrodes in citric acid electrolyte. As per cell configuration and pulse conditions, extraordinary phenomena such as tool electrode cut-off due to Joule heating followed by fractured tool welding to the work substrate, electrolyte capillary action around the tool electrode, and electrode vibration by evolved bubbles are observed Metal structure formed on the bottom of the blind hole under weak electric conditions hinders further drilling. By adjusting electrochemical conditions, micro holes, 37µm in diameter with 100µm depth and 26µm in diameter with 50µm depth, are drilled using a 10µm thick tungsten wire electrode. A complex micro hand pattern is fabricated by electrochemical milling on SS 304 substrate. Furthermore, high quality micro grooves with dimension of 34µm wide and 17µm deep are machined using 20µm thick stainless steel foil electrode.

Zhou et al. **[75]** fabricated micro grooves with a semicircular cross-section of tens of microns in radius on metal foils by stepwise manipulating process parameters in wire electrochemical micromachining to improve the profile accuracy of micro grooves with a semicircular cross-section via evenly distributing the machining gap. Firstly, a two-

dimensional model of the electric field was established to investigate the groove shaping process including the changes of machining gap distribution at all normal directions of a cylindrical wire electrode. Finally, a row of 20 microgrooves are produced simultaneously on a 5mm thick stainless steel block by multi-wire electrochemical machining with stepwise parametric manipulation.

Sethi et al. **[76]** analyzed the efficient electrochemical dissolution of tungsten carbide–cobalt alloy (WC-Co) micro-tools for micromachining operations with an eco-friendly electrolyte which is a combination of sodium nitrate (NaNO3) and a complexing agent citric acid (C6H8O7), which not only gives a higher dissolution rate of WC-Co but also gives similar dissolution efficiency. A detailed experimentation to optimize the concentration of complexing agent in the eco- friendly electrolyte was carried out through micro wire-electrochemical machining (micro-WECM) and was analyzed using yield parameters, topographical and material surface analysis as well as electrochemical analysis. This eco-friendly electrolyte produces higher dissolution rate and better surface finish.

Qu et al. **[77]** fabricated microstructures with superior surface quality using wire electrochemical micromachining (WEMM) in an effective and efficient way. Generating passive film on the workpiece is an alternative to improve surface quality in WEMM, which necessitates a delicate selection of electrolyte. $NaNO_3$ solution as a passive electrolyte is beneficial to obtain good surface quality, but it barely takes effect in WEMM. Hence combination of ethylene glycol (solvent) and $NaNO_3$ (solute) has been used to investigate its influences on surface quality in WEMM of stainless steel (304 SS). Electrochemical measurements reveal that 304 SS is subjected to secondary passivation in 1 mol/L $NaNO_3$-ethylene glycol. XRD analysis indicates that the compositions of the passive films formed at various potentials are not exactly the same. Both the secondary passivation and the passive films make dramatic contributions to the improvement of the machined surface quality.

(v)   Investigations on nitinol shape memory alloy

Keeping in view of the present research needs for investigations into WECM of nitinol shape memory alloy for microfeatures fabrication, it is necessary to explore challenges for machining. Once challenges are well known for machining of nitinol SMA, research plans for for experimental investigations can be drawn up leading to successful research findings that can cater the needs of industries for fabrication of nitinol microfeatures. Some of the important reported research papers are reviewed as follows:

Kedare et al. **[78]** did comprehensive study on the review of WEDM of SMAs. It is found that pulse on voltage, pulse off voltage, spark intensity and wok tensions are the most prominent parameters which affect the surface topography. White cast layer, debris and globules were found on the surface**.**

Chu et al. **[79]** demonstrated that anodic oxidation in an H_2SO_4 electrolyte leads to the production of a titania coating that is deficient in nickel on a nitinol SMA. Despite having a porous structure, the titania film can nonetheless successfully stop Ni from diffusing from Nitinol SMA. Additionally, anodic oxidation in an electrolyte of H_2SO_4 can enhance the wettability, biocompatibility, and thermal resistance of nitinol SMA**.**

Lee et al. **[80]** used data from numerous machining scenarios for the purpose of developing a consistent electrochemical polishing technique for Nitinol-based SMAs,. They used acid and neutral electrolyte during operation and found that acid electrolyte is appropriate for slow and precise operation. However, the neutral electrolyte produces holes on the nitinol surface rather than providing precision machining. The Nitinol surface with the most noticeable shape was polished up to a roughness of 0.37 μm, when acid electrolyte was used. The pulse off/on time was 200s and the adjusted current was 18A. Finally, a 0.31 μm surface roughness was attained**.**

Frensemeier et al. **[81]** acquired the pulse electrochemical machining to investigate the two-way shape memory impact on the nitinol alloys. However, it was discovered that pulse electrochemical machining is the more appropriate method for working with the nitinol alloy since it produced a microstructure devoid of distortion, heat damage, oxidation, and deformation. During pulse electrochemical machining, different protrusion architectures can be formed on the surface of nitinol by using groove and hole tools**.**

Ao et al. **[82]** experimentally investigated on how nitinol shape memory alloys were machined for fabricating microgrooves using electrochemical micromachining (EMM). To enhance surface quality, an ethylene glycol-NaCl electrolyte solution with varying ethanol percentages was utilized. The workpiece's $TiCl_4$ can be dissolved by the addition of ethanol to the electrolyte solutions, which also reduces the formation of oxide layer. The finest surface quality microgrooves are fabricated in electrolyte solutions with 20 vol% ethanol. The machining accuracy and surface quality will suffer if too much ethanol is used during machining**.**

Lee et al. **[83]** investigated on short pulse electrochemical machining for groove process on nitinol shape memory alloy and conducted experimental research on the machining settings, machining variables, and a reliable electrochemical polishing (EP) technique for

nitinol SMA. They investigated the outcomes of utilizing a neutral electrolyte and an acid electrolyte. First off, executing EP with a neutral electrolyte results in countless tiny holes on the nitinol surface and is not precise. Although the procedure is quick, using a neutral electrolyte is appropriate for machining where the main objective is metal removal. Second, employing an acid electrolyte for EP is preferable than neutral electrolyte for slow machining. Precision machining is also more suited to EP utilizing an acid electrolyte. Although the machining process becomes unstable when too much current is applied, final surface roughness is typically better when a larger current is applied.

Ma et al. **[84]** found that confined etchant layer technique (CELT) has been effectively used to micromachining of nitinol shape memory alloy using the proper etching solutions containing HF and HNO_3. The concentration of OH in the etching fluid affects the micromachining process. Micromachining experiments demonstrate that electro generated F and NO_2 can be effectively scavenged by OH. The etched patterns on the nitinol maintain the intricate geometry of the mould and are roughly the same size as the patterns on the mould.

Mineta [85] investigated the effects of pulse voltage on the basic characteristics of electrochemical etching of nitinol SMA in LiCl-ethanol solution. The effect of sludge and dissolves products on etching characteristics has been also considered. The etched surface tends to be rough in the case of pulse etching at low pulse duty ratio, pulse voltage and with a thick etching pattern. The etch rate was about 4μm/min in the case of DC etching; on the other hand, the etch rate could be suppressed below 0.5μm/min in the case of pulse etching with linear dependence on the duty ratio.

Mouliprashanth et al. **[86]** produced a precise geometrical micro hole in nitinol SMA of 0.25 mm thickness using electrochemical micromachining with 500μm tool electrode using the Non-passivating electrolyte (NPE), Passivating electrolyte (PE) and the Composite electrolyte (CPE) to study the machining characteristics. A effort is made to produce such a micro hole using a mixed electrolyte to improve machining process. Polarization studies are also conducted for all the chosen electrolytes and good machining accuracy and surface characteristics are obtained under optimized parametric conditions when the nitinol is machined with the composite electrolyte due to combined advantages of both the passivated and non-passivated electrolytes during electrochemical micromachining.

Hung et al. **[87]** used a 300μm diameter tungsten wire electrode to fabricate a fine slot into the nitinol wire. In order to obtain high machining accuracy and surface finish during

wire electrochemical micromachining (WECMM), an ultra short pulse power generator was utilized as a power source to reduce the stray current effect, thus enhancing the machining accuracy. During the process, various process parameters were experimented for their effects on machining characteristics using ultrasonic-vibration-aided WECMM to determine whether it benefited the machining characteristics and micro slots has been successfully fabricated on nitinol wire. Furthermore, with the process setting and combinations of best suitable process parameters, the machining accuracy was improved. Finally, a fine slot was fabricated under the optimum machining conditions and aided by ultrasonic vibration**. The overview of some of the important development and findings of the research work from various researchers has been presented in table1.4.

Table1.4 Development and finding of the research work from various researchers

Development and findings	Investigators
Conceptualization of process and modelling	Chikamori (1977) & Jain (1980)
Process improvement	Meada et. al(1984)
Analysis and optimization	Bejar et. al(1995)
Improvement in machining accuracy	Zhu et. al(2007) & Shin et. al(2008)
Enhancement of mass transport, improvement in machining efficiency and surface quality	Wang et. al(2011), Zeng et. al(2012), Ninsong et. al(2013), Xu et. al(2015), Volgin et. al(2015), Debnath et. al(2018)
Turning and threading operations	Taweel et. al(2011) & sharma et. al(2018)
Use of novel tool profiles	Fang et. al(2016), Zou et. al(2017), Meng et. al(2017), He et. al(2017)
Use of bipolar pulses	Gao et. al(2019)
pH of the electrolyte solution and working potential are the deciding factors which determines the nature of anodic dissolution	Aakash Tyagi et al (2017)
Applied voltage and the pulse duration significantly influence the side gap width in WEMM	N.S. Qu et al (2013)
NiTInol SMA with zinc coated brass wire electrode material	N Kulkarni et al (2020)
3D surface analysis and SEM and EDX analyses were performed to improve the surface integrity of the NITINOL machined samples	Rakesh Chaudhari et al (2020)
tube with an array of holes as the cathode that promotes the refreshment of electrolyte	Tao Yang, et al (2019)
Review on Wire Electrochemical Machining Process: Overview and Recent Advances	S. Debnath, et al. (2018)

Influence of wire feed rate on microslit width fabricated by wire ECM process	S. Debnath, et al. (2019)
Wire electrochemical machining of macro geometrics with a high rate of cutting	Klocke et.al (2018)
Reviewed exquisite properties of shape memory alloys.	Soni Kumari et al (2021)
Extensive review of available literature that the applications of SMAs, particularly NiTi SMAs	Barsharani Dash et al (2019)
Experimental Investigation on electrochemical micromachining (EMM) to machine microgrooves in NiTi SMAs.	Sansan Ao et al (2020)
Stable electrochemical polishing process for NiTinol SMA, machining factors and machining conditions.	Eun Sang Lee et al (2011)
Ozonated aqueous NaCl electrolyte along with TWECM	M. Kalaimathi et al (2017)
WEMM assisted with coupling axial and intermittent feed-direction vibrations	Haidong He et al (2019)
Axial electrolyte flow coupled with the application of tiny vibrations by PZT in WECM	S. Debnath et al (2017)
Anodic oxidation in H_2SO_4 electrolyte results in formation of titania film depleted in Ni on NiTi SMA.	C.L. Chu et al (2008)
Machining performance using non-traditional machining, especially with NiTi SMA	Kishan Zadafiya et al (2021)
Comprehensive study on the review of WEDM of SMAs	Rahul Kedare et al (2018)
Use of gas bubble chain in wire electrochemical micromachining to facilitate the emission of insoluble products	Ningsong Qu et al (2021)
Wire preposed jet electrochemical machining	Qi Jing et al (2020)
Characteristics of the stray-current attack in reciprocated travelling wire electrochemical machining and insulating methods	Yongbin Zeng et al (2014)
Vibration-assisted wire electrochemical micromachining	Kai Jiang et al (2020)
Machining of Ti-Al alloy using WECM with axial electrolyte flushing	Haidong He et al (2016)
Influence of electrolyte flow on micro wire ECM	Shaohua Wang et al (2011)

The literature review is essential in the design, development, and experimentation of this

research work. Here is a list of some of the major ideas that the literature review revealed. From the discussion above, it can be deduced that various researchers investigated the influence of different process parameters on various output criteria, constructed micro tool arrays with single and multiple wire electrodes and investigated the influence of different operating parameters on the homogeneity of the fabricated microfeatures, the influence of various operating parameters during machining presented methods for enhancing mass transport in the narrow IEG, and the influence of various operating parameters during machining on the homogeneity of the fabricated microfeatures. It has been shown the process capabilities to fabricate 3D complex microfeatures with different machining conditions. The experimental setting is based on the many needs described in the research cited above. The thorough investigation of each process parameter carried out by several researchers facilitates understanding the behaviour of each parameter for machining of variety of engineering materials. Ideas for developing the experimental setup that would be suitable for the current research work were gathered from the previous literature as per the requirement of machining difficult to cut shape memory alloy and enhancing the performance of wire electrochemical machining. The fundamental ideas behind different optimization methods were described in detail which further helps to improve the efficiency of machining. It has been discovered that an experimental investigation into WECM performance improvement during the micromachining of nitinol shape memory alloy is still pending. This investigation will take into account the most crucial process factors with overall enhancement in the machining performance during WECM. It is believed that more research needs to be done on WECM during the micromachining of the nitinol. More study and in depth research work is necessary to enhance WECM performance while machining difficult to cut nitinol shape memory alloy because of its phase transformation capabilities. It is inferred that further thorough research encompassing the greatest number of process parameters is required in order to attain machining accuracy and surface quality during micromachining of nitinol shape memory alloy without altering any properties and to improve process performance during WECM.

1.5 Existing knowledge gap to outline the research objectives

A relatively new electrochemical material removal technique is WECM. The research efforts described in this area clearly indicate where the process stands right now and can still be used to indicate its viability, applicability, capability, and potential in the future. Future plans for this novice include immediate attention, additional research works aimed

at tying up any loose ends for supporting its position, and providing a solid platform offering reliable alternatives and solutions not only for internal micro fabrication systems but also for more versatile, economical, and industry-scale implementations. As the process is under development, it has a wide scope of research in different areas which is concerned with machining process, power supply unit, wire electrodes, electrolytes, measurements and different handling. The various problematic areas for research has been shown if **figure1.11.** However, machining of difficult to cut shape memory alloy is a prime need in industrial and biomedical field.
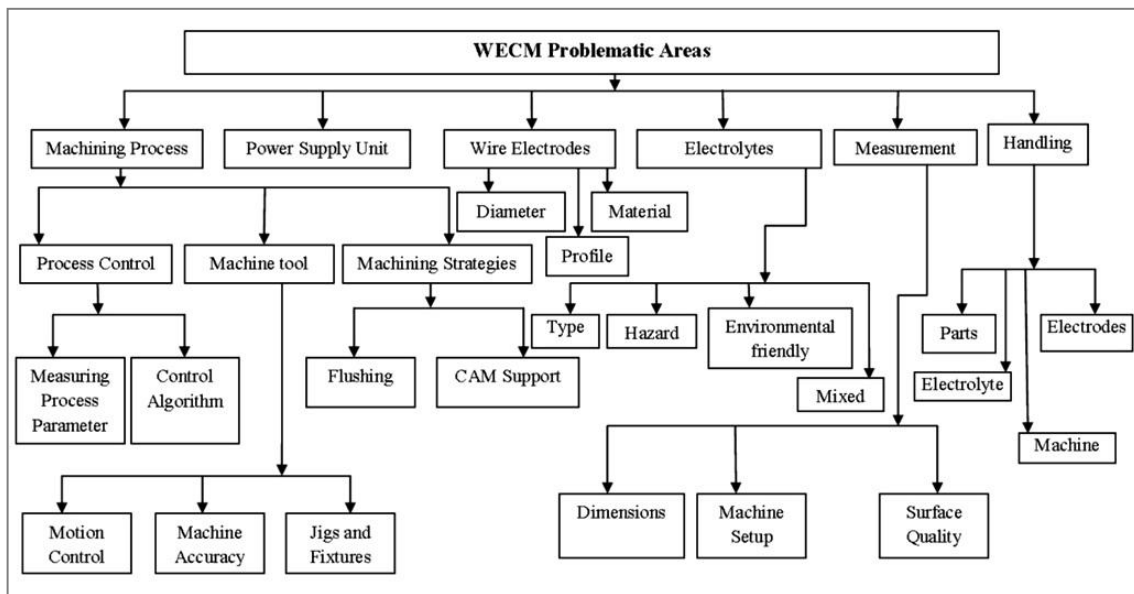
Figure1.11 WECM problematic areas for research

More focus has been given to fabricate microfeatures of nitinol shape memory alloy and investigations has been planned for performance enhancement of machining during micromachining of shape memory alloys using different developed novel methods. A thorough investigation of the available literature on WECM and nitinol shape memory alloy reveals that, in addition to the various research work covered in the previous section, the attempts can be broadly classified into five categories: where emphasis has been placed on the fundamentals and process improvement, mathematical modelling and simulations, influence of process parameters and other factors, enhancement of mass transport, machining accuracy and efficiency and investigations on nitinol shape memory alloy etc. The various types of work materials are taken into account and finally product fabrications. However, there is still more research work has to be done in this area for improvement in machining performance. On the other hand, product fabrication for advanced industrial or biomedical applications is the final step that can certainly justify

the capability but is more practical if more investigations are carried out for machining difficult to cut nitinol shape memory alloy without altering its properties and these approaches have been sufficiently completed which are able to stand alone with better control and stability. In general terms, it is possible to think about scaling up products from lab scale to industry scale right away by enhancing the wire electrochemical machining performance during micromachining of nitinol shape memory alloy.

Similar to the research endeavours described in the previous section, developing a good WECM setup locally should come first to fulfil all the requirements of nitinol shape memory alloy machining. To validate the necessity for specialized flushing procedures, pilot trials experiments are required to match the system's fundamental operating capabilities and stability in machining difficult to cut shape memory alloy. The use of different nozzle jet systems with varying standoff distances plays major roles in efficient flushing while machining difficult to cut shape memory alloy materials for performance enhancement during the process. To further fine-tune, gradual development is required, which can also go along with achieving distinct and various goals according to the objectives and priority. Then, taking into account the basic and fundamental parametric aspects of micromachining by WECM, mathematical model is developed that still fall short in the prescribed attempts, such as physics based on theoretical and mathematical modelling which can predict as well as provide a direct relationship with input parameters to output criteria. In contrast, one of the most important factors that addresses validity and determines whether a system can be scaled up to commercial size is reduction of microsparks and stray current effect during machining which affects the surface quality and accuracy of fabricated microfeatures. However, there are negligible attempts where the influence of different process parameters on reduction of overcut, micro sparks and stray current effects on surface of workpiece has been investigated. The novel insulation methods can be applied to reduce overcut and stray current effects during machining which has a wide scope for investigation for performance enhancement of machining process. The influence of different parameters using different wire insulation methods suggest towards a potential study need. Additionally, a mathematical model for vibration assisted axial nozzle jet machining under the impact of a number of key process parameters can be created. As a start-up, step is crucial for reaffirming the research facts and for determining how well the developed system aligns and behaves in this direction. It also allows researchers to gain firsthand research experience, understand the technical aspects of the system, and evaluate the system's status, condition, applicability, and

potential. Since axial flushing is simpler and more efficient when it comes to the fabrication of micro features, especially those with lower aspect ratios, conducting research in this direction may prove worthwhile in investigating how the new vibration assisted axial nozzle jet flushing approach actually stands out under various flushing parameter settings for machining of nitinol shape memory alloy and enhancing the performance of machining.

Till the date, no work was found in literature for understanding the anodic dissolution mechanisms for unique nitinol shape memory alloy material during WECM. As nitinol is used for number of advanced aerospace, automobile and biomedical applications due to its strength and magical super elastic properties, hence, in this research work, experimental investigation for performance enhancement of WECM during micromachining of nitinol shape memory alloy by developing novel experimental setups and planning with diversified advanced industrial applications in the fabrication of micro features is proposed. In these lines, this research tries to investigate the process of Wire Electrochemical Machining (WECM) for performance enhancement during micromachining of shape memory alloy.

In literature most of the work of WECM was carried out with common electrolytes like H_2SO_4, HCL and $NaNO_3$ as an electrolyte. Some of researchers used NaCl and Gelatinous Electrolyte. Diversified efforts are also needed to find alternate and novel eco-friendly electrolytes. Study on Influence of ozonated mixed neutral and acidic electrolytes in aqueous solutions and their different concentration with effect of addition of complexing agents i.e. EDTA, citric acid etc with vibration assisted axial nozzle jet flow for enhancement of mass transport and surface quality and effect of wire insulations and coating on reduction in stray current effect and overcut are still required to be done for further investigation. Experiments are to be conducted to understand the influence of the various WECM parameters during micromachining of nitinol shape memory alloy. This research mainly concentrates in finding optimum WECM process parameters for performance enhancement of WECM during micromachining of shape memory alloy by using in-house developed novel experimental setup. Lastly, as always, different types of microfeatures can also be generated to strictly affirm the system capability.

1.6 Objectives of the present research

According to the aforementioned endeavours, it can be said that numerous attempts have been made in this research work to close various gaps in our current understanding of the process and to offer an appropriate platform for this lab size procedure. Most of the work

in WECM was carried on mild steel, stainless steel, tungsten, copper, inconel718, cobalt alloy, nickel alloy, aluminium alloy, magnesium alloys, and titanium alloys and influence of various process parameters are studied by previous researchers but still any work is not conducted on shape memory alloy during wire electrochemical machining.

Apart from that, each alloy requires different process conditions in order to achieve desired results. Therefore, it is necessary to understand the process parameters that will allow for desired results in machining of nitinol which comes under the widely used shape memory alloy and has tremendous advanced applications in various industrial and biomedical fields. It is evident from a review of the literature that it still face difficulties in commercialising WECM. It is quite challenging to manage the machining process and the quality of the machining is not always good for the creation of small components. Investigations regarding the influence of process parameters on output criteria during machining of nitinol shape memory alloy for re-establishing the facts and establishing the competency of setup are focused on indigenous development of proper setup, mathematical modelling, use of different mixed ozonated neutral and acidic electrolytes for suitability of nitinol machining simulations, and experimental validation, application and influence of newly developed flushing approach, enhancing the feed rate and influence of process parameters on maximum achievable feed rate on manufactured micro features. As a matter of time, there is need to broadening of existing material processing window to understand dissolution mechanisms of nitinol shape memory alloy for performance enhancement of wire electrochemical machining by developing novel experimental setups and planning, proper setting of control parameters, and achieving different objectives as follows:

(i)   To develop in-house WECM setup utilizing different procured, customized and in house fabricated components and subsystems for details experimental investigation during micromachining of stainless steel and shape memory alloy (SMA).

(ii)   To develop vibration assisted axial nozzle jet flow system and to investigate the effect of different diameter nozzles at varying stand-off distances and compare vibration assisted axial nozzle jet flow system with other existing flow systems for performance enhancement of WECM during machining of nitinol SMA.

(iii)   To develop wire insulation methods and investigate the effect of wire coating and insulation on machining accuracy, surface quality in the region near machined zone using developed WECM setup for experiments with controlled process parameters for reduction of micros-parks, stray current and overcut etc.

(iv)   To investigate the use of different types of electrolytes e.g. neutral, acidic as well as mixed and ozonated mixed electrolyte with suitable eco-friendly complexing agents (ex. Citric acid, EDTA) for improvement in surface quality and homogeneity during micromachining of nitinol shape memory alloy during WECM.

(v)   To investigate the effect of different parameters and characterization of nitinol shape memory alloy using developed experimental setup with various processing conditions as well as to explore influence of energy input process parameters on maximum achievable wire feed rate for overall performance enhancement of WECM.

As mentioned earlier, the developed vibration-assisted axial nozzle jet flow wire electrochemical machining experimental setup will play a helpful role to justify the uniqueness and originality of the present research work by incorporating various novel methodologies i.e. insulations techniques, mixed and ozonated electrolytes and exploring the possibilities of micromachining of various microfeatures on stainless steel SS304 and difficult to cut nitinol SMA material. The investigation of different influencing parameters during WECM of nitinol SMA will help to understand the dissolution behaviour in different electrolytes. The analysis of fabricated microfeatures of nitinol SMA utilizing vibration assisted axial nozzle jet flushing based on critical examination of various SEM micrographs to determine the influence of significant WECM parameters on machining accuracy and surface roughness during micromachining may be another significant outcome. The extensive research work will help to move towards closing the existing research and knowledge gap by contribution of a cost effective machining system for fabricating intricate microfeatures on difficult to machine nitinol SMA materials for advanced engineering applications and by providing a appropriate platform for commercialization of this emerging anodic dissolution process at the end.

Chapter2: DEVELOPMENT OF WECM EXPERIMENTAL SET UP

2.1 Introduction

WECM configurations as well as in-house developed and built subsystems have been described here. Multiple components of the various specified subsystems have been employed because this is a step-by-step development that corresponds to specific development stages. The details in the development stages with utilization of various components are described in the following sections. The subsystems include ones that have been purchased, the specification, range, and capabilities of which have been chosen based on the requirement of setup configurations, machining circumstances and conditions, and needs; other subsystems have been developed and built locally as well as specifically tailored internally to meet the needs of the experiments. The main WECM experimental setup has undergone numerous modifications and upgrades based on research objectives and to enable improvements in experimental settings for the performance enhancement of WECM process. These have been covered in details. A schematic representation of the basic developed WECM setup is shown in **figure 2.1.**
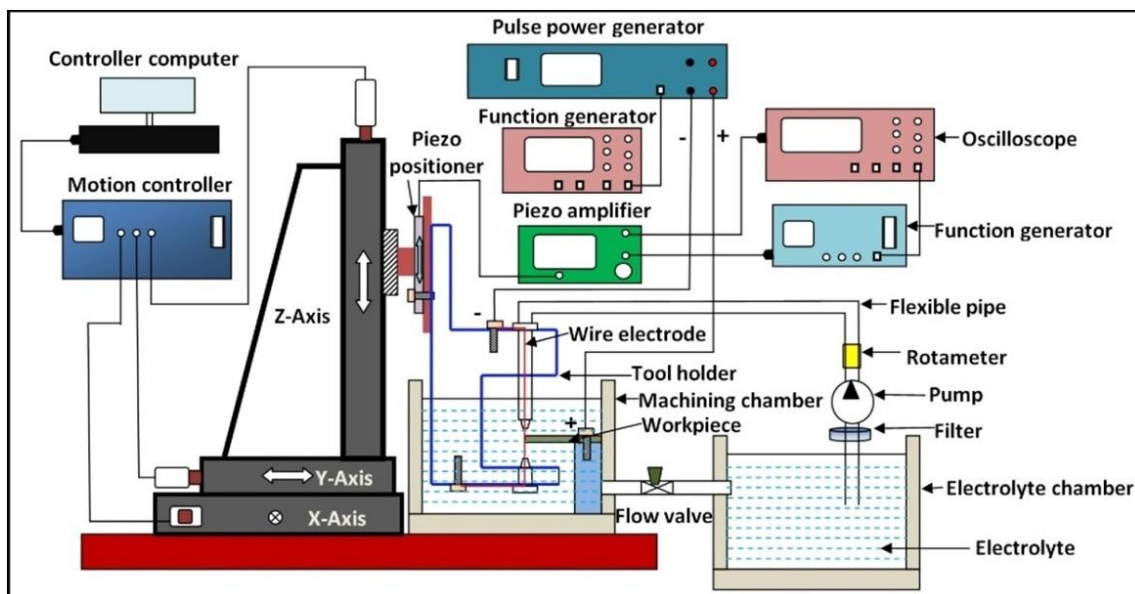
Figure 2.1 Schematic diagram of developed WECM setup.

The subsystem consists of requirement of basic components i.e. mechanical machining unit, power supply unit, motion control unit, machining chamber, ozone generator unit and accessory unit. Electrolyte flow system has three indigenously developed arrangements of systems i.e. axial flow system, vibration system and nozzle jet system. And finally wire electrode insulators have been used. The details of subsystems and components used for the development of experimental setup have been discussed as

follows:

2.2 Basic components of WECM System

The WECM setup has been carefully designed and developed to meet the research goals and function of wire electrochemical machining. Each component of the machining setup has been selected and created to prevent any issues during the machining process. Novel methods or techniques have also been incorporated into the development of the machining subsystems and components. The details of basic components used for the development of the WECM setup are discussed as follows:

2.2.1 Mechanical Machining Unit

One of the most complex and intricate components of the WECM setup is the XYZ micro-positioning stage. For machining operations, APN100PP MTN movement stage made by Newport Corporation has been used as shown in **figure2.2.**

Cz,	Normal centered load capacity	1000 N
+Cx,	Direct axial load capacity	200 N
-Cx,	Inverse axial load capacity	21 N
Kαx,	Compliance in roll	4.0 μrad/Nm
Kαy,	Compliance in pitch	6.0 μrad/Nm
Kαz,	Compliance in yaw	5.0 μrad/Nm
Q,	Off-center load (N)	Q ≤Cz ÷ (1 + D/100)
	Where D = Cantilever distance (mm)	
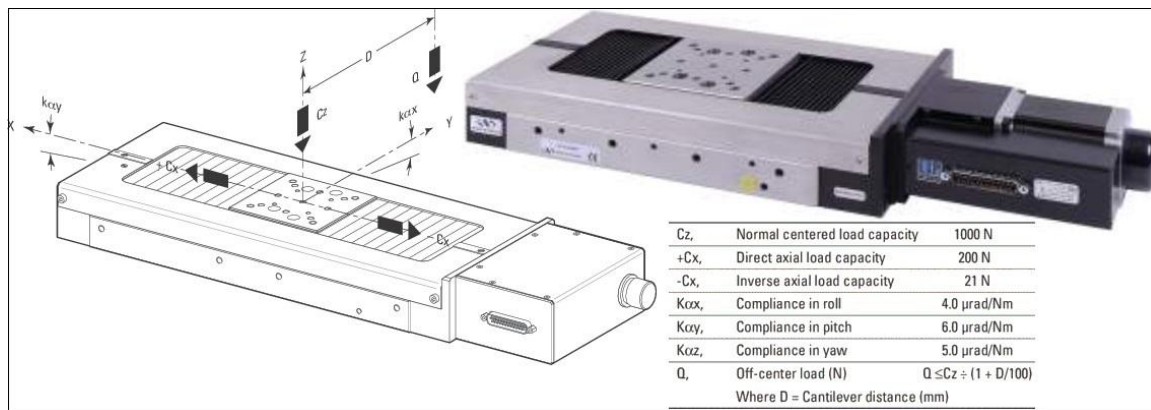
Figure 2.2 Schematic and actual MTN movement stage

This stage has 0.1 μm resolution and 100 mm travel in each axis. The three axes of the stage are precisely driven by three stepper motors. Three long linear steps make up the XYZ movement stage. These stepper-driven stages depict the X, Y, and Z principal Cartesian axis directions. It aids in holding the vertically mounted wire on Z axis and allowing it to move in all three directions at once, which is necessary for tool positioning, machining processes, and loading and unloading the wire holding and tensioning block. XYZ stage has been used during machining in the form of knee and a column type structure. The stages are stacked on top of one another in this design, providing room and flexibility for machining chambers with bigger surfaces. All three stages are movable, and any one of them can be used, depending on the situation. However, because the weight of the other stages is supported on it, all three stages have a rather high horizontal or normal load carrying capability. The stage has 0.1μm minimum incremental motion and resolution for each stage. To hold the wire mounting, a section of the flushing unit,

and to provide a specific off-center distance for setting the wire electrode on holding and tensioning block suitably within the machining chamber, appropriate fixtures that were made in-house are also attached with Z-stages. This whole mechanical machining unit of XYZ stage has been mounted on the worktable essentially which serves as a base and storage area where other components are also mounted i.e. machining chamber regardless of the stage on which it is loaded, PZT vibration unit, and other necessary equipment. The robust frame that supports the worktable ensures the essential structural stability while it is in use. The worktable holding the stages with column and knee type construction and the machining chamber has been placed on a breadboard made by Scientific Solution Ltd, New Delhi, with a grid of M6 holes for cushioning. Additionally, the breadboard has been appropriately leveled with pads.

2.2.2 Motion control Units

The motion control unit has been used for controlling the movement of all the three XYZ mechanical movement stage in a very precise manner to maintain the accuracy and resolution as specified by the manufacturer. The XYZ mechanical positioning stage motion control unit is shown in **figure2.3.**
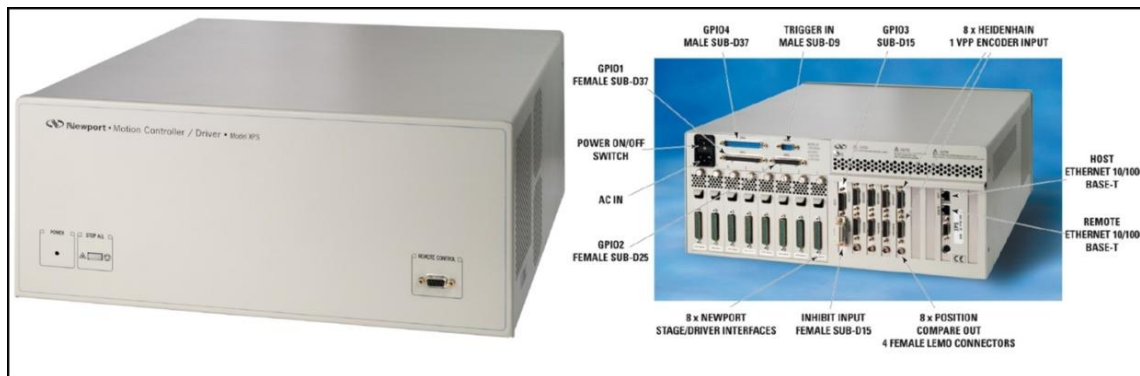
Figure 2.3 XYZ stage motion control unit

The motion controller is connected to the appropriate computer through an RJ45 Ethernet connector to execute the desired outcomes. The controller supports at least 4 axis movements, various stage types, numerous functions, languages, TCL-generated scripts, execution of simple and complex linear and nonlinear trajectories, linear or circular interpolations, spline execution, master-slave operations, and CAD interface. Additionally, these levels have a feedback mechanism that shows the corresponding positions in all three dimensions online. All the commands to the motion controller has to be given from the XPS –Q8 motion controller software from the computer connected to the controller as shown in **figure 2.4.** The various inputs can be directly given in the

software in digital form which is further converted into analog signal in motion controller through digital to analog convertor.
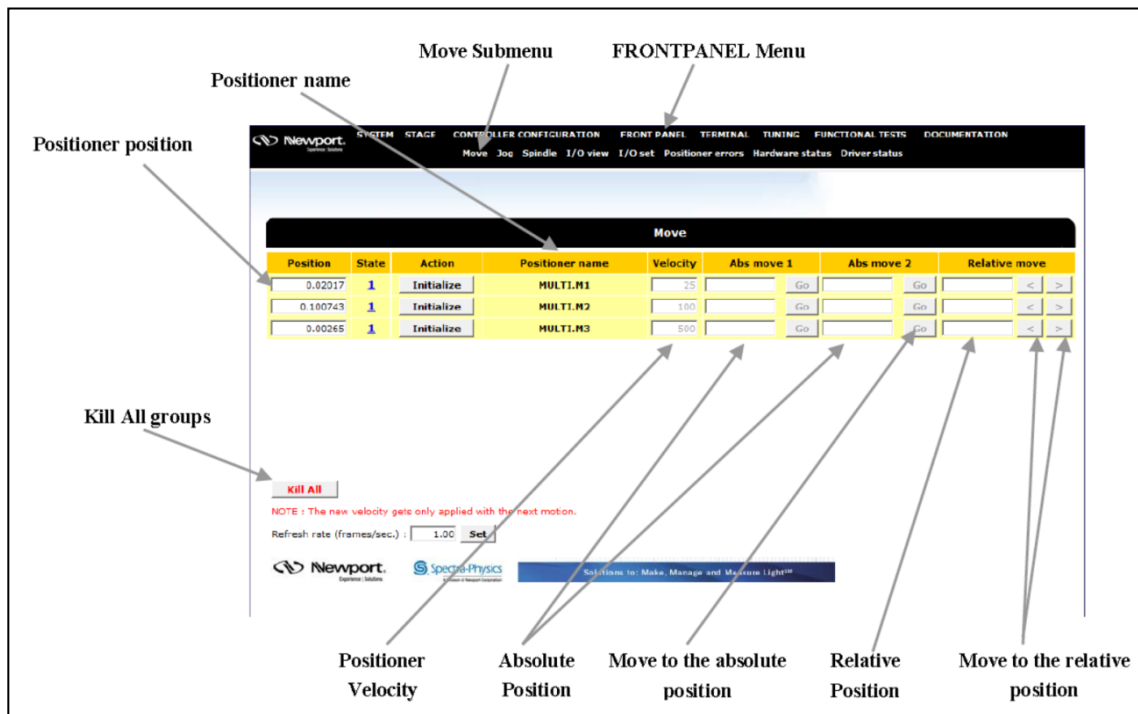
Figure 2.4 XYZ stage control unit software
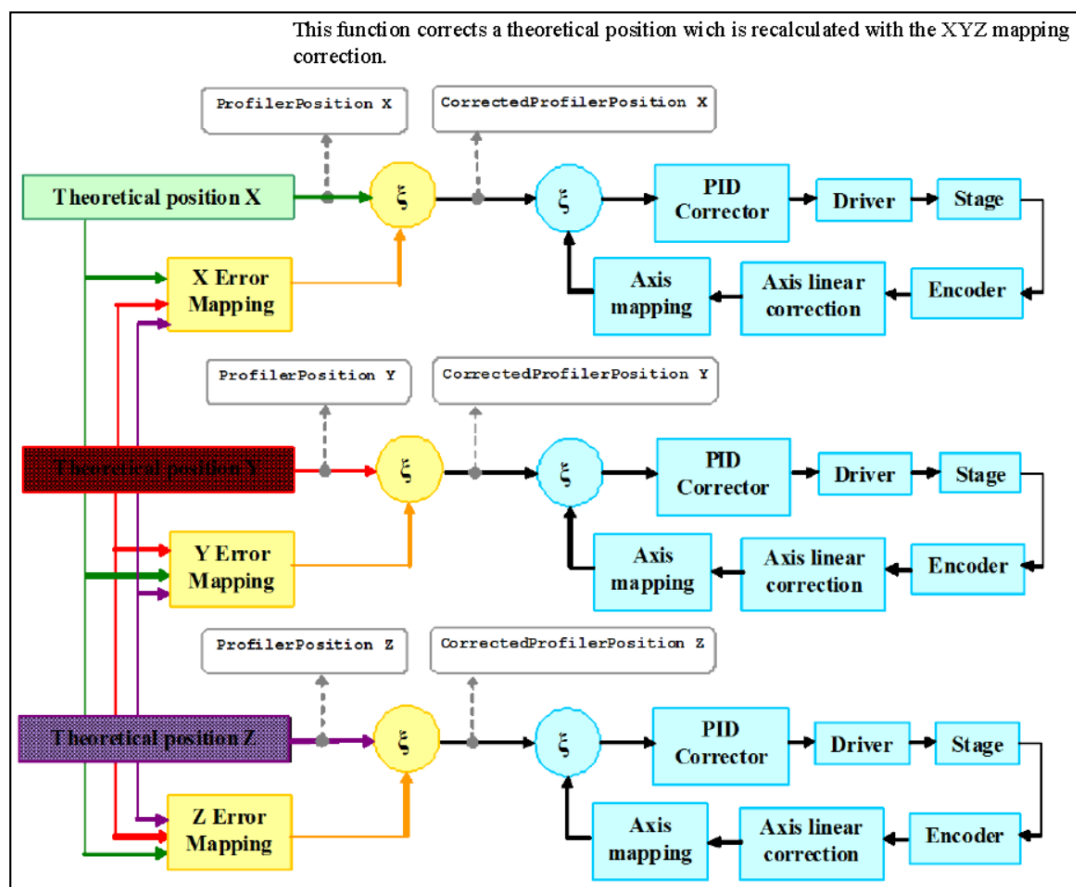
Figure 2.5 XYZ axis mapping

The motion control software displays positioner position, position name, move submenu in the frontal panel where positioned velocity can be given for giving specific feed rate to the wire electrode and stages can be moved absolute and relative mode. The jog mode can be used for continuous motion of the single stage till the limits. To drive these XYZ stages, various control inputs are provided. The precise movement of the stages can be confirmed through XYZ axis mapping through feedback control system of the controller as shown in **figure 2.5.** This function corrects a theoretical position which is recalculated with the XYZ mapping correction for any errors in the motion by PID corrector and encoders through closed loop feedback control system. To obtain a 3D curved machined product, we can move the three axes sequentially, two axes at a time, the third axis, and also three axes at a time. Programming is used to create profiles or to perform many repetitive tasks.

2.2.3 Power supply unit

The WECM configuration also includes a power supply unit, which is crucial. During experiments, it provides the necessary DC voltage pulses with the correct values, duty ratios, and frequencies. According to development conditions that can only be operated, the Matsusada Precision Inc, Japan, POA75-4 ultra high speed bi-polar power supply has been used for distributing appropriate current density through wire electrode, as well as an oscilloscope and function generators for monitoring different pulse parameters, has been used.
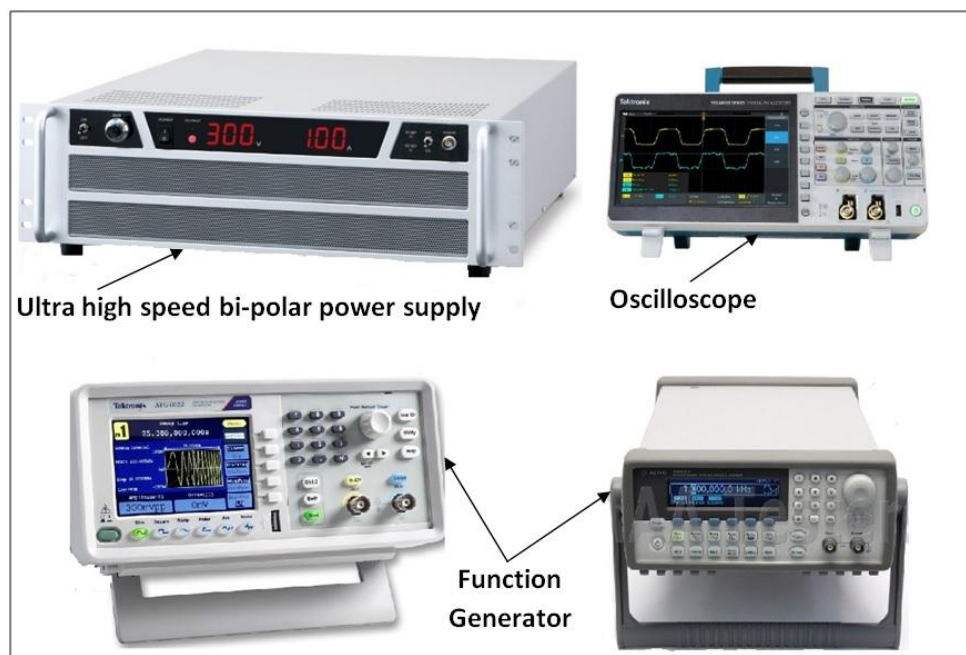
Figure 2.6 Power supply unit

The complete power supply unit including function generators and oscilloscope is shown in **figure 2.6.** The POA75-4 ultra high speed bi-polar power supply has a rated maximum current of 4A, a maximum output voltage of 75V, and a frequency of 1MHz. Since POA 75-4 lacks an internal function generator, external function generators have been employed to supply the required voltage pulses, with POA serving as voltage amplifier. During operations, the display panel on the POA displays the machining voltage and current to two decimal places. As it runs on 110V main voltages, a step down transformer has been fitted with POA. In order to start the pulse with increased voltage, POA also provides control via a front panel bias switch to add normal DC voltage amplitude in both positive and negative directions from mean value. This function is extra since it is simple to accomplish with an external function generator. The function wave generator supplies the input power. For the entire fabrication and machining process, an Agilent 33250A and Tektronix AFG1022 function waveform generators were utilized. This waveform function generators can produce a variety of waveforms from a 220V power source, including sine, square, pulse, ramp, and others. Pulse wave was chosen for the machining and fabrication processes. The Agilent 33250A function waveform generator offered pulses with a frequency of 5MHz and a duration of 400 ns and voltage amplification in the ratio of 1:25 with the connected power supply. Additional pulse width options from this function generator range from 8ns to 1999.9s. It has a peak to peak voltage of 6 volts with a maximum of 5 volts in the positive direction and 1V in the negative direction, with a maximum pulse frequency of 80 MHz. The intricacy that results from the potential for reverse etching of wire prevents the direction in negative from being used, so effort has instead been paid on enhancing flushing abilities. Tektronix AFG1022 has a peak to peak voltage of 10 volts with a maximum of 5 volts in the positive direction and 5V in the negative direction, with a maximum pulse frequency of 25 MHz and voltage amplification ratio of 1:10 to the power supply voltage input. An Agilent 33250A and Tektronix AFG1022 function waveform generator control the complete machining process and used for different energy parameter settings i.e. pulse voltage, pulse frequency, duty ratio and pulse width etc and helps to investigate the effect of these parameters during wire electrochemical machining.

Also, the digital storage oscilloscopes has been used for data acquisition tasks in order to monitor and record input power, waveform nature, continuous notation of machining current, and noting down various other parameters during the execution of WECM process. During micromachining, a digital storage oscilloscope is used to view and track

the pulse waveform. The designed arrangement makes use of the Tektronix TBS 2000B model, which has a bandwidth of 100 MHz and a sampling rate of 1GS/s and 20M record length on all channels. During machining, this oscilloscope shows an online image of the given pulse in addition to detailed information. The nature of the supplied pulse was observed during initial IEG setting, as well as during machining to determine the status of the operation. A digital storage oscilloscope was also used to detect the occurrence of any short circuits between electrodes. The wire feed rate and pulse power supply is immediately shut off upon detection of a short circuit, and the wire electrode is then retracted back a few microns to clear the IEG before machining can resume with the necessary parameter settings. The desktop computer can be connected to a digital storage oscilloscope as well for online monitoring, and pulse parameters can be directly stored on external storage devices for further analysis.

2.2.4 Machining chamber

The 3D schematic representation of the machining chamber is shown in **Figure2.7**. It is kept on the worktable, or in the X-Y plane, and contains the required electrolyte for the machining. The M6 threaded breadboard, which is attached to the worktable with screws and nuts, is used to anchor the chamber and limit movement.
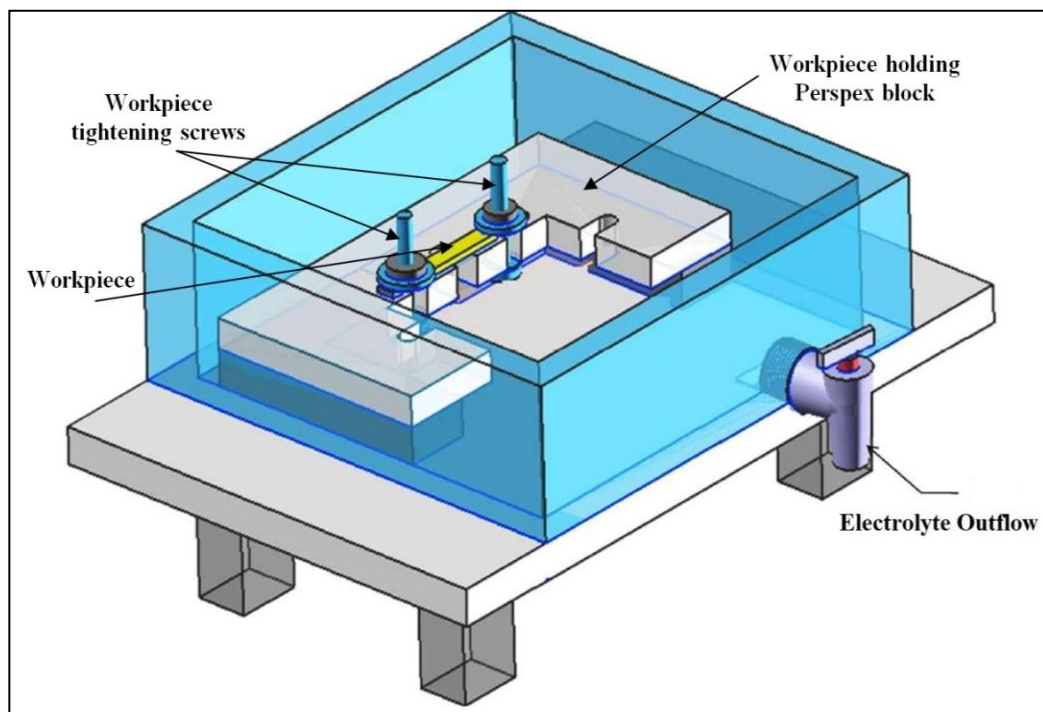
Figure 2.7 3D schematic of machining chamber

A non-conductive, non-corrosive perplex acrylic sheet is used to construct the machining chamber. Since the acrylic layer is transparent, we can see through it, making monitoring

much simpler. The necessary electrolyte solution is kept in the machining chamber, which also offers work specimen fixation and clamping. The work holding system has been made adjustable as well, making it simple to fit workpieces of various sizes and thicknesses in a variety of settings. After fabrication, the machining chamber is made leak-proof to the required dimensions and working conditions. Additionally, an outlet drain plug is fixed to the chamber's base to remove the amount of electrolyte after machining and to regulate the electrolyte level in a variety of situations where the electrolyte is flowing or standing still. There are two unique setups available in the machining chamber. One is used to steadily hold the workpiece during machining. The other is utilized to hold a workpiece sheet that will be used in fabrication.

2.2.5. Ozone generator unit

Ozone is a strong oxidant with very short life and can be easily decomposed in to secondary oxidants. Its decomposition in the aqueous solution can be affected by PH value, temperature and chemical composition presents in the electrolyte. Ozone has been generated in the machining chamber where it can be immediately consumed due to its very short life. The ozone generator used in the research work during wire electrochemical machining of nitinol shape memory alloy is shown in **figure.2.8** with detailed experimentations are included in chapter5.

Figure 2.8 Ozone generator unit

This ozone generator has an ozone output of 250mg/h. This ozone generator works on the principle of corona discharge because of its cost effective production and greater

durability. The high voltage power supply is utilized to obtain an electric discharge across the dielectric and air gap between the electrodes. The diffusion of dielectric across large contact area of electrode occurs due to dielectric and the high voltage breaks O_2 molecules and form three atoms of oxygen molecules which converts into ozone O_3. This generated ozone in the machining chamber helps to remove the sludge and dissolved products on the surface of the materials and clean surface will be always available for uniform anodic dissolution during WECM and can improves accuracy and surface quality.

2.2.6 Accessory unit

Apart from the various components required for development of WECM setup, some accessory units also required that include Dinolite 40X digital microscope for online monitoring of machining conditions. Agilent U1252A multimeter has been used for more precise monitoring of machining current. A multimeter needs to be linked in series in order to measure the current flowing through the circuit while it is being machined. It has a protective device against short circuit and overload circumstances in addition to a delicate protection circuit for the machining system. The use of multimeter has later been avoided to keep connection issues in check. Instead of it, in-built display panel on POA has been used. Also, Leica DM-2500 and Olympus STM6 measuring microscope for carrying out post experimental offline measurements, Taylor Hobson made CCI (Coherent Correlation Interferometer) profilometer for carrying out roughness and micro-depth measurements etc have been used. The magnifying glass is used for visually understanding the live micromachining process and fabricated microfeatures. Metrohm Autolab electrochemical workstation was used to conduct electrochemical analyses i.e. potentiodynamic (PDP) tests and electrochemical impedance spectroscopy (EIS), FESEM machine used for EDS and SEM images and XRD machine was used for XRD analysis.

2.3 Electrolyte flow system

According to the stage of development and needs outlined in the planned objectives and to fulfill the requirement for machining difficult to nitinol shape memory alloy, three flushing systems have either been utilized alone or in combination to improve mass transfer by rapidly regenerating fresh electrolyte. The axial flow system, vibration system and nozzle jet flow system are three different approaches for cleaning up machining debris, sludge and dissolved products produced during wire electrochemical machining. The description of these three different kinds of flow systems are as follows:

2.3.1 Axial flow system

The components of the axial flushing unit include a submerged pump, an electrolyte supply chamber, a rotameter, flexible hose with a nozzle, several valves, etc. In contrast to cumbersome gear pumps, the submerged pumps employed in this work are convenient, small, and handy. They also offer flexibility in stepwise building with extremely low to higher power levels. These pumps' compact design and ability to submerge enables for simple tabletop implementation, flexible relocation, and a significant decrease in vibrations, which could otherwise negatively affect the stability of the remaining subsystem assembly and machining operations. Additionally, the pumps are effectively furnished with rubber dampers that further obliterate minute vibrational impacts. These pumps have longer lifecycles without the need for frequent replacement because they are completely compatible with corrosion conditions and media. These pumps also have filters built in that prevent larger external contaminants from entering the flow system. It is also possible to utilize more filters. To prevent any reduction in electrolyte pressure, additional ultrafine filters were afterwards avoided. The electrolyte solution that needs to be passed via the submerged pump is kept in the electrolyte supply chamber together with other flow components like hose pipe work, a bypass valve, and a rotameter that are positioned over stranding. In order to drain off electrolyte and manage the amount of the solution, a plug is additionally attached to the bottom of the electrolyte chamber. The electrolyte chamber now has additional bypass control valve so that any extra electrolyte from the machining chamber can simply flow and recycle. The Perspex lids on top of the electrolyte chamber have accurate cut-outs and apertures, and they also prevent electrolyte spillage when the pump is operating. The rotameter, which was incorporated into the most recent configuration, was created and calibrated in India by Asiatic Engineers. It monitors the volume flow rate of electrolyte in either litres per minute (lpm) or litres per hour (lph). The flow control valve on the rotameter works in conjunction with the bypass valve to change the flow rate from zero to maximum. In order to make fractional measurements simple, the range of scale on the rotameter has been carefully tailored and chosen while considering the maximum volume of electrolyte flow rate at a time. Additionally, this reduces torque production and prevents the needless extension of the rotameter. The density and corrosiveness of the electrolyte medium were taken into consideration when designing the float for the rotameter. Through a threaded fastening, the flexible tubing connects the rotameter outlet to the nozzle. Furthermore, this attachment makes sure that vibrations are kept to a minimum and enables simple

positioning across the breadboard in any horizontal orientation. The internally manufactured nozzle has a projecting component on the front end. This projecting component is flexible, allowing for secure mounting in the Z stage to further reduce potential vibration and facilitate simple flow placement. To further reduce the diameter of the flow stream, a secondary nozzle with a lower exit diameter can also be added to the protruding component indicated. The secondary nozzle, however, was later removed due to its insignificant impacts under developed setup and machining circumstances, loss of flow pressure, and challenges in maintaining a reduced diameter flow stream surrounding wire.
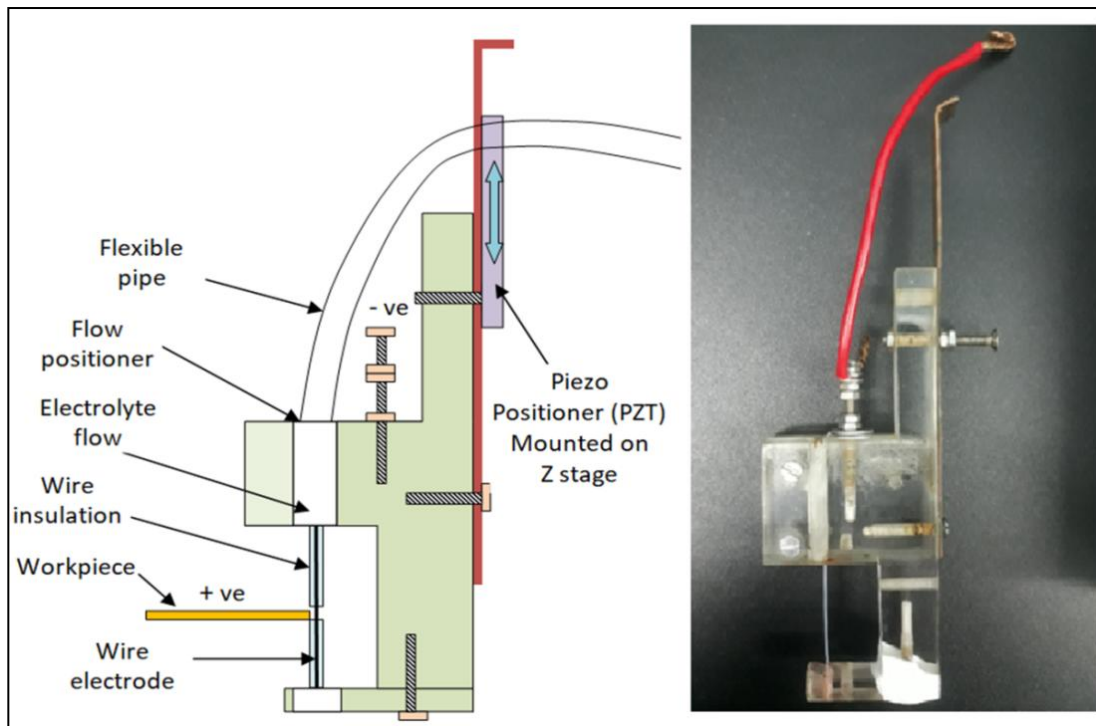
Figure 2.9 Schematic and photographic view of wire holder for axial flow system

Another important and key element of the WECM setup is the locally produced wire holding and tensioning block for axial flow system. The holding device's schematic is shown in **figure 2.9.** With the help of a screw, nut, and bolts, a wire of the desired diameter is held firmly and vertically in the block indicated. Wire is strained, and the tension can be manually controlled, to make it straight, stretched, and stable during machining. This block is also made of Perspex, which adds lightness, non-corrosiveness, and enhanced machinability, making it a flexible and universal component that matches with various setup configurations like stages and machining chambers, improvements, requirements, and changes in machining conditions occurring during various development stages. The block is mounted on the aforementioned fixture's Z axis, but it

can also be mounted in accordance with various piezoelectric transducer (PZT) variations and other flushing devices as needed. When axial flow system is used, the block additionally provides provisions for quickly changing the flow position in all three directions. Additionally, flushing at various angles and varied nozzle diameters can both be accommodated. The block's design also accommodates varying work thickness, form, and workpiece placements, as well as varied wire span as needed. It is also possible to successfully cover the parts of the block that were submerged in electrolyte during machining and had apertures for bare wire. This will lessen the impact of stray corrosion. It is crucial to hold the wire tool in a fixture when fabricating it. It has the ability to maintain the tension on the wire that is manually applied by the operator. The holding device features a number of extensions for carrying out various tasks. Acrylic, a clear plastic-like material with great strength and stiffness, was chosen as the material to build the extensions and the holding device. Furthermore, it is robust and simple to monitor. A little extension wire has been added to the holding device to make it easier to power the electrode. This cable also assures that nothing will be disturbed when the crocodile pin holder is being attached.

2.3.2 Vibration system

The voltage amplifier system and piezoelectric transducer (PZT) actuated single axis translation stage along with digital storage oscilloscope and function generator to control and monitor the online process for any disturbance make up the complete PZT vibration system. The components in complete vibration system are shown in **figure2.10.** A separate function generator supplies the PZT's needed and controlled frequency and amplitude via a voltage amplifier module. By adjusting the corresponding voltage values from -20V to +130V, this module also enables feed movements in micro ranges. The same range is employed to produce the requisite vibration amplitudes, but only when the function generator's voltage values are changed at a ratio of 1:10. PU65HR, a single axis positioned translator were employed during the machining process. PU translators are made up of a single metallic component that also houses the flexure guiding mechanism. This design results in the PU translation stages having high robustness, negligible friction, and exceptional mechanical stability. High loads may be supported by this actuator, which also produces 40–100 micron single-axis motion. It may be installed vertically or horizontally, making it easily flexible. PU65HR, a single axis positioned translator, has been tuned for a high resonance frequency. It has a resolution of 0.13 nm and a maximum stroke of 65 µm, and it is paired with ENT 400/ENV 800 voltage

amplifier devices. Without any load, it resonates at a frequency of 1320 Hz. The PZTs and their voltage amplifier technology are both produced by the German company Piezosystem Jena GmBH. While the ENV module serves as a voltage amplifier in a single housing, the ENT module serves as the main supply.
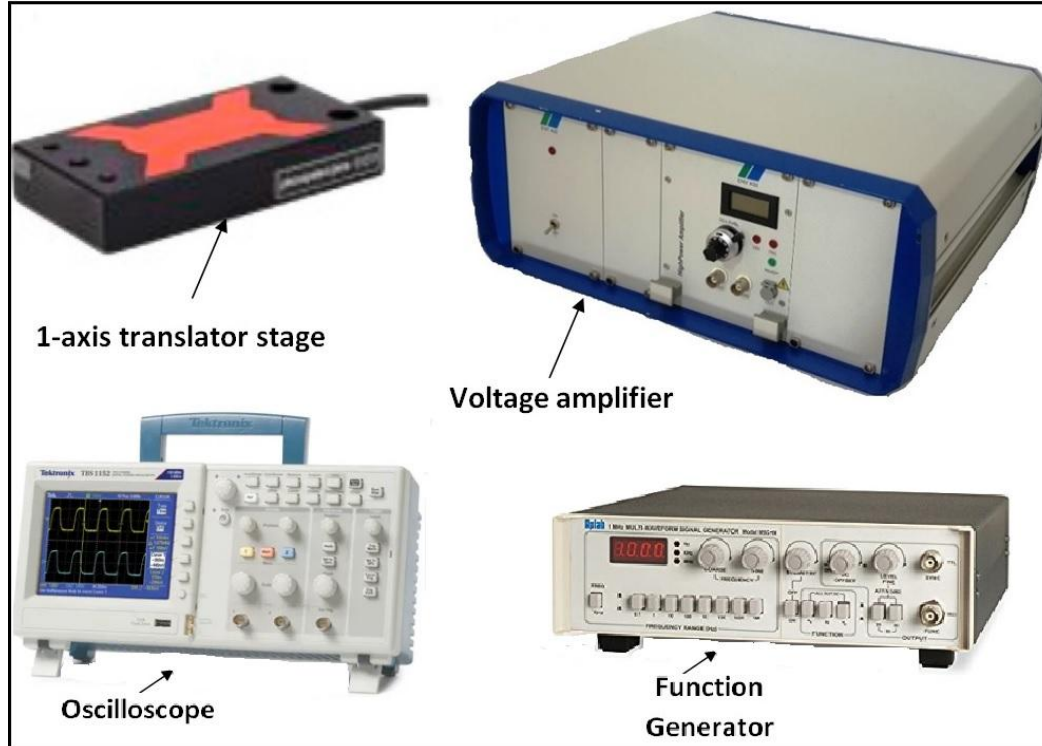
Figure 2.10 Components of vibration unit

For constant monitoring of the unit's stability under various vibration amplitudes, an overload indication is also present. Equipments like digital storage oscilloscopes Tektronix TBS 1062 model and Aplab U1252A function waveform generator have been used for data acquisition tasks in order to monitor and record input power, waveform nature, setting frequency and amplitude for the voltage amplifier of the vibration unit, and noting down various other parameters during the execution of WECM process. During micromachining, a digital storage oscilloscope is used to view and track the pulse waveform. The designed arrangement makes use of the Tektronix TBS 1062 model, which has a bandwidth of 60 MHz and a sampling rate of 1GS/s. During machining, this oscilloscope shows an online screen image of the given pulse for the frequency and amplitude settings in addition to detailed information. The nature of the supplied pulse was observed for any disturbances in the vibration unit during machining to determine the status of the operation.

2.3.3 Nozzle jet flow system

The nozzle jet flow system has been employed considering the requirement and needs as

per the outline objective to machine difficult to cut nitinol shape memory alloy with reduction in stray current and overcut of fabricated micro features and without other negative effects on properties of the material for performance enhancement of wire electrochemical machining.
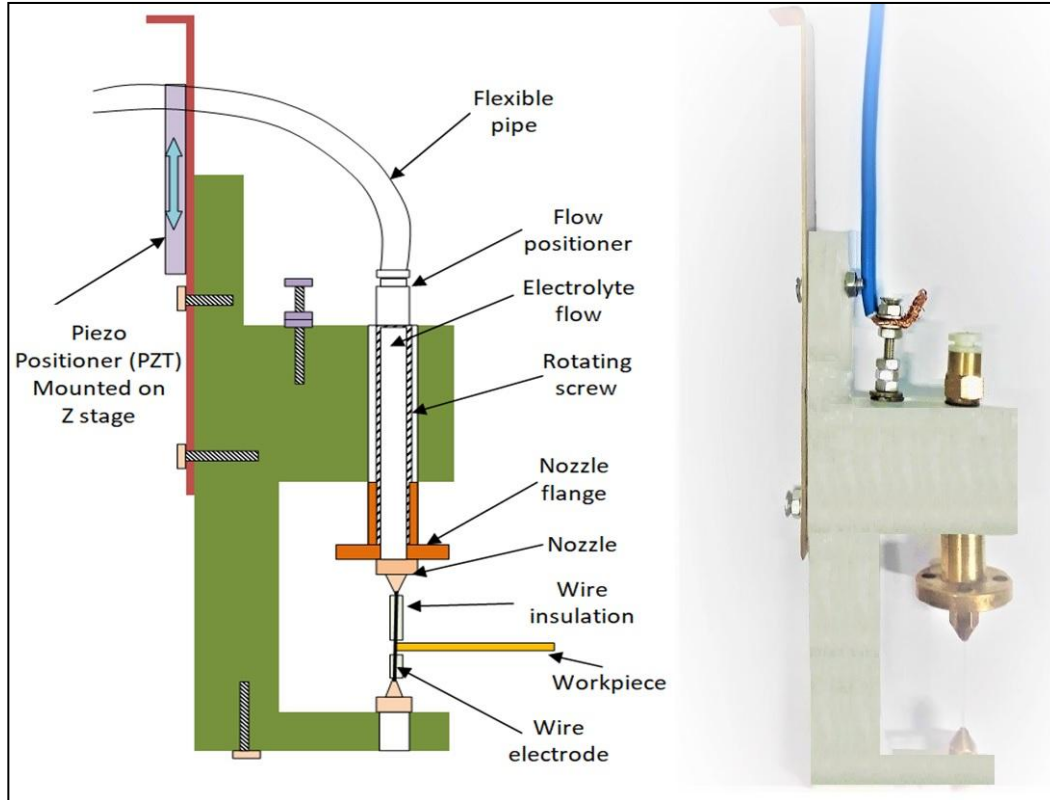
Figure 2.11 Schematic and photographic view of wire holder for nozzle jet flow system

The basic components of the nozzle jet flow system are same as axial flow system that includes a submerged pump, an electrolyte supply chamber, a rotameter, flexible hose with a nozzle, several valves, etc. The axial flow same system has been used in nozzle jet system expect development of crucial unique wire holding and tensioning block to create jet flushing of the electrolyte using different small diameter nozzles. The schematic and photographic view of wire holder for nozzle jet flow system is shown in **figure2.11.** It has provision to use nozzles of different small diameters and can vary the standoff distance of nozzle tip from the top surface of the workpiece. The distance can be varied maximum up to 30mm from the top the workpiece surface. The wire holder has a rotating screw having external threads to adjust the vertical distance. The nozzle flange made up of brass material has been connected from the outside of the rotating screw in its threaded portion to vary the distance. This nozzle flange has internal threads to connect different diameter nozzles at the bottom surface of the flange and nozzle can be tightly fasten in the flange so that there should not be any leakage of high pressure flowing jet used for

flushing and renewal of electrolyte during machining. The electrolyte flowing from the electrolyte chamber to the machining changer though flexible hose pipe which passes from the top inlet of 5mm diameter of wire holding block. This has been made leak proof using pneumatic valve so that it can withstand high electrolyte pressure and flow in the range from 5lph to 35lph using different diameter and standoff distances of nozzles. The final and most delicate nozzle characteristics to keep into mind are the internal bore diameter. The nozzle diameter from the range of 0.2mm to 1.0mm has been used in the machining process as shown in **figure2.12.** The diameter of the nozzle provides great balance between speed and accuracy of machining due to efficient nozzle jet flow system at IEG near machining zone. These nozzles are made up of brass material.

Figure 2.12 Nozzles of different diameters

The larger diameter nozzles will produce flow at more surface area and smaller diameter nozzles will produce efficient flushing effect exactly near the machining area which has to be investigated through various experimentations considering nozzle diameter and nozzle standoff distance from the top surface of the workpiece using nozzle jet flow system and included in chapter3. The insulated wire electrode inserted through the nozzle diameter and flushing in the form of electrolyte jet flow has been carried out through the diameter of the nozzles.

2.4 Wire electrode insulators

The stray current effect producing during wire electrochemical machining is a major concern and has to be eliminated. If the wire electrode is not properly insulated then it may worsen the machining conditions. Therefore, wire electrode insulators plays important role in reduction of stray current effect during machining. Further, the overcut in the fabricated microfeatures can be reduced due to controlled current density distribution at narrow inter electrode gap in the machining zone. To improve the performance of wire electrochemical machining, synthetic enamel and Poly Tetra Fluro

Ethylene (PTFE) tube insulation on the non machining surface of the wire electrode are used and presented in chapter4. The synthetic enamels have high adherence properties as it is made of different kind of oils. Synthetic material for insulating electrically conductive material has excellent electrical insulation properties and good compatibility with conductors and other materials. It has good electrochemical properties, thermal properties, mechanical properties, chemical stability, high heat and corrosion resistance. It forms an insulating protective layer with a uniform thickness to prevent stray current effect. The Plasti dip aerosol red synthetic rubber adhesive has been used as wire insulator in the preliminary experimentations. However, as the synthetic enamel coating has a tendency of insulation removal due to continuous machining, PTFE tube (100μm outer diameter and 60μm internal diameter) insulation has been used. It is a robust polymer material. The high dielectric strength and breakdown voltage of PTFE allows it to be used as standard insulation material to improve the performance of wire electrochemical machining by reducing the stray current effect and overcut to the large extent by further research and analysis.

2.5 Specifications of WECM Setup

The specification details of the developed WECM setup have been shown in **table2.1.**

Table2.1. Specifications of WECM setup

Positioning system and motion controller	MTN100PP XYZ Movement stage, 0.1µm resolution and 100mm travel length for each axis, Newport Corp. USA
Input power supply line	3-Phase, 440V AC
Pulse power generator	POA75-4 power supply, Matsusada Precision Inc, Japan voltage range of -75 to +75V, current rating of up to 4A
Piezoelectric vibration unit	ENV 800 voltage amplifier, PU65 HR Piezo 77ositioned stage of resolution – 0.13nm and maximum stroke – 65µm, Piezosystem Jena GmBH, Germany
Function generators	Agilent 33250A , U1252A function waveform generator, Tektronix AFG1022
Oscilloscopes	Tektronix's TBS1062
Tool electrode	Tungsten smooth cylindrical wire Diameter – 50 µm
Wire insulators	Synthetic enamels, Plastidip aerosol red synthetic rubber adhesive spray PTFE tube (100µm outer diameter and 60µm internal diameter)
Nozzles	Diameter of 0.2mm, 0.3mm, 0.4mm, 0.6mm, 0.8mm, 1.0mm
Electrolytes	H_2SO_4 (98% analytical grade), NaBr, $NaNO_3$, NaCl, citric acid and EDTA
Workpiece	Nitinol SMA, thickness –300 µm (Activation: 45°C +/- 10°C), 120µm (Activation: 15° +/- 10°C), 1mm (Heat treatments for 30 minutes at 550–750 °C; water quench, 80°C to 10°C for activation)) mfg. by Nexmetal Corp. Inc, USA
Ozone generator	Prestige POZ1.0, Ozone output 250 mg/h
Machining chamber	40cm x 40cm x 30cm
Flushing system	Electrolyte chamber (60cm x 60cm x 50cm), Pump
Accessory units	Dinolite 40X digital microscope, Agilent U1252A multimeter

The overall schematic with all used components is shown in **figure 2.13**. The photographic views of the developed WECM experimental setup with main machining unit and tool holding mechanism with machining chamber are shown in figure **2.14**.
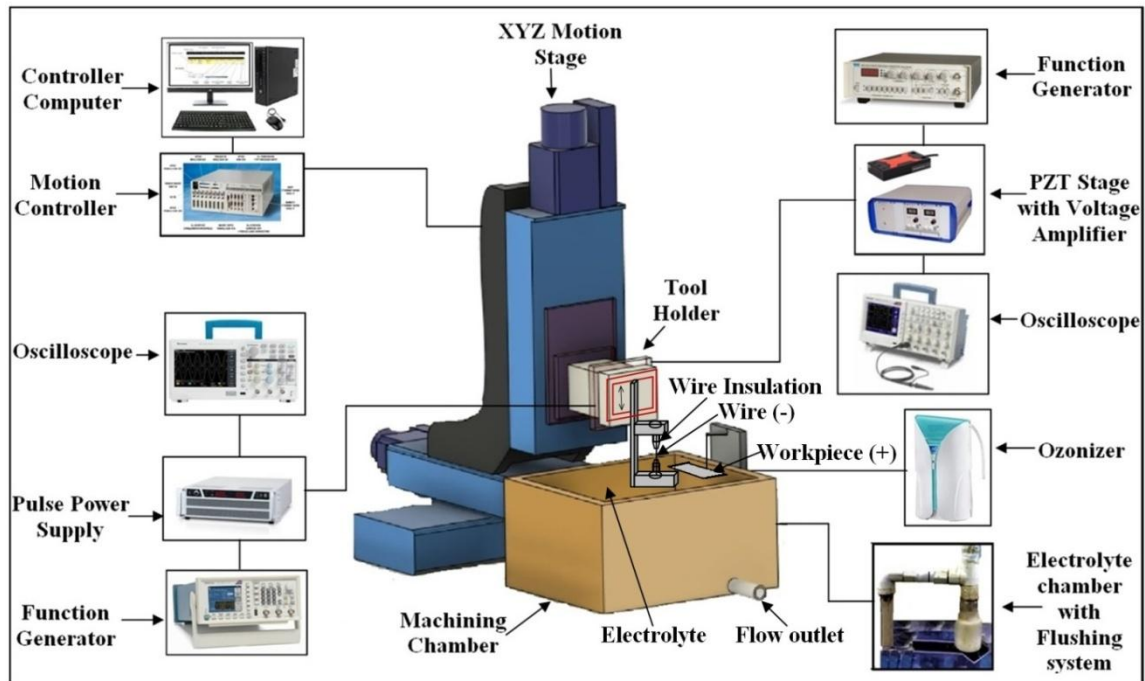
Figure 2.13 Schematics of developed WECM with all used components
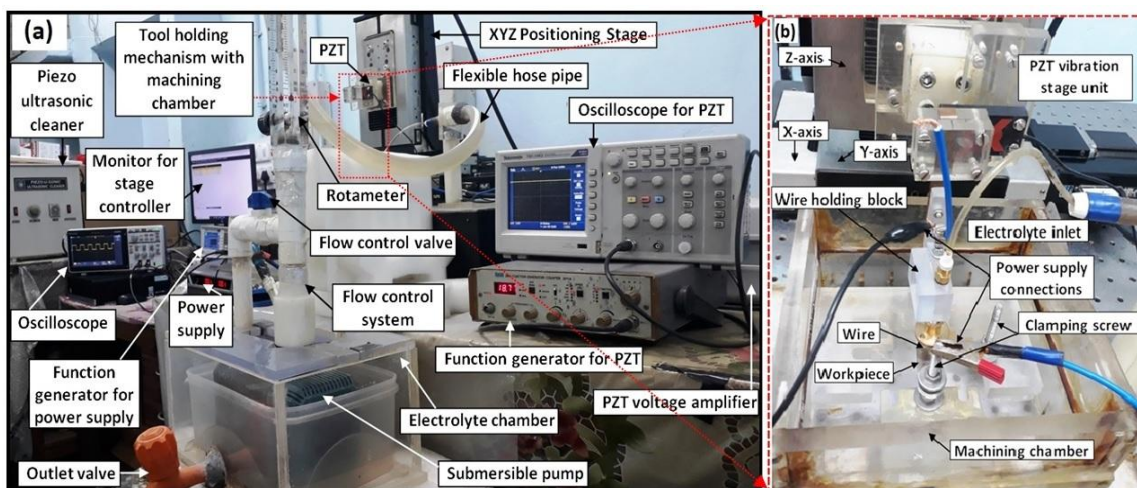
Fig.2.14 Photographic views of developed WECM experimental setup **(a)** Main machining unit **(b)** Tool holding mechanism with machining chamber

Chapter 3: INVESTIGATION ON VIBRATION ASSISTED AXIAL NOZZLE JET FLOW SYSTEM FOR PERFORMANCE ENHANCEMENT OF WECM

3.1 Introduction

The fabrication of advanced difficult-to-cut metallic complex microstructures with good surface integrity, without residual stress and metallurgical defects, has become an important issue in today's manufacturing industries. Moreover, from the various theoretical aspects on parametric analysis, efforts have been made to create mathematical model for predicting the microslit width using the principle of vibration assisted nozzle jet flow system. This chapter deals with the initiation of experiments. Hence, it firstly incorporates wire material, workpiece as well as electrolyte and the reason behind selecting those which have been maintained throughout the rest of research works. Secondly, this chapter deals with several pilot experiments, requirements, and implementation of vibration assisted nozzle jet flow system, analysis consisting of comparison of different flow systems and major process parameters in nozzle jet system, fabrication of linear micro features and concerned analysis, etc. All these have been achieved with simultaneous modifications and changes occurring in part of experimental setup as discussed earlier. Hence the detailed changes in developing setup have also been included.

Further, Investigations has been carried out to find the influences of nozzle parameters on corresponding micromachining criteria like slit width and standard deviations, three different flow systems i.e. axial flushing, axial electrolyte flow with piezoelectric transducer (PZT) and vibration assisted axial nozzle jet flushing has been used. In contrast to various separate and solo flushing strategies, combining flushing strategies may opt towards better mass transfer solution. The phenomenon consisting of fundamentals when this combined flushing strategy is employed has also been discussed. In the present work, vibration-assisted axial nozzle jet flow WECM is proposed as a newly developed method to improve mass transport efficiency by effective flushing of electrolysis by-products and renewal of fresh electrolytes. A straight narrow slit was fabricated with this process. The machining gap between the anode workpiece and cathode wire was reduced to a submicron scale that reduces slit width and machining accuracy. Further, machining can be controlled by the pulse voltage, duty ratio, and wire feed rate as the most influencing process parameters to fabricate homogeneous and

reduced micro slit width.

A comparison of the axial flow system, axial flow with PZT vibration with this newly developed flushing strategy was made. The effect of the most influencing parameters, i.e. pulse voltage, wire feed rate, and duty ratio, on the machining results of each flushing strategy being analyzed. The effect of nozzle diameter and workpiece nozzle stand-off distances on slit width machining results has also been investigated. There has been no research into the anodic dissolving mechanisms for nitinol shape memory alloy during WECM investigated in the literature to date. As a result, this study report also discusses microslit machining of nitinol memory shape alloy for improving WECM performance. The experiments have been carried out on final modified setup. The probable impact of machining setup on output or process efficiency that can still be there has also been pointed out. Lastly, to explore the experimental observations and discussions, an outcome has also been added.

3.2 Principle of vibration-assisted axial nozzle jet flow WECM

A schematic depicting the evolving mechanisms in are shown in **figure3.1 (a) and (b)** respectively.
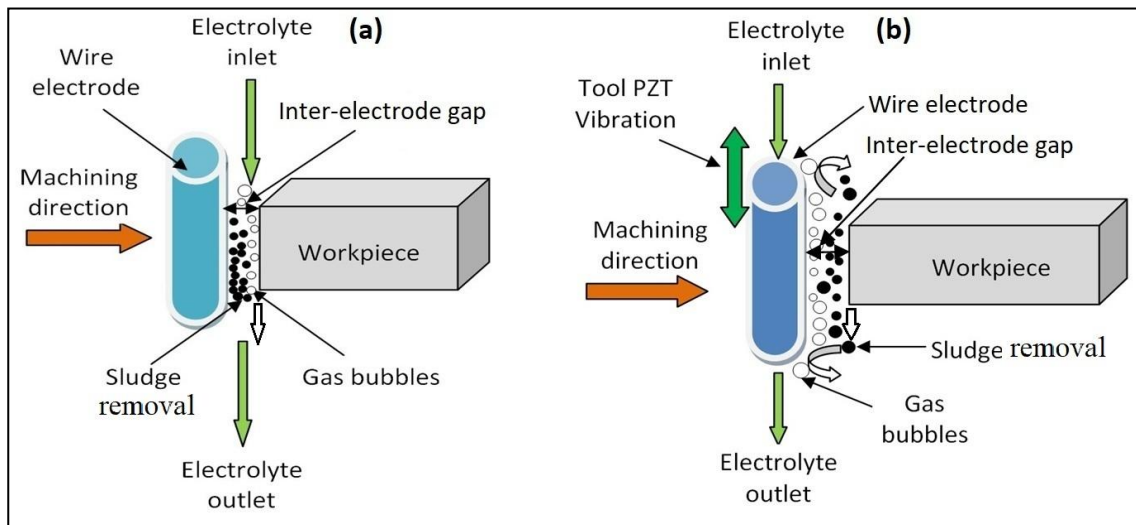
Figure 3.1 A schematic of evolving mechanism of inter-electrode gap **(a)** Axial flow system **(b)** PZT tool vibration assisted axial flow system

Figure 3.1(a) shows axial flow system which is the most basic and easy method for removing electrolysis products during machining. Moreover, as the electrode remains tense, it becomes difficult to employ a rotation of the wire. Also, the use of intermittently back wire becomes ineffective in machining high aspect ratio features. As such, in axial flushing, application of a stream of electrolyte with a forward flow pattern and a constant flow in the axial direction of the wire envelops the machining area, generates uniform

flow field, and removes the machining products by ensuring better renewal of fresh electrolyte. However, the flow entrance angle, as well as the flow rate of electrolyte, affects the machining quality, accuracy, and stability [3]. Figure 3.1(b) shows PZT tool vibration assisted axial flow system. Implementing axial vibrations on wire by piezoelectric transducer (PZT) or by the stage itself, is the easiest way of circulating electrolytic solution and removing reaction products from the IEG. The highly frequent upward and downward axial movement of the wire generates pressure wakes which in turn results in the reduction or elimination of sparking and short-circuiting and improvement of machining stability. The vibration frequency and amplitude have a great impact on machining quality due to improved flushing efficiency with timely removal of sludge and dissolved products at narrow inter electrode gap near the machining zone compared to ones without vibration assistance. However, the frequency, as well as the amplitude of the vibrations, also affects the machining quality. If the vibration amplitude and frequency remain very low, bubbles generate and accumulate in the machining gap, resulting in deformation of a micron-diameter wire with increased surface tension. On the other hand, if the vibration amplitude and frequency are higher, then radial swing of the wire may occur, which may lead to frequent short-circuiting and micro sparking. Also, implementation of very high vibration frequency can deteriorate the flushing efficiency as the rapid change in flow direction can bring the electrolysis products back into the machining zone after it has been flushed out. As such, an optimal amplitude and frequency of vibration should be maintained during WECM for adequate flushing [3]. Further, the improvement in the quality of machining process with more efficient flushing as compared to axial flow system and PZT vibration assisted axial flow systems was implemented with addition of nozzle jet flow system.

Figure 3.2 Schematic for the principle of vibration-assisted axial nozzle jet flow WECM process

The principle of vibration-assisted axial nozzle jet flow WECM is depicted in **Figure 3.2.** The pulse generator is used to dissolve material by electrochemical reactions between the cathode wire and anode workpiece soaked in a suitable electrolyte solution separated by a tiny inter-electrode gap (IEG) during machining. During the process, sludge and dissolved products such as hydrogen gas, bubbles, hydroxides must be efficiently removed for renewal of fresh electrolyte in the narrow IEG to avoid any micro-sparks and short-circuit for stable machining conditions. Therefore, vibration-assisted axial nozzle jet flow is used during the machining process to improve mass transport and flushing efficiency for sludge disposal and electrolyte renewal in the narrow IEG to continuously deliver fresh electrolytes under a constant flow rate to the machining area. The wire is fed towards the workpiece in a predetermined trajectory for anodic dissolution in the form of metallic ions with a given feed length to machine the workpiece with a small diameter nozzle jet flow electrolyte at a specific workpiece nozzle stand-off distance coaxial with a wire electrode along with the low frequency and small amplitude PZT vibration.

3.3 Development of Mathematical Model

Figure 3.3(a) illustrates the principle of the WECM process. The wire acts as the cathode traveling along its axis and the workpiece acts as an anode submerged in an electrolyte. The micro-slits are fabricated by controlling the workpiece feed path and the electrolyte is enforced to flow through the narrow inter-electrode gap (IEG) with the help of an axial nozzle jet flow system assisted with PZT vibration.

Figure 3.3 (a) basic WECM Principle **(b)** Schematic of side gap for micro-slit width

The Schematic of the side gap for micro-slit width is shown in **figure 3.3(b).** The wire electrode of diameter Dw is fed towards the workpiece at fw wire feed rate with an initial inter-electrode gap ℓ at a distance L from the center of the wire electrode. The anodic dissolution takes place in the machining area having a frontal gap Δ_b in Y-axis direction and side gap Δ_s in the X-axis direction. The slit width Sw and total length X with stray current effect near the machining zone at the edge of fabricated micro-slit is obtained during WECM. From the analysis of the stray current attack, it is clear that the workpiece upper surface is subjected to more severe stray current-induced pitting corrosion than the underside and near the slit edges during WECM.

Though the current in anode and cathode material is the same, current densities in anode and cathode are different which can be defined as the ratio of current to the area normal to the direction of flow of the current. There are two possible directions of the flow of current. In the axial direction, it may be downwards or upwards. In this direction, the current density remains similar throughout the height due to the same cross-sectional area. In the radial direction, the area normal to this axial direction of flow of current is the surface area. The surface area is minimum at the inner surface (frontal gap in the direction of machining zone) and maximum at the outer surface (back side of wire) and changes continuously with workpiece thickness due to the height of the workpiece. As the surface area changes, the current density also changes with the thickness. It is maximum on the inner surface and minimum on the outer surface.

In the electrolytic process, the current density j is:

$$j = -k_e . E \tag{3.1}$$

Where, E; the electric field strength and k_e ; the electrolyte conductivity.

The expression for effective electrolyte conductivity considering the effect of gas bubbles with dissolution hydroxide sludge produced during electrolysis product is given by **[88]:**

$$k_{e=} \ k_0 \ (1 + \alpha \Delta T)(1 - \alpha_v)^a [1 - \beta (1 - \frac{k_d}{k_0}) \alpha_s]^\gamma \tag{3.2}$$

Where, k_0 ; initial electrolyte conductivity, α; temperature coefficient, ΔT; temperature difference, α_v ; void fraction of bubbles, α_s ; void fraction of dissolution hydroxide sludge, k_d ; dispersed medium electrical conductivity, β and γ are constants with values are 0.994 and 1.5 for the specified arrangement.

$$\beta = \ \beta_1 + \beta_2 \tag{3.3}$$

Where, β_1 ; volume ratio of hydrogen, β_2 ; hydroxide volume ratio in electrolyte mixture.

The anodic dissolution process is interrupted because of the less current density near the

machining zone with reduced electrolyte conductivity. As per Faraday's laws, material removal is,

$$m = \frac{AIt}{zF} \tag{3.4}$$

Where, m; anodic mass material removal, A; atomic weight, I; current defined by the amount of charge transfer (number of electrons x charge of each electron) per second written as, $I = \frac{Q}{t}$, Where, t; machining time, z; metal ions valency, F; Faraday's constant(≈ 96500 c / mol), Q; total electric charge passed.

The eq. (3.4) can be re-written as

$$V = \frac{mR}{e_a t} \tag{3.5}$$

Where, $e_a = {A}/{zF}$ and is electrochemical equivalent, V; applied voltage, R; resistance for current flow in the machining zone.

Now, it is well known that,

$$R = \frac{\ell}{k_e a_r} \tag{3.6}$$

Where, k_e ; electrolyte and electrolysis product mixture conductivity, a_r; area of the wire in the machining zone, ℓ; distance between wire and workpiece during machining (IEG). Neglecting the effect of electrolyte temperature and bubbles during machining, electrolyte, and electrolysis product mixture conductivity can be re-written as **[89]:**

$$k_e = k_0 \frac{2[1-(\beta_1+\beta_2)]}{2+\beta_1+\beta_2} \tag{3.7}$$

Where, k_0 ; electrolyte conductivity, $\beta_1 = \frac{q_1}{q_g}$ and $\beta_2 = \frac{q_2}{q_g}$ is hydrogen and hydroxide volume ratio, q_1; hydrogen volume flow, q_2; hydroxide volume flow, and q_g; total volume flow through IEG. The pump output electrolyte volume flow is **[89]**:

$$q_p = k_1 k_2 f q_g \tag{3.8}$$

Where, q_p; pump output volume flow, k_1; overflow coefficient, k_2; leakage coefficient, and f; processing surface complexity coefficient.

The pump output flow and velocity is:

$$q_p = a_p v_p \tag{3.9}$$

Where, a_p ; cross-sectional area of the flow in pump output mouth and v_p ; average electrolyte velocity at pump output.

As the electrolyte is flowing along a pipe with decreasing nozzle radius, an equal quantity of fluid should flow past any point in the pipe and nozzle in a specified time to make sure

continuity of flow. In this case, the velocity must necessarily increase due to decreased nozzle diameter. Therefore, the flow rate must be the same at all points i.e. pump output volume flow q_p and flow rate of nozzle jet flow q_n equal.

The equation of continuity for electrolyte flowing through the pump output mouth and nozzle jet is:

$$a_p v_p = a_n v_n \tag{3.10}$$

Where, a_n ; cross-sectional area of the flow in nozzle output mouth and v_n ; average electrolyte velocity at nozzle output.

$$v_n = \frac{r_1^2}{r_2^2} v_p \tag{3.11}$$

Where, r_1 –radius of pump output mouth, r_2 –radius of nozzle,

$$q_g = \frac{a_n r_1^2}{k_1 k_2 f r_2^2} v_p \tag{3.12}$$

$$\beta_1 + \beta_2 = \frac{k_1 k_2 f r_2^2}{a_n r_1^2 v_p} (q_1 + q_2) \tag{3.13}$$

It can be seen that the area of the wire a_r which is in the machining zone equal to

$$a_r = \frac{\pi d_w t_a}{2} \tag{3.14}$$

From the geometry of the machined slit, the mass removed in the process can be determined as

$$m = \rho_a t_a \left(d_w L + \frac{\pi d_w^2}{8} \right) \tag{3.15}$$

Where, ρ_a ; anode material density, t_a ; anode thickness, d_w ; wire diameter, L; total travel length of wire within the workpiece excluding the initial IEG.

From eq.(3.5), eq.(3.6), and eq.(3.15), applied pulse voltage can be re-written as

$$V = \frac{\rho_a t_a \ell}{e_a t \, k_e a_r} \left(d_w L + \frac{\pi d_w^2}{8} \right) \tag{3.16}$$

The equation of frontal IEG is

$$\Delta_b = \frac{\eta \omega k_e V}{f_w} \tag{3.17}$$

$$\Delta_b = \frac{\eta \omega \rho_a t_a \ell}{f_w e_a t \, a_r} \left(d_w L + \frac{\pi d_w^2}{8} \right) \tag{3.18}$$

Where, η ; current efficiency, ω ; anode electrochemical equivalency, V; applied voltage.

Δ_s is side machining gap, at a distance s from the side edge of the slit at position P from the wire as shown in **Figure 1(b).** Wire feed along the Y-axis, side gap increases along X-axis. The anodic dissolution rate is:

$$\frac{ds}{dt} = \frac{\eta \omega k_e (V - \delta V)}{s} \tag{3.19}$$

Where δV is electrode potential difference ($(\delta V = V_{anode} - V_{cathode}$) is very small and it can be neglected. The eq.(19) can be written as

$$s\, ds = \eta \omega k_e V\, dt \tag{3.20}$$

From eq.(17) and eq.(20), it can be re-written as

$$s\, ds = \Delta_b f_w\, dt \tag{3.21}$$

Integrating the above eq.(21)

$$\frac{s^2}{2} = \Delta_b f_w\, dt + c \tag{3.22}$$

When $t = 0, s = s_0$ and $c = {s_0^2}/{2}$ so Δ_s can be given:

$$\Delta_s = \sqrt{2\Delta_b f_w t + \Delta_b^2} \tag{3.23}$$

When the wire diameter is at a micron scale, $s_0 \approx \Delta_b$ and the primary factor of the side gap expands from s_0 to Δ_s be the cathode width of the wire diameter.

$$\Delta_s = \sqrt{2\frac{\eta \omega \rho_a t_a \ell}{f_w e_a t\, a_r}\left(d_w L + \frac{\pi d_w^2}{8}\right) f_w t + \left[\frac{\eta \omega \rho_a t_a \ell}{f_w e_a t\, a_r}\left(d_w L + \frac{\pi d_w^2}{8}\right)\right]^2} \tag{3.24}$$

Slit width; W_s can be calculated as

$$W_s = D_w + 2\Delta_s \tag{3.25}$$

$$W_s = D_w + 2\sqrt{2\frac{\eta \omega \rho_a t_a \ell}{e_a\, a_r}\left(d_w L + \frac{\pi d_w^2}{8}\right) + \left[\frac{\eta \omega \rho_a t_a \ell}{f_w e_a t\, a_r}\left(d_w L + \frac{\pi d_w^2}{8}\right)\right]^2} \tag{3.26}$$

This empirical formula as developed will be useful for estimating the slit width considering the influence of different process parameters in WECM.

3.4 Selection of Electrolyte, wire electrode and workpiece

3.4.1 Selection of Electrolyte

In WECM, acidic electrolyte solutions of H_2SO_4 and HCl have been favored over neutral salt-based electrolytes like NaCl and $NaNO_3$ for the machining of stainless steel, nickel and cobalt-based alloys, etc. This is due to the fact that acid electrolytes don't form any insoluble materials as the primary reaction result during machining, which could build up in the IEG, reduce conductivity, and obstruct the dissolution process [90]. Therefore, using acid electrolytes produces microfeatures with a high aspect ratio and smoother surfaces. By utilizing H_2SO_4, greater surface quality and localization have been attained in addition to transpassive dissolving because of the formation of passive film, which also aids in electrochemical polishing. However, the usage of HCl has led to the creation of uneven surfaces as a result of pitting corrosion caused by chloride. This has already been discussed earlier. On the other hand, if a proper flushing strategy is not used, the amount

of reaction by-products created during machining in salt-based electrolytes is much greater and insoluble, which might block the machining gap. Additionally, unlike acidic electrolytes, salt-based electrolytes leave a thick coating of corrosion products on the surface of iron-based work materials after machining, making them unsuitable for machining microstructures with high aspect ratios **[91].**

In the preliminary experiments for performance enhancement of machining, dilute H_2SO_4 solution has been chosen for machining stainless steel (SS304) in light of the foregoing and same has been applied for machining of nitinol shape memory alloy. It is important to note that the concentration of H_2SO_4 solution has been maintained at 0.1M throughout the research activity due to the detrimental corrosive effect of flushing units and other machining setups with rising concentration. Even while there is a chance that blackened metallic precipitates will form on the wire when the concentration is that low, this has only seldom or never happened under extreme circumstances in the current configuration. Additionally, the possibility has been reduced even further under modified machining settings by optimizing flushing conditions and modifying operation parameters. In the process of electrochemical machining, the electrolyte is a crucial component. The electrical and thermal conductivity of the electrolyte has been found to have substantial effects on the machining process as reported in previous studies. Therefore, the choice of electrolyte and its concentration are crucial in the WECM process. The search for alternative and novel eco-friendly electrolytes as well as research on the influence of ozonated mixed electrolytes in aqueous solutions and their various concentrations as well as the effects of the addition of complexing agents such as citric acid are both in need of multifaceted efforts for micromachining of nitinol shape memory alloy during wire electrochemical machining.

3.4.2 Selection of Wire Electrode

In WECM, various wire electrode types have been employed. These are coated, platinum-iridium alloyed, copper, platinum, molybdenum, tungsten, CNF, stainless steel (SS304), and other metals. With the exception of platinum, none of these existing wires have a lower tensile strength than copper. Additionally, copper has poor strength and is prone to distortion, breaking, and the generation of precipitate, which can attach to the wire surface after construction. Additionally, when copper wire is idle for a long time after cutting, it produces a white precipitate due to its increased chemical reactivity under air circumstances. Additionally, copper wire cannot have its diameter decreased below a particular point because doing so will cause the wire to eventually break due to the

creation of necking from persistent tensile tension. However, even though platinum has excellent chemical stability, its tensile strength is lesser than copper's. Because of this, when reduced to micron or submicron dimensions, platinum can easily deform due to tiny gas bubbles forming in the IEG and may break due to the slightest and minute contact with the workpiece during machining. This causes short circuiting and deviations from the tool path and prevents its successful application in WECM. As a result, using a platinum wire with a few microns of diameter during WECM is more challenging. Again, molybdenum has better tensile strength than platinum and copper, followed by stainless steel (SS304). However, for the same obvious reasons as mentioned above, it is always desirable to utilize wire with the highest tensile strength possible rather than a weaker wire when machining with a micro diameter under various machining conditions. This allows for the checking and consideration of wire breaking.

The strongest of them all, surpassing even the tensile strengths of tungsten and platinum-iridium, is CNF wire. Because CNF wire is more wettable than tungsten, it has a higher surface hydrophilicity, which helps create a smooth surface. However, the preparation and preprocessing procedures for using CNF wire are far more difficult and time-consuming. Other existing coated and alloyed wires suffer similarly as a result of problems with availability, cost effectiveness, complex processing, and in some cases, tensile strength. The selection of the tool electrode will be made in accordance with the goals of the research project, previous study areas, and the most suitable tool materials. Some conclusions about the suitable tool materials have been obtained from earlier studies. In order to preserve the machined profile dimension during the WECM process, the tool material must be both conductive and wear-free.

As a result, tungsten, which is inexpensive and has a somewhat high tensile strength that can allow it withstand the formation of tensile stress when decreased to a few microns, emerges as a very credible and commendable alternative. It also possesses a high degree of toughness and strong corrosion resistance. However, the drawing process is used to create the commercially available tungsten wire, which makes it more difficult to produce in large batches and increases the cost of manufacturing overall. This is because it requires complex micro-mold hole preparation, particularly at very low ranges. In this study, WECM machining will be done using tungsten wire with a diameter of 50μm during micromachining of stainless steel SS3304 and nitinol shape memory alloy.

3.4.3 Selection of Workpiece

As the goal of this research project is to improve WECM performance, no initial

emphasis on the type of work material was placed; rather, the preliminary experiments were started using the widely available, frequently used, and versatile stainless steel (SS304) material as an anode. It is an austenitic grade that belongs to the well-known and classic 18-8 stainless steel family (at least 18% Cr and 8% Ni). Its great formability makes it simple to use, and its excellent corrosion resistance helps to preserve samples under adverse environmental conditions for a long time after operations. Its applications span, the technological spectrum, from the most fundamental such as traditional home appliances to the most cutting edge such as automotive, aerospace, marine, etc.

Shape memory alloys are a highly ideal material for many engineering applications in the automotive, healthcare, and aerospace industries thanks to their superb qualities. The creation of a knowledge-sharing platform that is more productive and efficient inside SMA-based communities. The end-user applications and implementation of shape memory alloys in the aforementioned application categories both heavily rely on machining. In WECM, the majority of the research work was done on steels such as mild steel, stainless steel, tungsten, copper, inconel 718, cobalt alloy, nickel alloy, aluminium alloy, magnesium alloys, and titanium alloys etc. Previous researchers have explored the effects of different process settings, but no work has been done on WECM for the nitinol shape memory alloy. In addition, each alloy has unique processing requirements that must be met in order to get the required outcomes. Therefore, it is crucial to comprehend the process variables that will enable the machining of the nitinol shape memory alloy to provide the appropriate outcomes. It will soon be necessary to extend the current material processing window in order to better understand the mechanisms of dissolution during WECM and improve the performance of the innovative nitinol SMA material.

3.5 Experimental planning

As a tool electrode, Ø50µm of tungsten wire (manufactured by Goodfellow Ltd, UK) was used for investigation. To limit the effect of stray current on the machining zone, For a better understanding of the influence of vibration-assisted axial nozzle jet flow system in machining slit width, workpiece specimens of 10mm x 10mm x 0.1mm stainless steel 304 sheets and 120µm thick nitinol shape memory alloy sheet were employed. Acidic electrolytes were favored for machining over aqueous salt solutions because they left fewer insoluble compounds on the workpiece surface and tungsten wire. According to preliminary investigations, the machined slit width reduces as the electrolyte concentration drops. However, at very low concentrations (0.05M), the surface quality deteriorates dramatically. As a result, a 0.1M H_2SO_4 electrolyte solution made from de-

ionized water and laboratory-grade H_2SO_4 was chosen. A variable pulsed DC power source was used in the experiments.

The most basic and straightforward approach for eliminating electrolysis products during machining is the axial electrolyte flow system. A stream of electrolytes with a forward flow pattern and the steady flow in the axial direction of wire envelops the machining zone, creates a uniform flow field, and eliminates the machining products by providing improved electrolyte renewal. However, machining accuracy and stability are affected by the flow entrance angle and electrolyte flow rate due to vibration of wire resulting in sparking and short-circuiting. The simplest flushing technique to circulate electrolytic solution and remove reaction products from IEG is to use a vibration-assisted axial-flow system as shown in **figure3.4.**
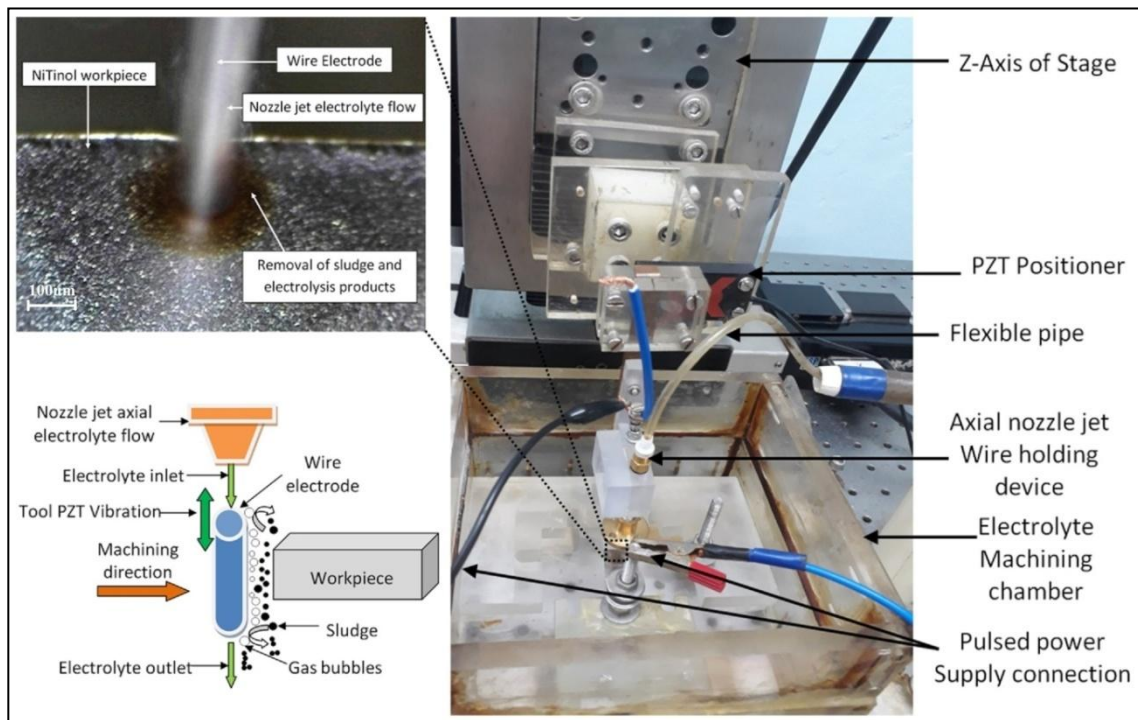
Figure 3.4 Actual microslits machining during vibration-assisted axial nozzle jet
flow WECM

The axial vibration on a wire via piezoelectric transducer creates pressure, which reduces or eliminates sparking and short-circuiting while also improving machining stability. This approach provides better control over tension and support for thinner wire implementation. The vibration frequency and amplitude have a great impact on machining quality. Very low vibration frequency and amplitude create bubbles in IEG resulting in deformation of microwire diameter with increased surface tension. On the other hand, very large vibration frequency and amplitude create a radial swing of wire

electrode resulting in frequent sparking and short-circuiting and can reduce flushing efficiency due to fast change in the flow direction. As a result, proper vibration frequency and amplitude should be maintained. These problems can be reduced to some extent by combining axial flow with PZT vibration for better machining quality. This is a topic that necessitates more in-depth investigation to ensure improved efficacy, determining coupling effects, and flushing parameter operating ranges. Therefore, vibration assisted axial nozzle jet flow wire electrochemical machining is introduced, together with a unique experimental setup and wire holding tool, to improve homogeneity, machining accuracy, and surface quality while reducing slit width. The wire holding device for a vibration-assisted axial nozzle jet flow system has a capability to hold various diameter nozzles with varying workpiece nozzle stand-off distances in the range up to 30mm. The jet flushing with nozzles is proposed to decrease the sludge and dissolved products stagnation area near the wire electrode. As a result, the removal of sludge and dissolved products in a narrow inter-electrode gap can be improved by using small diameter nozzles with variable stand-off distances. Whether the sludge and dissolved products renewal are better and improvement in machining accuracy, quality, and stability with controlled flow rate can be determined by comparison with axial flow and PZT vibration technique during wire electrochemical machining. If the flow rate isn't quite high enough, a thin electrolyte stream is unable to pass through the narrow IEG. As a result, electrolysis products built up which blocks small IEG, and limit electrolyte flow causes sparking and short-circuiting.

On the other hand, too much electrolyte flow during machining creates an unanticipated swing of wire electrode, which distorts it and may disturb the predetermined travel path and damage the process stability. Therefore, an appropriate controlled flow rate for a tiny size nozzle flow system should be selected. The micro wire tool mounting and holding, workpiece mounting, and an electrolyte flow system were all part of the experimental setup. The wire holding tool has a flushing nozzle attached to it, and the electrolyte is flushed axially along the wire electrode. With the help of the rotameter attachment of the flushing system, the electrolyte flow rate can be adjusted as needed. To avoid any contacts between wire and workpiece material, all experiments maintained the required amount of inter-electrode gap, i.e., 100 μm, by moving the wire electrode towards the workpiece in a forward direction by rotating the stepper motor of the stage controller through the microprocessor and checking the inter-electrode gap with a continuity tester. To move the wire electrode towards the workpiece, all machining parameters were set

according to the designed experimental planning and provided the wire feed rate in the stage controller. Switch off all machine units in a sequential manner at the end of the machining operation. While machining, the experimentation scheme was established to investigate the impact of nozzle diameter and nozzle workpiece standoff distance, as well as other influencing process parameters such as feed rate, duty ratio, pulse voltage, and so on. Details of parameters identified to carry out the experiments were identified based on data from a literature survey, review of experiences, and trial experiments for micro-slits machining carried out to understand the effect of nozzle diameter and nozzle workpiece standoff distance with vibration-assisted nozzle jet flow wire electrochemical machining.

Table 3.1 Operating Conditions

Working condition	Value
Workpiece material	Stainless Steel 304, Nitinol
Workpiece Thickness	SS304-100μm, NiTi-120 μm
Wire Electrode Material	Tungsten (Smooth cylindrical)
Diameter of Wire Electrode	Ø50μm
Nozzle Diameter	0.4 - 1 mm
Nozzle Workpiece Distance	5 -20 mm
Applied Pulse Voltage	7 - 10V
Wire Feed rate	1-1.6μm/sec
Duty ratio	35-50%
Voltage Pulse frequency	250KHz
Type and concentration of	0.1M H_2SO_4
Electrolyte Flow rate	35 lph-axial , 5 lph-Nozzle Jet
IEG	100μm
PZT Tool vibration frequency	20Hz
PZT Tool vibration amplitude	12.94μm

Table3.1 shows the operating conditions for all of the process parameters, along with the ranges that were used in the experiments. For the experimental analysis, micro slits were machined and the influence of nozzle diameter, workpiece nozzle standoff distance, and other influencing parameters was studied. To assess the experimental results and improve the quality of the micro machined product, the diameter of the nozzle with the workpiece nozzle standoff distance was adjusted at each stage of the experimental investigation while other process parameters remained constant during micro slit machining. Standard deviation, which shows homogeneity of the machined microslit, is used to represent machining accuracy. The standard deviation is used to calculate machining accuracy in terms of slit width using the equation below.

$$SD = \sqrt{\frac{\sum_{i=1}^{n}(S_i - S_{mean})^2}{n-1}} \tag{3.27}$$

Where, n, number of measurements taken; S_i, each measurement value; S_{mean}, mean of S_i;

Each experiment was repeated multiple times with the same axial electrolyte flow rate and PZT vibration, but with different distances between the nozzle and the workpiece and nozzle diameter. For vibration-assisted axial nozzle jet wire electrochemical machining, the machined slit-width was measured using an Olympus STM6 measuring optical microscope for each operating condition machined with all flushing conditions, and machining accuracy was obtained for various nozzle diameters and workpiece nozzle standoff distances.

3.6 Comparison of vibration-assisted axial nozzle jet flow system with other flushing methods during wire electrochemical machining

Here, a basic comparison among different flushing strategies is analyzed to get the best electrolyte flushing technique that can help to meet the desired criteria of generating high-quality micro features with the WECM process. Experimental results of different electrolyte flow systems regarding average slit width for different pulse voltage, wire feed rate, and duty ratio imply that vibration-assisted axial nozzle jet flow wire electrochemical machining process has a great impact on reduction in slit width with better homogeneity and machining accuracy. On the other hand, during axial electrolyte flushing, the value of the generated slit width cannot attain the desired lower value and the machining accuracy is also reduced due to improper flushing and removal of sludge. PZT vibration-assisted axial-flow system has a better result than the axial-flow system. It can also be concluded that these three flushing techniques individually have limitations in the maximum acceptable pulse voltage, wire feed rate, and duty ratio to continue proper machining. Accuracy of machining in WECM deteriorates if micro sparks occur, clogging of gas bubbles and sludge generate on the wire as well as in the machining gap during machining. In the case of using PZT vibration in wires, micro sparks occur at high feed rates that also deteriorate the accuracy of machining though it can generate minimum slit width. On the other hand, the axial flow of electrolyte generates improper accuracy due to the instability of wire electrodes due to the impingement of electrolyte flow on the wires during machining. However, the most important investigation of this research work may be the positive impact of vibration-assisted axial nozzle jet flow wire electrochemical machining that offers higher machining accuracy and process stability with greatly reduced micro slit width and standard deviation.

Micro slits fabricated with axial flow WECM are shown in **Figure3.5** under different

parametric operating conditions. It is observed that the slit width of the fabricated micro slits is quite high with a minimum of 190 μm and a maximum of 227μm.
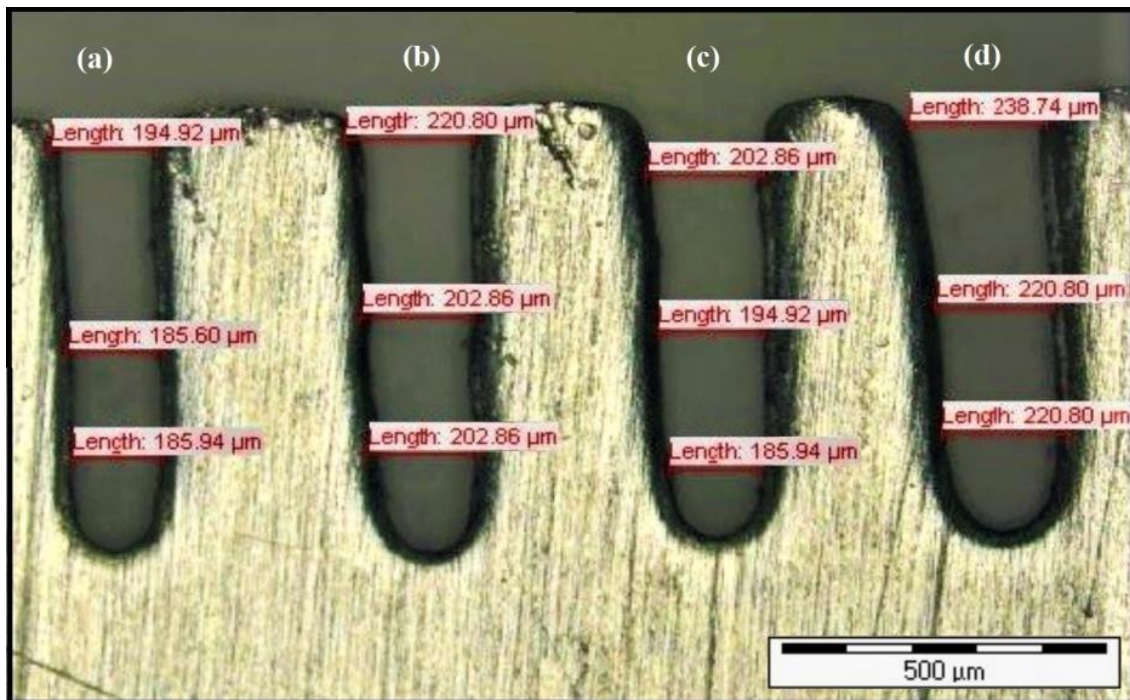
Figure 3.5 Axial flow WECM fabricated microslits under the following conditions (a) 7V pulse voltage, 45% duty ratio, 1.4 μm/sec feed rate (b) 9V pulse voltage, 35% duty ratio, 1.6 μm/sec feed rate (c) 8V pulse voltage, 40% duty ratio, 1.2μm/sec feed rate (d) 10V pulse voltage, 50% duty ratio, 1μm/sec feed rate

The more slit width may be because the axial flushing was not sufficient to remove sludge and dissolved products efficiently in the inter-electrode gap and it creates a problem for renewal of fresh electrolyte and electrolysis products during machining. As the electrolyte flow inlet diameter is quite high and the height of the workpiece surface from the electrolyte inlet is a minimum of 30mm in the wire holding tool, flow entrance angle may distort results in distortion of the wire due to the impact force of the electrolyte flow, and worsen the machining stability. Further, it is seen that the initial overcut of the fabricated micro slit is quite high which may be due to the setting of a high initial inter-electrode gap of 100μm resulting increase in the side gap. Micro slits fabricated with axial flow with PZT vibration WECM are shown in Figure.3.6 under different parametric operating conditions. It is observed that the slit width of the fabricated microslits has better results than the axial-flow system with a minimum of 165μm and a maximum of 181μm. Overcut in slit width is reduced due to the combined effect of PZT vibration with the axial flow system.
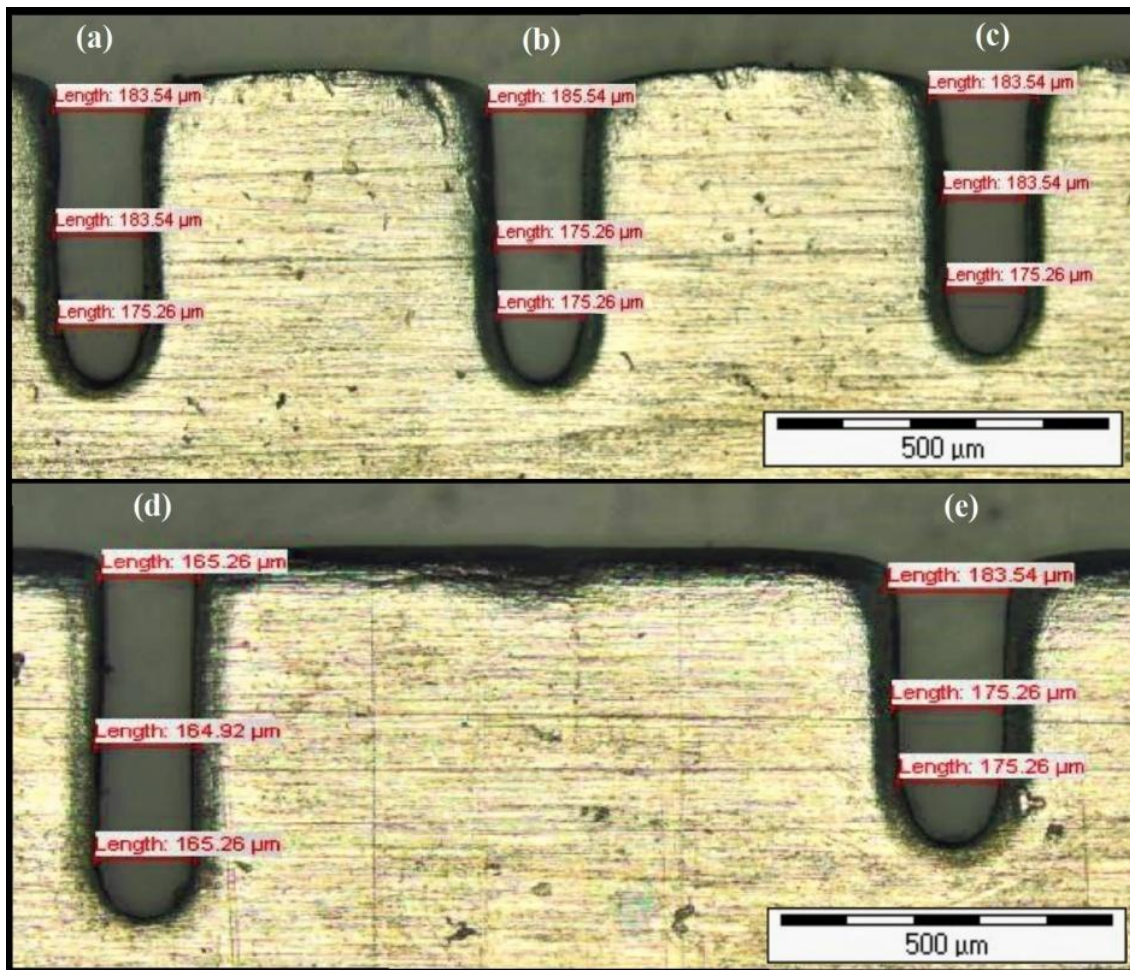
Figure 3.6 Axial flow with PZT vibration WECM fabricated microslits under the
following conditions (a) 10V pulse voltage, 50% duty ratio, 1.6 μm/sec
feed rate (b) 9V pulse voltage, 35% duty ratio, 1.2μm/sec feed rate (c)
9V pulse voltage, 40% duty ratio, 1μm/sec feed rate (d) 7V pulse
voltage, 45% duty ratio, 1.4 μm/sec feed rate (e) 8V pulse voltage, 40%
duty ratio, 1.2μm/sec feed rate

Also, initial overcut was reduced due to better control and support of wire tension and
support of wire electrode which creates pressure waves for renewal of fresh electrolyte in
the inter-electrode gap with controlled machining conditions and to avoid any sparking
and short-circuit during machining. The micro slits fabricated with axial flow with
vibration-assisted axial nozzle jet flow WECM are shown in **Figure3.7** under different
parametric operating conditions. It is observed that slit width of the fabricated micro slits
has better results than the axial-flow system as well as axial flow with PZT vibration
WECM with minimum 110μm and maximum 150μm. Overcut in slit width is reduced
due to the combined effect of PZT vibration with the axial flow system. Also,
homogeneity with better slit width was obtained during machining because small nozzle

diameter and variable workpiece nozzle stand-off distance have seen more positive impact during machining.
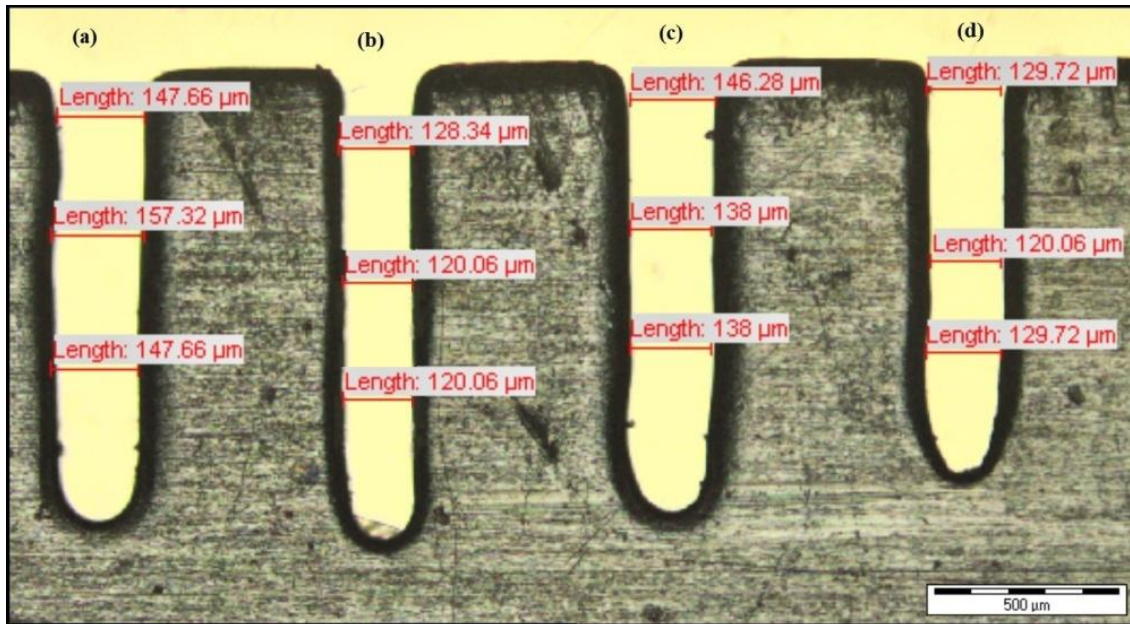
Figure 3.7 Vibration assisted axial nozzle jet flow WECM fabricated microslits under the following conditions of workpiece nozzle stand-off distance (a) 10V pulse voltage, 45% duty ratio, 1.6 μm/sec feed rate (b) 8V pulse voltage, 45% duty ratio, 1.4μm/sec feed rate (c) 9V pulse voltage, 35% duty ratio, 1.2μm/sec feed rate (d) 8V pulse voltage, 40% duty ratio, 1.4μm/sec feed rate

Further, the effect of variable nozzle diameter and workpiece nozzle stand-off distance should be investigated for further improvement in the fabrication of micro slits. Vibration-assisted axial nozzle jet wire electrochemical machining proved to be a better strategy for overall performance improvement of WECM during micromachining of complex micro features.

3.6.1 Effect of pulse voltage on slit width and accuracy

The experiment results reveals the effect of applied pulse voltage on slit width produced during different electrolyte flow systems as shown in **figure3.8.** As per the past research and literature review, the operating condition for micro slits fabrication was 1.4μm/sec feed rate, 45% duty ratio, with 7 to 10V variable pulse voltage, and other constant process parameters as per the given operating conditions in **table3.1.** The range of 7 to 10V variable pulse voltage was selected because, below 7V, the machining creates micro-pits or no machining at all due to unstable process and continuous sparking and short-circuiting and pulse voltage above 10V becomes too high which creates heavy overcut

during machining. Flow rate at axial flow and PZT vibration axial-flow system was 35lph found suitable after previous investigations on this experimental setup since the diameter of electrolyte flow inlet was 6mm which is quite large and minimum workpiece surface height from electrolyte flow inlet opening was 30mm which necessitates a higher range of flow rate for sufficient flushing of sludge and dissolved products with a renewal of fresh electrolyte. On the other hand, vibration-assisted axial nozzle jet flow systems had a flow rate of 5lph which is quite low as compared to individual axial flushing methods, because, nozzle diameters used in the range of 0.4 to 1mm at a workpiece nozzle stand-off distance of 5 to 20mm. High flow pressure creates due to the use of a small diameter nozzle with a low flow rate which is sufficient for efficient flushing and renewal of fresh electrolytes in the inter-electrode gap.
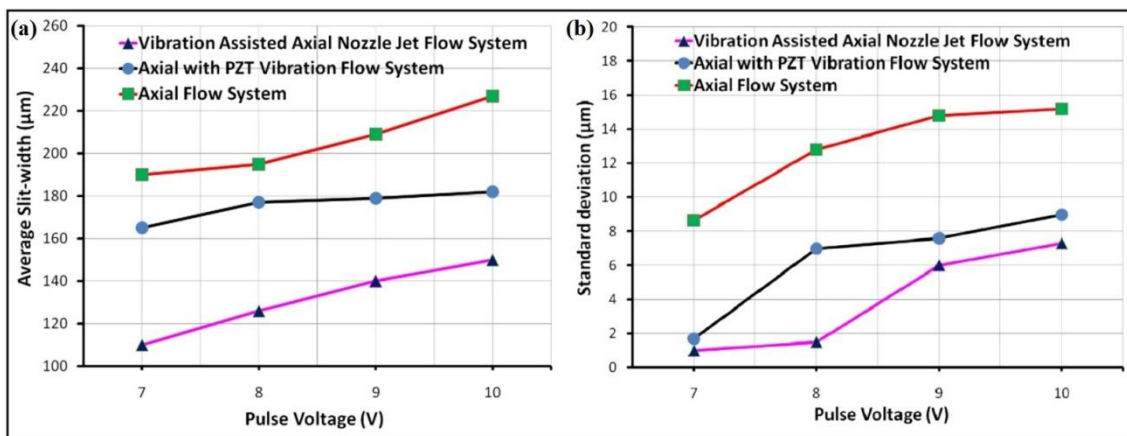
Figure 3.8 Effect of pulse voltage on **(a)** slit-width **(b)** machining accuracy

More flow creates large flow pressure and may vibrate the wire which in turn reduces process stability and machining accuracy. It is observed from **figure3.8(a)** that with the increase in applied pulse voltage, the value of the average slit width increases for all three different types of the flow system. Moreover, Slit width is very less with vibration-assisted axial nozzle jet flow system as compared to axial flow system and PZT vibration-assisted axial-flow system. Homogeneity and machining accuracy of slit width is more at 7V pulse voltage which decreases with further increase of pulse voltage up to 10V as represented by graphical plot shown in **figure3.8(b).** Again further increase in pulse voltages leads to continuous micro sparks and large overcut on the machined slit width. However, the effect of micro sparks and overcut was greatly reduced with a vibration-assisted axial nozzle jet flow system. It is also observed that a vibration-assisted axial nozzle jet flow system has a more positive impact for obtaining less slit width with greater machining accuracy under the same operating conditions used for axial flow

system and PZT vibration-assisted axial-flow system. Average of minimum 110µm slit width is obtained at 7V pulse voltage using vibration-assisted axial nozzle jet flow system which is much less than other flushing strategies. Further, the Standard deviation is also low with this newly introduced flushing strategy as compared to other available flushing strategies as shown in **figure 3.8(b).** Again experiment reveal that the standard deviation at 7V was minimum and it increases with an increase in pulse voltage. The rate of increase in standard deviation is quite high above 7V pulse voltage for vibration-assisted axial nozzle jet flow system due to fact that more flow may increase sudden flow pressure during machining and vibrate electrode wire which in turn reduces machining accuracy. Vibration-assisted axial nozzle jet flow system proved a better flushing method with different pulse voltage conditions for enhancement in machining accuracy, homogeneity, and efficiency for difficult-to-cut materials in industrial applications.

3.6.2 Effect of wire feed rate on slit width and accuracy

Based on the preliminary experiments on different flushing strategies, stable parameter setting of 7V pulse voltage, 45% duty ratio, with 1 to 1.6 µm/sec variable wire feed rate was used to analyze the effect of wire feed rate on slit width and machining accuracy. Flow rate at axial flow and PZT vibration axial-flow system was 35Lph and for vibration-assisted axial nozzle jet flow system was 5Lph as discussed herewith previously for the reason of choosing different flow rate. The comparison is made for machined average slit width obtained at different variable wire feed rates and graphically plotted as shown in **figure3.9(a).** It is observed that a very low wire feed rate below 1 µm/sec generated micro-pits or overcut during machining. Wire feed travel was very less which facilitates a higher dissolution rate and removal of more material from the workpiece leads to overcut in machining. With a further increase in wire feed rate, overcut is reduced due to restricted and reduced dissolution rate during machining. The axial flow system has a large overcut due to improper flushing of sludge and dissolved products in a narrow IEG and a higher stray current effect on the surface of the machined micro slit. For micromachining, a high wire feed rate is preferred. However, the stability of machining deteriorates at a certain high range of wire feed rates. The axial flow system shows that for the wire feed rate from 1.0 to1.4 µm/sec, the average slit width is reduced. With further increase in wire feed rate above 1.6µm/sec, large overcut and reduction in machining accuracy occurs due to restriction in the anodic dissolution process in the machining zone where proper electrolyte flushing is not completed for sludge removal due to narrow IEG and short circuit occurs at the time of machining. This problem was

resolved to some extent with a PZT vibration-assisted flow system with an increased wire feed rate. High overcut occurs due to very low wire feed travel and large metal removal with very less wire feed rate and the effect of wire vibration.PZT vibration helps to restrict the anodic dissolution process with less material removal in narrow IEG by removal of sludge and other dissolved products which produces very little overcut at a high wire feed rate. Machining accuracy also improved with the PZT vibration-assisted flow system.
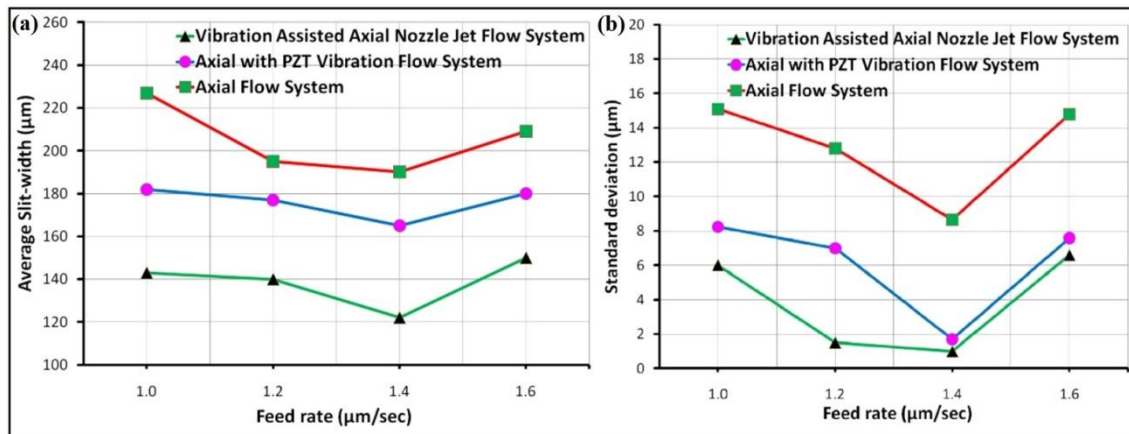
Figure 3.9 Effect of wire feed rate on **(a)** slit-width **(b)** machining accuracy

It is observed from **figure3.9** that vibration-assisted axial nozzle jet flow wire electrochemical machining has a great impact on machining accuracy due to the use of small nozzle diameters. The graph is plotted for machining accuracy as shown in **figure3.9(b).** Experiment results reveal that the standard deviation obtained at 1.4 µm/sec wire feed rate was minimum. Removal of sludge and dissolved products and renewal of fresh electrolyte in narrow IEG were most effectively obtained with the help of vibration-assisted axial nozzle jet wire electrochemical machining. The average slit width of 122µm is obtained at a 1.4 µm/sec wire feed rate which is very less as compared to other flushing strategies. Vibration-assisted axial nozzle jet flow system proved better flushing method with different wire feed rate conditions for enhancement in machining accuracy and homogeneity.

3.6.3 Effect of duty ratio on slit width and accuracy

The duty ratio effect on the machining of slit width with different flow systems is illustrated in **figure3.10.** The parameter setting of 7V pulse voltage, 1.4 µm/sec wire feed rate, with 35% to 50% variable duty ratio and other constant process parameters as per the operating conditions in **table3.1** is used to analyze the effect of wire feed rate on slit width and machining accuracy. The duty ratio 35% to 50% selected for the experiments

since, below 35% duty ratio, creates frequent sparking and short-circuit results in the unstable machining process, and duty ratio above 50% results in heavy overcut to more current density distribution in the inter-electrode gap as high duty ratio has a high pulse on time which is directly proportional to the increase in current flow. Increase in the duty ratio means more time has been made available for carrying out machining because material removal takes place only during pulse on time. However, after 50% duty ratio, the increase in slit width is much more rapid. This is due to the increased accumulation of reaction products which adhere to the wire surface and increase the effective diameter of the wire under constant flushing conditions.
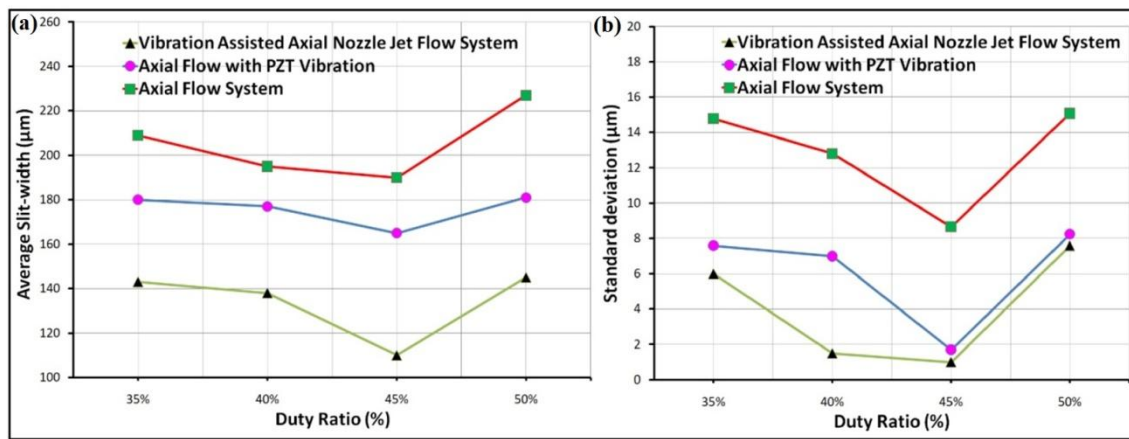
Figure 3.10 Effect of duty ratio on **(a)** slit-width **(b)** machining accuracy

Flow rate at axial flow and PZT vibration axial-flow system was 35lph and for vibration-assisted axial nozzle jet flow system was 5lph as discussed above. Below 35% duty ratio for all flushing strategies, short circuits, micro sparks and a thick layer of black colored precipitates on wire with micro-pits and heavy overcut have been observed. At 35% duty ratio, machining has been quite controlled with uniformity in slit width but with overcut which get reduced at 45% duty ratio with very less deviation in machined slit width. Further increase in duty ratio above 50% during axial flushing increases average slit width to a large extent. The increase in duty ratio implies that more time has been given to machine the workpiece for a fixed duration because only during pulse on-time material removal takes place. With an increase in duty ratio, the dissolution rate increases, which results in large metal removal with an increase in average slit width.

The experiment results also reveal that machining with the increased duty ratio has facilitated the formation of the increased amount of reaction products for which sludge and other debris started clogging the IEG. PZT vibration-assisted flow system and vibration-assisted axial nozzle jet flow system has less effect of the increase of average

slit width above 50% duty ratio. However, following the increasing trend of slit width. These identify the effect of adequate flushing and proper removal of sludge and other dissolved products at narrow IEG and machining zone. Slit width has been decreased as sludge and dissolved products are effectively removed during machining. 45% duty ratio had controlled machining where the slit width is very less as compared to other combinations of duty ratio with proper homogeneity and machining accuracy. It is observed that the vibration-assisted axial nozzle jet flow system obtained less average slit width of 110 µm at 45% duty ratio with all other stable parametric combinations for all flushing strategies which is very less as compared to other flushing strategies. Moreover, the deviation between the values of various slit widths is found to be lower with a particular stable parametric setting.

Vibration-assisted axial nozzle jet flow system proved a better flushing method with different duty ratios for enhancement in machining accuracy and homogeneity. A plot of standard deviation for slit width using different duty ratios for all flow systems is graphically represented as shown in **figure3.10(b)** which represents the machining accuracy of obtained slit width. Experiment results reveal that standard deviation had an increasing trend below and above 45% duty ratio with other constant operating conditions for all flushing strategies. Further, if the duty ratio was below 35% and higher above 50%, the tendency of increase in standard deviation was more due to short–circuits and micro-sparks at lower duty ratio and sudden increase in current density in the narrow IEG at higher duty ratio. Machining accuracy was reduced to a greater extent at these conditions. Standard deviation was minimum at 45% duty ratio. Using novel technique, the overall improvement of 36% slit width reduction and 75% increase in machining accuracy as compared to axial flow WECM and 23% slit width reduction and 40% increase in machining accuracy compared to axial flow with PZT vibration WECM was observed with micro slits machined on 100µm thick stainless steel SS304.

3.7 Effect of nozzle diameter on slit width and accuracy

To understand the effect of a varying range of nozzle diameter in case of vibration assisted axial nozzle jet flow system, experiments were conducted for the fabrication of micro slits on 100µm thick SS304 workpiece with 7V pulse voltage, 45% duty ratio, 1.4µm/sec feed rate, 5lph flow rate as more flow may vibrate the wire which in turn reduce the machining accuracy, and 10mm workpiece nozzle stand-off distance. The influence of nozzle diameter ranging from 0.4 to 1.0 mm on micro slit machining during vibration-assisted axial nozzle jet wire electrochemical machining was investigated. Also,

a graph is plotted to understand the effect of nozzle diameter on slit width obtained as shown in **Figure3.11.**
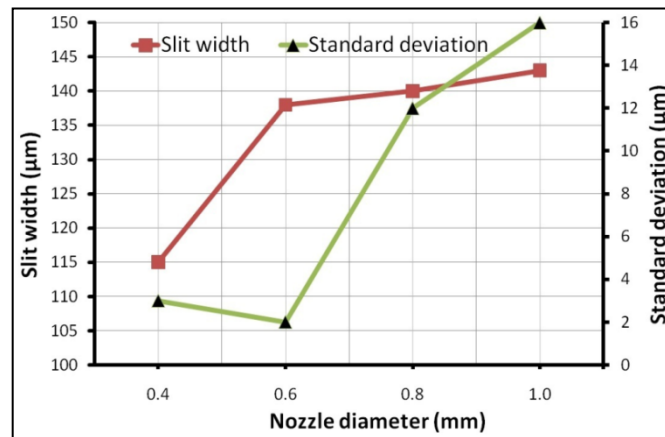
Figure 3.11 Effect of nozzle diameter
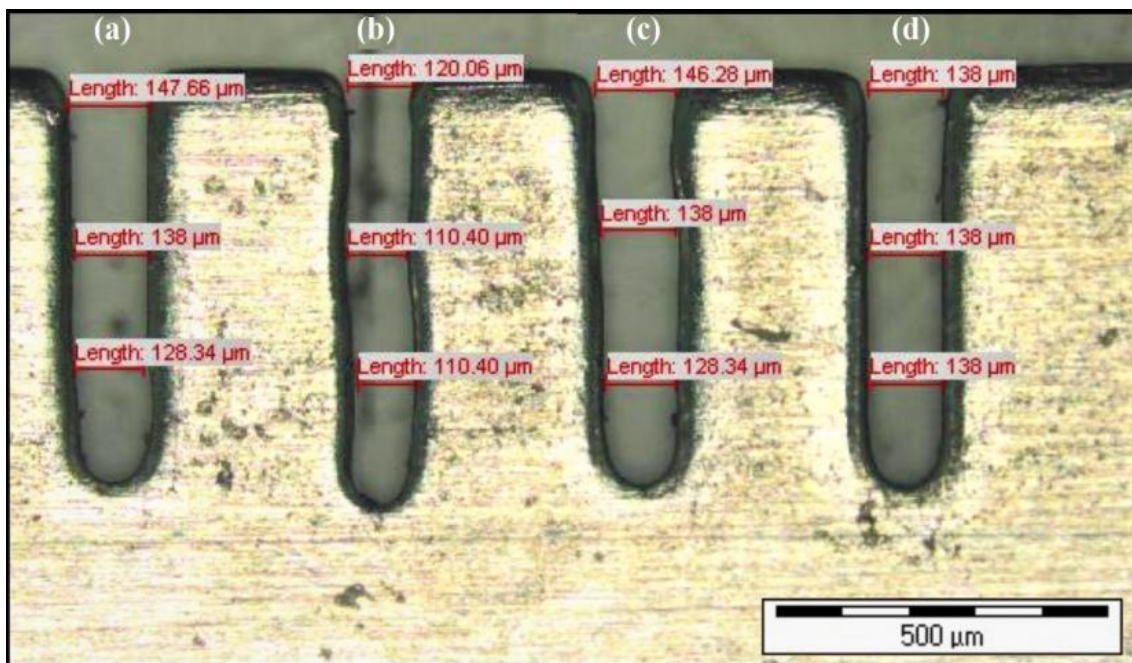
Figure 3.12 Vibration assisted axial nozzle jet flow WECM machined microslits at different nozzle diameter (a) 1.0mm (b) 0.4mm (c) 0.8mm (d) 0.6mm

It indicates that the slit width becomes large with the increase of nozzle diameter. The slit width is very less with the nozzle diameter of 0.4 mm, and it increases with the increase of nozzle diameter. However, standard deviation was less at 0.6mm nozzle diameter which further increased with increase in nozzle diameter Therefore, the diameter of the nozzle has a great impact on the flushing and renewal of fresh electrolytes into IEG. The machined micro slits of SS304 are shown in **Figure3.12.** The average slit width is only 115 μm with the nozzle diameter of 0.4 mm, and it rises to 143 μm with the nozzle diameter of 1 mm. Larger nozzle diameter results in lower fluid flow velocities and thus

sludge and dissolved products are removed slower. Standard deviation increases with an increase in nozzle diameter, which in turn, reduces machining accuracy. Small slit width obtained using small diameter nozzle.

3.8 Effect of workpiece nozzle stand-off distance on slit width and accuracy

Experiments were conducted for the fabrication of micro slits on 100μm thick SS304 workpiece with 7V pulse voltage, 45% duty ratio, 1.4μm/sec wire feed rate, 5lph flow rate as more flow may vibrate the wire which in turn reduce the machining accuracy, 0.4mm nozzle diameter, to understand the effect of a varying range of workpiece nozzle stand-off distance. The workpiece nozzle stand-off distances of 5 to 20mm were considered to find the effect on micro slit width machining during vibration-assisted axial nozzle jet wire electrochemical machining. Also, a graph is plotted to understand the effect of a varying range of workpiece nozzle stand-off distance on slit width obtained as shown in **figure3.13**. The machined microslits of SS304 are shown in **figure3.14.**
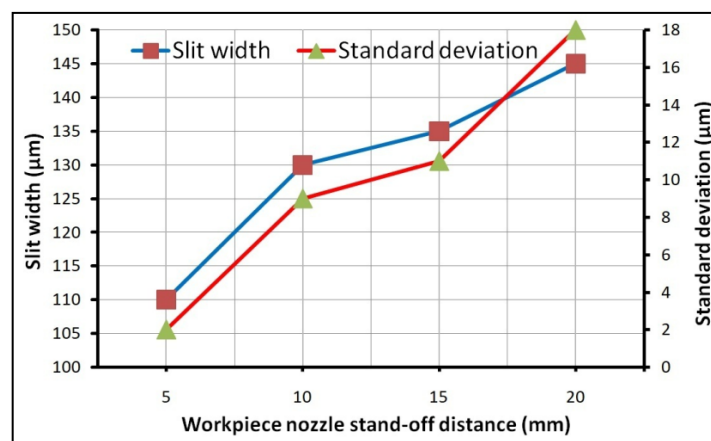
Figure 3.13 Effect of workpiece nozzle stand-off distance

It indicates that the slit width becomes large with the increase of workpiece nozzle stand-off distance. The average slit width is only 110 μm with the workpiece nozzle stand-off distance of 5 mm, and it rises to 145 μm with the workpiece nozzle stand-off distance of 20mm during fabrication of microslits. The slit width is very less with the workpiece nozzle stand-off distance of 5 mm, and it increases with an increase in the stand-off distance. Increased workpiece nozzle stand-off distance reduces electrolyte pressure, allowing the electrolyte to loosely enclose the wire and diffuse further away from the nozzle over the workpiece surface while maintaining a steady flow flux.

Flushing should be optimized to get better homogeneous slit width, therefore for effective flushing of the IEG; the velocity of the fluid flow should be as high as possible for the removal of sludge and dissolved products. The velocity of fluid flow gets reduced with an

increase in workpiece nozzle stand-off distance results in an increase in slit width. Standard deviation increases with an increase in workpiece nozzle stand-off distance results in reduced machining accuracy. Also, more flow may vibrate the wire which in turn reduces the machining accuracy. Small slit width and higher machining accuracy can be obtained with the use of a small workpiece nozzle stand-off distance.
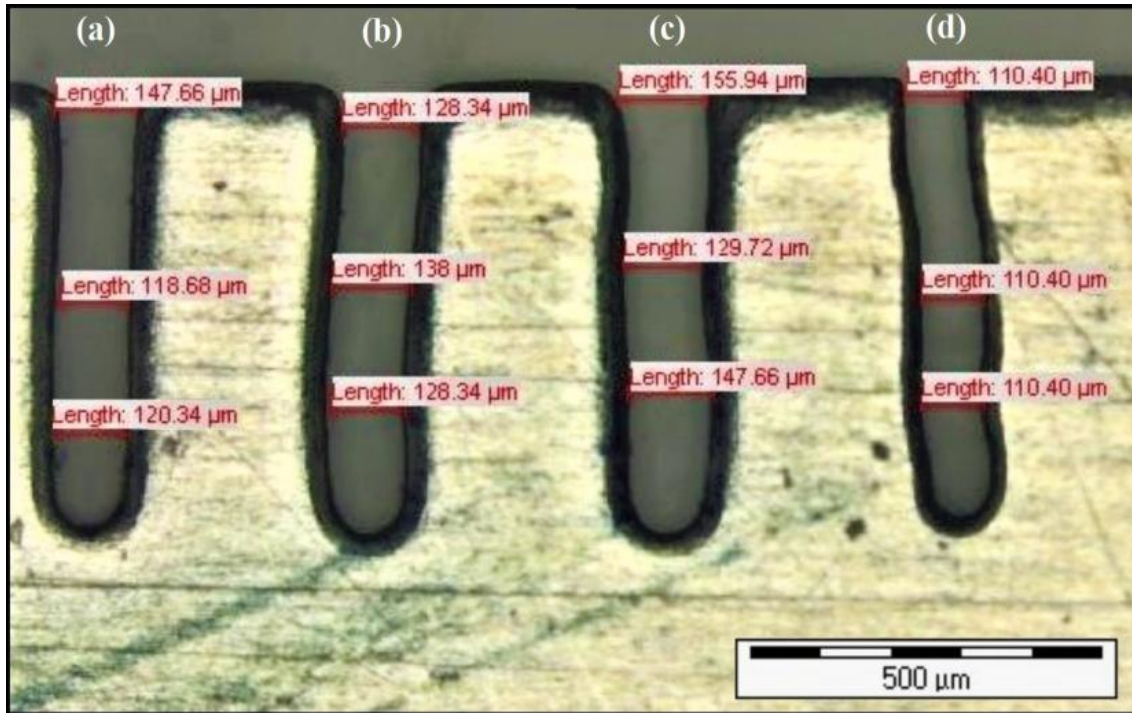
Figure 3.14 Vibration assisted axial nozzle jet flow WECM machined micro-slits at different workpiece nozzle stand-off distance (a) 15mm (b) 10mm (c) 20mm (d) 5mm

3.9 Micro-slit fabrication of nitinol shape memory alloy

Micromachining and nanotechnology play an increasingly decisive role in the development of miniaturized components ranging from electronics semiconductors, sensors and actuators, energy conversion, automotive parts, aerospace, biomedical, surgical instruments, and robotics, etc. nitinol shape memory alloy (SMA) has wide applications in all these manufacturing industries. Traditional machining is not suitable for machining nitinol SMA due to high cutting forces, more tool wear, poor surface finish, and heat generation due to contact between tool and workpiece. To conquer this complexity, nontraditional processes have become inevitable for machining nitinol SMA. Nontraditional machining processes prove improved machinability and surface finish but have certain limitations due to heat sensitivity, super-elasticity, biocompatibility, and severe strain hardening. Wire electrochemical machining is heat-free, mask-free, and

strain-free micro-fabrication machining processes and therefore compatible for micromachining of nitinol SMA. There has been no research into the anodic dissolution mechanisms for nitinol shape memory alloy during WECM discovered in the literature to date. As a result, this research report also discusses micro slit machining of nitinol memory shape alloy for improving WECM performance.

After successfully identifying vibration-assisted axial nozzle jet flow wire electrochemical machining as one of the best techniques amongst axial flow and PZT vibration-assisted axial flow systems, and determining the effect of the most influencing machining parameters during WECM, with number of preliminary trial experiments, a parametric combination of 6V pulse voltage, 1.4µm/sec feed rate, 45% duty ratio, 0.4mm nozzle diameter with 5mm nozzle workpiece stand-off distance, 5lph flow rate and keeping all other parameters constant as per the operating conditions, nitinol shape memory alloy micro-slit has been successfully fabricated.

Figure 3.15 Machined nitinol SMA microslit

As demonstrated in **figure3.15**, the vibration-assisted axial nozzle jet WECM machined nitinol SMA microslit is quite smooth and homogeneous. However, it was difficult to achieve the uniform dissolution of nitinol SMA due to its tendency of passivity due to formation of titanium oxide layer on the surface. The average slit width of 131.56µm was fabricated with shows some stray current effect at the edges which needs further investigations

3.10   Outcomes of experiments

This chapter deals with comparison and the influences of different flow systems on the

performance criteria of fabricated microslits and based upon the experimental results, different outcomes have been mentioned here. WECM is a very newer process of removing material electrochemically. The process retains almost every benefits of ECM and boosts some of the opportunities for machining macro, micro and even sub micron features. However, flushing is till the problem for this anodic dissolution process due to which several researches are still ongoing. In this context, the present research work deals with introducing combined method of different flushing techniques which is new to the field. The combined approach points to be very beneficial in comparable to single flushing strategy by improving the flushing condition, allowing the possibility of further increase in feed and by generating features with good homogeneity. Experiments with better electrolyte flow prevent formation of black colored metallic precipitates on wire. Upon increasing the flow rate, better disposal of sludge and dissolved products that improves the slit width. However, few effects of short circuiting may be observed when flow rate is extreme. With increase in flow rate, standard deviation decreases and then increases. Obviously, the point where the standard deviation is lowest falls in the region where slit width increases with increase in electrolyte flow, i.e. where the phenomenon is proper, justifiable and not influenced by other factors like precipitate formation and deficiency in setup.On the other hand, incorporation of vibration with PZT along with the axial flushing and nozzle jet flow system clearly reveals the fact that when the machining and setup is ideal, it is possible to further increase the flushing efficiency and by applying perpendicular vibrations, standard deviation almost unaffected. It is also revealed that, increase in slit width by application of combined flushing allows further increase in maximum achievable feed rate that can give WECM, an upper hand when it is compared with commercial process like WEDM.

Comparison between axial flow, axial flow with PZT, and novel vibration-assisted axial nozzle jet wire electrochemical machining and analysis on the effect of most influencing parameters i. e pulse voltage, feed rate, and duty ratio on machining result of each flushing strategy reveal that vibration-assisted axial nozzle jet wire electrochemical machining has a most positive impact on machining accuracy and efficiency as compared to other flushing strategies. The overall improvement of 36% slit width reduction and 75% increase in machining accuracy compared to axial flow WECM and 23% slit width reduction and 40% increase in machining accuracy compared to axial flow with PZT vibration WECM was observed using this developed novel technique with micro slits machined on 100μm thick stainless steel SS304.

The results obtained for different flow systems with different selected variable experimental parameters at constant 7V pulse voltage, 1.4 µm/sec wire feed rate and 45% duty ratio is shown in table3.2.

Table3.2 Selected experimental parameters and Results

Sr. No.	Experimental parameters		Results					
			Axial flow WECM		Axial flow with PZT vibration WECM		Vibration assisted axial nozzle jet flow WECM	
			Average slit width (µm)	Standard deviation (µm)	Average slit width (µm)	Standard deviation (µm)	Average slit width (µm)	Standard deviation (µm)
01	Pulse voltage (V)	7	188.8	8.66	165.1	1.7	110	1
		8	195.1	12.8	177	7	126.5	1.5
		9	209.2	14.8	179.2	7.6	140.1	6
		10	227.1	15.2	182	9	150.2	7.3
02	Wire feed rate (µm/sec)	1.0	227.2	15.09	182.3	8.24	143.1	6
		1.2	195.1	12.8	177	7	140	1.5
		1..4	190.3	8.66	165.1	1.7	122.3	1
		1.6	209.1	14.79	180.1	7.6	150	6.6
03	Duty ratio (%)	35	209.1	14.79	180.1	7.6	143.2	6
		40	195.2	12.8	177	7	138	1.5
		45	190.4	8.66	165	1.7	110	1
		50	227.1	15.09	181.2	8.24	145	7.6
04	Nozzle diameter (µm)	0.4	-	-	-	-	113.6	3
		0.6	-	-	-	-	137.5	2
		0.8	-	-	-	-	140	12
		1.0	-	-	-	-	141.9	16
05	Workpiece nozzle stand-off distance (mm)	5	-	-	-	-	110.4	2.1
		10	-	-	-	-	131.5	9.3
		15	-	-	-	-	128.9	11.2
		20	-	-	-	-	144.4	18

The slit width is very less with the nozzle diameter of 0.4 mm, and it increases with an increase in the nozzle diameter. Experiments with increasing nozzle diameter have increased in slit width. The average slit width is only 115 µm with the nozzle diameter of 0.4 mm, and it rises to 143 µm with the nozzle diameter of 1 mm. The larger nozzle diameter results in lower fluid flow velocities and thus sludge and dissolved products are removed slower. For obtaining a small slit width, a small nozzle diameter is recommended. It indicates that the slit width becomes large with the increase of workpiece nozzle stand-off distance. The average slit width is only 110 µm with the workpiece nozzle stand-off distance of 5 mm, and it rises to 145 µm with the workpiece

nozzle stand-off distance of 20mm. The slit width is very less with the workpiece nozzle stand-off distance of 5 mm, and it increases with an increase in the distance. Using the vibration-assisted axial nozzle jet flow system and finding out the effect of most influencing machining parameters during WECM, with a parametric combination of 6V voltage, 1.4µm/sec wire feed rate, 45% duty ratio, 0.4mm nozzle diameter with 5mm nozzle workpiece stand-off distance and keeping all other parameters constant as per the operating conditions, on nitinol shape memory alloy homogeneous microslit has been successfully fabricated.According to a preliminary study on SS304 for vibration-assisted axial nozzle jet wire electrochemical machining, the dissolution mechanism of nitinol shape memory alloy differs from SS304, as do the effects of various parameters. As a result, additional in-depth research including a larger number of process parameters is needed to improve machining accuracy and surface quality during micromachining of the nitinol shape memory alloy for WECM performance. This is the first step towards the application of this process for machining of nitinol shape memory alloy.

This research work has a future scope to understand the dissolution mechanism of biocompatible, superelastic nitinol shape memory alloy without affecting any exquisite properties. Apart from the above approaches of enhancing the performance of WECM, reduction in micro sparks, stray current attack and overcut reductions using different insulation and coating of wire electrodes plays very important role for achieving higher surface quality machined micro features. For this to achieve and exploit the same, proper coating and insulation of wire electrodes is required to be used and influence of different flushing and process parameters has to be carried out and detailed investigations is needed.

Chapter4: EXPERIMENTAL INVESTIGATION INTO REDUCTION OF MICROSPARKS, STRAY CURRENT AND OVERCUT FOR PERFORMANCE ENHANCEMENT OF WECM

4.1 Introduction

WECM has enormous potential for the fabrication of high aspect ratios and complex micro features of any conducting materials with better surface quality. However, the reduction of stray current attack and overcut during machining plays important role to achieve improved surface quality using different insulation methods and recent development of WECM. Performance of the WECM can be enhanced to a large extent during machining of microslit through diminishing micro-sparking removal and reducing overcut by proper controlling of predominant machining parameters. The available literature shows that WECM is a transport limited electrochemical dissolution process and continuous removal of electrolysis products, namely the hydroxides and hydrogen gas, and renewal of fresh electrolytes becomes more difficult in the tiny inter-electrode gap which results in instability and occurrence of frequent micro-sparks during micromachining. Moreover, of the several research works for investigating the influence of various process parameters, no effort has been focused to control the effect of micro-sparks and reduction in overcut on wire electrochemical micromachining process considering most of the influencing parameters which is a primary requirement during machining. In this chapter, therefore, emphasizes on finding out the effect of various controllable parameters such as feed rate, pulse voltage, pulse voltage frequency, and wire vibration frequency & amplitude with PZT on corresponding slit width for micro-spark effect as well as formation of overcut. First, the experimental planning I was made for influence of different process parameters for reduction in micro-sparks and overcut and then next experimental planning II was carried out for reduction of stray current and overcut using different coating and insulation techniques.

The application of various wire electrode coating and insulation methods and the effect of various prominent parameters for reduction of stray current attack and overcut play a more important role in the enhancement of machining accuracy, homogeneity, and surface quality during the fabrication of microfeatures. Therefore, the characteristics of the stray-current attack in WECM were identified through simulation for electrolyte potential and current density distribution at narrow IEG in the machining zone and overcut model is presented in this chapter. Also, the use of synthetic enamel and novel

PTFE (polytetrafluoroethylene) tube insulation method were used to reduce the stray current effect and overcut during WECM and a comparative study has been made with uncoated wire. The elimination of stray current during WECM is needed in practice for effective utilization of this process in the area of micro-fabrication. WECM have now reached at a noteworthy level of research activities but still it is a lab based process and needs more attention towards achieving higher machining quality. This chapter, therefore, further emphasizes on finding out the effect of various special coating and insulation methods such as synthetic enamel coating and novel PTFE pipe tube insulation method and also compared the results with machining without coating and insulation on corresponding slit width for stray current effect as well as the formation of overcut. A comparative study was made between all these methods investigating the effect of most prominent parameters such as pulse voltage, IEG, duty cycle, and wire electrode feed rate, and stray current effect in WECM are first identified. No research has been carried out for the machining of nitinol SMA during WECM using PTFE tube insulation process method for enhancement of machining accuracy and surface quality. Therefore, this material has been considered for the experimental investigation due to the benefit of WECM process and applications of material. Further, the array of nitinol shape memory alloy (SMA) microslits has been fabricated and analyzed based on SEM (Scanning Electron Microscope) and EDX (Energy Dispersive X-ray Spectrum) for understanding the anodic dissolution mechanism and effect of PTFE pipe tube wire insulation method for reduction of stray current attack and overcut.

4.2 Experimental planning-I: Influence of process parameters

In the present work, tungsten wire of Ø50μm with very thin layer of coating of synthetic enamel on non-machining area was used as a tool electrode. The workpiece specimens were 15mm x 15mm x 0.1mm stainless steel 304 sheet was used for better understanding the effect for micro sparks generation and overcut in machined slit width. The electrolyte used for experimentation was 0.1M H_2SO_4. Experimentations are done with variable rectangular DC power supply. Micro slits were machined and effect of micro-sparking and overcut considered for experimental analysis. To analyze experimental results and to enhance the quality of the micro machined product, numbers of micro sparks were counted with the help of oscilloscope at each stage of varying conditions of process parameters during machining of microslits and overcut measured with optical microscope for each operating conditions by considering the mathematical model, as follows:

$$\text{Overcut} = 2\Delta s = 2\Delta b \sqrt{\frac{2d}{\Delta b} + 1} \qquad\qquad (4.1)$$

Where, Δb, inter electrode frontal gap; Δs, inter electrode side gap; d, diameter of wire electrode;

Experimental setup was prepared for micro wire tool mounting and holding, workpiece mounting and electrolyte flow system. For all the experimental trials maintained the required amount of inter-electrode gap i.e., 100μm. All the machining parameters have been set according to the designed experimental planning and given the feed rates in stage controller to move wire electrode towards workpiece. The experimentation scheme was designed in such a way to explore the influence of various parameters on generation of micro sparks and responsible for production of overcut while machining are considered. Sketch of side gap for overcut in WECM machining process shown in **figure4.1.**
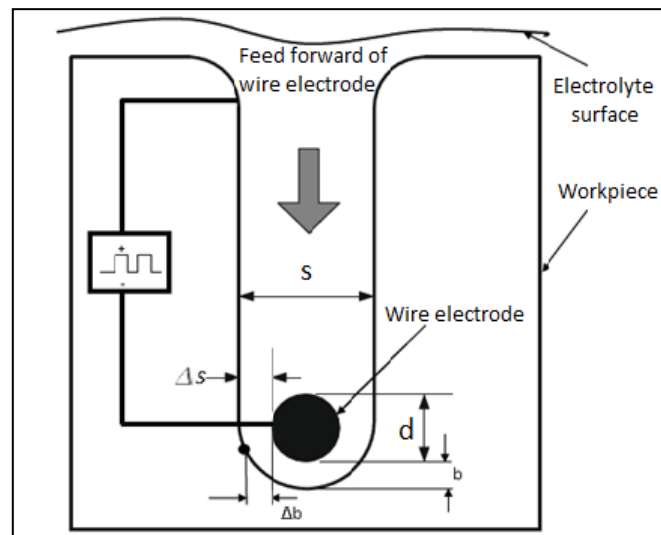
Figure 4.1 Sketch of side gap for overcut in WECM process

Table 4.1 Operating Conditions

Working condition	Value
Workpiece material	Stainless Steel 304
Workpiece Thickness	100μm
Wire Electrode Material	Tungsten
Diameter of Wire Electrode	Ø50μm
Applied Pulse Voltage	4 to 12V
Wire Feed rate	1.0μm/sec to 1.8μm/sec
Duty ratio	50%
Voltage Pulse frequency	50KHz to 500KHz
Type and concentration of	0.1M H_2SO_4
Electrolyte Flow rate	35lph
IEG	100μm
PZT Tool vibration frequency	0 to 100Hz
PZT Tool vibration amplitude	0 to 50μm

Operating conditions for all the process parameters with their ranges used in experimentations are shown in **Table4.1.** In this experimental study, feed rate, pulse voltage, pulse voltage frequency, PZT tool vibration frequency and amplitude were identified to carry out the experiments keeping other parameters fixed for all experiments and working ranges were selected on the basis of data given in literature survey, review of experiences and trial experiments for microslits machining to understand the effect for generation of micro-sparks and as well as formation of overcut.

4.2.1 Experimental observations and discussions

4.2.1.1 Influence of feed rate on micro spark and overcut

Experimental trials were taken for the fabrication of microslits with 4V applied voltage, 200 KHz voltage pulse frequency, 40Hz PZT vibration frequency, 12.94μm PZT vibration amplitude and 1μm/sec to 1.8μm/sec ranges of feed rate. It is observed that average current is increases with increase in tool feed rate and micro sparks occurs at higher currents but overcut is reduced with increase in feed rate.
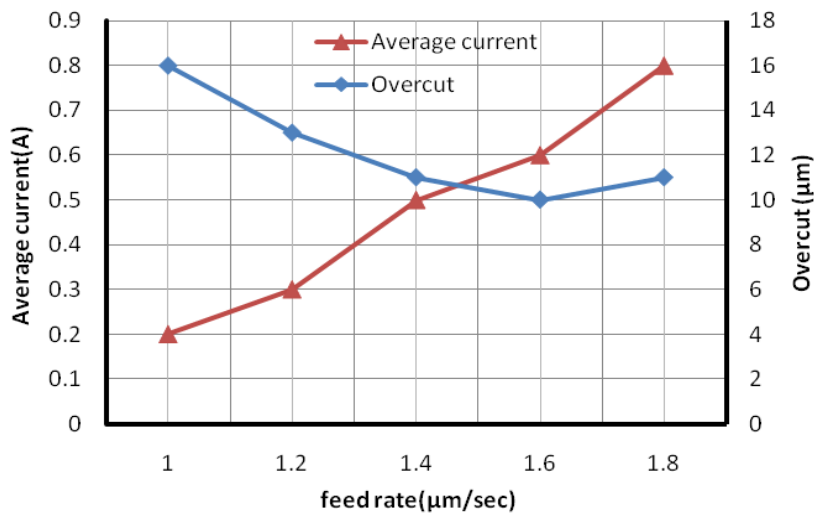
Figure 4.2 Influence of tool feed rate on average current and overcut

It is observed that wire feed rate in the range of 1.4 to 1.6μm/sec gives better control for the reduction of average current and overcut. Moreover, the average overcut is at a bit higher side regarding the fact that tungsten wire of diameter 50μm and IEG of 100μm has been used during experiments due to application of such low feed rate. In order to achieve better accuracy and efficiency, as well as prevent the occurrence of micro sparks and to reduce overcut, influence of feed rate with number of micro-sparks and overcut was investigated and plotted on graph as shown in **figure4.2.**

Microslits fabricated with lower feed rate is homogeneous as controlled dissolution occurred and due to absence of micro-sparks effect. If the feed rate was too high, it was

difficult for the flushing electrolyte to carry away the electrolysis products from the extremely narrow machining gap effectively, leading to micro-sparks.

4.2.1.2 Influence of machining voltage on micro spark and overcut

The influence of applied voltage on overcut without tool vibration and with PZT tool vibration was investigated at 1.4μm/sec tool feed rate, 50% duty ratio, 250KHz voltage pulse frequency, 35lph electrolyte flow rate, 100μm thick SS304 workpiece, Ø50μm tungsten wire electrode, 0.1M H_2SO_4 and 60Hz frequency with 12.94μm amplitude of PZT vibration and with a range of 4V to 12V applied voltage. It is observed that overcut is much less when the micro-machining operation is performed for wire vibration with PZT as shown in **figure4.3.** Further experimental trials were taken to investigate the effect of applied voltage on overcut and number of micro-sparks produced with same above parametric conditions with PZT tool vibration and it is observed that when applied voltage on lower side, inter-electrode gap becomes smaller, the micro-sparks occurs often due to poor removal of electrolysis products from the further narrowing machining gap.
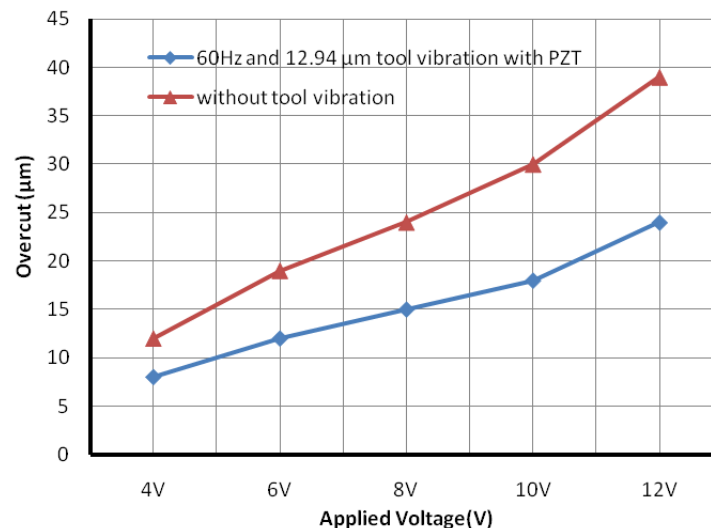
Figure 4.3 Influence of applied voltage on overcut with and without PZT vibration

With tool vibration, the electric short circuit is avoided and the overcut is improved due to pressure waves created in the electrolyte which can promotes excellent circulation of electrolyte and removal of sludge and precipitates from the narrow zone of micromachining, which improves the overall machining performance. It is again observed that the overcut and micro sparks increases with increase in applied voltage and decreases with decrease in applied voltage. A large voltage leads to a high current density, which induces a high material removing rate then a wide side gap is obtained which ultimately increases the overcut. Micro sparks could be seen at the beginning of the process. As the cutting process continued, micro sparks disappeared while the average current decreased.

Furthermore, the wire electrode loses its straightness and tension and the electrolyte could not be flushed along the wire electrode into the machining gap. As a result, the machining target could not be completed. As per the Faraday's and Ohm's laws, greater machining current into the machining gap created with higher applied voltage which increases the material removal rate (MRR) leads to increase in overcut and more micro-sparks which reduces homogeneity and accuracy of machining. It is found that applied voltage in the range of 4 to 6V gives better control on reduction of number of micro-sparks and overcut. The influence of applied voltage on overcut and number of micro-sparks are plotted graphically as shown in **figure4.4.**
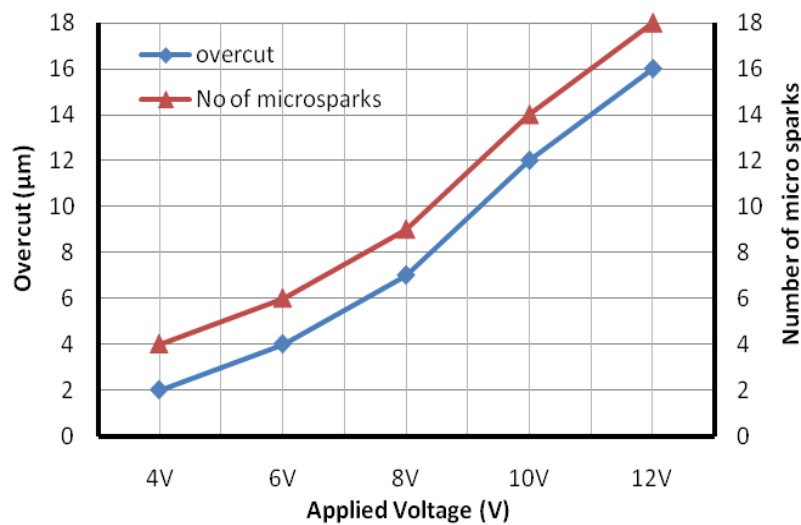
Figure 4.4 Influence of applied voltage on overcut and number of micro-sparks

4.2.1.3 Influence of pulse frequency on micro spark and overcut

Experimental results reveal the effect of applied voltage pulse frequency on overcut and number of sparks produced during machining of microslits with 6V applied voltage, 1.4μm/sec feed rate, 40Hz PZT vibration frequency, 12.94μm PZT vibration amplitude and 50 KHz to 500 KHz range of voltage pulse frequency. A voltage pulse frequency of 250 KHz is optimal for reduction of micro-sparks and overcut. The graph for Influence of voltage pulse frequency on overcut and number of micro sparks plotted as shown in **figure4.5.** It is observed that with the increase in applied voltage pulse frequency, the value of the overcut of the microslit decreases almost linearly. Moreover, with a further increase in frequency beyond 500 KHz under the constant duty ratio, if the pulse-on becomes smaller than the double layer charging time, then no machining will occur.
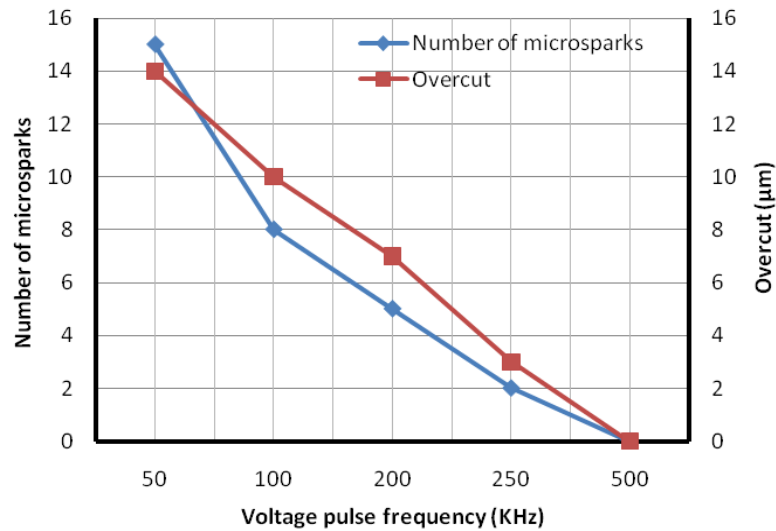
Figure 4.5 Influence of pulse frequency on overcut and number of micro sparks

It is also observed that with a decrease in the frequency value may be up to 50 KHz, generation of more heavy micro sparks occurs and the machining product will fully clog the inter-electrode gap. As a result, micro-sparks will be prevalent and machining will stop after starting.

4.2.1.4 Influence of PZT tool vibration frequency on micro spark

The influence of micro-tool vibration frequencies on number of micro sparks generated is investigated by conducting experiments with 6V applied voltage, 1.4 µm/sec feed rate, 200KHz voltage pulse frequency, 12.94 µm PZT vibration amplitude.
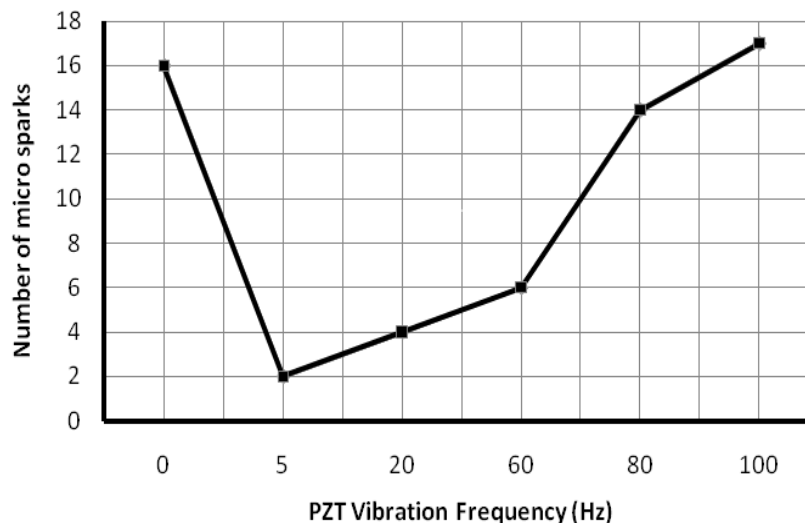
Figure 4.6 Influence of PZT vibration frequency on number of micro-sparks

It is observed that for vibration frequencies of 0 to 5 Hz, it is inadequate to remove the micro-sludge and precipitates from the very narrow machining gap, and number of micro spark generations is quite large which leads to unstable process stability. Hence with proper range of micro-tool vibration frequency has significant effect on better renewal of

electrolyte which improves the machining stability and machining accuracy as shown in **figure4.6.** When vibration frequencies are higher than 40 Hz, number of micro-sparks increases quickly due to wire electrode radial vibration which is more frequent at 80Hz frequency. It is observed that vibration frequencies of 5 to 20 Hz has better control for reduction of micro-sparks.

4.2.1.5 Influence of PZT vibration amplitude on micro-sparks

Experimentation has been conducted with 6V applied voltage, 1.4µm/sec wire feed rate, 200 KHz voltage pulse frequency, 20Hz PZT vibration frequency with 0 to 50µm range of PZT vibration amplitude of wire vibration. The influence of PZT vibration amplitude on number of micro-sparks observed as shown in **figure4.7.**
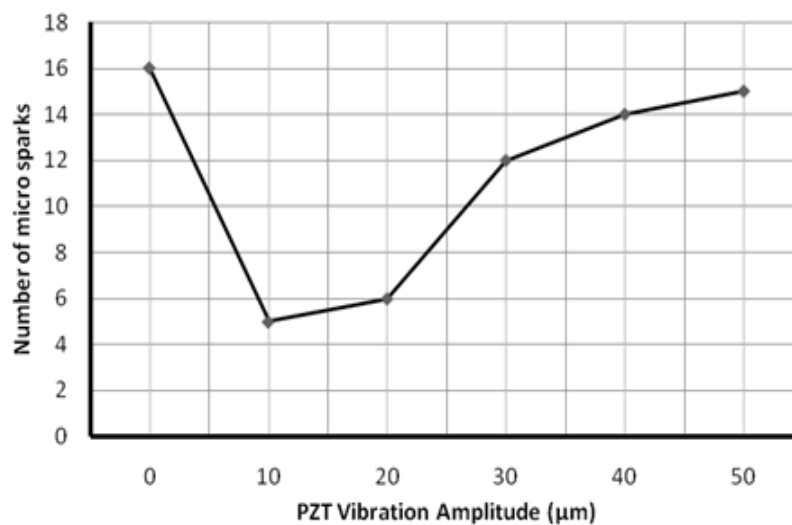
Figure 4.7 Influence of PZT vibration amplitude on number of micro sparks

It is observed that when vibration amplitude is lower than 10µm, pressure waves are too low to renew electrolyte completely in machining gap, hence micro-sparks occurs with high frequency with unstable processing stability and range of 10 to 20µm micro-tool vibration amplitudes generates quite less micro-sparks which leads to better processing stability during micromachining. However, in the case of the amplitude is higher than 20µm, number of micro-sparks between the tool and the workpiece increases due to radial swing of the wire electrode, and hence the processing stability becomes very poor.

4.2.1.6 Fabrication of microslit with controlled parametric conditions

As IEG is 100µm which is quite large, it has taken a considerable amount of time to overcome the effect of micro sparks and to reduce the chances of overcut at the entry point of machining but microslit is quite smooth and homogeneous as shown in **figure4.8.**
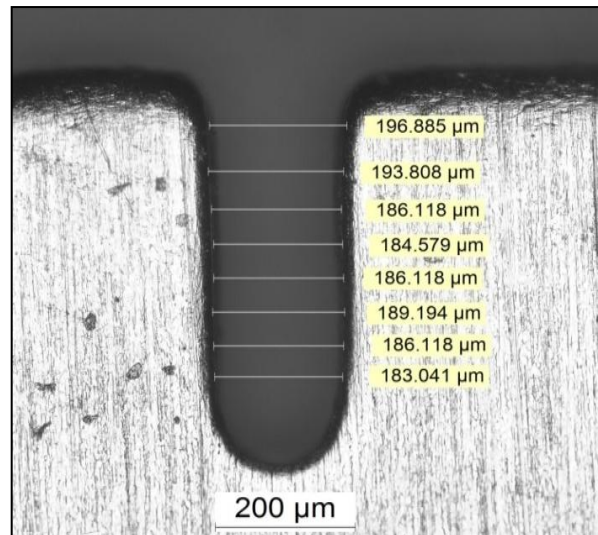
Figure 4.8 Micro-slit fabricated with controlled parametric condition

After finding out the influence of various predominant machining parameters and using controlled parametric combination of 6V voltage, 1.4μm/sec feed rate, 250 KHz voltage pulse frequency, 20Hz PZT vibration frequency, 10μm PZT vibration amplitude, microslit has been fabricated.

4.3 Experimental planning II: Insulation methods

4.3.1 Principle of insulation method for WECM

Figure4.9 illustrates the principle of WECM for uncoated wire. The double-layer equivalent circuit made up of distributed capacitances and resistances forms at electrode and electrolyte interface. The electrolyte solution receives some positive ions from the metal electrodes. This results in an excess of negative charge on the electrode from the electrons involved in ion production. The positively charged ions in the electrolyte solution are subsequently drawn to the electrode's negative charge. The electrical potential within the electric double layer has a maximum value on the stern layer. The potential drops with the increase of distance from the surface and reaches zero at the boundary of the electric double layer affecting machining quality during WECM. During the machining process, the pulse generator is used to dissolve material into metallic ions by electrochemical reactions between the cathode wire and the anode workpiece, which are separated by a thin inter-electrode gap (IEG). The required shape can be obtained by using a scheduled path. Beyond this, hydrogen gas bubbles and sludge are generated during the reaction. Therefore, in this study, to enhance mass transport and increase flushing efficiency for the disposal of sludge and renewal of fresh electrolyte in the machining gap, vibration-assisted axial nozzle jet flow is executed to take advantage of both axial flushing and vibration during the machining process**.** Also, the stray current

has significant impact produces poor machining accuracy and surface quality at uncoated wire condition with more overcut on obtained microfeatures.
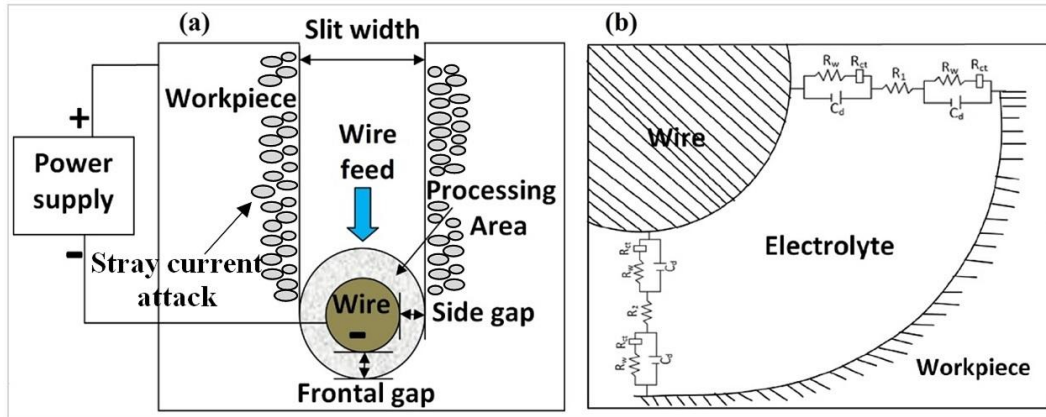
Figure 4.9 WECM principle for uncoated wire with double layer equivalent circuit

According to the theory of electrochemical double layer, the charging voltage U_c can be expressed as follows:

$$U_c = U_0 \left(1 - e^{-\frac{t}{\tau}} \right) \tag{4.1}$$

$$\tau = R_{eq} \, C_d \, \propto \frac{C_d}{k} \Delta_s \tag{4.2}$$

Where, U_0, a steady-state potential that depends on the power's output characteristics and amplitude of the supplied pulses; τ, the time constant of an equivalent circuit of a double layer which is equal to the product of circuit resistance and capacitance; t, charging time; k, actual electrolyte conductivity; R_{eq}, the equivalent resistance of the circuit; C_d, double layer capacitance; Δ_s, inter-electrode side gap. The insulation on the wire electrode surface and coating distance from the workpiece upper surface can be a most efficient approach to increase machining accuracy. In this method, current can be precisely released from the required machining area. The schematic for WECM principle for insulation method is shown in **figure4.10.** Due to the precise and long-lasting insulation of the wire electrode at narrow IEG in the machining zone, the insulating layer prevents current from flowing in unwanted areas of wire electrode acting as a barrier in an electric circuit and concentrates the current flux lines at machining zone at varying insulation distance from workpiece upper surface and uniform electrolyte conductivity, eliminating the effect of secondary counterfeit current on the sidewall of the electrodes results in reduction of stray current attack as shown in **figure4.10 (a) and (b).** The side gap for 360^0 exposed wire angle is largest which further reduces with reduction in angle i.e. 180^0, 150^0, and minimum at 90^0 as shown in **figure4.10 (c).** The lower exposed wire angle has a tendency to minimize stray corrosion to a larger extent due to controlled

current density distribution near the machining zone at narrow IEG with significant improvement in machining accuracy with minimum overcut due to less side gap.
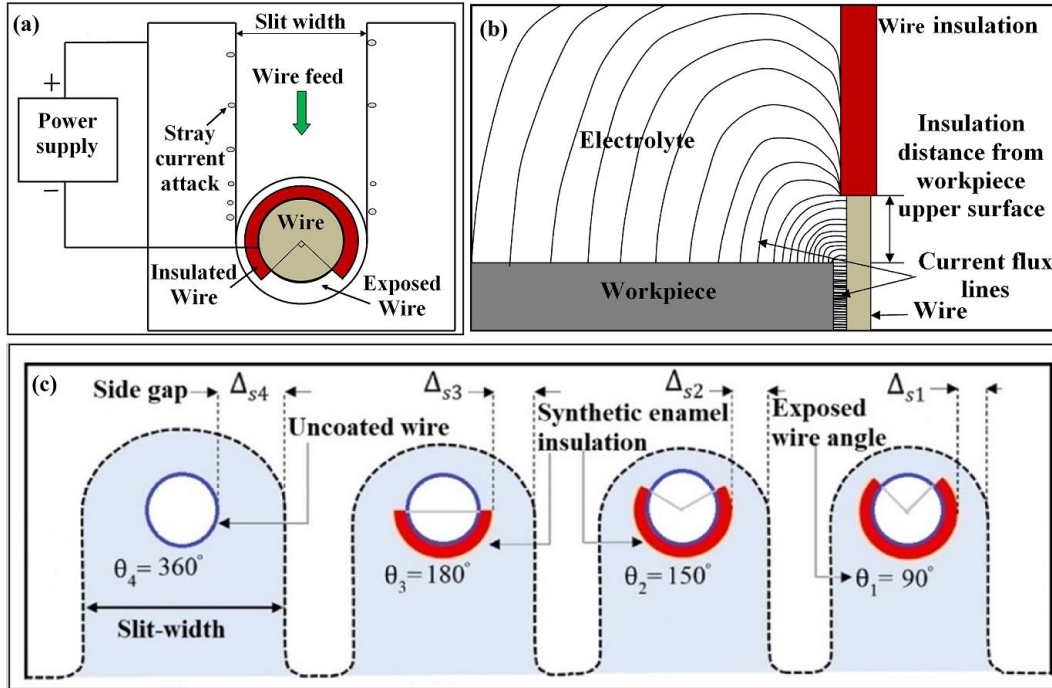
Figure 4.10 WECM principle for insulation method

The slit width of fabricated microslits is used to evaluate the machining accuracy of WECM during machining with the effect of wire feeding and different energy input parameters i.e. pulse voltage, pulse frequency, duty ratio and wire feed rate, which can be defined with a mathematical model shown in figure4.1 as follows **[48]**;

$$W_S = d_w + 2\sqrt{2d_w \frac{\alpha k_e (D_r - \tau f)V}{f_w} + \left(\frac{\alpha k_e (D_r - \tau f)V}{f_w}\right)^2} \tag{4.3}$$

$$W_S = d_w + 2\Delta_s \tag{4.4}$$

$$\text{Overcut} = 2\Delta_s \tag{4.5}$$

$$\text{Overcut} = 2\sqrt{2d_w \frac{\alpha k_e (D_r - \tau f)V}{f_w} + \left(\frac{\alpha k_e (D_r - \tau f)V}{f_w}\right)^2} \tag{4.6}$$

Where, W_S, slit width; d_w, the diameter of wire electrode; α, volumetric electrochemical equivalent; k_e, electrolyte conductivity; D_r, duty cycle; τ, double layer charging time; f, applied frequency; V, applied voltage; f_w, wire feed rate. This model shows that an increase in pulse voltage and duty cycle increases overcut. Also, it is seen that increase in wire feed rate results in a decrease in overcut. The results are validated with the experimental investigation for the effect of these parameters and compared with different wire insulation methods.The actual WECM machining process with PTFE pipe tube

insulation is shown in **Figure4.11.** All the experimental investigation using novel wire insulation methods has been carried out using this in-house developed setup.
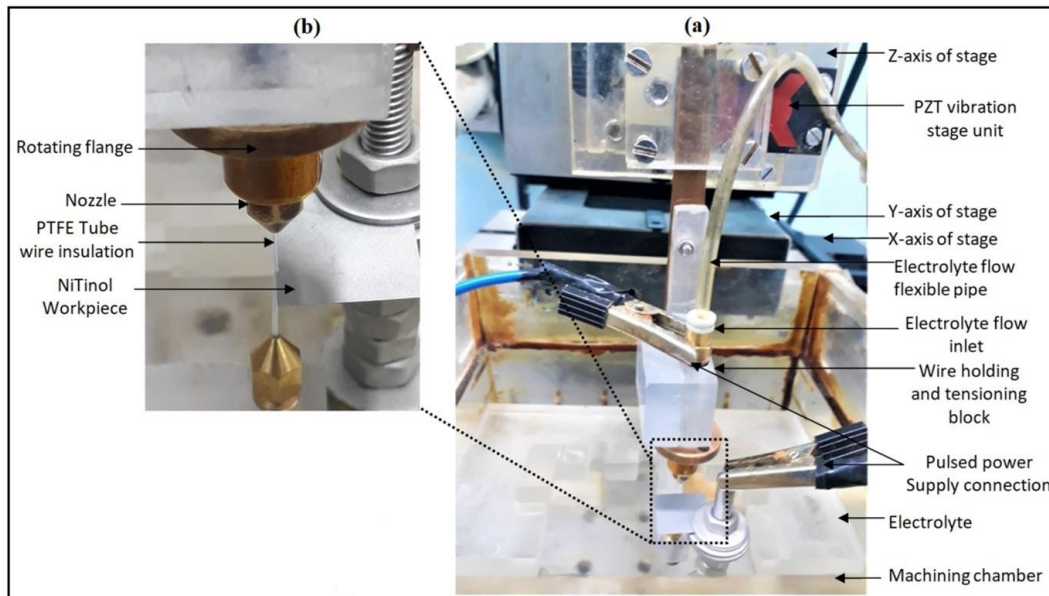
Figure 4.11 Actual WECM machining process with PTFE pipe tube insulation

4.3.2 Simulations for insulation

Wire electrochemical machining operation is simulated in COMSOL multi-physics software to analyze the distribution of electrolyte potential and current density distribution on the surface of workpiece at narrow IEG in the machining zone using primary current distribution and deformation geometry chemical electro-deposition module with stationary study. The parameters used in the calculations are listed in **Table4.2.**

The electrolyte potential and current density distribution in the machining gap for different coating angles and coating distances were simulated using this model with following assumptions:

    (i) The IEG in WECM is same for the different kind of coating methods and coating parameters,

    (ii) The electrolyte in the narrow IEG in machining zone is clean, without any electrolysis products, bubble formations and electrolyte has a single phase flow. The electrolyte conductivity and temperature are assumed to be constant,

    (iii) The simulation is a static process with stable electrical parameters without any deformation on the slit boundary,

    (iv) The concentration polarization, the electrochemical polarization, and the boundary effect are negligible,

(v) Electrode surfaces are formed on the cathode and the anode, and the other boundaries are considered as zero flux.

Table4.2 Simulation parameter machining Conditions

Parameters	Values
Concentration of electrolyte	0.1 M H_2SO_4
Electrolyte density	1.83 gm/cm^3
Electrolyte electrical Conductivity	3.66 S/m
Work material density (SS304)	8.03 gm/cm^3
Molar mass (SS304)	9779.825 g/mol
Workpiece electrical conductivity	1.37 x 106 S/m
(SS304) Slit width	120 μm
Workpiece relative permittivity	1.002
Initial IEG	40 μm
Applied anode Potential	7 V
Coating exposed wire angle	90°, 360°
Coating distance from workpiece surface	100 μm, 400 μm
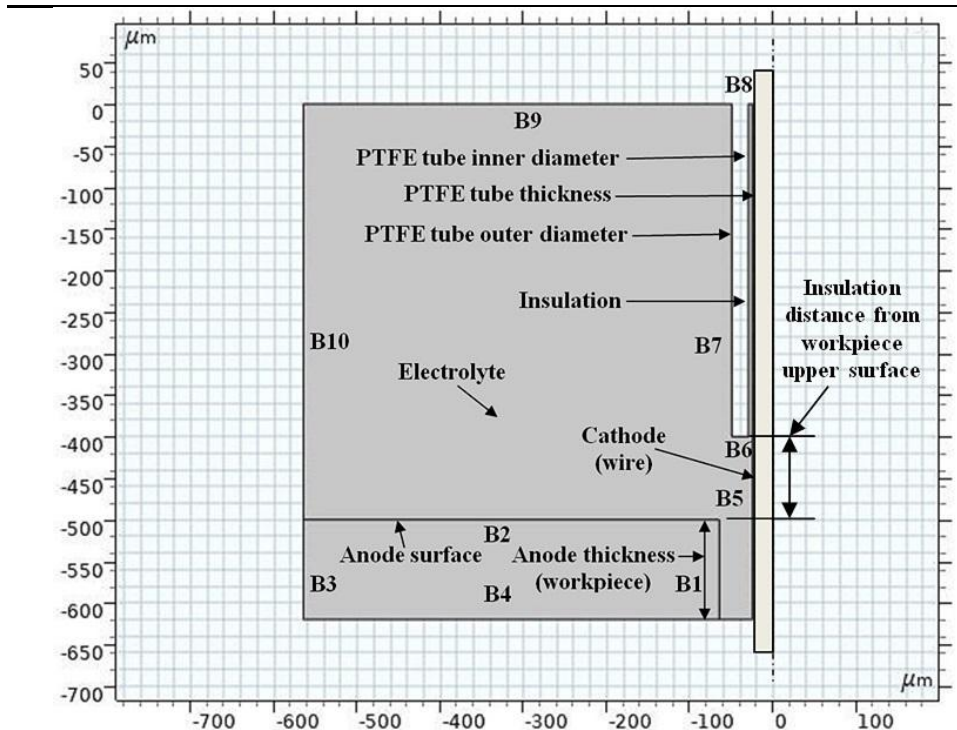
Figure 4.12 Geometric model of electric field for insulation distance from workpiece upper surface

The electric potential, namely, $\emptyset(x, y)$, within the region Ω can be described by Laplace's equation. That is $\Phi(x, y)$ is the potential distribution function in electrolyte domain.

$$\Omega: \nabla^2 \emptyset = \frac{\partial^2 \emptyset}{\partial x^2} + \frac{\partial^2 \emptyset}{\partial y^2} = 0 \tag{4.7}$$

2-D model indicating X–Y plane of the geometry as shown in **figure4.12** has been considered for simulation using different coating and insulation distances from the upper surface of the workpiece and for assigning different boundary conditions and listed in **Table 4.3.**

Table 4.3 Simulation boundary Conditions for exposed wire angle

Boundary no.	Boundary condition	Mathematical form
B1,B2,B3,B4	Anode (Positive terminal)/ Workpiece surface	$\emptyset = E$ (7V)
B5	Cathode (Negative terminal)/ Wire electrode surface	$\emptyset = 0$ (0V)
B3.B7.B8	Electrical Insulation (Synthetic enamel (Varnish)/ PTFE tube)	$\frac{\partial \emptyset}{\partial \emptyset} = 0$
B9, B10	Zero Flux (The boundary conditions)	$\frac{\partial \emptyset}{\partial \emptyset} = 0$

Using electrolyte potential and current density distribution for PTFE tube insulation at a distance of 400 μm and 100 μm from the surface of the workpiece, respectively, the views in **figure4.13** and **figure4.14** illustrate the deformed geometry that is created in front of the wire. The PTFE insulating tubes are closed to both sides of the workpiece surfaces and it is hollow inside to allow the wire electrode to pass through constant inner and outer diameter. The distribution of electric field lines near the cathode indicates the presence of stray current, which prevents the dissolution from localizing and significantly reduces the machining accuracy, as shown by the contour in the electrolyte domain at the initial stage of machining in static condition. According to **figure4.13**, material removal may take place in the area where the dispersion of electric flux lines is farther from the tool, 400 μm from the workpiece upper surface. The process of material dissolution is stopped if the conductivity of the electrolyte is sufficiently decreased so that the current density over this zone is below a threshold value. These coating techniques will localize

the distribution of the electric field and somewhat lessen the effect of stray current on the workpiece surface. The current density distribution changes with the change of the coating distance from the workpiece surface. The closer is the distance from the workpiece surface; the smaller is the current density distribution range as shown in **figure4.14**.
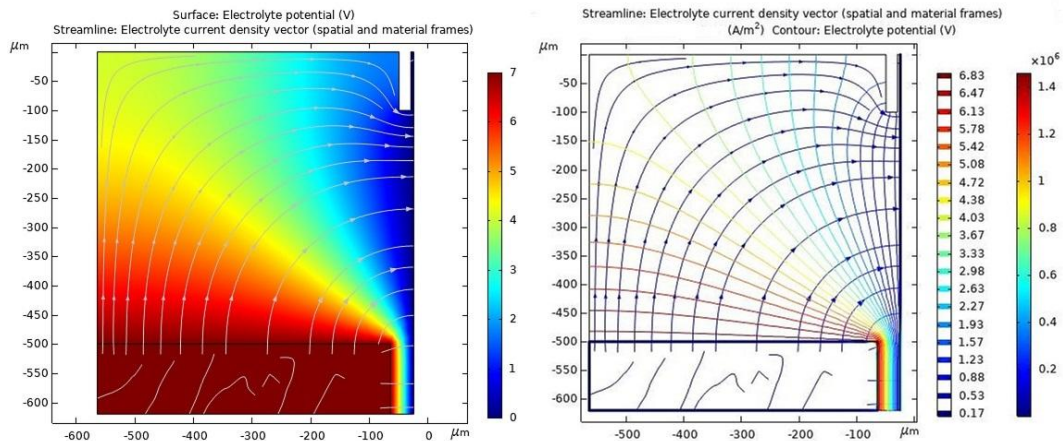
Figure 4.13 Simulation analysis of the current density distribution in the machining gap at 400µm insulation distance from workpiece surface
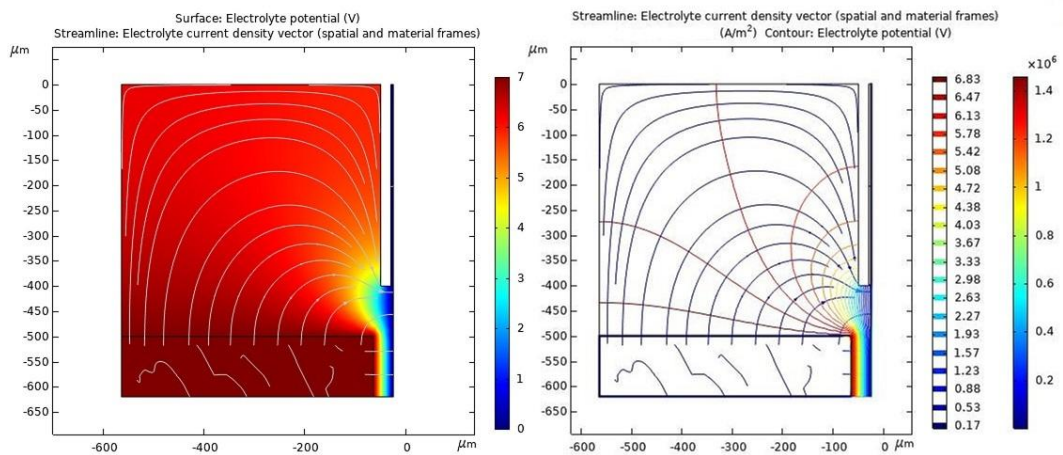
Figure 4.14 Simulation analysis of the current density distribution in the machining gap at 100µm insulation distance from workpiece surface

The synthetic enamel coating and PTFE insulating tube can limit the current density distribution and lower the chance of stray-current attacks on the workpiece surface, resulting in a greater surface quality. Further, in order to study insulating wire efficiency in reducing the stray current effect and overcut, the process is simulated for different coating exposed wire angle. **Fig4.15** shows X–Y plane of the geometry considered for simulation using different coating exposed wire angle and boundary conditions for a 2-D case of this problem are listed in **Table4.4.**
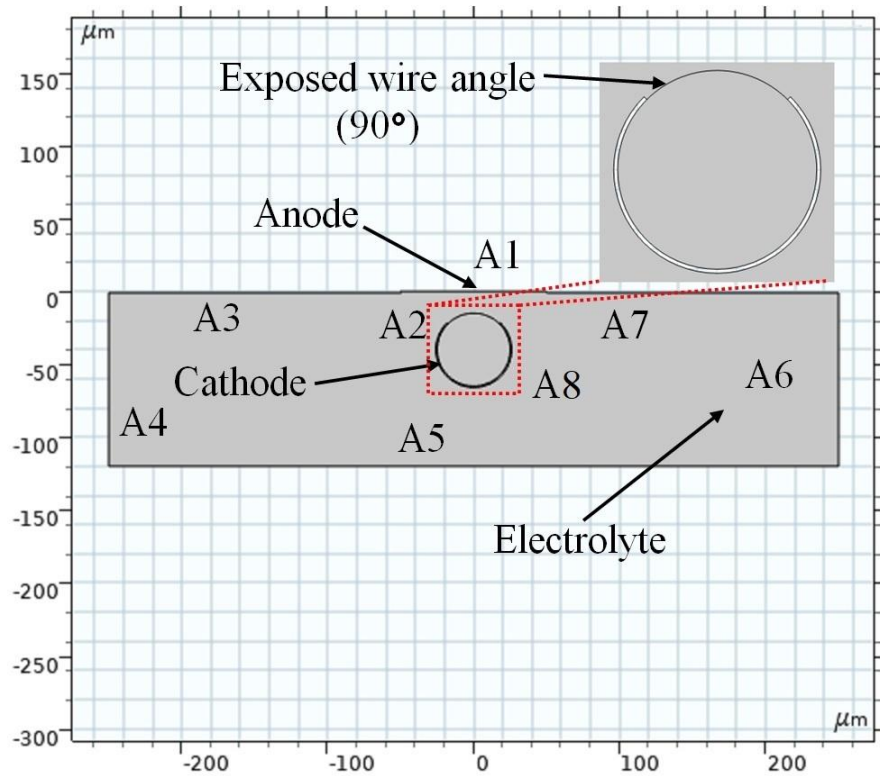
Figure 4.15 Geometric model of electric field for exposed wire angle

Table 4.4 Simulation boundary conditions for exposed wire angle

Boundary no.	Boundary condition	Mathematical form
A1	Anode (Positive terminal)/ Workpiece surface	$\emptyset = E$ (7V)
A2	Cathode (Negative terminal)/ Wire electrode surface	$\emptyset = 0$ (0V)
A8	Electrical Insulation (Synthetic enamel (Varnish)/ PTFE tube)	$\dfrac{\partial \emptyset}{\partial \emptyset} = 0$
A3, A4, A5, A6, A7	Zero Flux (The boundary conditions)	$\dfrac{\partial \emptyset}{\partial \emptyset} = 0$

Figure4.16 and **figure4.17** show views of deformed geometry created in front of wire by representing electrolyte potential and current density distribution for uncoated wire (360° exposed wire angle) and 90° exposed wire angle respectively. The distribution of electric field lines near the wire indicates the existence of stray current, which prevents the dissolution from localizing and severely reduces the machining accuracy and surface quality, as seen by the contour in the electrolyte domain during the first stage of

machining. The process is reproduced by insulating the wire, leaving just a portion of it (the exposed angle) open to participate in electrochemical dissolution in order to examine the efficiency of wire insulation in minimizing the stray current effect.When the coated exposed wire angle is 90° for electrochemical dissolution, the lowest value of slit width can be obtained due to controlled current density distribution near the machining zone as shown in **figure4.16.** The highest value of slit width can be obtained at maximum value of exposure angle (360°) for bare wire electrode as shown in **figure4.17.** It shows that with an increase in wire exposed angle, slit width also increases. Thus, wider slit widths are obtained with bare tool or tool with minimal insulation. Also, minimum overcut can be obtained with maximum portion of the wire electrically insulated.
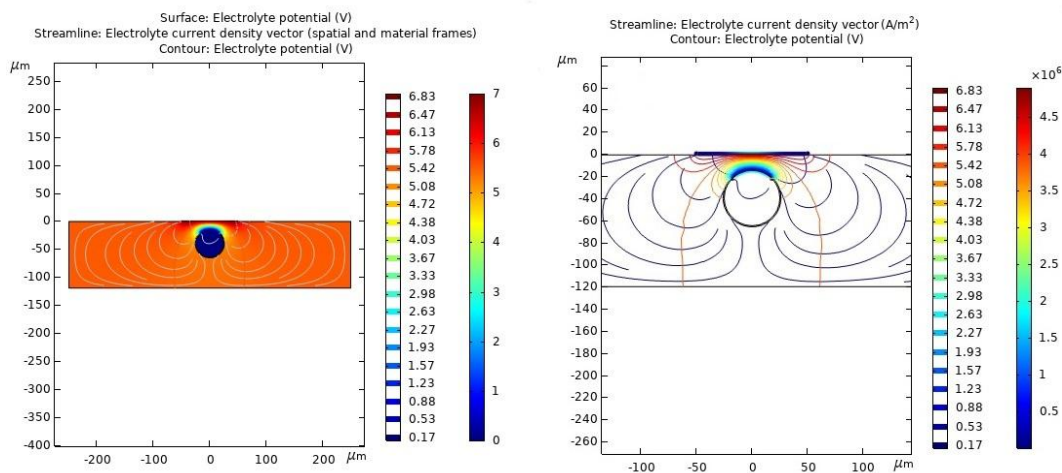
Figure 4.16 Simulation analysis of the current density distribution in the machining gap at 90° exposed wire angle
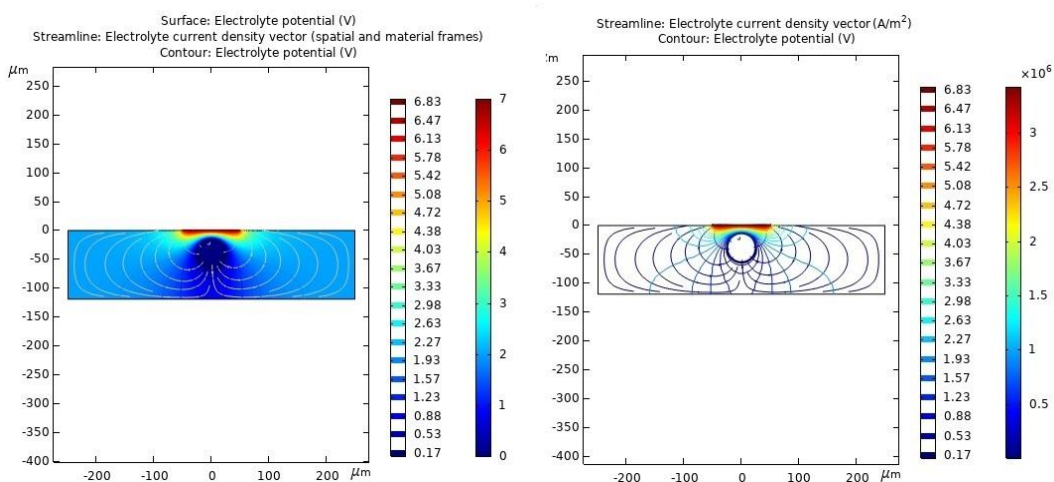
Figure 4.17 Simulation analysis of the current density distribution in the machining gap for without wire coating at 360° exposed wire angle

With the increase in wire exposed angle, the overcut is observed to increase. As the area of cathode available for machining increases, the magnitude of the current flowing in the circuit also increases leading to an increase in MRR, and hence, increase in overcut has been obtained. Another important finding from the aforementioned study is that as the exposed angle increases, the rate of overcut and stray current attacks increases at a steadily declining rate until it becomes comparatively extremely low when the exposed angle surpasses 180°. This is mostly due to the fact that, after 180°, the exposed area grows from the wire back face, which is not right in front of the workpiece surface. The impact of exposed angle on MRR is lessened as a result. According to the aforementioned study, insulating the wire electrode allows for improved machining precision with little to no overcut and little stray current impact. The study conducted through simulation has been validated with experimental investigation using different coating exposed wire angles and distances from the workpiece upper surface within selected range.

Planning for validation

During experiments, the machining chamber is positioned on the bench and houses the appropriate electrolyte solution as well as the workpiece in a unique arrangement. The bench is used to keep the machining chamber in place and prevent it from moving around during experiments. In the specified block, the wire is held vertically straight with adequate tension with coating and insulation on non-machining portion at specific distance from the workpiece surface. An appropriate axial electrolyte flow system has been devised for regulating proper flow, and the wire holding and tensioning block has the configuration to attach the PZT for introducing tiny amplitude wire vibration during machining. The flushing system includes a pump connected to the electrolyte supply chamber through a flexible pipe to maintain the required flow with a flow meter. The DC pulse generator is used for generating various pulse types with variable pulse voltage, pulse period, duty cycle, etc. In the present work, a tungsten wire of Ø50 μm has been used as a tool electrode. The workpiece specimens were 15mm x 15mm x 0.1mm stainless steel SS304 sheets used for a better understanding of the effect of stray current and overcut in machined micro-slit. The electrolyte used for experimentation was 0.1M H_2SO_4. Experimentations have been carried out with a variable pulsed DC power supply. Microslits were machined and the effect of different wire coating and insulation methods for the analysis of stray current attack and overcut was considered for experimental investigation. In this experimental study, at first, high pulse voltage, high duty cycle, and inter-electrode gap were identified to carry out the experiments while keeping other

parameters fixed for all experiments. Working ranges of parameters were selected based on trial experiments for microslits machining to understand the effect for analysis of stray current attack and as well as the formation of overcut. Also, a comparative study and investigation have been planned with non-coated wire electrodes. Machining conditions are shown in **Table4.5.** The coating and insulating methods were experimentally verified for stray-current attack reduction and compared with the results of uncoated wire. From the analysis, synthetic enamel coating with a thin layer of coating thickness and a PTFE insulation tube with 60µm inner diameter and 100µm outer diameters were used.

Table 4.5 Process parameter machining Conditions

Parameters	Value
Workpiece material	SS 304, Nitinol SMA
Workpiece Thickness	100 µm (SS304), 190 µm
Wire Electrode Material	Tungsten smooth cylindrical
Diameter of Wire Electrode	Ø50 µm
Applied Pulse Voltage	5 to 12 V
Wire Feed rate	1.0 µm/sec to 1.8 µm/sec
Duty cycle	45 % to 60 %
Voltage Pulse frequency	250 KHz
Type and concentration of electrolyte	0.1 M H2SO4
Nozzle diameter	0.4 mm
Workpiece nozzle stand-off distance	5 mm
Electrolyte nozzle jet Flow rate	5 lph
IEG	40 µm to 100 µm
PZT Tool vibration frequency	20 Hz
PZT Tool vibration amplitude	12.94 µm
Insulating material for wire	Synthetic Enamel, PTFE
Exposed wire angle	90° to 360°
Insulation distance from workpiece upper	100 µm to 400 µm

All the experiments were planned for insulating tube and synthetic enamel coating distance from the workpiece upper surface and exposed wire angle with a comparative study of different electric input supply and wire feed parameters to fabricate microslits on 100µm SS304 samples. The fabricated micro-slits were measured by an optical microscope. The experimental trials were also carried out with varying initial inter-electrode gaps to understand the effect during different coating and insulating methods by electrode forward direction motion. All experimental parameters have been set accordingly and given the wire feed rates in the stage controller to move wire electrode towards workpiece to explore the influence of various parameters on generation of stray current attack and responsible for the production of overcut while machining is

considered. The oscilloscope is used for measuring various pulse power characteristics during tests. Other tools utilized in the research included a multimeter, stereo zoom microscope, and optical camera, among others.

4.3.3 Experimental observations and discussions

The stray current has the most visible influence in areas adjacent to the actual machining zone. The researchers have advocated using synthetic enamel coating on the additional segment of the wire electrode both above and below the workpiece to address this issue. However, there is always a risk of the coating layer being removed due to poor adhesion or the force generated by the electrolyte jet. The use of PTFE tube insulation in place of a synthetic enamel coating layer is recommended as a solution for this problem. The simulation has been done for understanding the flow of electrolyte potential and current density distribution through anodic dissolution process in the narrow inter-electrode gap using minimum and maximum range of coating angles and distances from workpiece upper surface at constant anode potential and initial IEG, during WECM. Further, for validating the simulation results, several experiments have been carried out for investigating the effect of different parameters with synthetic enamel coating and PTFE tube electrode insulation for the analysis of stray current attack in the region near the machining zone which is easily visible on the machined surface in microscopic views and reduction in overcut to improve machining accuracy, homogeneity, and surface quality during WECM and described as follows:

4.3.3.1 Effect of process parameters on overall performance

The effect of high pulse voltage

The effect of high pulse voltage on the generation of stray current attack and overcut has been experimentally investigated with a varying pulse voltage of 9 V to 12 V at 1.4 µm/sec wire electrode feed rate at 100 µm IEG, pulse period of 4 µsec and pulse width of 1.8 µsec with other constant machining parameters during WECM. **Figure4.18.** indicates that at the increasing pulse voltage, high pulse voltage leads to an increase in the overcut to a greater extent. It also reveals that an increase in the current signal from 0.06 A to 0.4 A at pulse voltage from 9 V to 12 V produces a significant increase in the current density distribution on the surface of the workpiece near the machining zone. Due to the increased current density distribution at a narrow IEG near the machining zone, the metal removal rate during the anodic dissolution process significantly increases resulting increase in the overcut of fabricated microslit. The deposition rate of electrolysis products during anodic dissolution on the workpiece upper surface is more due to the generation of

more sludge and dissolved products which lead to the sudden increase in stray current attacks on the upper surface of the workpiece.

Figure4.19 reveals that stray current attack on the upper surface of the workpiece is more at high pulse voltage with high current density distribution at the edge of the microslits near the machining zone. In addition, the quality of the edge of the machined slit at high pulse voltage is not quite uniform and homogeneous due to an uneven and higher range of current density distribution and accumulation of more electrolysis products in the narrow IEG. It is seen that the stray current zone in the fabricated microslit at 12 V is much higher than the microslit fabricated at 9 V. Also, the average slit width of 350 μm was obtained at 12 V which was significantly reduced to 310 μm for the pulse voltage of 9 V.

Figure 4.18 Effect of high pulse voltage on overcut and average current without wire coating
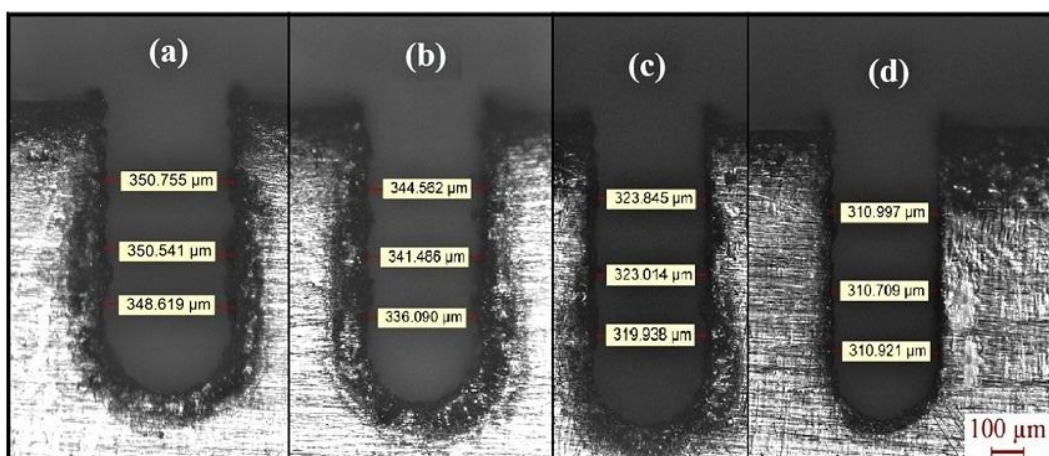
Figure 4.19 Fabricated microslits without wire coating with the following high pulse voltage conditions **(a)** 12 V **(b)** 11 V **(c)** 10 V **(d)** 9 V

It is clear that the appropriate current density distribution near the machining zone with a proper range of pulse voltage as per the requirement for anodic dissolution of workpiece material leads to a reduction in stray current attack and overcut and achieves better surface quality and machining accuracy during machining.

The effect of duty cycle

The duty cycle is directly related to the distribution of electric fields in the form of pulse duration and pulse period. A significant amount of hydrogen bubbles and dissolved products are produced per unit time when the duty cycle is high. They are unable to be removed from the microslit edges during machining time, resulting in an uneven current density distribution near the machining zone at narrow IEG. As a result, the stray current effect becomes more pronounced, resulting in poor machining quality. The overcut can be reduced to lower pulse duration and feed rate. The influence of duty cycle on stray current and overcut has been experimentally investigated using 9 V applied pulse voltage due to the less overcut and stray current attack based on results on effects of high pulse voltage without coating as discussed. To investigate the effect of duty cycle more clearly on overcut and duty cycle, the range of 45 % to 60 % of duty cycle with other constant machining conditions was selected and results are graphically represented as shown in **figure4.20.** It also reveals that an increase in the current signal from 0.16 A to 0.28 A at duty cycle from 45 % to 60 % increases the current density distribution linearly on the surface of the workpiece near the machining zone. Due to this, the metal removal rate during the anodic dissolution process significantly increases resulting increase in the overcut of fabricated microslit. Also, the effect of stray current is more prominent at high range of duty cycle.
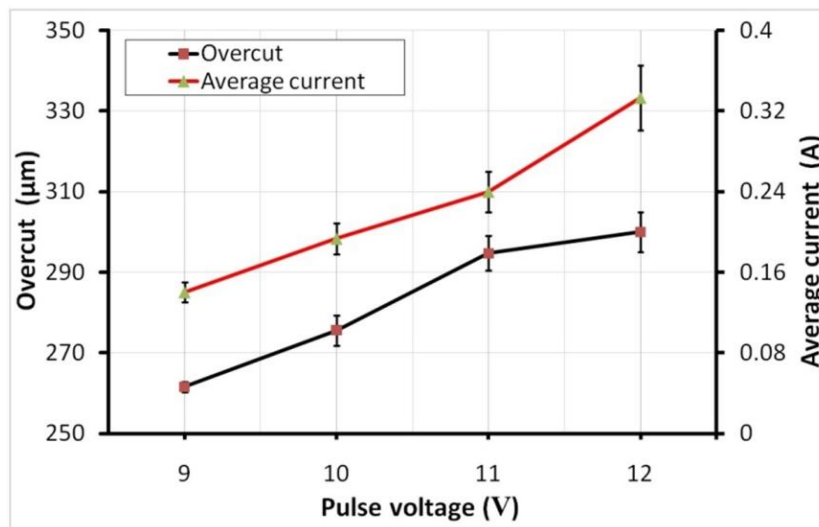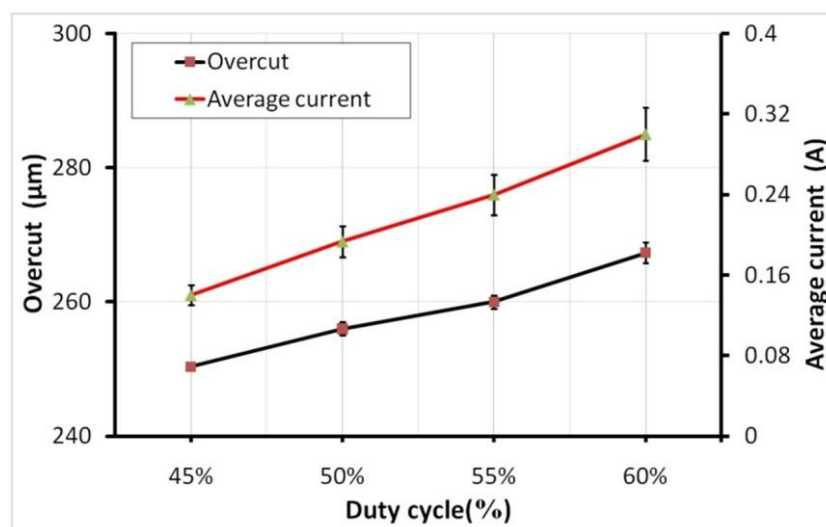

Figure 4.20 Effect of duty cycle on overcut and average current without wire coating
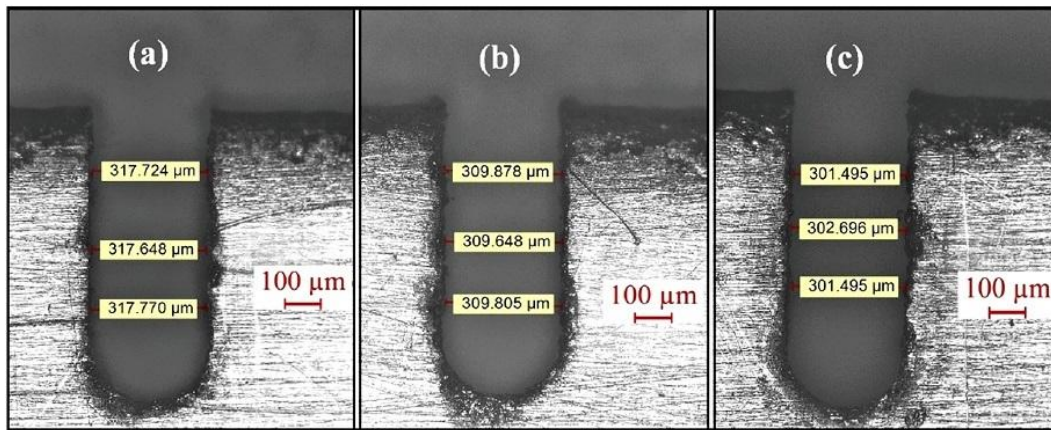
Figure 4.21 Fabricated microslits without wire coating and insulation with the following duty cycle **(a)** 60 % **(b)** 55 % **(c)** 45 %

The experiment result reveals that a minimum duty cycle of 45 % is recommended for reducing overcut for a stable machining operation with even electric field distribution in the machining zone. In addition, increasing the duty cycle from 45 % to 60 % increases the overcut in the machined microslit with the unstable process and uneven distribution of the electric field. The fabricated microslits shown in **figure4.21** indicate that the high duty cycle affects the machining quality during WECM with the increase in overcut.

The effect of initial inter-electrode gap

The effect of initial inter-electrode gap on stray current and overcut has been experimentally investigated using 7 V applied pulse voltage, 250 KHz pulse frequency with 45 % duty cycle, and 1.4 μm/sec wire feed rate due to the less overcut and stray current effect. These values of parameters were selected based on the previous experimental results to obtain higher machining accuracy and homogeneity for a better understanding of the anodic dissolution process during WECM for the effect of overcut and stray current effect. All these experiments were carried out with very thin synthetic enamel coating on the surface of wire electrode on both upper and lower side of wire electrode at approximately 500 μm distance. This synthetic enamel is kind of varnishes coated on the surface of the tungsten wire and cured to form electrical insulation film possessing certain mechanical strength, thermal resistant and chemical resistant properties.

From **figure4.22**, it is revealed that the increase in the initial inter-electrode gap (IEG) increases the overcut. In consequence, a decrease in initial IEG leads to the reduction of overcut. Due to narrow initial IEG, removal of electrolysis products becomes very difficult during electrochemical deposition on the surface of the workpiece which leads to

restriction of the further dissolution process, and the metal removal process gets stopped. As the wire electrode fed towards the workpiece in a forward direction for machining and initial IEG is very small below 20 µm, the electrode wire touches the workpiece cutting edge leading to the generation of heavy micro-sparks and pitting corrosion at the edge of microslits resulting in the reduction of machining quality. The average slit width of 183 µm at an initial IEG of 40 µm has been obtained which increases to an average slit width of 205 µm at an initial IEG of 100 µm as shown in **figure4.23.**
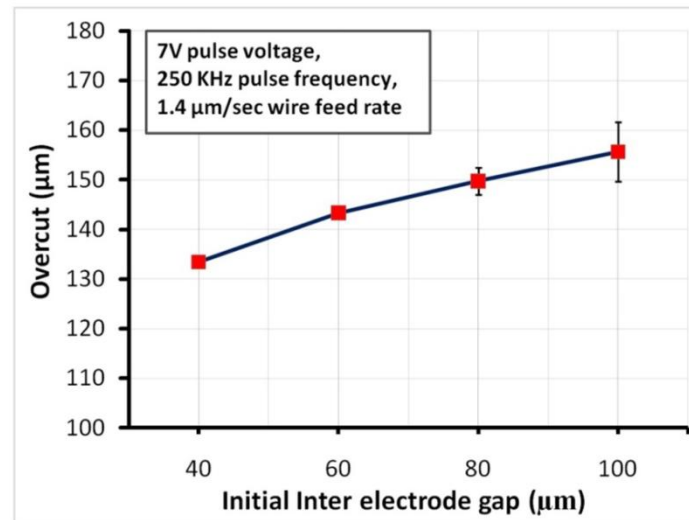
Figure 4.22 Effect of initial inter-electrode gap on average overcut
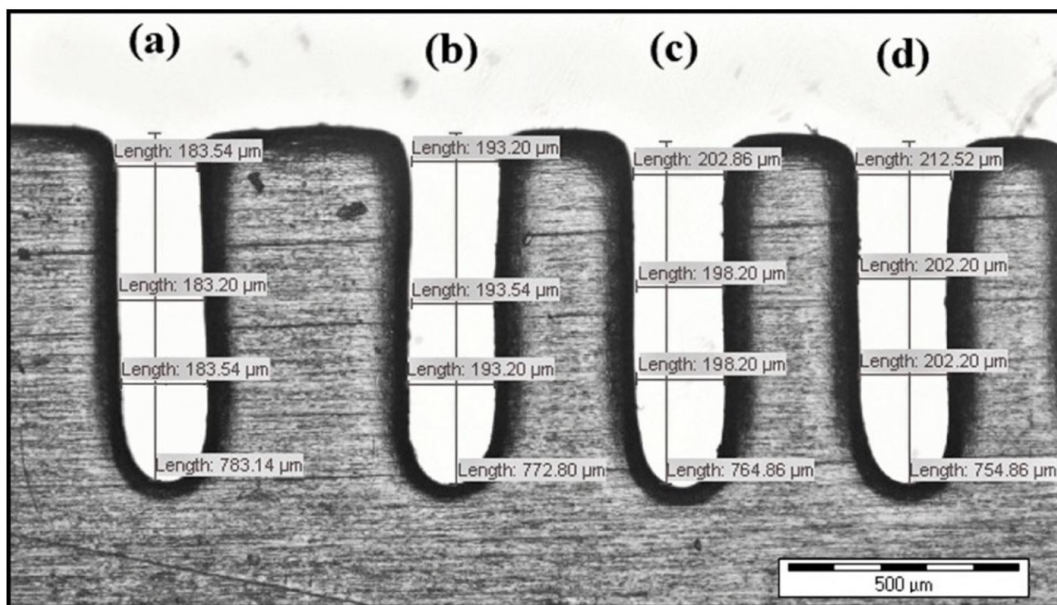
Figure 4.23 Fabricated microslits with synthetic enamel wire coating at the following initial inter-electrode gap conditions **(a)** 40 µm **(b)** 60 µm **(c)** 80 µm **(d)** 100 µm

The initial IEG has more effect on the stray current attack on the workpiece surface. It is clear from the experimental investigation that the initial IEG has a significant effect on the reduction of overcut during WECM.

4.3.3.2 Effect of synthetic enamel wire coating parameters

As per the above experimental investigation for the effect of high pulse voltage, duty cycle, and initial inter-electrode gap with synthetic enamel wire coating, it is observed that the effect of stray current and overcut has been significantly reduced. Therefore, the synthetic enamel is suitable as an insulation coating for WECM and further in-depth experimental investigation has been proposed to understand its effect on stray current and overcut with different wire coating features during WECM. The very thin layer of coating has been used to understand the effect of synthetic enamel coating wire on stray current and overcut. In the coating method, a diluted varnish enamel thin layer is sprayed over the wire electrode uniformly and the coating dries up for generating a strong protective layer of coating. Then the unwanted coating surface is cleaned to remove the remaining enamel as per the required exposed wire angle and coating distance. Also, the synthetic enamel coating exposed wire angle and coating distance from the upper surface of the workpiece is considered for analyzing stray current effect and overcut during WECM. The synthetic enamel coated wire with 90^0 exposed wire angle and 100 μm synthetic enamel coating distance from the workpiece upper surface is shown in **figure4.24.**
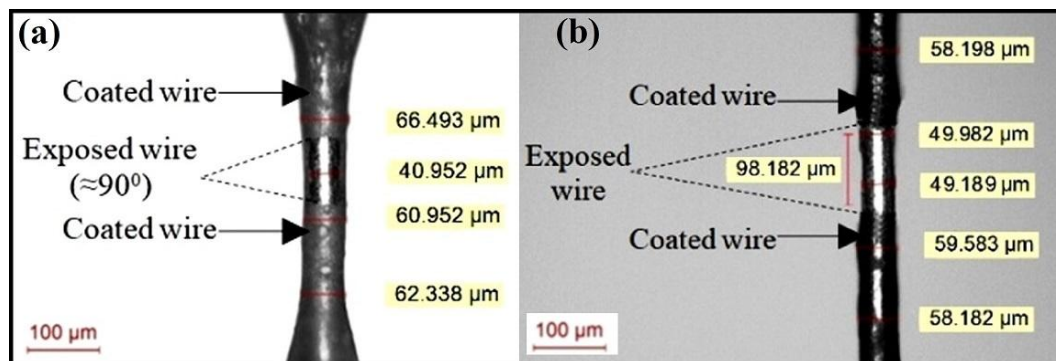
Figure 4.24 Wire electrode (a) exposed angle (90^0) (b) synthetic enamel coating distance

The effect of synthetic enamel wire coating distance from the upper surface of the workpiece

The experiments were carried out for analyzing the effect of synthetic enamel wire coating distance from the workpiece upper surface under bare wire electrode conditions. The parametric combination of 7 V pulse voltage, 250 KHz pulse frequency, and 1.4 μm/sec wire electrode feed rate with other constant machining conditions and synthetic

enamel wire coating distance from 100 µm to 400 µm from the workpiece upper surface has been selected for the experimentations.
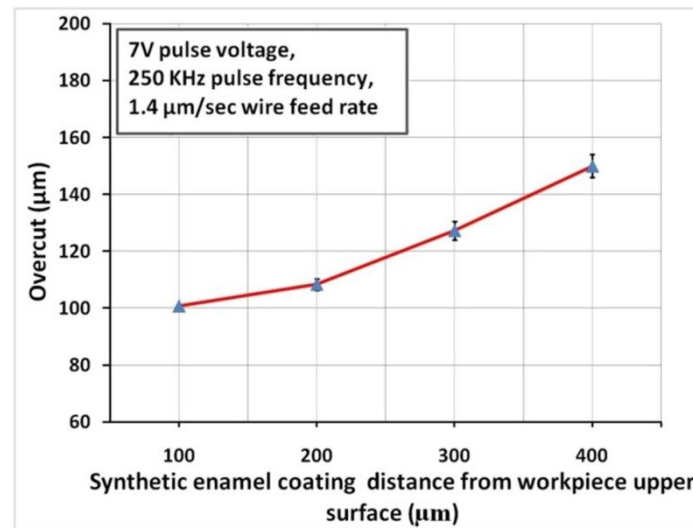
Figure 4.25 Effect of synthetic enamel coating distance from workpiece

upper surface on overcut
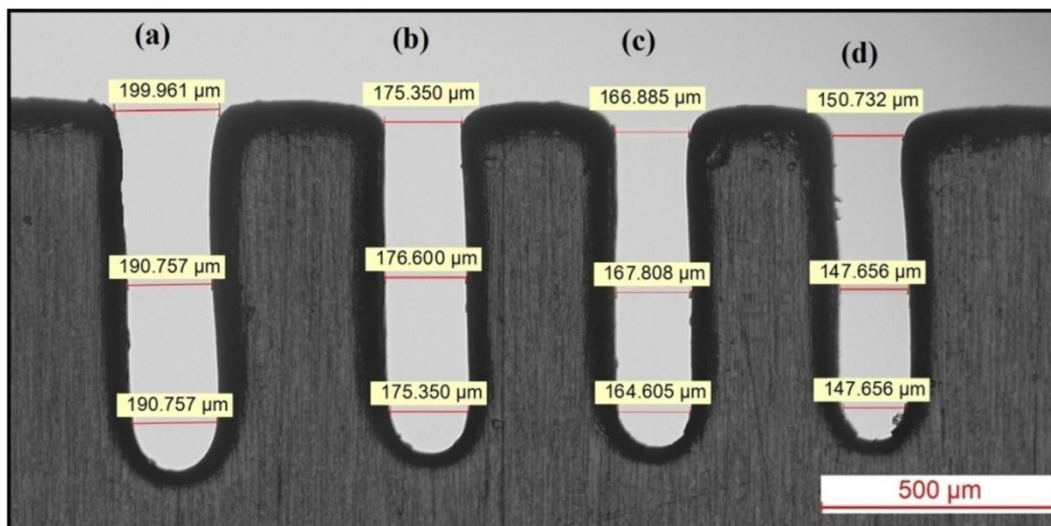
Figure 4.26 Fabricated microslits with synthetic enamel coating at following conditions of workpiece upper surface coating distance (a) 400 µm (b) 300 µm (c) 200 µm (c) 100 µm

From the experimental results, it is revealed that the overcut of fabricated microslits is minimum at 100 µm synthetic enamel wire electrode coating distance from workpiece upper surface and overcut increases with increase in the distance as shown in **figure4.25.** The average slit width of 147 µm was obtained using 100 µm synthetic enamel wire electrode coating distance from the workpiece upper surface which further increases to average slit width of 190 µm at 400 µm distance. Also, the homogeneity and machining accuracy of fabricated microslit at 100 µm is higher compared to the 400 µm synthetic

enamel wire electrode coating distance from the workpiece upper surface. Further, it is observed that the negligible stray current effect on fabricated microslits is seen only at the edge of the microslit and its minimum compared to the uncoated wire electrode as shown in **figure4.26.**

The effect of exposed wire angle

The coating was carried out under the closed microscopic observation for exposed wire angle in the range of 90^0 to 360^0 (bare wire electrode) with a very thin layer of thickness of coating with 100 μm synthetic enamel coating distance from the workpiece upper surface and parametric combination of 7 V pulse voltage, 250 kHz pulse frequency and 1.4 μm/sec wire electrode feed rate with other constant machining conditions. The effect of synthetic enamel coating exposed wire angle with overcut is shown in **figure4.27.** The experimental results reveal that overcut is minimum at 90^0 coating exposed wire angle and it is increased with increase in coating exposed wire angle with maximum overcut at 360^0 coating exposed wire angle (bare tool) wire electrode. Also, machining accuracy is better at 90^0 coating exposed wire angle compared to other increasing exposed wire angles.
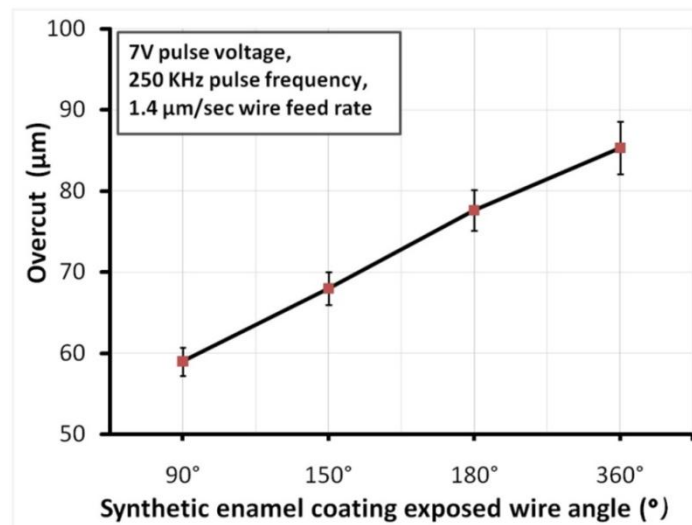
Figure 4.27 Effect of synthetic enamel coating wire exposed angle on overcut

The less overcut during 90^0 coating exposed wire angle may be due to controlled current density distribution and current flux line are uniform in the narrow IEG which is responsible for stable machining process throughout the machining operating condition. It greatly reduced the side gap of the microslits resulting in minimum overcut at 90^0 coating exposed wire angle and increasing with an increase in angle. The fabricated homogeneous microslits with reduced overcut and higher machining quality were also obtained as shown in **figure4.28.**
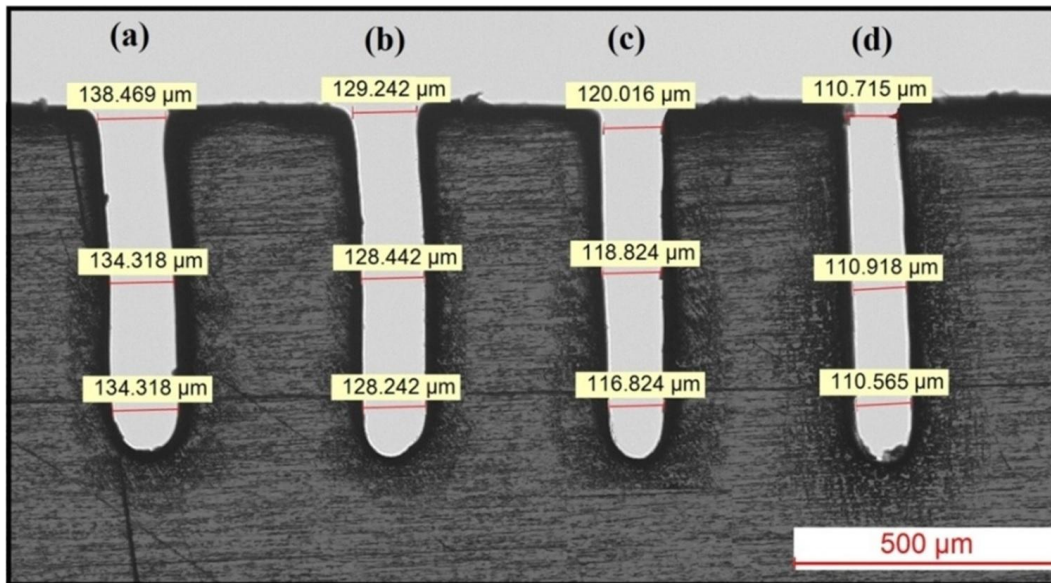
Figure 4.28 Fabricated microslits with synthetic enamel wire coating with the following conditions of exposed wire angles (a) 360^0 (b) 180^0 (c) 150^0 (d) 90^0

It is found that there is the least amount of pitting corrosion on the microfeatures surface when the synthetic enamel coating methods were used**.** The experimental results indicate that the proposed synthetic enamel coating method is quite efficient to reduce the stray current attack and overcut during WECM.
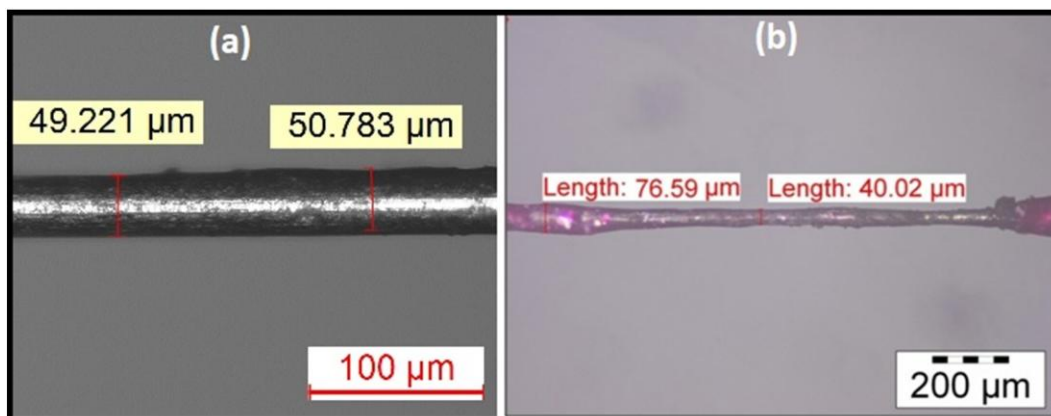
Figure 4.29 wire electrode (a) non-coated (b) synthetic enamel coating after machining

It is also observed that the synthetic enamel coating was removed during the machining process and affects the wire electrode due to the burning of synthetic enamel coating on the surface of the wire electrode. The diameter of the wire electrode was reduced from 50 µm to 40 µm after the removal of synthetic enamel coating in the machining zone as shown in **figure4.29.** It indicates that the wire etching process has been initiated during the machining process which results in the wire electrode getting a reduction in wire

diameter. Therefore, it is needed to explore the effectiveness of tube coating which may reduce the drawback of synthetic enamel coating during WECM.

4.3.3.3 Effect of PTFE tube wire insulation parameters

As the synthetic enamel wire electrode coating has some limitations due to burning and removal of the coating during wire electrochemical machining even though proved best than uncoated wire electrode for reduction of stray current attack and overcut. It happens when a current flows incorrectly due to uneven current density distribution anywhere other than the intended machining path. The above drawback can be avoided using a novel PTFE (polytetrafluroethylene) tube wire electrode insulation method. It has extreme chemical resistance with its inertness and durability, a massive temperature range with high thermal stability, outstanding corrosion protection and excellent electrical insulation properties. Also, it is eco-friendly material and provides excellent resistance to solvents, alkali and acids. The stray effect can be prevented by decreasing the electrical resistance near the machining zone.
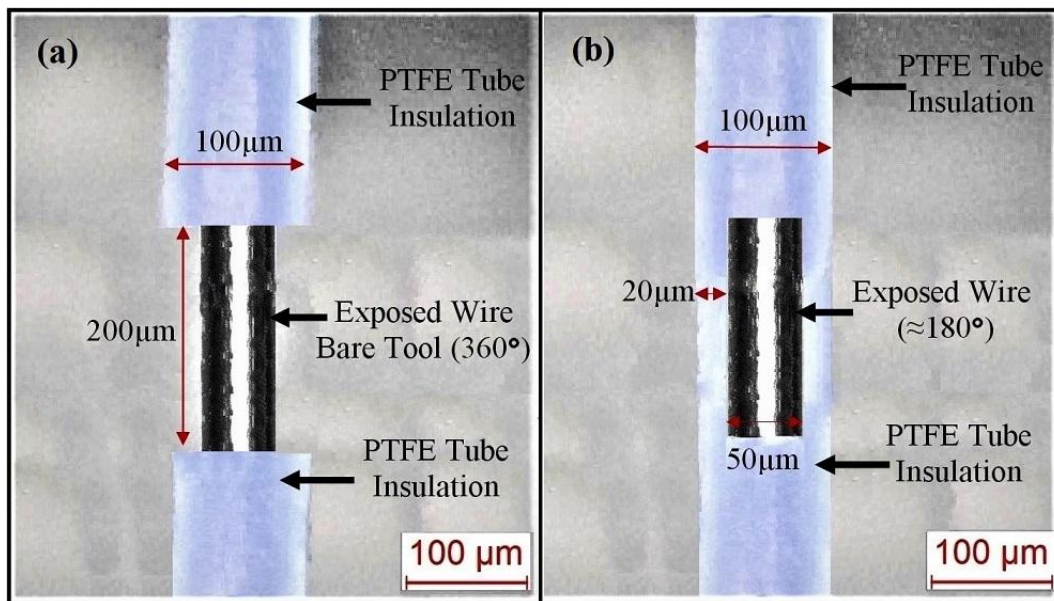
Figure 4.30 PTFE tube insulation **(a)** exposed angle (360^0) **(b)** exposed angle (180^0)

The outer and inner diameters of the PTFE tube are of utmost importance for the reduction of stray current effect and overcut during machining process. The PTFE tube insulation wire with 360^0 exposed wire angle and 180^0 exposed wire angle with insulation distance is shown in **figure4.30.** Using this method, the distribution of the electric field may be confined and the influence of stray current on the workpiece surface and overcut can be reduced to a great extent. The experiments are carried out with 100 µm outer diameter PTFE tube insulation with 60 µm inner diameter and microslits are fabricated

and effect of PTFE tube insulation distance from workpiece upper surface and exposed wire angle were investigated and results are discussed hereunder.

The effect of PTFE tube wire insulation distance from the workpiece upper surface

The experiments were carried out for the effect of PTFE tube insulation distance from the workpiece upper surface with bare wire electrode conditions. The parametric combination of 7 V pulse voltage, 250 KHz pulse frequency, and 1.4 µm/sec wire electrode feed rate, 45 % duty cycle with other constant machining conditions, and PFTE tube insulation distance from 100 µm to 400 µm from the workpiece upper surface was selected for the experimentations. From the experimental results, it is revealed that the overcut of fabricated microslits is minimum at 100 µm PTFE tube insulation distance from the workpiece upper surface and increases with an increase in the distance as shown in **figure4.31.**
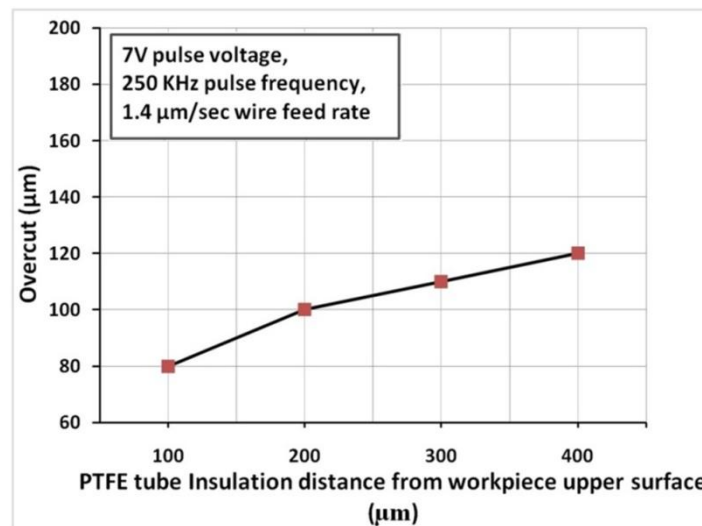
Figure 4.31 Effect of PTFE tube insulation distance from workpiece

upper surface on overcut

Further, the overcut of microslits can be reduced with a distance below 100 µm but it is very difficult to control the machining process due to nozzle jet flushing which may result in coverage of machining zone with the insulated portion of the wire electrode. The experimental results reveal that the closer the distance between the synthetic enamel coating and the workpiece, overcut is reduced to a greater extent with negligible stray current effect on the workpiece surface. The reduction in overcut was due to the uniform and required current density distribution with the parallel flow of current flux near the machining zone at narrow IEG. The average slit width of 130µm was obtained using 100 µm PTFE tube insulation distance from the workpiece upper surface which further increases to the average slit width of 170 µm at 400 µm distance as shown in **figure4.32**.

Also, the homogeneity and machining accuracy of fabricated microslit using PTFE tube insulation distance from workpiece upper surface is better compared to figure4.26. Further, it is observed that the stray current effect on fabricated microslits is seen only at the edge of the microslit and it is negligible compared to figure4.19, 4.21, 4.23, 4.26 and 4.28.
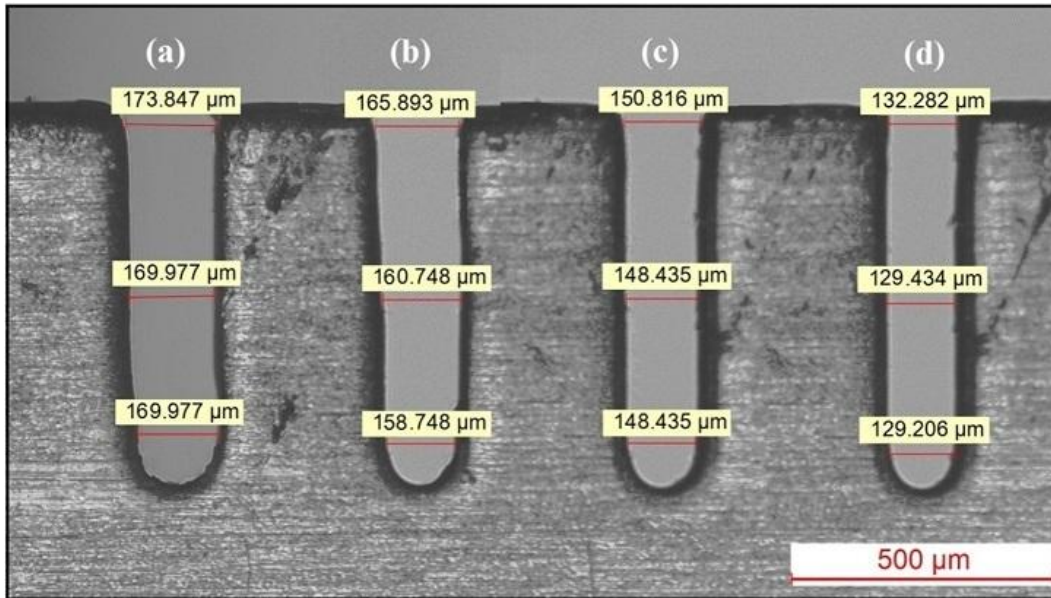
Figure 4.32 Fabricated microslits with PTFE pipe tube wire insulation with the following conditions of workpiece upper surface insulation distance (a) 400 µm (b) 300 µm (c) 200 µm (d) 100 µm

The stray current effect is negligible using PTFE pipe tube insulation compared to synthetic enamel coating This is maybe due to the uniform current density distribution during the process as the PTFE insulation has strong insulation capacity and synthetic enamel has a poor coating capability. The overcut of microslits fabricated with the PTFE tube insulation method at different insulation distances is less compared to the synthetic enamel wire coating for the same machining condition. Therefore, the PTFE tube insulation method is the most promising method for reducing overcut and stray current attacks during wire electrochemical machining for the fabrication of complex microfeatures.

The effect of PTFE tube insulation exposed wire angle

The experiments were carried out under the closed microscopic observation for exposed wire angles in the range of 180^0 and 360^0 (bare wire electrode) with 100 µm PTFE tube insulation distance from the workpiece upper surface and parametric combination of 7 V pulse voltage, 250 KHz pulse frequency and 1.4 µm/sec wire electrode feed rate with

other constant machining conditions. The use of 90^0 and 150^0 exposed wire angle was quite complicated due to the difficulty in maintaining it with PTFE tube insulation in micron level therefore it is not included in this experimental investigations. But it can be possible to use minimum exposed wire angle using some special mechanisms for micro cutting the edges of PTFE tube in required angle for required distance which may further improves the machining accuracy. The fabricated microslits using PTFE tube insulation exposed wire angle of 360^0 and 180^0 with reduced overcut with better machining quality is shown in **figure4.33.**
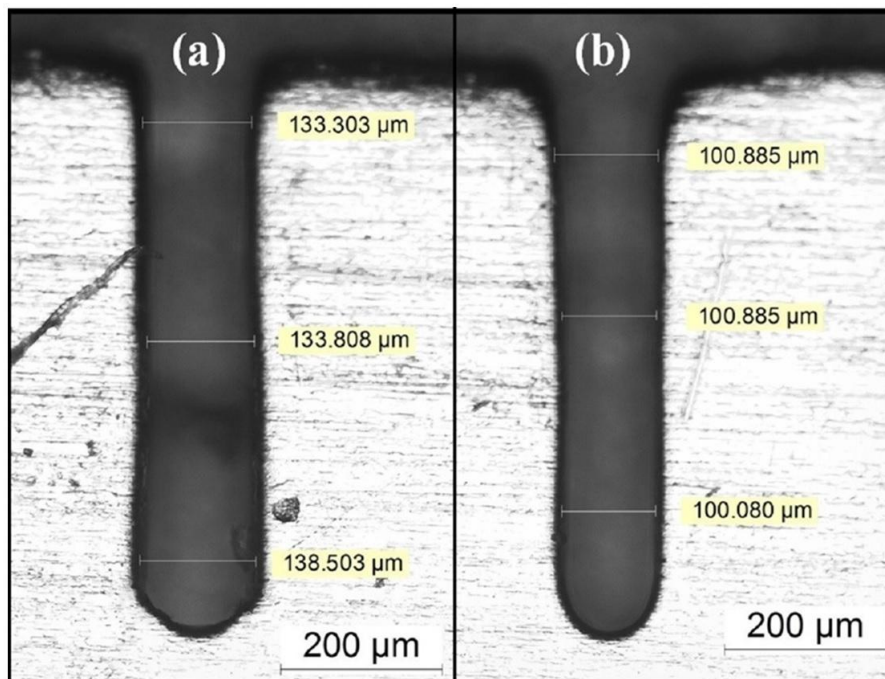
Figure 4.33 Fabricated microslits with PTFE tube wire electrode coating with the following conditions of exposed wire angles (a) 360^0 (b) 180^0

It is revealed from figure4.33 that overcut is minimum at 180^0 PTFE tube insulation exposed wire angle and it is increased with an increase in coating exposed wire angle 360^0 PTFE tube insulation exposed wire angle with better machining accuracy. The less overcut during 180^0 coating exposed wire angle may be due to controlled current density distribution and current flux line are uniform in the narrow IEG which is responsible for stable machining process throughout the machining condition and stable insulation efficiency throughout the machining process. It greatly reduced the side gap of the microslits resulting in minimum overcut at 180^0 coating exposed wire angle and increasing with an increase in angle. However, the effect of overcut reduction will be low as the coating exposed wire angle exceeds 180^0. This may be due to the increased exposed area from the back side of the electrode which is not in frontal IEG which results in

minimum MRR. But, as the coating strength and durability of the PFTE tube insulation is very high compared to synthetic enamel coating, there is no evidence of stray current effect and pitting corrosion observed in the fabricated microslits using the PTFE tube wire electrode insulation method.

4.3.3.4 Comparison of synthetic enamel coating and PTFE tube wire insulation with uncoated wire electrode

In WECM, stray current attacks and overcut in machined microfeatures play a significant task in efficient machining. The uniform and required current density distribution in the machining zone at a narrow IEG is difficult because improper wire electrode coating and insulation result in uncontrolled anodic dissolution.
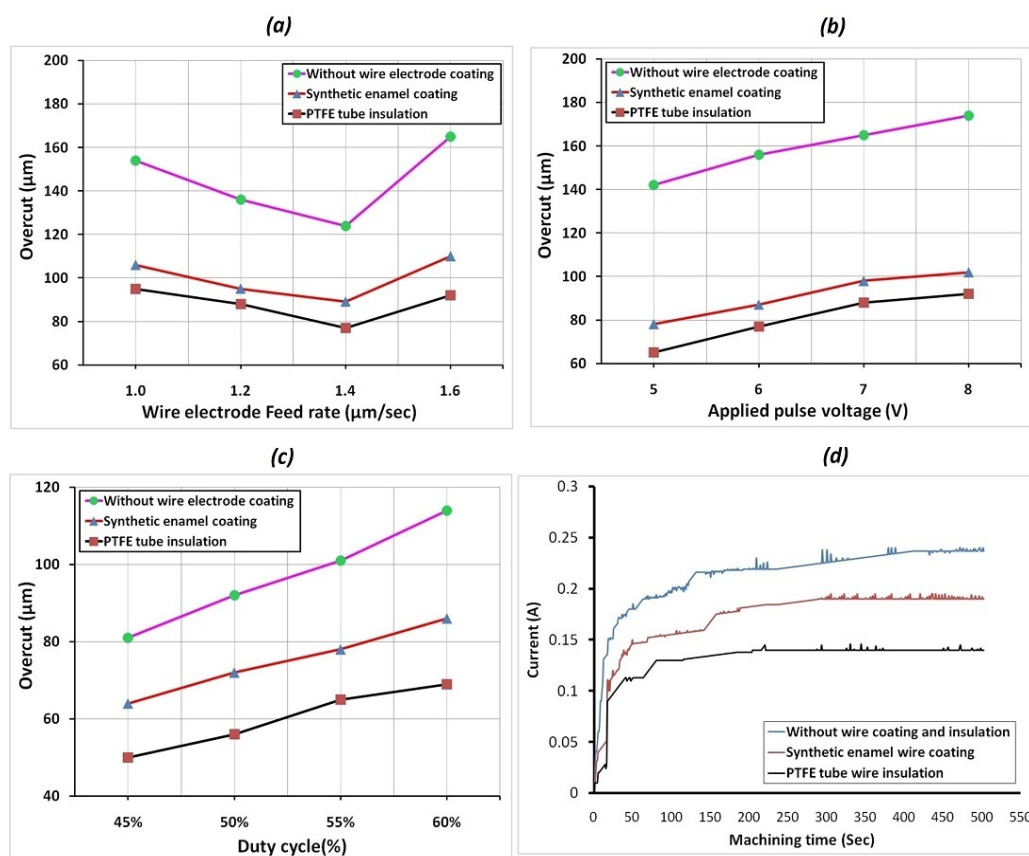
Figure 4.34 Effect of various parameters on overcut with different coating conditions

(a) Wire feed rate **(b)** Pulse voltage **(c)** Duty cycle **(d)** Machining time

Appropriate and efficient current density distribution in the machining zone is required for the reduction of stray current attacks and overcut for obtaining better machining accuracy and quality. Therefore, a basic comparison among various parameters responsible for appropriate current density distribution and the effect of different coating and insulation methods are focused on micromachining with WECM. Experimental results of different process parameters i.e. wire feed rate, pulse voltage, duty cycle, and

current signal with machining time using electrode coating and insulation methods and plotted graphically as shown in **figure4.34.** The 40 μm IEG was used for all the experiments. The results reveal that the PFTE tube wire insulation method has a great impact on reduction in stray current attack and overcut of fabricated microslits with better homogeneity and machining accuracy as discussed hereunder.

In these experiments, a wire electrode feed rate in the range of 1 μm /sec to 1.6 μm /sec with other machining conditions was used and the effect on stray current and overcut is shown in figure4.34 (a). The applied pulse voltage was 7 V and the duty cycle was 45 % for all the conditions. It is observed that the overcut is reduced with an increase in wire electrode feed rate from 1 μm /sec to 1.4 μm /sec in all three cases but overcut start increasing at 1.6 μm /sec may be due to the higher feed rate than the required for above parametric conditions. However, the overcut was greatly reduced with synthetic enamel and PTFE tube insulation method as compared to uncoated wire electrode. Further, the experimental investigation reveals that the overcut generated is less with the PTFE tube insulation method compared to synthetic enamel wire electrode coating. The minimum microslit overcut of 75 μm was obtained at a 1.4 μm /sec wire feed rate using the PTFE tube insulation method which increases to 90 μm for synthetic enamel and 125 μm for uncoated wire electrode during the WECM process.

Further, applied pulse voltage in the range of 5 V to 8 V with other constant parametric machining conditions has been used and the effect on stray current and overcut is shown in figure4.34 (b). The duty cycle was 45 % and the 1.4 μm/sec wire electrode feed rate for all the conditions. It is observed that the overcut increases with an increase in applied pulse voltage in all three cases. However, the overcut was greatly reduced with synthetic enamel and PTFE tube insulation method as compared to uncoated wire electrode. Further, the experimental investigation reveals that the overcut generated is less with the PTFE tube insulation method compared to synthetic enamel wire electrode coating. Also, if the applied voltage is over 8 V, machining control is too difficult and overcut increases to a greater extent with more effect of the stray current attack observed on the workpiece upper surface. The minimum microslit overcut of 64 μm was obtained at 5 V pulse voltage using the PTFE tube insulation method which is increased to 78 μm for synthetic enamel and 142 μm for uncoated wire electrodes during the WECM process. As the durability of PTFE tube insulation is much higher than synthetic enamel coating, there is even current density distribution in the machining zone at narrow IEG with no loss in electrolyte conductivity throughout the process during WECM. Whereas, synthetic

enamel coating may get removed due to current flux flow while machining results in uneven current density distribution.

Also, the duty cycle in the range of 45 % to 60 % with other constant parametric machining conditions was used and the effect on stray current and overcut is shown in figure4.34 (c). The IEG was 40 μm and the applied pulse voltage was 5 V for all the conditions. It is observed that the overcut increases with an increase in applied pulse voltage in all three cases. However, the overcut was greatly reduced with synthetic enamel and PTFE tube insulation method as compared to uncoated wire electrode. Further, the experimental investigation reveals that the overcut generated is less with the PTFE tube insulation method compared to synthetic enamel wire electrode coating. Also, if the duty cycle is below 40 % and above 60 %, machining control is too difficult and overcut increases to a greater extent with more effect of stray current attack and micro-sparks were observed on the workpiece upper surface. The minimum micro-slit overcut of 50 μm was obtained at 45 % duty cycle using the PTFE tube insulation method which is increased to 64 μm for synthetic enamel and 82 μm for uncoated wire electrodes during the WECM process.

The effect of the synthetic enamel coating and PTFE wire tube insulation with uncoated wire is studied for the received current signals to time for analysis of stray current attack during WECM as shown in figure4.34 (d). The parametric combination of 12 V and 60 % duty ratio is used to analyze the effect of machining time on the production of the current signal. The higher range of pulse voltage and duty cycle has been selected to understand the capability of all these methods to produce a higher range of current signals with even current density distribution throughout the process for more stable machining conditions. The current single produced at a higher value than required may lead to an increase in stray current attack and generates overcut due to more current density distribution near the machining zone. It is observed that the current signals generated at the PTFE tube wire insulation method are less as compared to synthetic enamel coating and current signals generated at uncoated wire are much higher among the coating methods. Further, it is seen that the current signal generated using PTFE tube insulation is quite uniform throughout the machining time compared to synthetic enamel wire coating and uncoated wire. It indicates that the current flux lines are parallel and uniform near the machining zone and density distribution is controlled and uniform during the machining process using the PTFE tube insulation method as compared to synthetic enamel coating and uncoated wire. When the applied current is appropriate as per the required machining

condition, the surface quality is improved with no stray current effect on the upper surface of the workpiece. However, when excessive current is applied, the machining state becomes unstable and overcut generated with loss of homogeneity of machined microslits during WECM. Therefore, the reduction in the stray current attack on the upper surface of the workpiece is completely overcome and which in turn improves the surface quality and homogeneity of fabricated microslits. Further, controlled current signals also helped to reduce the overcut in machined microslit using the PTFE tube wire insulation method as compared to synthetic enamel wire coating and uncoated wire.

4.4 Fabrication of microslits array for Nitinol SMA

Nitinol SMA is widely used in medical industries because it has anti-magnetic properties with excellent dust protection. Conventional machining is not suitable due to high cutting forces, more thermal damage, and tool wear. Nonconventional machining processes have better machining quality but have certain restrictions due to heat affected zone (HAZ) effect, and rigorous strain hardening.
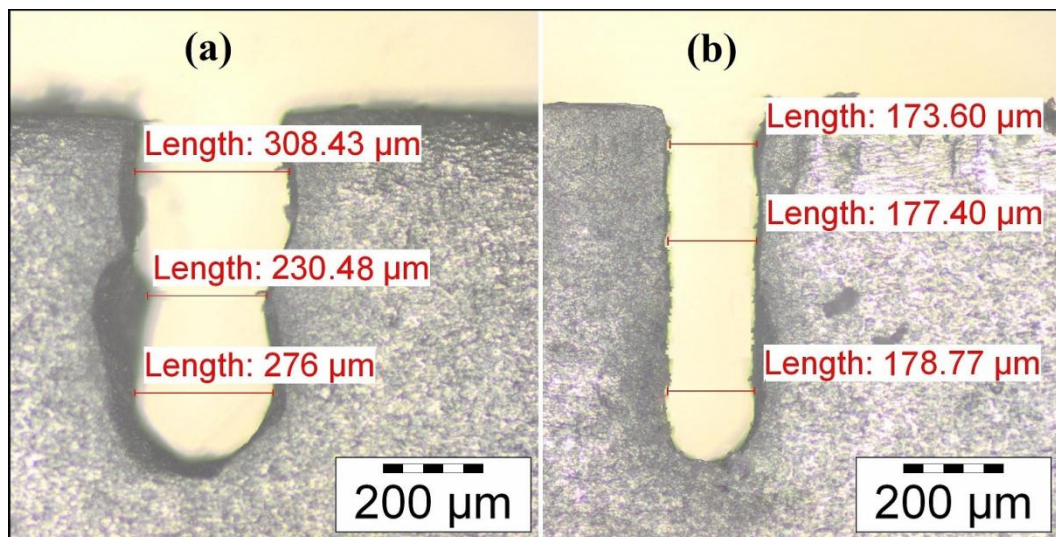
Figure 4.35 Nitinol SMA fabricated microslits at (a) without wire Coating (b) with synthetic enamel wire coating

The major difficulty in nitinol SMA machining is due to its phase transformation which changes with HAZ during traditional machining resulting in poor surface finish. WECM is heat-free, mask-free, and strain-free micro-fabrication machining processes and therefore well-suited for nitinol SMA machining with selective anodic dissolution. For the experimentations, 0.19 mm thick nitinol SMA (Activation: -10^0C $\pm$ 10^0C, Martensite below-10^0C) composed of 56 % nickel and 44 % titanium made by Nexmetal Corp. Inc, California, USA was used as a workpiece. After successfully identifying PTFE tube insulation method for wire electrodes as one of the best techniques among others, wire

feed rate of 1.4 µm/sec, an applied voltage of 9 V, pulse frequency of 250 KHz, and pulse width of 1.8 µsec used for the fabrication of nitinol SMA microslits array and compared with microslits machined without coating and with synthetic enamel coating with similar process parameters and at 180^0 exposed wire angle with 100 µm insulation and coating distance from workpiece upper surface.
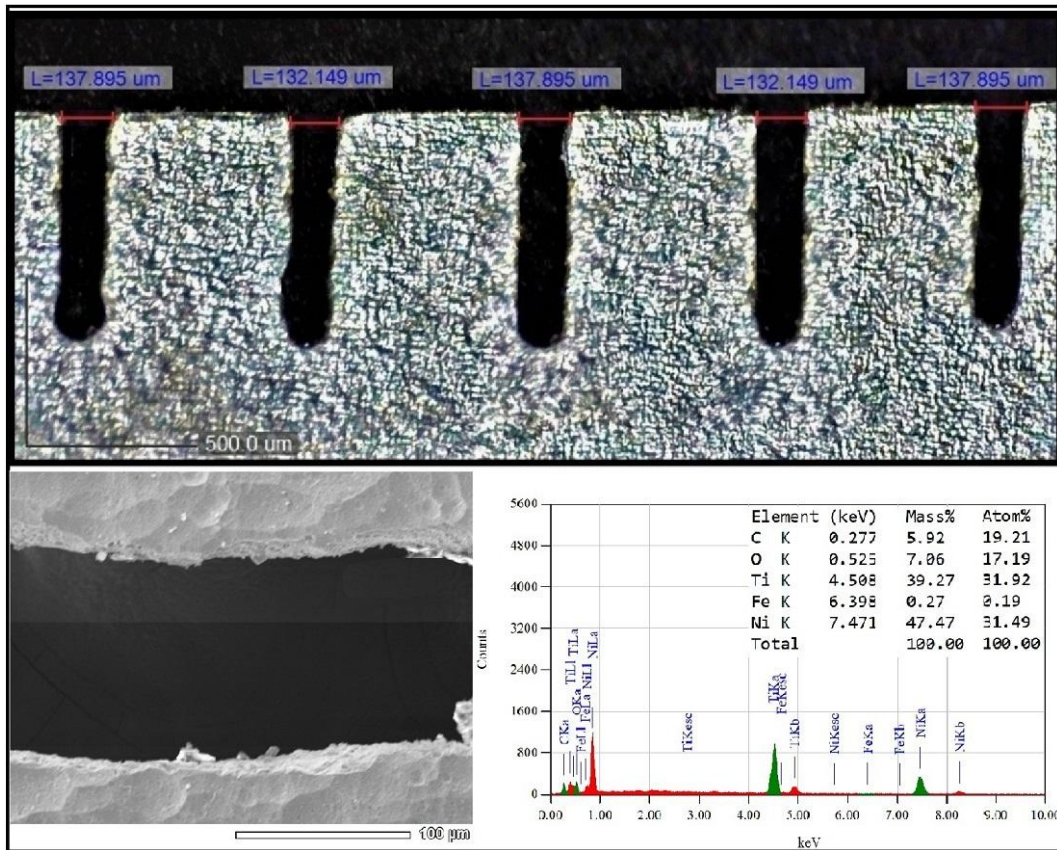
Figure 4.36 The array of nitinol SMA fabricated microslits with SEM and EDX

The pulse voltage below 9 V unable to generate enough current to attain metal removal in the machining zone and more pulse voltage resulting in stray current effect and increase in overcut in a fabricated microslits. The average slit width of 271 µm with very poor machining accuracy and more stray current effect without wire electrode coating and 176 µm with good machining accuracy and minimum stray current effect near machined surface has been obtained using synthetic enamel coating as shown in **figure4.35.** It shows that 100 µm slit width overcut reduction has been obtained using synthetic enamel coating compared to uncoated wire electrode. Further, the average slit width of 135 µm with very good machining accuracy with negligible stray current has been obtained using PTFE tube insulation method as shown in **figure4.36** with SEM and EDX analysis**.** The experimental results reveal that the average 23% reduction in overcut has been obtained using PTFE tube insulation method compared to synthetic enamel coating which shows

best method among others. The generation of oxide layers due to passivation limits the current flow across the circuit and tries to create hindrance further electrolytic dissolution of material during machining. The thickness of the oxide films increases with an increase in energy input i.e. pulse voltage and duty cycle. Thus, there is a need to control this oxide layer for maintaining the process continued with the use of appropriate parametric combination during WECM. The wire feed rate above 1.4 µm/sec generates short circuits and fabricated microslits shows uneven edge. The wire electrochemical process avoids pitting corrosion and is more effective to provide high resistance for nitinol SMA machined surface. The corrosion resistance is further enhanced in the H_2SO_4 electrolyte solution. It is seen that the mass of oxygen (O_2) has been increased to 7.06% after machining which shows the formation of a thin protective passive layer of TiO_2 on the surface of the microslit. Also, the increase in 5.92% mass carbon after machining shows that it oxidizes away the toxic carbon monoxide or carbon dioxide. Further, a decrease in Ni mass from 56% to 47.47% shows the removal of more toxic Ni atoms. Ni is selectively dissolved and Ti remains passive. Ti is protected by oxide film formation. The negligible defects on the machined surface of nitinol SMA were observed with fewer precipitated particles. The machined surface has a protective layer of TiO_2 and shows consistent corrosion resistance resulting in smoothing of the machined surface during WECM. The oxides formed on the surface of nitinol alloy always contain a certain amount of toxic nickel resulting increase in nickel release and associated nickel toxicity. The results are eventually expected to be applied in biomedical, automotive, and aerospace industries for the production of nitinol SMA complex microfeatures in near future using WECM.

4.5 Outcome of experiments

This chapter highlights that effect of micro sparks measured with the help of oscilloscope and overcut measured with optical microscope on machining accuracy and dimensional characteristics of the machined products. The application of various novel wire electrode coating and insulation methods for reduction of stray current attack and overcut of fabricated microfeatures during WECM has significant original research outcomes due to its uniqueness. After fabrication, enhancement of dimensional accuracy of smaller cross-section has been achieved. Moreover, investigations on different process parameters for reduction of micro sparks and overcut reduction as well as different wire electrode coating and insulation methods have been used. The present experimental investigation highlights that the machining accuracy and dimensional characteristics of the machined products during wire electrochemical machining is greatly influenced by the various

predominant machining process parameters due to the influence of different process parameters on generation of number of micro-sparks and overcut during machining. Experiments with increasing feed rate has resulted decrease in overcut and with higher value of feed rate started showing abrupt change and increasing trend in overcut problem due to coagulation of reaction products in the IEG due to uncontrolled micromachining process. Average current increases with increase in feed rate and micro-sparks occurs at higher currents. The overcut and number of micro-sparks increases as applied voltage increases. Again, it is observed that overcut is less when the micro machining operation is performed with tool vibration PZT system. Also, experimental results reveals that with the increase in applied voltage pulse frequency, the value of the overcut of the microslits decreases almost linearly but at the very low frequency, number of micro-sparks increases which reduces the process stability and homogeneity. It can be concluded that low frequency and small amplitude vibration of wire electrode with PZT significantly improves processing stability by reducing generation of micro sparks and overcut

Further, this research work presented simulation analysis and experimental investigation into the wire electrochemical machining of SS304 stainless steel and nitinol SMA using a 0.1M H_2SO_4 electrolyte with different anode potential, duty ratio, initial inter-electrode gap in uncoated wire condition, coating angle and distances using synthetic enamel coating and PTFE tube insulation method. The effect of some of the prominent parameters for analysis of stray current attack and reduction of overcut was studied, including applied pulse voltage, IEG, synthetic enamel coated electrode, The PTFE tube insulation exposed wire angle, synthetic enamel coating, and PTFE tube insulation distance from the upper surface of the workpiece. The experiments were also conducted for the fabrication of nitinol SMA microslit array under controlled parametric conditions using the PTFE tube insulation method during WECM. Simulation analysis for electrolyte potential and current density distribution have been carried out using COMSOL multi-physics software for different coating exposed wire angle and distances from workpiece surface and results are validated experimentally. The application of PTFE tube insulation is a remarkably efficient method compared to synthetic enamel coating to reduce the stray current attack and overcut during WECM. The overcut has been greatly reduced which is below 5 μm at 180^0 wire exposed angle with 100 μm coating distance from workpiece upper surface with better homogeneity and machining accuracy and no stray current effect on the workpiece surface. After successfully identifying PTFE tube insulation method for wire electrode, wire feed rate of 1.4 μm/sec,

pulse voltage of 9 V, pulse frequency of 250 KHz, and pulse width of 1.8 µsec, 180^0 exposed wire angle with 100 µm PTFE tube insulation distance from workpiece upper surface were used successfully for fabrication of nitinol SMA microslits array with an average slit width of 135 µm. The machined surface analyzed based on SEM and EDX has a protective layer of TiO_2 and shows consistent corrosion resistance resulting in a smooth machined surface.

Based on the outcomes, microslits with better machining accuracy and surface quality were fabricated using different coating and insulation methods with a reduction of stray current and overcut during WECM. This work has been carried out keeping in mind every possible aspect of effective utilization of wire coating and insulation for reduction of stray current and overcut to promote ongoing research activities for performance enhancement during WECM. The machining of nitinol SMA is quite difficult as compared with SS304 due to its capability of shape memory effect, hardness, strength and other properties. The parameter combinations for machining of nitinol SMA are different as compared to SS304 during WECM. This experimental investigation shows the suitability of WECM for industry scale complex microfeatures production in biomedical, automotive, and aerospace industries. However, in-depth research is still needed to enhance further process capability and effectiveness of WECM by determining suitable electrolytes and its combinations with complexing agents under ozonated and non ozonated conditions as well as strict control of operating parameters during machining nitinol shape memory alloy.

Chapter5: ELECTROCHEMICAL CHARACTERIZATION AND MICROMACHINING OF NITINOL SHAPE MEMORY ALLOY USING DIFFERENT ELECTROLYTES

5.1 Introduction

Nitinol is a special material that can change shape when heated; as a result, it is referred to as a shape memory alloy. This chapter deals with the fabrication of microgrooves and microslits of nitinol shape memory alloy using wire electrochemical machining (WECM), a material that is well suited for use in biomedical and MEMS applications. The goal of this work was to investigate the precise methodology for creating microgrooves on nitinol utilizing different neutral aqueous electrolytes i.e. NaBr, NaCl, $NaNO_3$ electrolytes for dimensional and surface characteristics analysis at different electrolyte concentrations. These electrolytes are salt combined with water, the resultant electrolytes displays enhanced electrochemical stability. This allow the electrolyte more ecofriendly and lessening the risks associated with traditional organic solvents and reduced reliance on harmful chemicals and scarce resources which makes them sustainable electrolytes in the purview of green ECM. Further, non-ozonated and ozonated mixed electrolytes with and without addition of EDTA as complexing agent i.e. $NaCl+NaNO_3$ and $NaCl+NaNO_3+EDTA$ electrolyte have been used to analyze the homogeneity and surface integrity of fabricated microfeatures and investigated with FESEM, EDS analysis and measurement of 3D surface profile for average surface roughness (Ra) values.

Further, this chapter seeks to look into the surface morphology and biocompatibility of nitinol SMA in relation to the H_2SO_4 electrolyte and complexing agent of environmentally friendly citric acid electrolyte. The performance of nitinol SMA in the highly corrosive environment has been characterized using potentiodynamic polarization (PDP) tests and electrochemical impedance spectroscopy (EIS) in 0.1M H_2SO_4 and mixed 0.1M H_2SO_4 + 0.1M citric acid electrolyte solutions to assess the viability of its applications. Additionally, during wire electrochemical machining (WECM) of nitinol SMA, for the machined microgrooves, an examination of surface roughness with groove depth and width overcut has been investigated. These investigations' findings have been evaluated, and it has been highlighted how changes in electrochemical behavior are caused by micro structural variables. Finding the best and most efficient settings using these mixed ozonated aqueous neutral electrolytes in experimental planning-I and mixed acidic electrolyte in experimental planning-II for machining nitinol SMA with improved

accuracy and high surface integrity was the main outcome of this work. The experimental findings indicate that the wire electrochemical machining performance has significantly improved, which could assist to lessen the negative effects of using nitinol SMA microfeatures that have been created. The aforementioned studies encouraged the production of nitinol SMA microfeatures using wire electrochemical machining while examining the machining and surface integrity of the process.

5.2 Experimental planning I: Influence of mixed ozonated aqueous neutral electrolyte

In this study, 1mm thick commercially-available nitinol sheets of 15mm x 15mm dimensions (Martensite below 80°C, Heat treatments for 30 minutes at 550–750 °C; water quench, 80°C to 10°C for activation) were employed and used after undergoing ultrasonic cleaning in acetone to eliminate any dirt or impurities. Also, 200μm nitinol sheet has been used for microslits fabrication. A cylindrical tungsten wire with a diameter of 50μm was used as electrode. From the previous literature, it was recommended that NaBr is suitable for titanium [102] and $NaNO_3$, NaCl electrolytes are appropriate for efficient dissolution of nitinol [95]; and hence, the same was used for the present experiments. Also, it has been observed that addition of suitable complexing agents proven the best solution for improvement in the surface finish of microfeatures therefore EDTA is also used in the experimentations in combination with most suitable electrolytes for machining of nitinol amongst all these electrolyte solutions. Also, ozone generator with ozone output of 250 mg/h has been used for experimentation in ozonated electrolytes during WECM of nitinol. The microfeatures fabrication was carried out using in-house developed experimental setup. The Newport XPS QS motion controller software is used to control the 0.1 μm/step resolution stepper motors. The machining chamber mounted and fixed on breadboard of the stage and the wire holder is mounted on Z-axis stage and feed motion. The power supply used producing maximum current at different pulse voltages up to 4A. The electrolyte chamber has enough ozone in it created using ozonator. For controlling appropriate flow, a suitable axial electrolyte flow system has been created. The ozone has been produced using ozonizer in the machining chamber for improvement in the performance of WECM process [68]. A pulsed DC power supply (Matsusada DOA75) is employed to keep the polarity consistent during WECM. The power supply is readily available and offers a voltage range of -75 to +75V, a current rating of up to 4A, and a maximum power output of 300W. A pulse generator device is used to produce the necessary types of pulses. To determine the pulse's nature and to keep track of the

machining conditions, a function generator (Tektronix AFG1022) is utilized. A tool holding device fabricated from acrylic material is developed and attached to the Z axis of stage. The tool is positioned on an XYZ translation stage with a resolution of 0.1μm and a total travel distance of 100mm for each axis. The machine is featured with continuity setting for micro sparks recognition using Tektronix TBS 2000 series digital oscilloscope. To evaluate the effect of different electrolytes i.e. NaBr, NaCl, NaNO₃ with and without ozonated conditions and addition of complexing agent i.e. EDTA on the accuracy, homogeneity and surface integrity of microfeatures, experiments were conducted using wide range of electrolyte concentrations with constant pulse voltage, feed rate and duty ratio for analyzing material removal rate and surface roughness. To begin the experiment and get the electrolyte flowing via the gap between the electrodes, place the workpiece on the work holding platform. Mount the wire electrode in the tool holder and feed it towards the workpiece to ensure the just in contact condition, which is tested for with a continuity tester. All of the machining settings have been changed in line with the anticipated experimental planning and provided feed rates in the stage controller for the forward movement of the wire electrode towards the workpiece. **Table5.1** displays the machining parameters for each process parameter and the experimental ranges that they were employed in. The wire is positioned on an XYZ translation stage that has an overall travel distance of 100 mm for each axis and a resolution of 0.1μm. For the purpose of creating linear micro grooves on nitinol SMA, the workpiece and wire were maintained in a vertically straight posture.

Table 5.1. Machining Parameters

Working condition	Value
Workpiece material	Nitinol SMA
Workpiece Thickness	1mm, 200μm
Wire Electrode Material	Tungsten
Diameter of Wire Electrode	Ø50μm
Applied Pulse Voltage	5V -8V
Wire Feed rate	1.4μm/s
Duty ratio	50%
Voltage Pulse frequency	250KHz
Type and concentration of Electrolyte	0.2 to 0.4M NaBr, NaNO₃, NaCl and EDTA
Electrolyte Flow rate	35lph
IEG	50μm
PZT Tool vibration frequency	50Hz
PZT Tool vibration amplitude	12.54μm
Ozone output from ozone generator	250 mg/h

The arrangement was kept steady while the wire electrode was supplied linearly. Both the

workpiece and the fixture were submerged in the electrolyte bath. All the experimentations have been carried out using this in-house developed vibration assisted axial nozzle jet wire electrochemical machining process. The experiments were repeated three times with three different concentrations for these entire electrolytes. Surface roughness and dimensional characteristics have been assessed at each step of varied circumstances of process parameters during WECM of machined micro grooves for each operating conditions. During tests, the oscilloscope has been utilized to track various pulse power characteristics. The studies have also been conducted using a multimeter, a stereo zoom microscope, an optical camera, and a microscope, among other tools. The output responses were measured and machined microgrooves parameters were carefully examined under an optical microscope Lieca, Germany and CCI (Coherent correlation interferometer) profilometer made by Taylor Hobson for their dimensions, i.e. width and depth and surface roughness and 3D profile of the microgrooves. Further, in-depth analysis and characterization of the fabricated microfeatures have been carried out for these electrolytes using FESEM and EDS for changes in the surface characteristics and chemical compositions during WECM on nitinol shape memory alloy. The elemental composition of the fresh nitinol sample used for fabrication of microgrooves and microslits has been presented herewith through SEM, EDS and 3D surface profile as shown in **figure5.1.** It has equiatomic mass element combination of Ni and Ti with 48.65% and 48.12% with a surface roughness Ra of 0.7395μm.
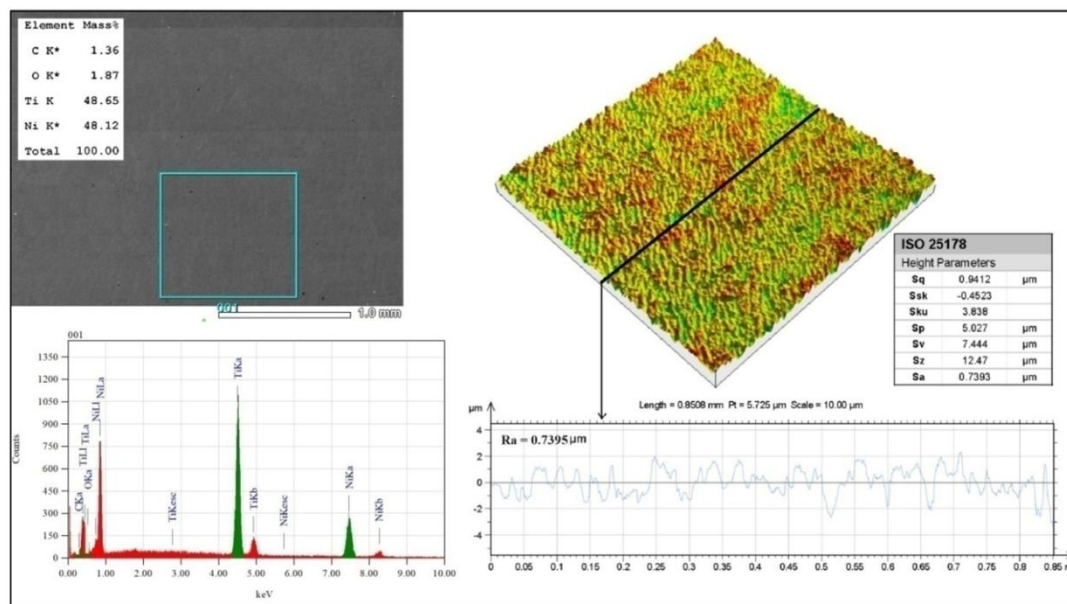
Figure 5.1 Elemental composition and 3D surface roughness profile of
non-machined nitinol SMA sample

5.2.1   Experimental observations and discussions

5.2.1.1 Influence of pulse voltage

Previous research has shown that pulse voltage has a significant impact on wire electrochemical micromachining. Hence, choosing the appropriate pulse voltage during WECM is crucial. It has been observed that the surface roughness shows increasing trend with increase in pulse voltage in both 0.2M nonozonated and ozonated aqueous $NaNO_3$ electrolyte as shown in **figure5.2.**
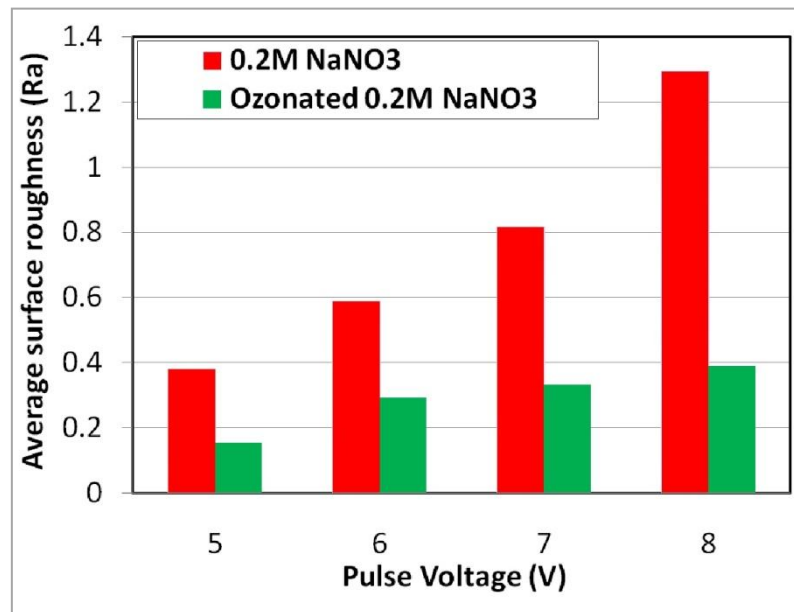
Figure 5.2 Influence of pulse voltage on average surface roughness (Ra)

Because the applied pulse voltage directly affects the rate at which metal is removed, as pulse voltage raises, the rate at which material is removed is also increases. When the current is constant and satisfies the machining requirement, the quality of the machining is improved. On the other hand, when excessive current is used, the machining situation becomes unstable and more material is removed at high pulse voltage. Only continuing micro sparks were seen at the beginning of machining when the pulse voltage is below 4V and other parametric variables are constant. According to experimental findings, the tiny micro pits have been created at 4V pulse voltage. Because of the extremely poor machining depth in this situation, it was advised against using pulse voltages lower than 4V to obtain effective machining while micromachining nitinol under the other parametric circumstances employed in this experiment. The range of 5V to 8V is therefore appropriate with these additional operating circumstances with the created setup, according to subsequent experimental study. It has been noted that the average surface roughness is lowest at 5V pulse voltage for both 0.2M nonozonated and ozonated aqueous

NaNO$_3$ electrolyte. Further, surface quality has been improved using 0.2M ozonated NaNO$_3$ electrolyte at 5V pulse voltage with the minimum average surface roughness (Ra) of 0.1542μm as shown in **figure5.3.**
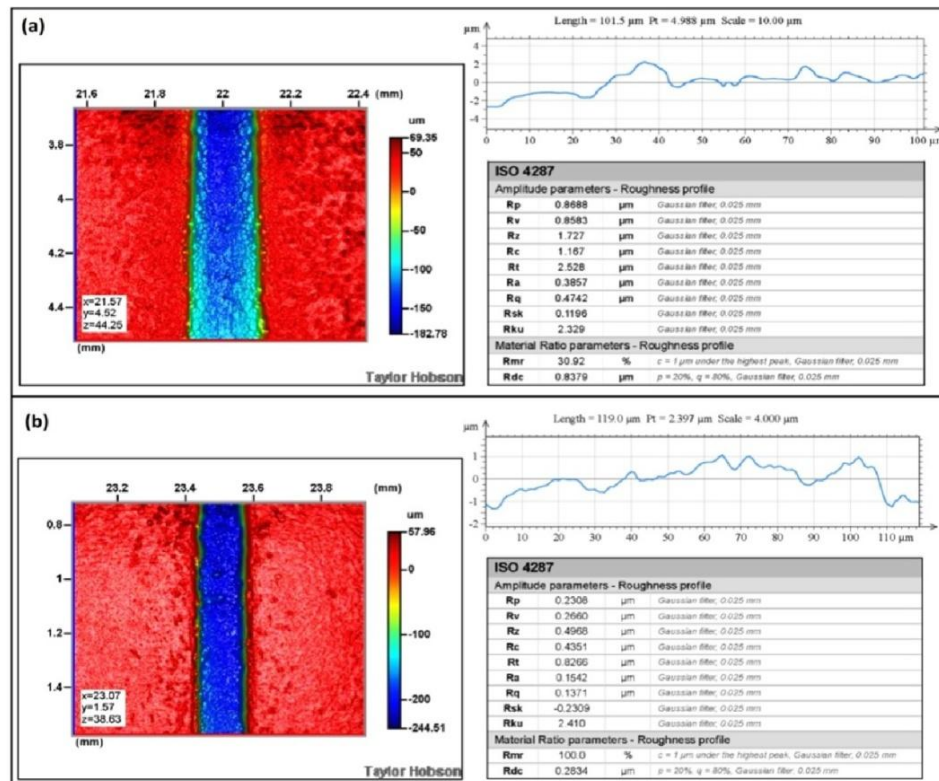
Figure 5.3 Surface roughness at 5V using (a) nonozonated NaNO$_3$ electrolyte (b) ozonated NaNO$_3$ electrolyte
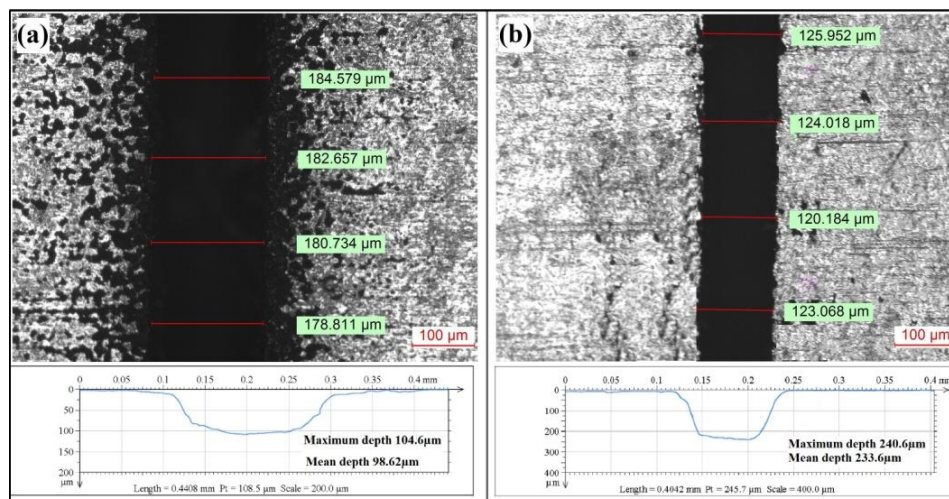
Figure 5.4 Analysis of groove width and depth at 5V using (a) nonozonated NaNO$_3$ electrolyte (b) ozonated NaNO$_3$ electrolyte

Further, the experimental results revealed that the mean groove depth of 233.6 μm and groove width of 123.30 μm have been obtained at 5V using ozonated 0.2M NaNO$_3$ compared to groove mean depth of 98.62 μm and groove width of 181.69 μm using non

154

ozonated $NaNO_3$ electrolyte for same parametric conditions as shown in **figure5.4.** It shows the higher capability of ozonated electrolytes to remove sludge and dissolved products as well as removal of oxides to avoid passivation in the process during WECM of nitinol. Due to the ozonation process, there is enough oxygen available to further oxidize the sludge and oxides. The nitrate is converted into nitrite during the anodic metal dissolution using aqueous $NaNO_3$ as electrolyte. The primary cause of the passive layer development on the workpiece surface is nitrite content. This passive layer acts as an insulating layer and is difficult to remove, slows the anodic dissolution rate. It is seen that the sidewall of the machined microgroove in nonozonated $NaNO_3$ electrolyte has more pitting effects with poor homogeneity due to non-uniform dissolution of nitinol during machining. However, the pitting effect using ozonated $NaNO_3$ electrolyte has lower pitting effect and produces smooth surface with homogeneous microgroove. Further, the microgroove with nonozonated electrolyte has circular in cross-section may be due to less machining depth and microgroove with trapezoidal cross-section has been obtained with ozonated $NaNO_3$ electrolyte which is almost double depth compared to nonozonated electrolyte.The EDS analysis was carried out to determine the composition of nitinol in nonozonated and ozonated aqueous $NaNO_3$ electrolyte, and the result is shown in **figure5.5.**
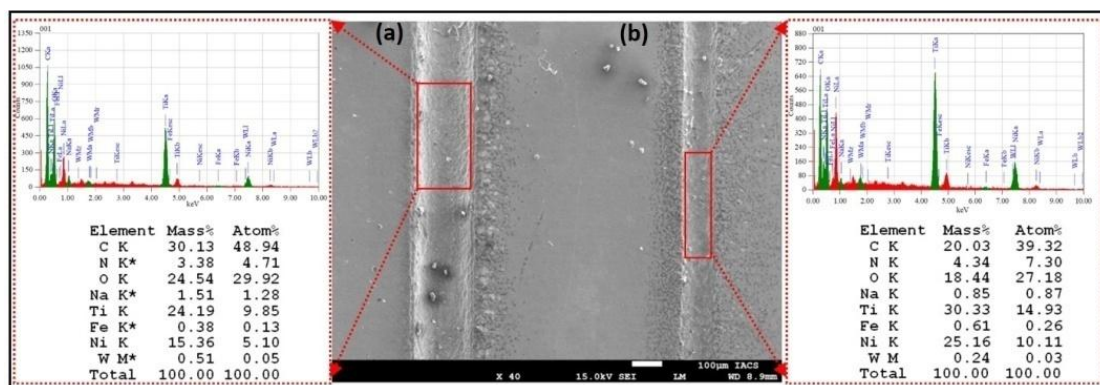
Figure 5.5 FESEM and EDS with element composition of machined microgrooves at (a) nonozonated $NaNO_3$ electrolyte (b) ozonated $NaNO_3$ electrolyte

The oxygen O and carbon C have higher peaks and titanium Ti and nickel Ni have lower peaks in nonozonated $NaNO_3$ electrolyte as compared to ozonated $NaNO_3$ electrolyte. It shows that thick oxide layer has been formed in nonozonated electrolyte compared to ozonated $NaNO_3$ electrolyte. This analysis was carried out to confirm about oxides and sludge formed during nitinol dissolution in electrolyte. It has been observed that the

increase in element composition of carbon mass% and oxygen mass% is observed in EDS analysis of microgrooves surface in both nonozonated and ozonated conditions during the WECM process. The 24.19 Ti (Titanium), 15.36 Ni (Nickel), 30.13 C (Carbon) and 24.54 O (Oxygen) mass % is observed in nonozonated condition which reduced to 30.33 Ti , 25.16 Ni, 20.13 carbon and 18.44 oxygen mass % in ozonated condition of aqueous $NaNO_3$ electrolyte. The presence of carbon C and oxygen O provides information on carbide and oxide layer development on the machined surface of nitinol. However, the thin oxide layer has been formed due to presence of less oxygen O in ozonated $NaNO_3$ electrolyte which helps for uniform anodic dissolution of nitinol and improvement in machined microgrooves surface quality.

5.2.1.2 Effect of neutral electrolytes on the accuracy and surface finish

When compared to the anodic dissolution of the other metals in WECM, nitinol is particularly difficult to machine. Because there is thin coating of passive TiO_2 on the surface, it offers good resistance to anodic dissolution. Surface oxidation under atmospheric circumstances is one of the main issues with nitinol electrochemical dissolution. Nitinol develops a passive oxide deposit on its surface when exposed to an oxygen-containing solution. Nitinol creates an oxide layer consisting of TiO_2 and NiO in aqueous solution, according to the equations below **[92]**.

$$Ni + 2H_2O \rightarrow NiO + 4H^+ + 2e^- \tag{5.1}$$

$$NiO + 2H^+ \rightarrow Ni^{2+} + H_2O \tag{5.2}$$

$$Ti + 2H_2O \rightarrow TiO_2 + 4H^+ + 2e^- \tag{5.3}$$

$$TiO_2 + 4H^+ \rightarrow Ti^{4+} + 2H_2O \tag{5.4}$$

According to certain investigations, the oxide film is dual in nature, with TiO_2 layer on top and interacting with the NiO sub layer. Ni dissolves through pores in the thinnest TiO_2 layer due to the substantially reduced resistance of these NiO sub layers to pitting.The initial experimentations were carried out using different aqueous neutral electrolytes successfully utilized in past research work i.e. NaBr, NaCl and $NaNO_3$ electrolytes.

NaBr electrolyte

First NaBr electrolyte has been used for machining of nitinol as it has proven suitability for titanium alloys but till date no experimentations are carried out for understanding the dissolution behavior of nitinol in wire electrochemical machining using tungsten wire electrode. From **figure5.6 (a, b, c),** it is observed that a huge amount of sticky sludge is accumulated on the surface of nitinol for all the mentioned electrolyte concentrations due

to which machining has not been carried out uniformly and also produced uneven rough surface in the machined area. In aqueous NaBr solution, the subsequent reactions may take place as follows [93, 94]:

$$NaBr_{(s)} + H_2O \rightarrow Na^+_{(aq)} + Br^-_{(aq)} \tag{5.5}$$

$$Ni^{2+} + 2Br^- \rightarrow NiBr_2 \tag{5.6}$$

$$NiBr_2 + 2H_2O \rightarrow NiO_2 + 4H^+ + 2Br^- \tag{5.7}$$

$$Ti^{4+} + 4Br^- \rightarrow TiBr_4 \tag{5.8}$$

$$TiBr_4 + 2H_2O \rightarrow TiO_2 + 4H^+ + 4Br^- \tag{5.9}$$
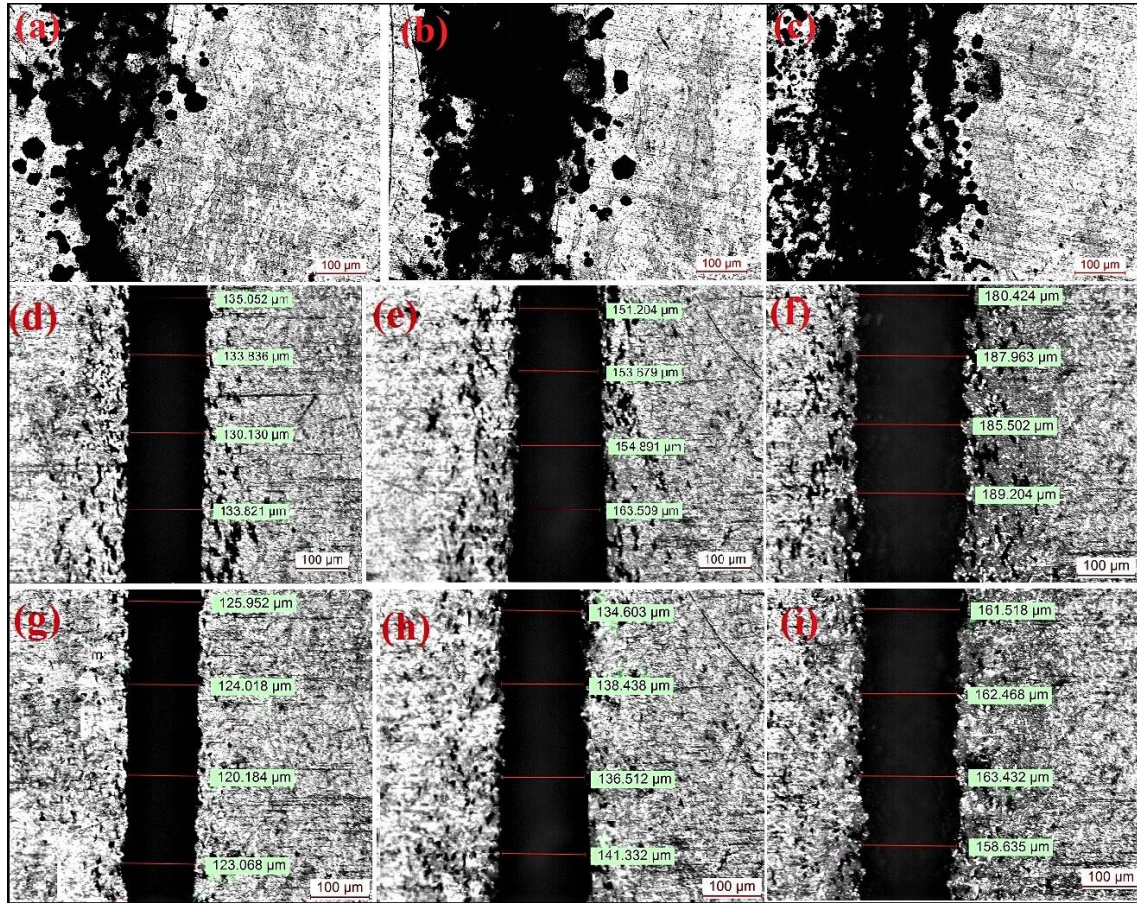
Figure 5.6 Fabricated microgrooves in NaBr (a, b, c), NaCl (d, e, f) and NaNO₃ (g, h, i) electrolytes at 0.2M, 0.3M and 0.4M concentration

In the aqueous NaBr solution, the oxide layers NiO_2 and TiO_2 form complexes like $NiBr_2$ and $TiBr_4$. Thus, the solubility of these two compounds controls how easily nitinol dissolves in aqueous NaBr solution. The highest capacity of Br^- ions to permeate TiO_2 results in local dissolution, often known as pitting. $TiBr_4$ molecule clusters act as the pit's nucleus, and they form in locations where the oxide layer electrical conductivity is higher. When the concentration of electrolyte is high, the anodic product $TiBr_4$ concentration at

the nitinol surface is very high and would surpass the solubility product, precipitating the salt as a thick layer on the surface that would then obstruct the dissolving and produces hindrance in the machining of nitinol. Further, it is seen from the **figure5.7 (a, b, c)** that the microgrooves mean depth of 20.02μm, 8.62μm, 10.86μm has been obtained at 0.2M, 0.3M and 0.4M aqueous solution of NaBr electrolyte with increasing surface roughness Ra of 0.5777μm, 0.8123μm, 0.9489μm. It is observed that the aqueous solution of NaBr electrolyte is not suitable for machining of nitinol during WECM.
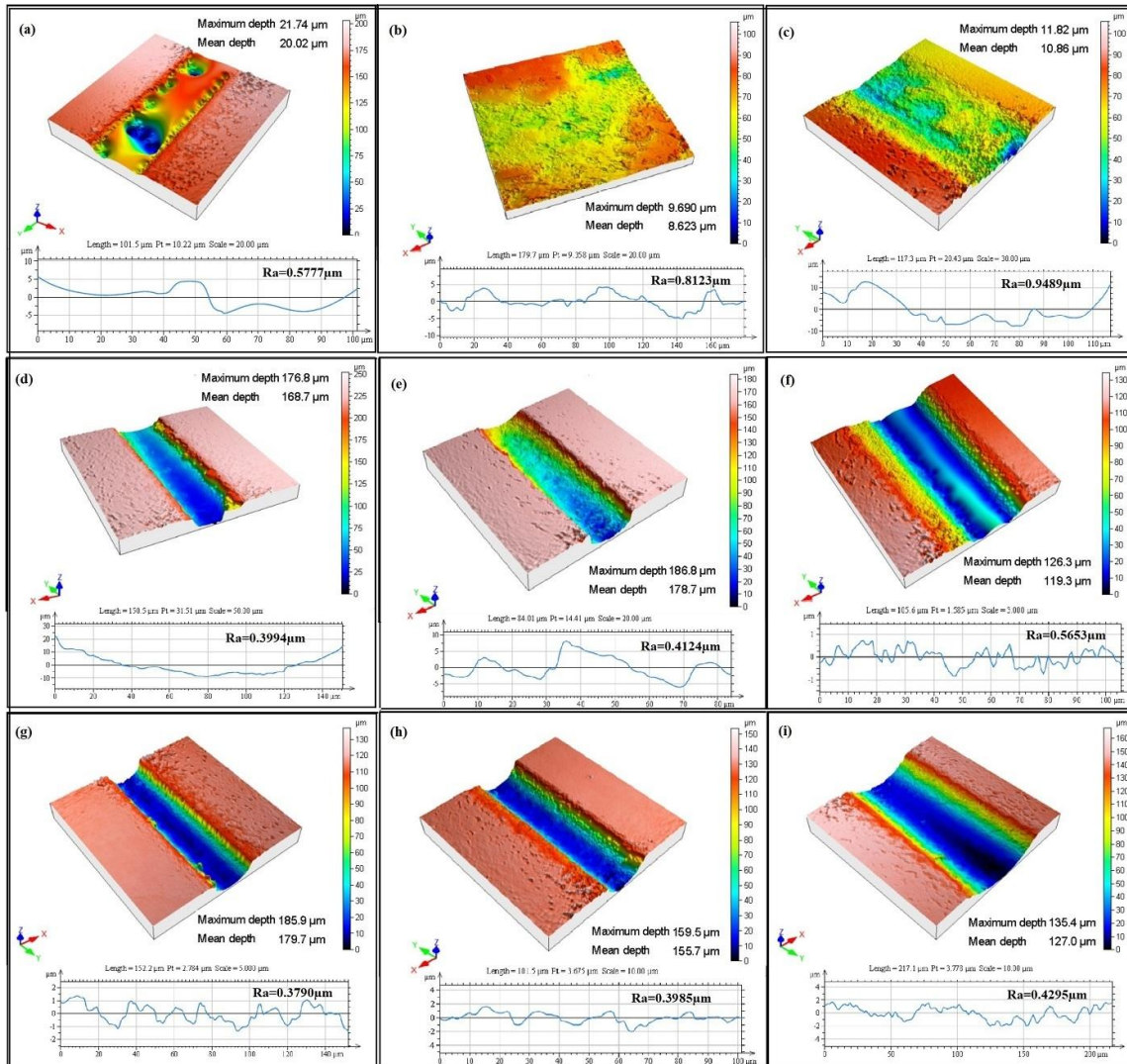
Figure 5.7 3D profile with surface roughness and depth of microgrooves in NaBr (a, b, c), NaCl (d, e, f) and NaNO$_3$ (g, h, i) electrolytes at 0.2M, 0.3M and 0.4M concentration

NaCl electrolyte

Further experiments were carried out using aqueous electrolyte of NaCl. It can be seen from **figure5.6 (d, e, f)** and **figure5.7 (d, e, f)** that in the case of aqueous NaCl solution at 0.2M electrolyte concentration, microgroove is fabricated with average groove width of

133.20µm having width overcut of 41.6 µm, mean groove depth of 168.7 µm with a surface roughness Ra of 0.3994µm. However, in the case of 0.3M and 0.4M electrolyte concentration, the anodic dissolution of nitinol is increased to a large extent with an increase in width overcut i.e. 56.75µm, and 69.6µm and surface roughness (Ra) i.e.0.4124µm, and 0.5653µm respectively. It shows highly non-uniform dissolutions with non-uniformity in machined surface. In aqueous NaCl solution, the reactions may take place as follows [95]:

$$NaCl_{(s)} + H_2O \rightarrow Na^+_{(aq)} + Cl^-_{(aq)} \tag{5.10}$$

$$Ni^{2+} + 2Cl^- \rightarrow NiCl_2 \tag{5.11}$$

$$NiCl_2 + H_2O \rightarrow NiO + 2H^+ + 2Cl^- \tag{5.12}$$

$$Ti^{4+} + 4Cl^- \rightarrow TiCl_4 \tag{5.13}$$

$$TiCl_4 + 2H_2O \rightarrow TiO_2 + 4H^+ + 4Cl^- \tag{5.14}$$

The formation of $TiCl_4$ on the surface, which alters how nitinol dissolves, may be the cause of the higher Ra value in the case of aqueous NaCl electrolyte. The aggressive Cl^- ions assault the oxide layer, causing NiO to dissolve off the surface. The metal's ability to dissolve is constrained by TiO_2, which has a thick and tenacious character. According to the equations, Ni^{2+} and Ti^{4+} ions combine with Cl^- in the solution to generate $NiCl_2$ and $TiCl_4$, respectively, which then combine with H_2O to form NiO and TiO_2. The majority of the $NiCl_2$ dissolves into the electrolyte because $NiCl_2$ is readily soluble in water. $TiCl_4$, on the other hand, is incredibly sticky and adheres to the anode surface. Another factor that strongly binds the nitinol surface is the production of TiO_2 once more on the anode. Nitinol cannot dissolve uniformly in the aqueous NaCl solution due to the production of $TiCl_4$ and subsequent TiO_2.

NaNO₃ electrolyte

NaNO₃ is a well-known passivating electrolyte that is utilized in ECM-based micromachining to improve accuracy. **Figure5.6 (g, h, i)** and **figure5.7 (g, h, i)** in the case of neutral electrolyte aqueous NaNO₃ show that at lower concentrations of electrolyte, the sludge quantity adhering to the surface is smaller than at larger concentrations of electrolyte. Also, it has been observed that the accuracy parameters like groove width, mean groove depth increase with the increase in the electrolyte concentration as the dissolution rate increases, hence the overcut increases. The average groove width of 123.30µm, 137.72µm, 161.51µm and mean groove depth of 179.7µm, 155.7µm, 127µm and the surface roughness (Ra) of 0.379µm, 0.3985µm, and 0.4295µm

are measured for 0.2M, 0.3M, and 0.4M $NaNO_3$ electrolyte concentration, respectively; thus, a uniform dissolution of nitinol can be considered and smoother surface in comparison to NaCl electrolyte has been obtained. Any of the following reactions might occur in an aqueous $NaNO_3$ solution **[96]**:

$$NaNO_3(s) + H_2O \rightarrow NaOH + NO + O \tag{5.15}$$

$$Ti + 2NaOH + H_2O \rightarrow Na_2TiO_3 + 2H_2 \tag{5.16}$$

$$3Ni + 8NaNO_3 \rightarrow 3Ni(NO_3)_2 + 2NO + 4H_2O \tag{5.17}$$
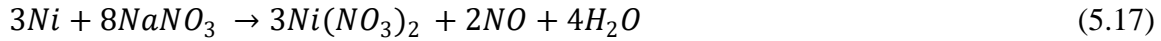
$NaNO_3$ reacts with H_2O to form NaOH and TiO_2 reacts with NaOH to generate a soluble complex Na_2TiO_3. After the outermost TiO_2 layer dissolves, Ni $(NO_3)_2$ is formed, which dissolves the lower Ni layer. The aforementioned dissolving process improves both the localized dissolution and the uniform electrochemical response in all electrolyte concentration conditions as compared to NaCl electrolyte solution.

Figure5.8 (a) (b) and **(c)** shows that the average groove width, mean groove depth and the average surface roughness for all theses electrolytes at different concentrations. In case of NaBr, machining of microgroove fabrication was not successful due to non-uniform dissolution and depth of machining is also very shallow throughout the nitinol surface area and the surface roughness (Ra) also very high compared to both NaCl and $NaNO_3$ electrolytes, and the uniform dissolution was obtained in $NaNO_3$ electrolyte with smaller groove width, larger groove depth and minimum average surface roughness (Ra).
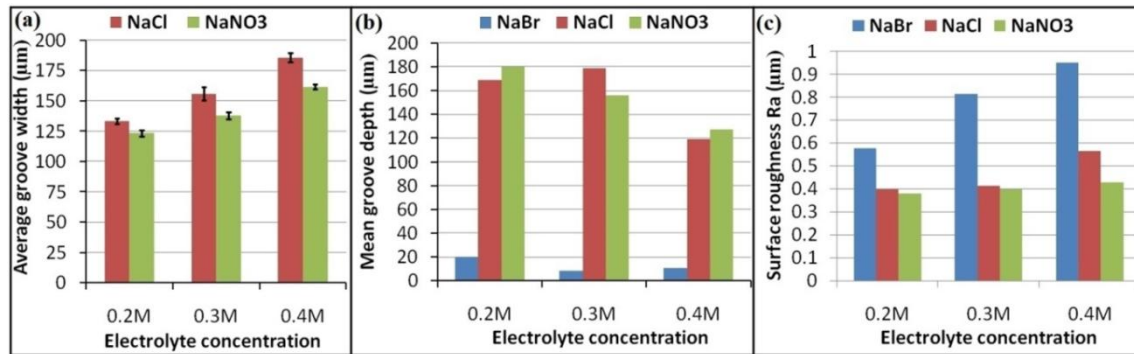
Figure 5.8 Effect of different electrolyte concentrations on fabricated microgrooves for (a) average groove width (b) mean groove depth (c) surface roughness (Ra)

The energy-dispersive spectroscopy (EDS) analysis for FESEM image of nitinol surface in aqueous neutral solutions of NaCl, $NaNO_3$, and NaBr electrolytes under nonozonated conditions is as shown in **figure5.9** reveals major components in the WECM machined surface layer such as Ti, Ni, C, and O etc. The machining parameters completely determine the surface morphology of the WECM process for nitinol shape memory alloy. The anodic dissolution of nitinol in simple aqueous NaBr solution is completely unstable

and non proper machining has been occurs. It may be due to the production of highly sticky sludge by bromide content in the solution. When using a simple aqueous NaCl solution, it is demonstrated in EDS that chlorides and oxides are present on the surface in significant amounts which creates hindrance to the nitinol anodic dissolution. However, the metal removal is higher in NaCl solution due to its non-passivating behavior.
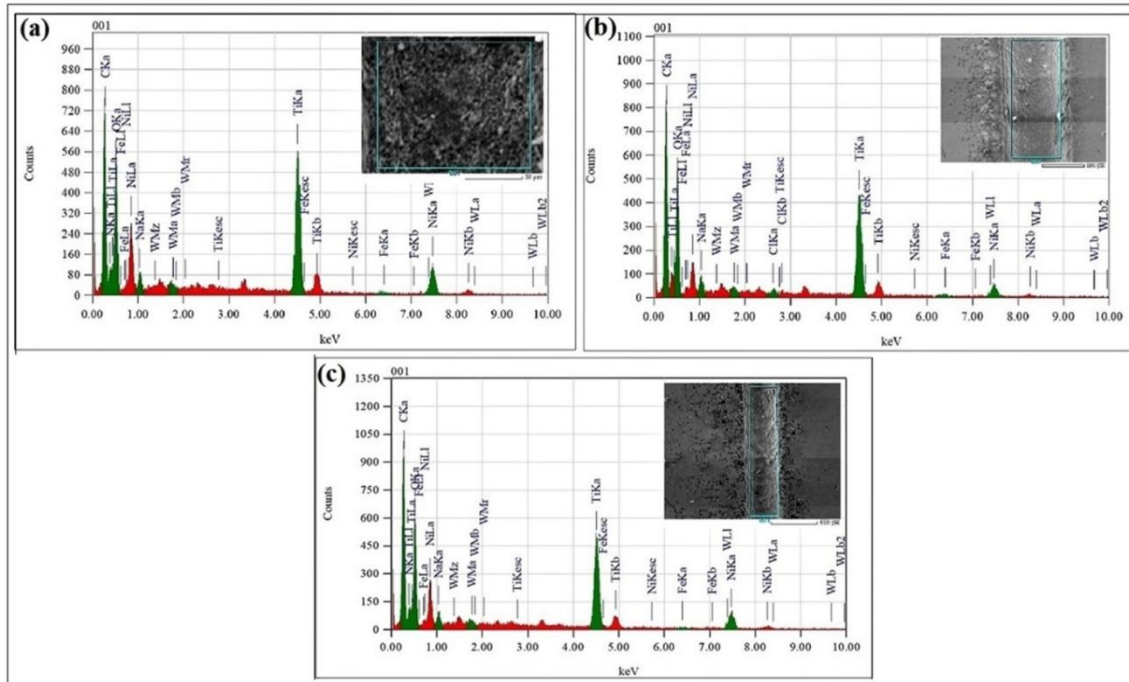
Figure 5.9 EDS of microgrooves surfaces with aqueous electrolytes (a) NaBr (b) NaCl (c) NaNO$_3$

Moreover, because of passivation in NaNO$_3$ due to its passivating behavior, the WECM process was characterized by oxide layers in aqueous NaNO$_3$ solution. As a result, the WECM machined surface layer contains TiO$_2$, NiO, C, TiC, WC, and a Ni-rich phase in all these aqueous electrolytes. The machined surface is composed of a thin oxide layer of TiO$_2$, NiO, and consumed W electrode deposition particles, as well as the dissolved electrolyte medium. **Table5.2** shows the element composition of machined microgrooves surface, which demonstrates the existence of titanium, nickel, and oxygen at all electrolyte conditions in 0.2M electrolyte concentration, showing the presence of titanium and nickel oxides. The high activity of Ni and Ti atoms was attributed to TiO$_2$, TiC, and Ni complexes. WC occurs as a result of the deposition of the consumed W electrode. TiC and C are also the impacts of the all these electrolytes. At low electrolyte concentration, the volume of Ti exceeds that of Ni. However, for the higher values of concentration, the quantity of Ni in the sludge is more than that of Ti. The oxygen and carbon contents in NaNO$_3$ electrolyte are lower as compared to NaBr and NaCl electrolyte. The nitinol

dissolution occurs in two stages.

Table 5.2. EDS Analysis for element composition of NaBr, NaCl and NaNO$_3$

Element (K)	NaBr		NaCl		NaNO$_3$	
	mass %	atom%	mass%	atom%	mass%	atom %
Ni	9.78	2.51	10.78	3.51	15.60	5.30
Ti	25.13	9.42	26.13	10.42	27.19	12.85
O	30.30	36.46	28.60	34.16	24.30	29.72
C	33.42	50.98	31.42	49.98	27.13	45.94
Fe	0.53	0.18	0.83	0.28	0.38	0.13
Na	0.66	0.38	1.66	1.38	1.51	1.28
N	-	-	-	-	3.38	4.71
Cl	-	-	0.49	0.26	-	-
Br	0.09	0.06	-	-	-	-
W	-	-	-	-	0.51	0.05

The first process is the adsorption of OH ions results in passivity, and the second is the adsorption of anions (Br, Cl, NO$_3$, etc.). The adsorption of anions on the oxide layer produces soluble salts through cations from the oxide, resulting in the formation of pits. Once formed, these pits maintain to start local dissolution via the autocatalytic process. The oxygen and carbon mass % is lower in NaNO$_3$ electrolyte solution compared to NaBr and NaCl shows its suitability for surface improvement during machining of nitinol using WECM.

5.2.1.3 Effect of mixed neutral electrolyte on the accuracy and surface finish

From the above experimental investigations for microgroove dimensions and surface roughness, it is observed that the NaNO$_3$ electrolyte is most suitable electrolyte for obtaining better dimensional accuracy and surface finish and NaCl for better metal removal rate. Therefore, further investigation has been carried out using mixed NaCl and NaNO$_3$ electrolyte and also used EDTA (Ethylenedinitrilotetraacetic acid disodium salt dehydrate) as a complexing agent for enhancing the performance of machining during WECM. Primarily to understand the effect of mixed electrolyte on nitinol for understanding the dissolution mechanism in both the electrolytic conditions, the electrochemical impedance spectroscopy (EIS) has been conducted for mixed NaCl+NaNO$_3$ and NaCl+NaNO$_3$+EDTA electrolyte and results are obtained from the generated data and graphs as shown in **figure5.10**. The imaginary impedance component (Z″) is shown against the real impedance component (Z′) for each excitation frequency in an EIS data shows Nyquist plot. The frequency (Hz) with respect to real component Z (Ω) and phase (°) enable analysis of absolute impedance has been shown as Bode plot. To correct the capacitor's non-ideal behavior, the constant phase element (CPE) concept can

be applied to the modeling of an electrical double layer, and the surface-deposited double layer capacitor is linked in parallel with the polarization resistor (Rp), which is coupled in series with the bulk resistor (Rs).
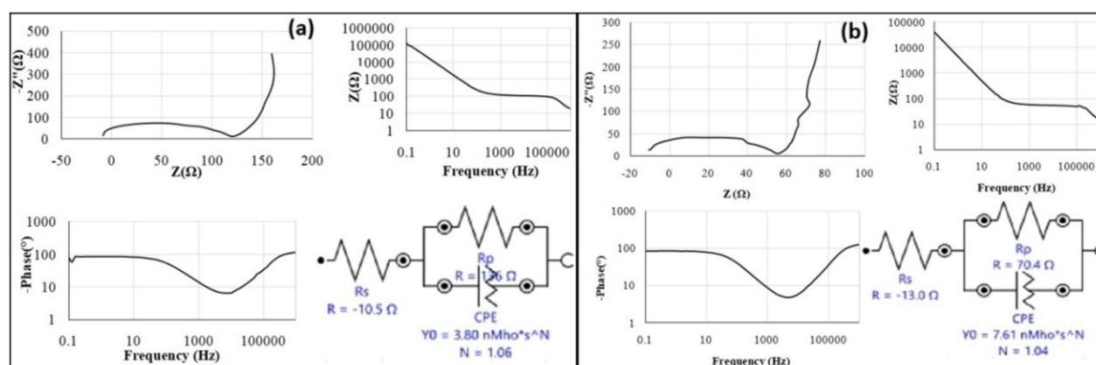
Figure 5.10 EIS with mixed electrolytes **(a)** 0.2M NaCl +NaNO$_3$ **(b)** 0.2M NaCl +NaNO$_3$ +EDTA

The diameter of the semicircle also represents the polarization resistance. The Rs, Rp, and CPE components of the equivalent circuit are fitted to the semicircle, which depicts the quick oxidation and reduction kinetics. Nitinol alloys with high Rp have good corrosion resistance. Roughness values are low during an electrochemical reaction when there is decrease in corrosion rate. The polarization resistances (Rp) were measured and evaluated using the Nyquist and Bode plots. To support this result and quantify the corrosion behavior of the nitinol samples in both electrolytes, the EC system was modeled using equivalent electric circuits. Using the Nyquist and Bode plots of each circuit, the optimal circuit for each sample was determined. To account for electrolyte behavior and oxide layer resistance, each circuit has CPE and Rs, which causes a potential drop between the working electrode, nitinol, and the reference electrode, Ag/AgCl cell, generating errors, and Rp, which behaves like a resistor. In 0.2M NaNO$_3$+NaCl electrolyte as shown in **figure5.10(a),** the polarization resistance of the nitinol sample was 136Ω shows higher corrosion resistance, while in 0.2M NaCl+NaNO$_3$ +EDTA electrolyte, it was 70.4Ω shown in **figure5.10(b)** shows lower corrosion resistance as indicated by the values of the resistances Rp and Rs. The CPE readings can be relied on to determine the thickness of the oxide deposit. The lower current density produces due to lower Rp in 0.2M NaCl+NaNO$_3$+EDTA electrolyte leading to formation of smooth surface and enhancement in surface finish as compared to 0.2M NaNO$_3$+NaCl electrolyte. The EIS data support the notion that the corrosion resistance of nitinol alloy is linked to the formation of a strong titanium oxide layer on the surface. The current investigations show that process induced surface smoothing and the spontaneous formation of a passive layer

boost the corrosion resistance of nitinol. The smoothening of the surface and the formation of a thin coating of TiO_2 on it are associated with the alloy's higher corrosion resistance and uniform corrosion behavior. It is widely acknowledged that the outcome of an EIS measurement can be utilized to effectively define the surface state of a material.
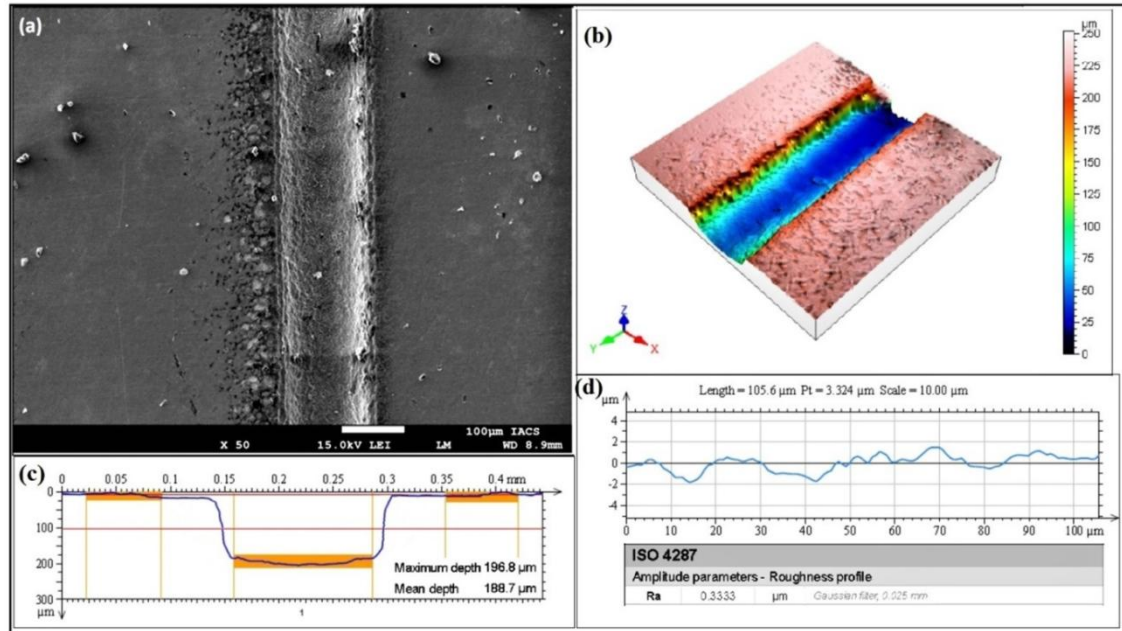
Figure 5.11 FESEM, mean depth, 3D surface and roughness profile of fabricated microgroove with mixed $NaNO_3$ + NaCl electrolyte

The suitability of an acceptable electrolyte for further machining during WECM was determined using this electrochemical characterization investigation for nitinol utilizing 0.2M $NaCl+NaNO_3$ and 0.2M $NaCl+NaNO_3+EDTA$ electrolytes. The capacity to create smooth surfaces makes $NaNO_3$ solutions the preferred electrolyte. However, the passive layer that the $NaNO_3$ electrolyte forms on the surfaces further impedes accurate machining, leading to normal machining capabilities. A correct machining performance is required while fabricating nitinol microfeatures. So, in order to improve the performance of the WECM, NaCl is mixed into the aqueous $NaNO_3$ electrolyte. Among all these aqueous neutral electrolyte solutions used under mixed electrolyte conditions, both the electrolytes was capable to effectively machine nitinol with improved anodic dissolution efficiency. However, the oxide layer formed on the machine surface during machining with $NaCl+NaNO_3$ electrolyte impairs the machining accuracy and surface finish which also affects the machined surface due formation of pitting near the sidewall of the microgroove as shown in **figure5.11.** It is observed that the average groove width of 118.35μm with a mean depth of 188.7μm and average surface roughness Ra of 0.3333μm have been obtained in mixed $NaNO_3$ + NaCl electrolyte. Also, tapering effect has been

found on the top initial machined surface of the nitinol compared to bottom surface and homogeneity of sidewall of the microgroove is poor in mixed $NaNO_3$ + $NaCl$ electrolyte. The addition of EDTA as a complexing agent helps to reduce excessive oxide layer on the surface of nitinol due to lower passivating effect and hence, clean surface will be existing for machining during WECM. With the chemical formula $C_{10}H_{14}N_2Na_2O_8.2H_2O$ i.e.Na_2H_2Y where Y is $C_{10}H_{12}N_2O_8$), EDTA disodium salt is a kind of complexing agent that has the capacity to interact with most metal ions and produce a soluble complex molecule. The probable chemical reactions in $NaNO_3$ and EDTA for nitinol are as follows [97]:

At cathode:

$$2H^+ + 2e^- \rightarrow H_2 \uparrow \tag{5.18}$$

At the interface of anode and electrolyte:

$$2H_2O \rightarrow 4H^+ + O_2 \uparrow + 4e^- \tag{5.19}$$

$$Ti^{2+} + 2NO_3^- \rightarrow TiO_2 + N_2 + 2O_2 \uparrow \tag{5.20}$$

$$Ti^{2+} + H_2O \rightarrow TiO^{2+} + H_2 \uparrow \tag{5.21}$$

$$TiO^{2+} + 2OH^- \rightarrow TiO_2 + H_2O \tag{5.22}$$

$$TiO^{2+} + H_2Y^{2-} \rightarrow TiOY complex + 2H^+ \tag{5.23}$$

It is discovered that increasing the TiO_2 layer reduces the metal removal at higher electrolyte concentrations.
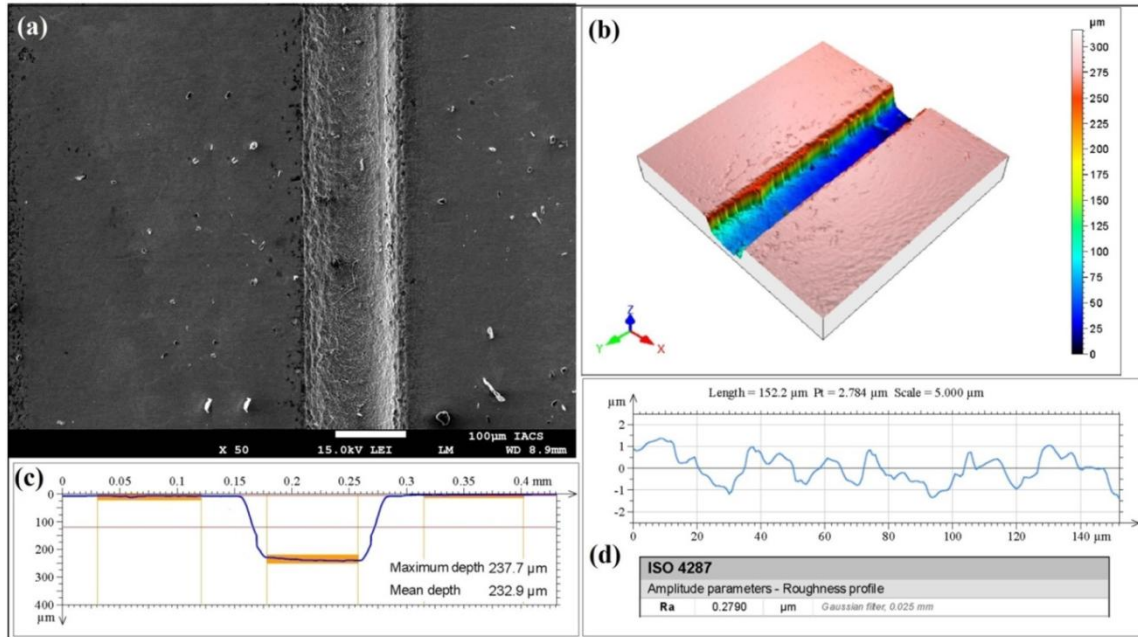
Figure5.12. FESEM, mean depth, 3D surface and roughness profile of fabricated microgroove with NaCl +NaNO₃+ EDTA electrolyte

Because NaNO$_3$ is passive in nature, it promotes the formation of a passive layer on the surface of nitinol, slowing the dissolution process and reducing overcut and NaCl is non-passive in nature which improves the material removal rate. Because EDTA is a chelating agent that forms soluble complexes with titanium ions, it can be used to minimize the production of TiO$_2$ layers in these electrolytes. Hence, the combination of these electrolytes improved the performance of machining in terms of accuracy, material removal rate and surface finish as shown in **figure5.12.** The pitting effect has been lowered and the homogeneity of microgroove has been improved the addition of EDTA as compared to the microgroove fabricated with mixed NaNO$_3$ + NaCl electrolyte shown in **figure5.12(a) (b) (c) and (d).** It has been observed that the mean depth of machined microgroove with mixed NaCl+NaNO$_3$+EDTA electrolyte has been improved to 232.9μm which is more as compared to mean depth of mixed NaCl+NaNO$_3$ electrolyte but tapering effect also increased.
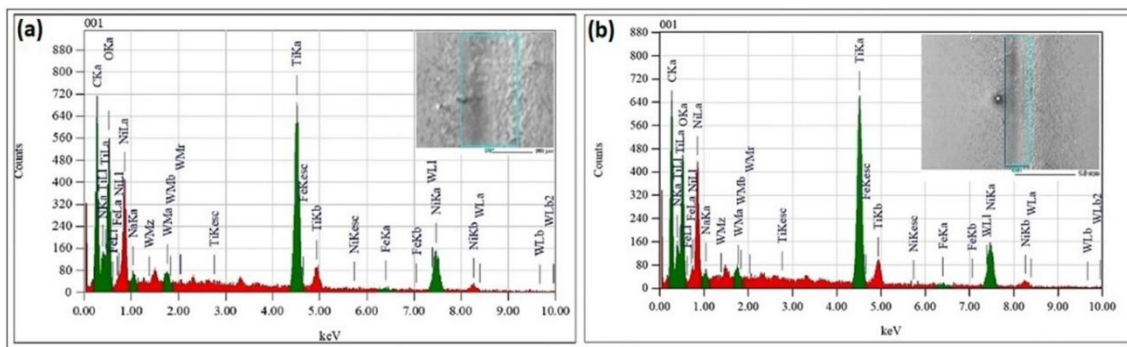
Figure5.13. EDS of microgrooves surfaces with mixed aqueous electrolytes (a) NaCl+NaNO$_3$ (b) NaCl+NaNO$_3$+EDTA

As far as width overcut is concerned in both these combination of electrolyte, there is no remarkable difference. Also, the average surface roughness (Ra) is 0.2790 μm in this electrolyte which is better than mixed NaCl+NaNO$_3$ shows improvement in the machining process. Further, the analysis for machined surfaces has been carried out using mixed NaCl+NaNO$_3$ and NaCl+NaNO$_3$+EDTA aqueous electrolyte solutions using EDS and FESEM images with generated plots are shown in **figure5.13.** The oxygen concentration is 20% without EDTA and 17.99% with EDTA, according to the EDS results presented in **Table5.3.** It has been confirmed from the EDS analysis that the lower content of oxygen in presence of EDTA forms thin oxide layer on the machining surface and occurs uniform dissolution during machining. This implies that an EDTA-based solution forms only a thin coating of titanium oxide, allowing for the machining of microgrooves with fewer overcuts and more mean depth. The mixed electrolyte with

addition of EDTA has better machining capability due to uniform dissolution compared to machining in individual electrolytes producing larger oxygen and carbon contents.

Table5.3. EDS Analysis for element composition of mixed electrolyte

Element (K)	NaCl +NaNO$_3$		NaCl +NaNO$_3$+EDTA	
	mass%	atom%	mass%	atom%
Ni	21.87	9.23	23.16	9.04
Ti	30.16	12.57	32.33	18.04
O	20.00	27.39	17.99	26.08
C	23.19	45.20	20.78	39.67
Fe	0.36	0.14	0.44	0.18
Na	1.66	1.54	0.88	0.88
N	2.35	3.58	3.68	6.02
Cl	0.41	0.24	-	-
W	-	-	0.74	0.09

When EDTA is present in the mixed NaCl+NaNO$_3$ electrolyte solution, this results in a uniform and controlled anodic dissolution of nitinol, which is also responsible for the reduction in overcut and increase in mean depth with better surface finish as compared to mixed NaCl+NaNO$_3$ electrolyte solution without EDTA.

5.2.1.4 Effect of ozonated mixed electrolytes on the accuracy and surface finish

From the above investigation, it is observed that the mixed electrolytes have capability to create smooth surfaces with fewer overcuts in width and more mean depth in fabricated microgrooves. However, the passive layer that the NaNO$_3$ electrolyte forms on the surfaces and large amount of sludge produced on the machining surface in NaCl electrolyte due to more metal removal further impedes accurate machining, leading to low grade machining capabilities. A correct machining performance is required while fabricating nitinol microfeatures. So, in order to improve the performance of the WECM, ozone gas is pressurized into the mixed aqueous NaCl+NaNO$_3$ by creating an ozonated mixed aqueous NaCl+NaNO$_3$ electrolyte. With the ozonated aqueous solution, metal removal is shown to be greater than with the non-ozonated electrolyte for all runs. This results in the prevention of an ozonation-caused passive layer and removal of sludge. Ozone (O$_3$) is enhanced to increase the oxidizing ability and corrosive behavior of basic aqueous electrolytes [98]. Ozone must be created in an area where it will be consumed since it is extremely unstable and quickly becomes O$_2$. This explains how adding ozonated aqueous NaCl and NaNO$_3$ solution to the WECM for nitinol affects how well the machine can function. Ozone is a powerful oxidant with a relatively short half-life that has been employed in many different chemical applications. The most reactive secondary

oxidants, hydroxyl and peroxyl radicals, are produced as ozone decomposes. The procedures that cause ozone to degrade in aqueous solutions are listed below **[99]**.

$$O_3 + OH^- \rightarrow HO_2^- + O_2 \uparrow \tag{5.24}$$

$$HO_2^- + O_3 \rightarrow HO_2 + O_3^{*-} \tag{5.25}$$

$$HO_2 + OH^- \rightarrow H_2O + O_2^- \tag{5.26}$$

$$O_3 + O_2^- \rightarrow O_3^{*-} + O_2 \uparrow \tag{5.27}$$

$$H_2O + O_3^{*-} \rightarrow OH + O_2 \uparrow + OH^- \tag{5.28}$$

$$HO^* + O_3^{*-} \rightarrow O_2^- + HO_2 \tag{5.29}$$

$$HO^* + O_3^{*-} \rightarrow O_3 + OH^- \tag{5.30}$$

$$HO^* + O_3 \rightarrow HO_2 + O_2 \uparrow \tag{5.31}$$

Ozone reacts with OH ions that have been severed from water molecules. The chain reaction also creates superoxide anion (O_2) and HO radicals. Equation demonstrates how the ozone (O_3) equilibrium reaction is significant **[100]**.

$$O_3 \rightarrow O_2 + O \tag{5.32}$$

The interaction between the water molecules and the atomic O continues, most likely creating the energetic O_3^*. Equations demonstrate that this O_3^* reacts with water to produce hydrogen peroxide.

$$O + H_2O \rightarrow 2HO^* \tag{5.33}$$

$$O_3^* + H_2O \rightarrow H_2O_2 + O_2 \tag{5.34}$$

The other O_2/HO_2 radicals appear as the species continue to react. When the byproducts of HO* and HO_2 contact with O_3, the chain reaction continues. Large amounts of radicals and products are produced, and they interact intensely with the workpiece's surface **[101]**.

$$HO^* + HO^* \rightarrow H_2O_2 \tag{5.35}$$

$$HO^* + HO_2 \rightarrow H_2O + O_2 \tag{5.36}$$

$$HO_2 + HO_2 \rightarrow H_2O_2 + O_2 \tag{5.37}$$
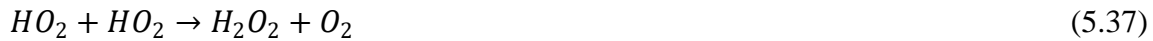
All of the dissolved chemicals experience quick and free radical interactions with these radicals. These hydroxyl radicals react with organic pollutants to produce hydrogen peroxide (H_2O_2) and certain aldehydes. The presence of hydrogen peroxide (H_2O_2) in electrolyte may raise material removal rate. The pH level, temperature, and substances in the solution all have an impact on how quickly ozone decomposes in aqueous solutions. The oxidative capability of ozone is increased via controlled ozone breakdown. The flow rate of the electrolyte is taken into account since it is required to assist ozonation for stability and to remove oxides and sludge from the tiny gap. The surface of the workpiece

would react with hydroxyl ions to produce hydroxides, which would then precipitate as sludge. For all experiments, it has been found that metal removal is greater for the ozonated aqueous solution. This is as a result of the O_3 mixed electrolyte's efficient removal of deposited contaminants from the surface. Deposits are continually removed, leaving a clean surface that may be machined further. The ozonation technique fully eliminates the metal sludge that is accumulated on the workpiece surface. Oxides on the workpiece surface can be removed with the help of the ozone, which frequently breaks down into oxygen form. Surface roughness is caused by active dissolving on the workpiece surface, which is caused by the present electrolyte concentration settings and ozonation during machining of nitinol.

Figure 5.14 FESEM, mean depth, 3D surface and roughness profile of fabricated microgroove with mixed ozonated NaCl +NaNO$_3$ electrolyte

Figure5.14. shows the FESEM, mean depth, 3D surface and roughness profile of machined microgroove at 0.2M mixed ozonated aqueous NaCl+NaNO$_3$ electrolyte. Ozone presence has a greater impact on the specimen's surface. The anodic dissolution is impacted by the increase in electrolyte conductivity. By rapidly oxidizing an oxide layer on the metal surface, ozonation exposes the workpiece's brand-new surface. As a consequence, ozonation effectively removes sludge and oxides, leaving the surface clean and improving surface roughness Ra. There are no more deposits on the uniformly machined surface. The removal of oxides from the nitinol sample surface increases the metal removal in the ozonated aqueous NaCl+NaNO$_3$ electrolyte. Ozone breaks down into extremely reactive secondary oxidants made of hydroxyl and peroxyl radicals, which

react quickly with dissolved oxide and metal hydroxide complexes. From the experimental investigation, the microgroove average width of 115.365μm, mean depth of 245.9μm and average surface roughness (Ra) of 0.2258 μm have been obtained which shows improved results as compared to mixed aqueous $NaCl+NaNO_3$ due to application of ozonization. The pitting effect is very less and homogeneity has been improved in this electrolyte as compared to nonozonated mixed $NaCl+NaNO_3$ electrolyte.

 As it is seen in the investigation of mixed $NaCl+NaNO_3+EDTA$ that the dimensional characteristics and surface finish have been improved compared to mixed $NaCl+NaNO_3$ electrolyte, further analysis has been carried out with mixed ozonated $NaCl+NaNO_3+EDTA$ electrolyte solution. The FESEM image, mean depth, 3D surface and roughness profile of machined microgroove with 0.2M mixed ozonated aqueous $NaCl+NaNO_3+EDTA$ electrolyte as shown in **figure5.15**.
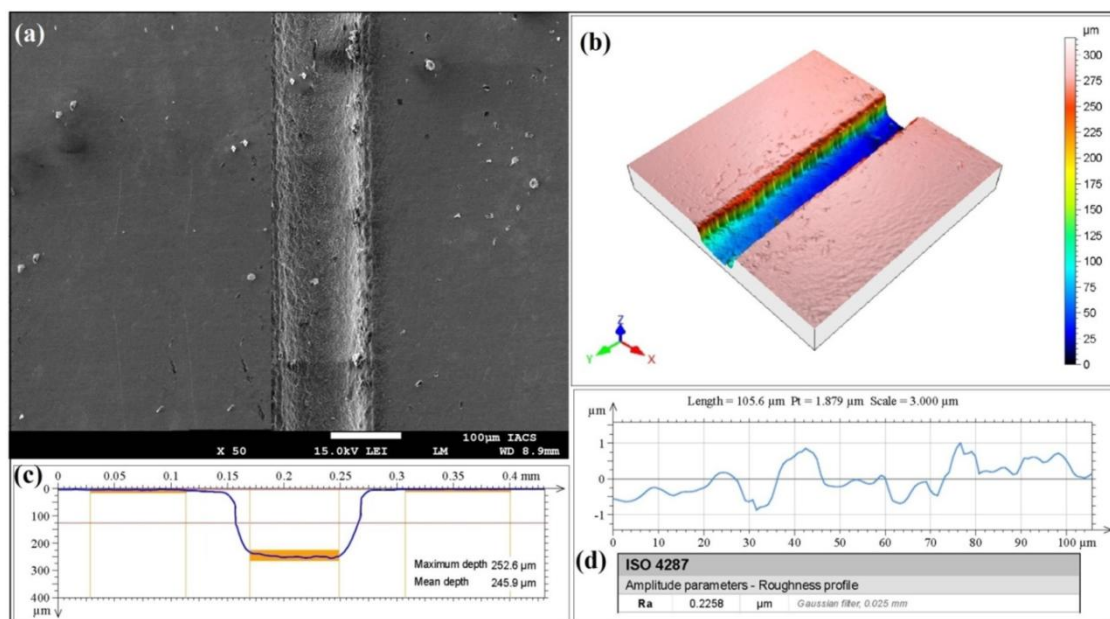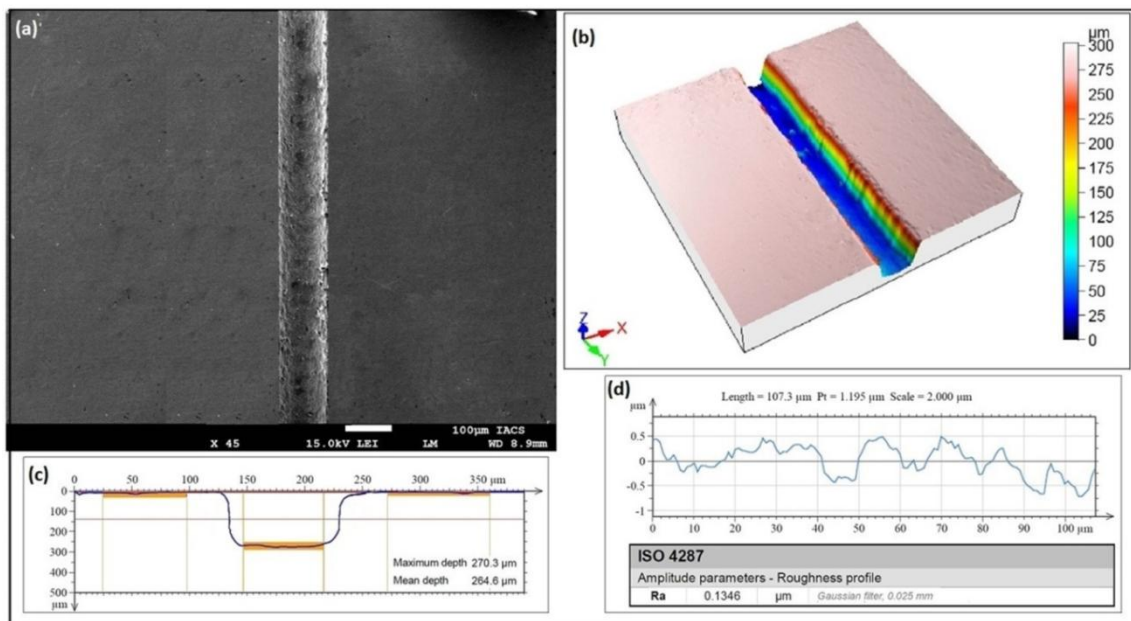

Figure 5.15 FESEM, mean depth, 3D surface and roughness profile of fabricated microgroove with mixed ozonated $NaCl+NaNO_3+EDTA$ electrolyte

From the experimental investigation, the microgroove average width of 105.86μm, mean depth of 264.6μm and average surface roughness (Ra) of 0.1346μm have been obtained with mixed ozonated aqueous $NaCl+NaNO_3+EDTA$ electrolyte during nitinol machining. The homogeneous microgroove with smooth surface finish has been obtained and pitting effect was not seen on the sidewall of the machined microgrooves with negligible tapering effect. It shows that mixed ozonated $NaCl+NaNO_3+EDTA$ electrolyte solution has been proven as best electrolyte combination for obtaining better accuracy and surface finish during microgroove machining of nitinol shape memory alloy using wire

electrochemical machining. The EDS analysis for machined surfaces of ozonated mixed $NaCl+NaNO_3$ and $NaCl+NaNO_3+EDTA$ aqueous electrolyte solutions as shown in **figure5.16.** The peaks of the titanium Ti and nickel Ni has been improved while peaks of oxygen O and carbon C have been reduced. It shows that the use of ozonization in electrolyte has great influence on formation of oxide layer on the machining surface of the nitinol to produce uniform anodic dissolution.
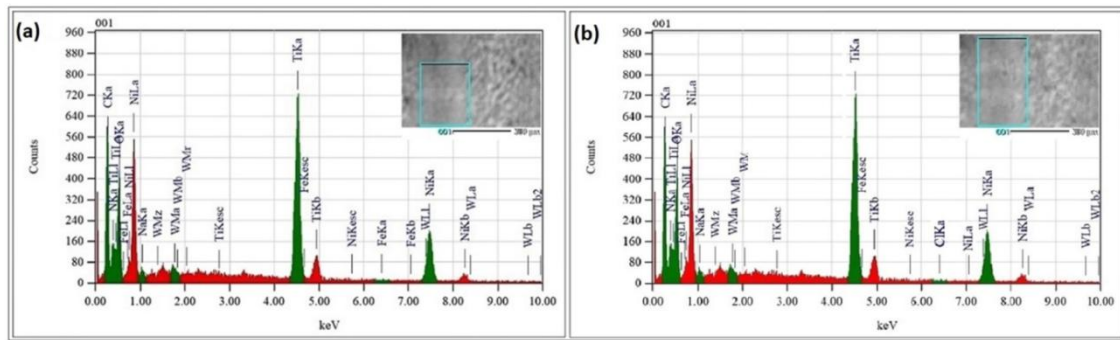
Figure 5.16 EDS of microgrooves surfaces with ozonated mixed aqueous electrolytes (a) $NaCl+NaNO_3$ (b) $NaCl+NaNO_3+EDTA$

The oxygen concentration (mass %) is 18.44% without EDTA and 14.66% with EDTA in ozonated conditions of both these electrolytes, according to the EDS results presented in **Table5.4.** The EDS findings reveal that oxygen present on the machined surface has lower value, implying that the nitinol surface has no more passivity in the electrolyte solution containing EDTA under ozonated condition as compare to other nonozonated conditions. In the case of the ozonated $NaCl+NaNO_3+EDTA$ electrolyte, this implies that the machined surface dissolves uniformly.

Table5.4. EDS Analysis for element composition Ozonated mixed electrolytes

Element (K)	Ozonated NaCl +NaNO₃		Ozonated NaCl +NaNO₃+EDTA	
	mass%	atom%	mass%	atom%
Ni	25.16	10.11	32.11	19.41
Ti	32.09	14.73	33.74	19.17
O	18.44	27.18	14.66	20.18
C	18.03	39.32	14.63	33.26
Fe	0.61	0.26	-	-
Na	0.85	0.87	0.62	0.69
N	4.34	7.30	3.92	7.08
Cl	0.24	0.20	0.24	0.20
W	0.24	0.03	0.08	0.01

This implies that an EDTA-based solution forms only a very thin coating of titanium oxide as compared to nonozonated mixed simple aqueous electrolytes, allowing for the

machining of homogeneous microgrooves with more depth of penetration due to uniform anodic dissolution of nitinol during WECM. When comparing results for average groove width, mean depth and surface roughness (Ra) for 0.2M mixed $NaCl+NaNO_3$ and mixed $NaCl+NaNO_3+EDTA$ electrolytes under nonozonated and ozonated conditions as depict in **figure5.17**, It is observed that that the average groove widths have no more differences in dimensional characteristics. However, there is improvement in mean depth and surface roughness Ra. The minimum mean depth has been obtained with 0.2M mixed $NaCl+NaNO_3$ under nonozonated condition and maximum mean depth has been obtained with mixed $NaCl+NaNO_3+EDTA$ under ozonated condition. In the same way, surface roughness Ra is maximum with $NaCl+NaNO_3$ under nonozonated condition and minimum with mixed $NaCl+NaNO_3+EDTA$ under ozonated condition. The average groove width of 118.35μm, 115.365μm, 112.68 μm, 105.86μm, mean depth of 188.7μm, 232.9μm, 245.9μm, 264.6μm and the surface roughness (Ra) of the machined surface achieved was 0.3333μm, 0.2790μm, 0.2258μm, and 0.1346μm for 0.2M of mixed $NaCl+NaNO_3$, mixed $NaCl+NaNO_3+EDTA$, ozonated mixed $NaCl+NaNO_3$, ozonated mixed $NaCl+NaNO_3+EDTA$ electrolytes respectively. It shows that ozonated mixed $NaCl+NaNO_3+EDTA$ electrolyte has been proven as most suitable electrolyte combination to achieve better dimensional characteristics and surface finish of nitinol during wire electrochemical machining.
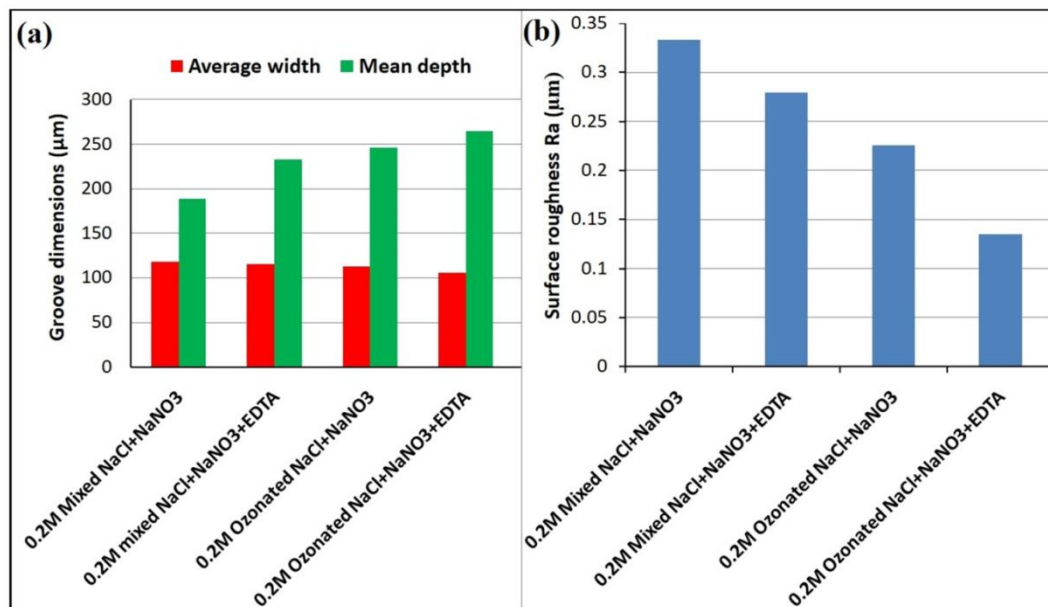
Figure 5.17 Comparison of microgrooves in various mixed ozonated electrolytes for (a) average width and mean depth (b) surface roughness Ra

5.2.1.5 Fabrication of micro slits with ozonated mixed electrolytes

The fabrication of perfect microslits is complicated for WECM due to the inaccuracies and the poor surface finish developed during machining. This investigation verified that the use of EDTA as a complexing agent, in combination with ozonated NaCl and $NaNO_3$ electrolyte, can improve the microfeatures accuracy of nitinol. The process used to fabricate the microslits involved wire electrochemical machining where constant wire feed has been given for material removal to fabricate microslits on the nitinol sheet of 200μm thickness. The concentration of the mixed $NaCl+NaNO_3$ and mixed $NaCl+NaNO_3+EDTA$ electrolyte was kept constant at 0.2 M, while other machining parameters, like pulse duty ratio of 50%, Pulse frequency of 250 kHz initial IEG of 50μm, wire diameter of 50μm, and pulse voltage of 5V at a wire feed rate of 1.4μm/s, remained unchanged. The optical images are presented in **figure5.18.**
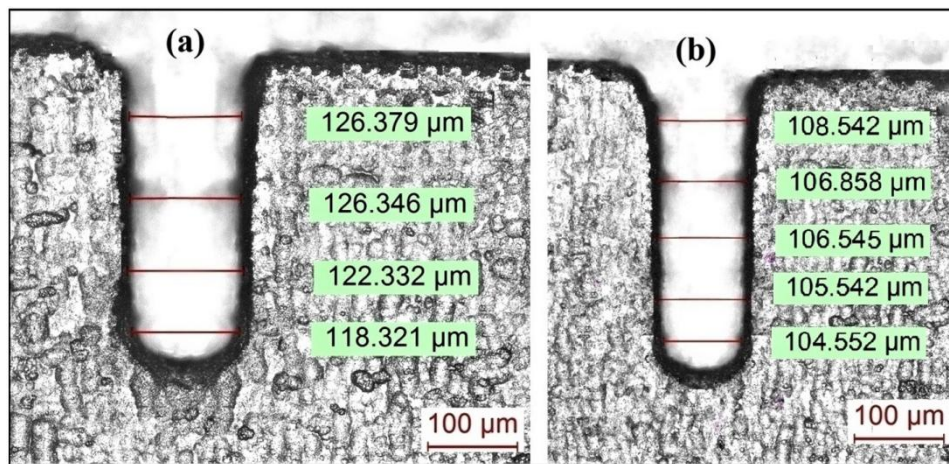
Figure 5.18 Fabricated microslits with (a) Mixed Ozonated $NaNO_3+NaCl$ electrolyte (b) Mixed Ozonated $NaNO_3+NaCl+EDTA$ electrolyte
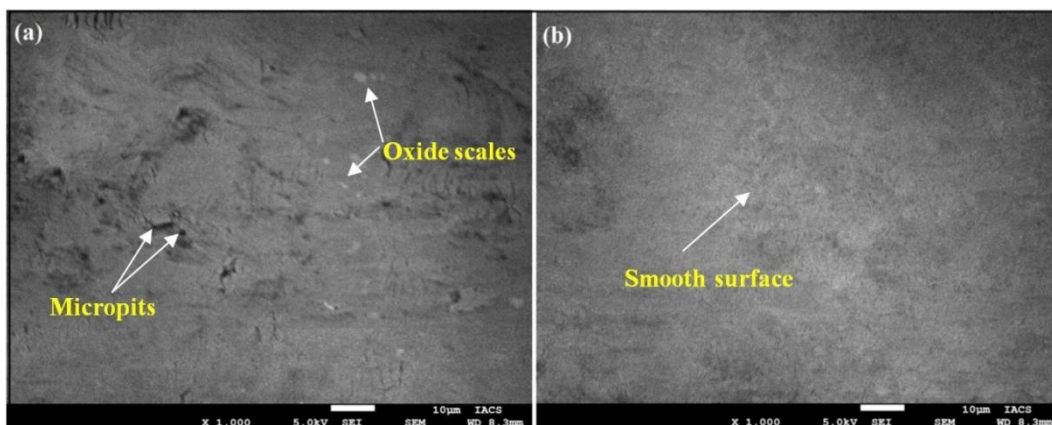
Figure 5.19 FESEM microstructure of machined microgroove surfaces at (a) 0.2M Ozonated $NaCl+NaNO_3$ (b) 0.2M Ozonated $NaCl+NaNO_3+EDTA$

For 0.2M $NaNO_3$ ozonated mixed $NaCl+NaNO_3$ electrolyte and 0.2M mixed

NaCl+NaNO3+EDTA ozonated electrolyte, the average slit width of 123.34μm, and 106.40μm, respectively, whereas the surface roughness (Ra) is calculated as 0.1546μm, and 0.1261μm, respectively, for the corresponding electrolytes measured using coherent correlation interferometer (CCI). Thus, with the usage of the EDTA as a complexing agent in combination with $NaCl+NaNO_3$ electrolyte, accurate and precise microslits with lowest surface roughness could be successfully fabricated. The machined surface conditions using 0.2M ozonated $NaCl+NaNO_3$ and mixed 0.2M ozonated $NaCl+NaNO_3+EDTA$ is shown in **figure5.19.** It can be seen that the machined microslits surface obtained with 0.2M ozonated $NaCl+NaNO_3$ has few micro pits and very small oxide scales. These micro pits form as the electrolyte temperature rises with increasing current density in the machining zone. However, the machined surface condition with mixed 0.2M ozonated $NaCl+NaNO_3+EDTA$ is smoother with negligible defects on the surface. Hence, it has been proven that the application of EDTA with mixed $NaCl+NaNO_3$ electrolytes in ozonated condition improve the machining accuracy and surface finish of fabricated nitinol shape memory alloy microfeatures during wire electrochemical machining.

5.3 Experimental Planning II: Influence of mixed acidic electrolytes

For electrochemical characterization of nitinol SMA, a standard three electrode configuration was used to perform cyclic potentiodynamic polarization (PDP) tests and electrochemical Impedance Spectroscopy (EIS) for acidic electrolytes as shown in **figure5.20.**

Figure 5.20 Schematic of Potentiodynamic and EIS test setup

An electrochemical workstation (PGSTAT model 302 N, Metrohm Autolab B.V, Netherlands) was used to conduct electrochemical analys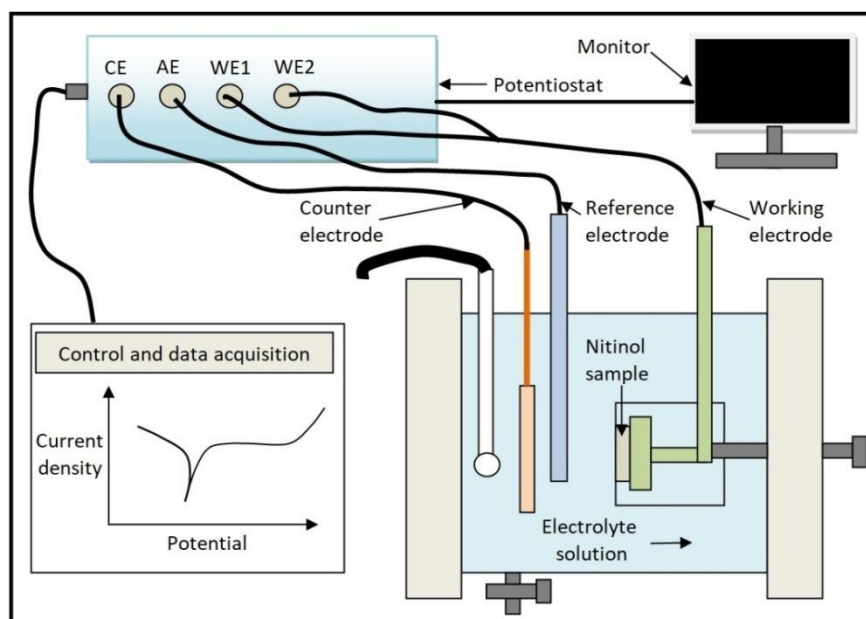es of the test samples. Before performing polarization tests, test specimens were carefully washed with distilled water after being placed in acetone for one hour. In this electrochemical workstation, it is unquestionably maintained static on the electrochemical cell utilizing a screw-type mechanism. In an effort to examine how surface integrity affects corrosion behavior, no specimens were passivised prior to corrosion testing. In order to suit the anode size of 15mm x 15mm x 1mm for corrosion testing, nitinol test specimens were made to that size. The working electrode for EIS and PDP testing was a nitinol SMA specimen, whereas the reference and counter electrodes for those tests were Ag/AgCl cells. The potentiodynamic curve was generated by scanning at a rate of 10 mV/sec from -1 V to 1 V. A condition known as Open Circuit Potential (OCP) was used for the EIS measurement. Standard Nyquist and Bode charts are used to present the results. Using the EIS analyzer programme, the precise parameters for the EIS observations were determined. The electrolyte solutions of 0.1M H_2SO_4 and mixed 0.1M H_2SO_4 + citric acid were utilized for electrochemical testing. To account for repeatability, PDP tests and EIS were carried out on two samples. The ASTM standard G61 was used to determine the susceptibility to localize corrosion on Nitinol SMA with a value of current cutoff as 5mA. The measurement has been stopped when the potential reaches the corrosion potential. Due to the wire electrode's side cross-section, WECM machining kinematics differs from those of other ECM techniques. **Table5.5** displays every WECM parameter that was applied to create the micro grooves.

Table 5.5 Process parameter conditions

Sr.No.	Process parameters	Nature	Range
1	Electrolyte concentration	Fixed	0.1M
2	Applied pulse voltage	Variable	6 to 8 V
3	Wire feed rate	Variable	1.2 to 1.8μm/s
4	Pulse frequency	Fixed	250KHz
5	Duty ratio	Variable	35 to 50%
6	PZT vibration frequency	Fixed	25Hz
7	PZT vibration amplitude	Fixed	12.54 μm
8	Flow rate	Fixed	5 Lph

In order to determine the best electrolyte for machining, two distinct acidic electrolytes were selected, including an inorganic acidic aqueous solution and a mixture of an inorganic and environmentally friendly organic acidic solution. All of the experiments for the machining of nitinol SMA employed 0.1M H_2SO_4 and 0.1M H_2SO_4 mixed with 0.1M environmentally friendly citric acid as the electrolyte **[74, 77].** To determine the appropriate input process parameters, such as pulse voltage, duty ratio and wire feed rate, a broad variety of trial experiments were carried out for fabrication of micro grooves. Additionally, the noncontact type CCI profilometer made by Taylor & Hobson was used to measure the depth of the groove and the surface roughness of the machined micro groove. This technique provided 3D surface roughness data for the surfaces, and a Lieca optical microscope was used to determine the groove width.

5.3.1 Experimental observations and discussions

In this section, the polarization studies using potentiodynamic polarization (PDP) tests and electrochemical impedance spectroscopy (EIS), experimental results, SEM analysis, observations and the performance characteristics were discussed in detail to analyze the surface integrity and surface roughness. After conducting wide range of trial experiments and obtaining best possible parameter combinations, the machined microgrooves have been cautiously observed. To find out the effect of 0.1M H_2SO_4 and mixed 0.1M H_2SO_4 + 0.1M citric acid electrolyte on machined micro-groove dimensions i.e. width and depth as well as surface characteristics and to get further insight; the experimental observations with results and discussions have been given hereunder.

5.3.1.1 Potentiodynamic Polarization Tests

The potentiodynamic polarization (PDP) investigation has been carried out on Nitinol SMA, and the resulting voltammograms as per the ASTM standard are shown in **figure5.21.** as polarization curves created by two different electrolytes and their consequences. For Nitinol, two distinct electrolytes i.e. 0.1M H_2SO_4 and mixed 0.1M H_2SO_4 + 0.1M citric acid electrolyte were used in the corrosion investigations. The electrolyte conductivity plays very important role in all electrochemical experiments, especially in the cyclic polarization technique. The externally polarized current-potential behavior of a metal near its corrosion potential gives an excellent estimate of the rate of corrosion. The polarization curve depicts corrosion potential against current and the effect of these electrolytes on nitinol susceptibility to localized corrosion was studied. It is evident from the ensuing voltammograms in both PDP tests that localized corrosion is not present under either electrolyte state, but uniform corrosion in the transpassive or oxygen

evolution zone may occur. These graphs show that nitinol SMA is more resistant to the start and spread of localized corrosion, assuming that the corrosion potentials of nitinol SMA in both the electrolyte obtained at a fixed scan rate in these tests are similar or having negligible difference. The voltage at which the anodic current grows quickly in this test method indicates the vulnerability to the start of localized corrosion. It shows that the corrosion potential shifted towards the anodic forward direction with decrease in corrosion current as the surface roughness decreased without significant difference in cathodic currents among both the nitinol SMA samples with different surface roughness in different electrolyte due to the different anodic behavior of the alloy.
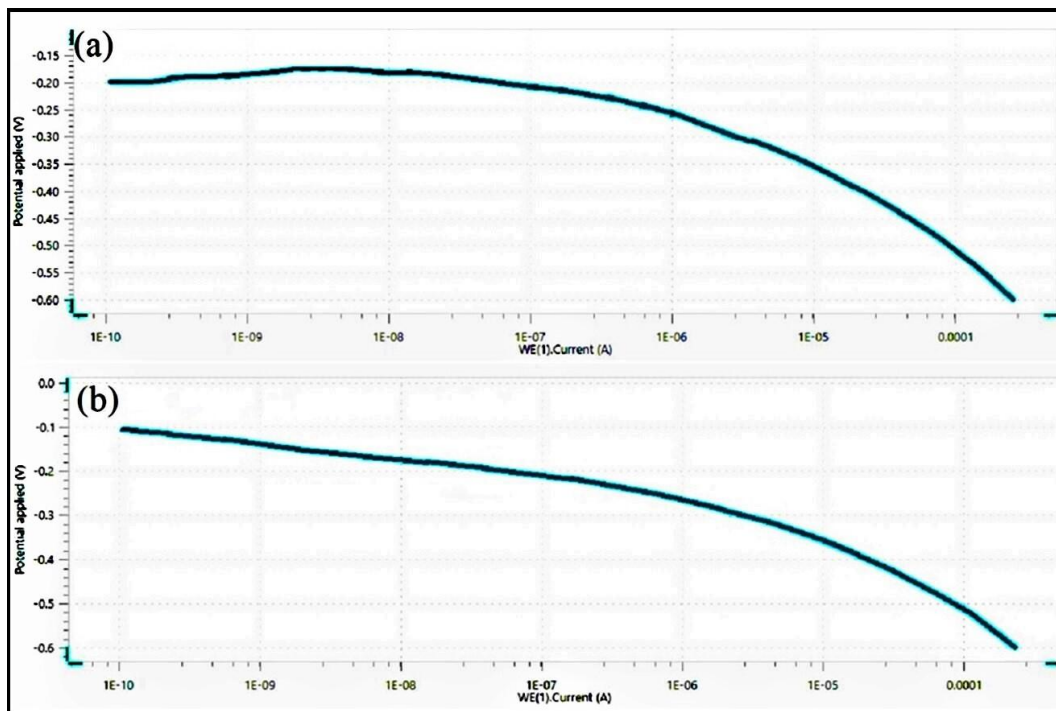
Figure 5.21 Voltammogram of (a) 0.1M H_2SO_4 (b) Mixed 0.1M H_2SO_4 + 0.1M citric acid electrolyte

The specimens in 0.1M H_2SO_4 electrolyte showed increase in the anodic current compared to mixed 0.1M H_2SO_4 + 0.1M citric acid electrolyte which may be responsible for increase in surface roughness due to increase in corrosion rate. The decrease in surface roughness occurs with lower corrosion rate and very high corrosion rate results in pitting due to rougher surface. The passive oxide layer can form due to formation hydroxide and gas bubbles. The overall surface-to-electrolyte contact area is greatly reduced by the heterogeneous interface that forms between the solution and the surface, which significantly slows down corrosion. The corrosion current of 1x 10^{-10} A is achieved with the acidic H_2SO_4 electrolyte, which is identical to the mixed 0.1M H_2SO_4 + 0.1M

citric acid electrolyte, but this mixed electrolyte reached the corrosion potential of -0.1 V, which is higher. This test demonstrates the acidic H_2SO_4 electrolyte's excellent active dissolution process. It demonstrates that the controlled dissolution of nitinol SMA with low current of mixed 0.1M H_2SO_4 + 0.1M citric acid electrolyte gives lower corrosion rate, further improving the surface roughness. Among the selected electrolytes, 0.1 M H_2SO_4 electrolytes were discovered to be the most corrosive solution. Due to a low passive current and a greater potential, Ni ions present in electrolyte show a lesser tendency to corrode when used in an electrolyte solution containing mixed 0.1 M H_2SO_4 + 0.1 M citric acid. It was discovered that the composition of the electrolyte caused differences in the passive zone of the polarization curves of various electrolytes.
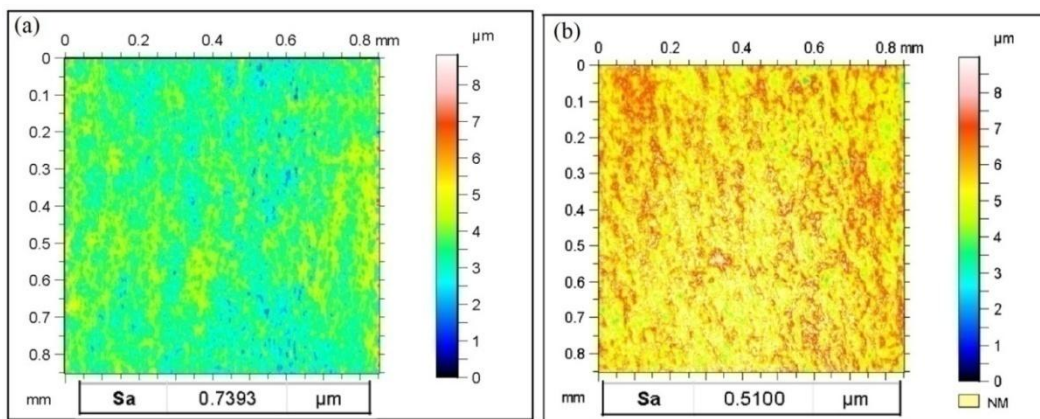
Figure 5.22 Surface roughness after PDP at **(a)** 0.1M H_2SO_4 **(b)** 0.1 M H_2SO_4 + 0.1 M citric acid

The precise ions present, especially anions, have a considerable impact on the corrosion behavior of nitinol. According to the polarization research, machining of nitinol can be properly done with mixed 0.1M H_2SO_4 and citric acid electrolyte solution. In contrast to other electrolytes, 0.1M H_2SO_4 in the presence of citric acid electrolyte can be used to generate the smooth surface. The surface topography in the solution of 0.1 M H_2SO_4 electrolyte and mixed 0.1 M H_2SO_4 + 0.1 M citric acid, as shown in **figure5.22 (a) and (b).** To achieve high surface quality, the citric acid solution serves as a safe organic acidic electrolyte. According to the findings of the potentiodynamic tests, the surface roughness of the nitinol sample in mixed 0.1M H_2SO_4 + 0.1M citric acid electrolyte solution was 0.5100 μm, which is much less than the surface roughness 0.7393 μm of 0.1 M H_2SO_4 electrolyte solutions. Thus, it is considered that the electrochemical machinability of the nitinol alloy is slightly better in mixed acidic electrolyte.

5.3.1.2 Electrochemical Impedance Spectroscopy

The working electrode i.e. nitinol SMA is applied a modest amplitude sinusoidal voltage across a broad frequency range in electrochemical impedance spectroscopy (EIS) using 0.1 M H_2SO_4 and mixed 0.1 M H_2SO_4 + 0.1 M citric acid electrolyte. Another sinusoidal signal with amplitude (I) and a phase shift in relation to the input signal is produced at each frequency.

Figure 5.23 EIS of H_2SO_4 electrolyte

Figure 5.24 EIS of mixed 0.1M H_2SO_4 and citric acid electrolyte
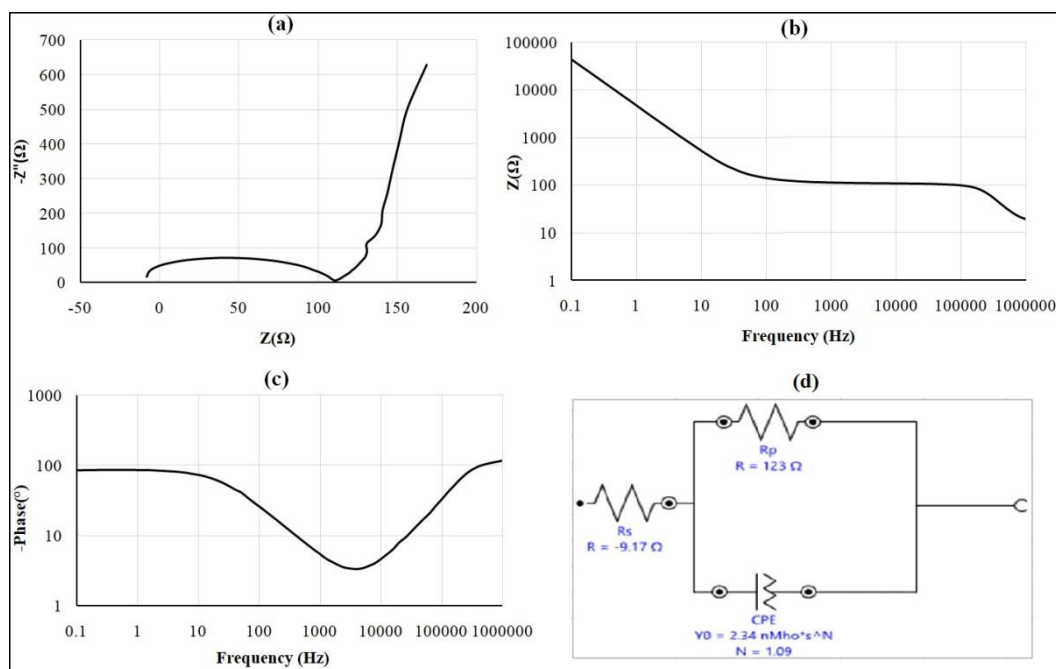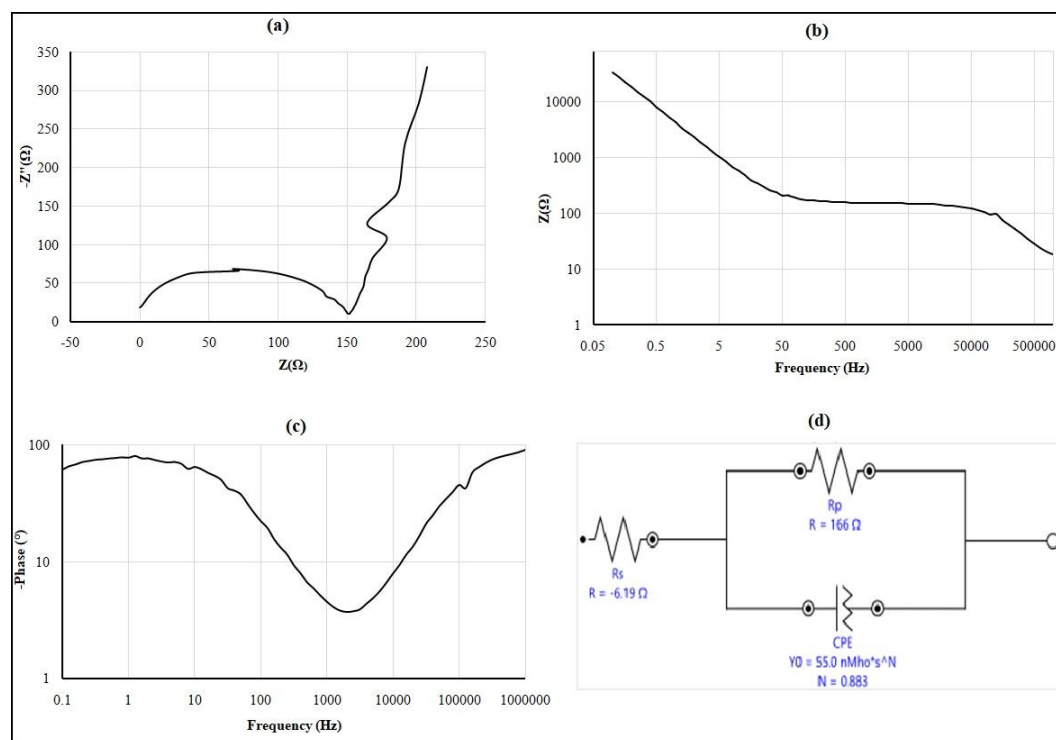
The imaginary component (Z″) is shown against the real component (Z′) for each excitation frequency in an EIS data Nyquist plot as shown in **figures5.23 (a) and 5.24(b)**. Plots of Bode-magnitude and Bode-phase enable analysis of absolute impedance as shown in **figures5.23 (b, c) and 5.24 (b, c)**. The notion of CPE may be applied to the modeling of an electrical double layer to correct the capacitor's non-ideal behavior. A double layer capacitor with bulk resistance and polarization resistance is part of the condensed Randles model. As illustrated in **figures5.23 (d) and 5.24(d)**, the surface-deposited double layer capacitor is linked in parallel with the polarization resistor (Rp), which is connected in series with the bulk resistor (Rs). An electrochemical system analysis starts with this model. The resistance of Rs moves the semicircle's beginning point to higher Z_{real} values in the Nyquist plot of a simplified Randles cell. The polarization resistance is also represented by the semicircle's diameter. The equivalent circuit's Rs, Rp, and CPE component is fitted to the semicircle, which represents the rapid oxidation and reduction kinetics. The amount of the current during the polarization of nitinol SMA as working electrode is governed by reaction kinetics and the diffusion of reactants both towards and away from the electrode. The lower corrosion current results from higher polarization resistance. When an electrode's potential is deviated from its value at open circuit or corrosion potential, the electrode becomes polarized. Due to electrochemical processes that are triggered at the electrode surface by the polarization of an electrode, current flows. This effect has significant effects on interpretation and needs to be made up for Nitinol SMA with high polarization resistance Rp have good corrosion resistance, whereas those with low Rp have low corrosion resistance. During an electrochemical reaction, the roughness values are low at strong corrosion resistance and a drop in corrosion rate. Additionally, a higher number of pits have been seen on rougher surfaces than on smooth surfaces, which is consistent with a lower corrosion rate. The strength of the corrosion current reduces as the electrolytes' provided resistance rises. A smart way to manage corrosion, incidentally, is to increase the solution resistance since a reduction in corrosion current results in a reduction in corrosion rate. In this approach, the solution resistance (Rs) is obtained from the high-frequency intercept of real impedance, and the sum of Rs and Rp is obtained from the low-frequency intercept. When Rp is known, the Stern-Geary equation may be used to calculate the metal corrosion rate.

To confirm the conclusion drawn in the EIS section, the polarization resistances (Rp) were determined and examined using the Nyquist and Bode plots as can be shown in **figure5.23 and 5.24**. The potentiodynamic tests order of the polarization resistances and

the EIS findings order of the resistances accord with one another. When an AC voltage is delivered to an electrochemical cell, resistance (R), capacitance (C), and inductance (L) are measured by watching the current response. When a DC voltage is supplied, the relationship between R, V, and I satisfies Ohm's law. Similar to this, the impedance Z (= 2f is the angular frequency of the applied AC voltage) may be represented as V / I, which is the equation for Ohm's law in an AC circuit, when an AC voltage is applied to an electrochemical cell. As a result, the resistance that prevents current flow when an AC voltage is introduced to the circuit is known as impedance. The many circuit components that make up a circuit's total impedance, including conductors, inductors, and resistors, represent these interruptions. The electrochemical cell in a real system incorporates multiple circuit components in a variety of arrangements. In order to accurately depict an electrochemical system, the idea of impedance should be used rather than a circuit model that only includes a resistor. Additionally, V and I have zero phase difference when applied with the angular frequency. A qualitative indicator of corrosion resistance is the capacitive loop's diameter in the Nyquist plot; a greater diameter denotes stronger corrosion resistance for nitinol SMA in respective electrolytes. It shown that for the case of metal under corrosive conditions, the resistance behavior predominates in the low frequency zone and that the Bode impedance values at low frequency may be used as a gauge of the corrosion resistance.

The electrochemical system was modeled using comparable electric circuits in order to support this result and quantify the corrosion behavior of the nitinol samples in both electrolytes. The ideal circuit for each sample was chosen using the Nyquist and Bode plots of each circuit. In order to account for the electrolyte behavior and the resistance of the oxide layer, each circuit contains a Constant Phase Element (CPE) and non faradic solution Resistance Rs causes a potential drop between the working electrode i.e. nitinol SMA and reference electrode i.e. Ag/AgCl cell causing errors and polarization resistance (Rp) is the transition resistance between the electrodes and the electrolyte which behaves like a resistor and can be calculated by taking the inverse of the slope of the current potential curve at open circuit or corrosion potential. The polarization resistance of the Nitinol sample in 0.1 M H_2SO_4 electrolyte was 123 Ω is improved to 166 Ω when compared to the Nitinol sample in 0.1 M H_2SO_4 with citric acid electrolyte. It is evident from the values of the resistances Rp and Rs that the corrosion resistance of the nitinol SMA sample dissolute in 0.1M H_2SO_4 electrolyte is significantly lower than that of the 0.1M H_2SO_4 and citric acid electrolyte. The values of the capacitance CPE can be reliably

used to find the thickness of the oxide film. Thus, any change in the thickness would change the capacitance C. The sample which shows the highest resistance also has the lowest oxide layer thickness. The reasoning for this contradiction is the porous structure of the oxide film leading to a surface area several times bigger than the geometric surface area.

It shows that the nitinol SMA using mixed 0.1 M H_2SO_4 + 0.1 M citric acid electrolyte has lower oxide layer thickness which is responsible for uniform anodic dissolution.The EIS findings are consistent with the fact that the corrosion resistance of the Nitinol alloy is linked to the development of a tough titanium oxide layer on the surface. The Bode plot only has one sloping section, which suggests that any potential time constants were likely to be near to one another and so irresolvable. The Bode modulus charts in the high frequency region showed continuous log|Z| values with a phase angle near to 0°. The electrolyte resistance, cell geometry, conductor impedance, and reference electrode all responded to the electrode's ohmic resistance, which is what caused the high frequency plateau of the modulus of impedance |Z|. The layer is displaying pure capacitive behavior when the phase angle is near to 90° in the low frequency band. The Bode-phase charts, where the greatest phase angle obtained was around 10° below 90°, show a considerable amount of departure from perfect capacitive behavior. Others have also noted a similar discrepancy for layers on Ti alloys. Changes in electrolyte conductivity are to blame for variations in the passive oxide layer's resistance. Changes in the surface's roughness are what caused the observed increase in corrosion resistance. The results of frequency response study are connected with the electrochemical process model at the corrosion system interface. The most common way to describe that concept is in terms of an electrical equivalent circuit. The results of the current experiments demonstrate that the nitinol SMA's corrosion resistance is increased by the process-induced surface smoothing as well as the spontaneous creation of a passive layer. The electrolyte made of a combination of sulfuric acid and citric acid, according to the results, produces the greatest results when machining nitinol SMA. Application of these greatly improves the nitinol alloy's resistance to corrosion. The smoothening of the surface and the development of a thin layer of TiO_2 on it are related to the alloy's increased corrosion resistance with uniform corrosion behavior. The corrosion resistance of the nitinol SMA in mixed 0.1 M H_2SO_4 + 0.1 M citric acid electrolyte solution is marginally superior to that of sulfuric acid alone. It is commonly recognized that the EIS measurement's outcome may be used to effectively define a material's surface condition.

Using this electrochemical characterization research for nitinol SMA using 0.1 M H_2SO_4 and mixed 0.1 M H_2SO_4 + 0.1 M citric acid electrolyte, the best and most appropriate electrolyte was identified for further machining during WECM. The concentrations used in the tests and the electrolytic concentrations used in this experimental investigation during WECM were identical. The nitinol SMA has higher electrochemical machinability in terms of machining potential and dissolved surface roughness. Its micro structural properties are determined by the WECM, which also has a significant impact on how well it resists corrosion as discuss below.

5.3.1.3 Effect of electrolytes on groove dimensions

In the WECM process, it is crucial to regulate the groove dimensions (width and depth) by establishing certain input process parameters. These geometrical parameters talk about the process's precision, quality, and controllability. It is seen that the pulse voltage is most influencing parameter during machining of nitinol SMA micro grooves using WECM. Under the same set of process settings, the effect of pulse voltage on various grove dimensions i.e. groove width, groove depth and surface roughness has been investigated in order to conduct meaningful research. The primary driving force behind this investigation is how different electrolytic media affect how electrolysis products at the tool and workpiece behave. The effect of different pulse voltages ranging from 5 to 8V on average machined groove width using 0.1M H_2SO_4 electrolyte and mixed 0.1M H_2SO_4 + 0.1M citric acid electrolytes has been shown in **figure5.25**. As the current density rises due to increase in pulse voltage, the groove's width also increases due to higher dissolution as material removal rate increases with increase in current density.
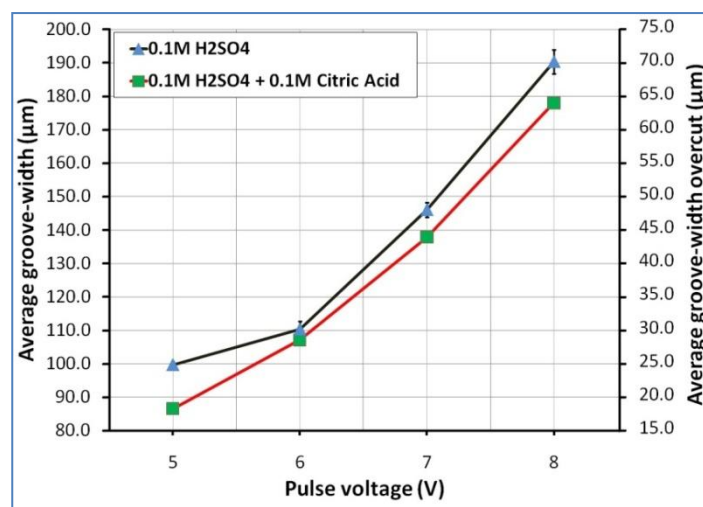

Figure 5.25 Micrograph of average groove width to pulse voltage

It is well known that H_2SO_4 is strong inorganic acid and citric acid is weak organic tri carboxylic acid which is commonly found in citrus fruits. A strong acid will have higher dissociation constant than a weak acid. The dissolution rate of citric acid electrolyte is quite lower as compared to H_2SO_4 electrolyte. When the citric acid is added to water, a reaction occurs in which hydrogen ions from the acid are released. An electrolyte with low water content can inhibit the formation of the passive layer since water is thought to play a significant part in the passivation process. **Figure5.26 and 5.27** shows the machined microgrooves of nitinol SMA during WECM at pulse voltages ranging from 5 to 7V in 0.1M H_2SO_4 electrolyte and mixed 0.1M H_2SO_4 + 0.1M citric acid electrolytes, respectively.

Figure 5.26 Groove width using 0.1M H_2SO_4 electrolyte at (a) 7V (b) 6V (c) 5V
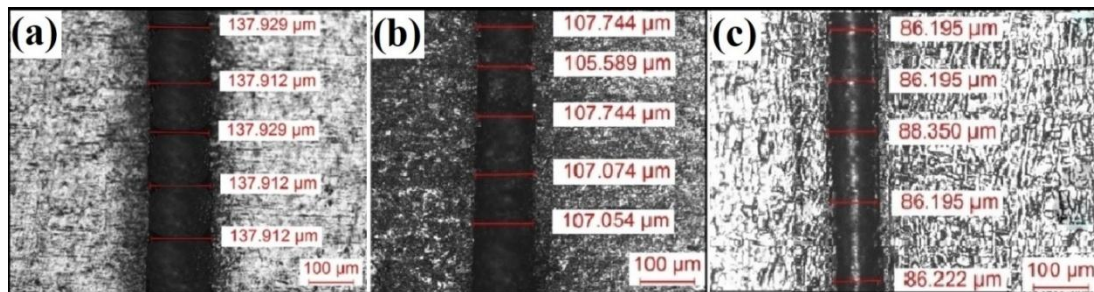
Figure 5.27 Groove width using 0.1M H_2SO_4 and 0.1M citric acid (a) 7V (b) 6V (c) 5V

As can be seen, at constant wire feed rate of 1.4μm/s , 45% duty ratio and other fixed parameters as per Table5.5, the minimum average machined groove width is 86.20 μm in 0.1 M H2SO4+0.1M citric acid at 5V pulse voltage. When the pulse voltage is 7V, the groove width is 137. 927 μm which is larger in 0.1 M H2SO4+ 0.1 M citric acid because the dissolution reactivity is greater and passive layer is less stable according to the polarization characteristics. It is thought that high pulse voltage produces more stray currents than tiny, low pulse voltage. At mixed 0.1M H_2SO_4 + 0.1M citric acid electrolyte solution, the machining groove width reduces as the electrolyte concentration was most suitable for acquiring proper anodic dissolution of nitinol SMA because the specific electrolyte resistivity is inversely proportional to the electrolyte concentration. The groove

width overcut ($\Delta_g = \frac{W_g - d_w}{2}$, where Δ_g; goove width overcut, W_g; groove width, d_w; diameter of wire) has been greatly reduced with addition of eco-friendly organic citric acid in sulphuric acid due to controlled current density distribution and toxicity of the H_2SO_4 electrolyte reduced by taking advantages of eco-friendly citric acid in the electrolyte solution for microgroove fabrication during WECM of nitinol. Citric acid-containing solutions enable for less current to be created than citric acid-free solutions. When citric acid is present in the electrolyte solution, this leads to a lower material removal rate, which also accounts for the decrease in width overcut. The production of the insoluble precipitates is decreased when an environmentally friendly citric acid complexing agent is added to the 0.1M H_2SO_4 aqueous electrolytes. In contrast to acids, these complexing agents are non-toxic and non-corrosive, making them acceptable for use in WECM. The minimum average machined groove width overcut was 18.10μm in 0.1 M H_2SO_4 + 0.1M citric acid at 5V pulse voltage which is less compared to width overcut of 24.85μm produced at 0.1 M H_2SO_4 electrolyte in same parametric machining condition.The effect of pulse voltages on maximum groove depth are as shown in **Figure5.28**.
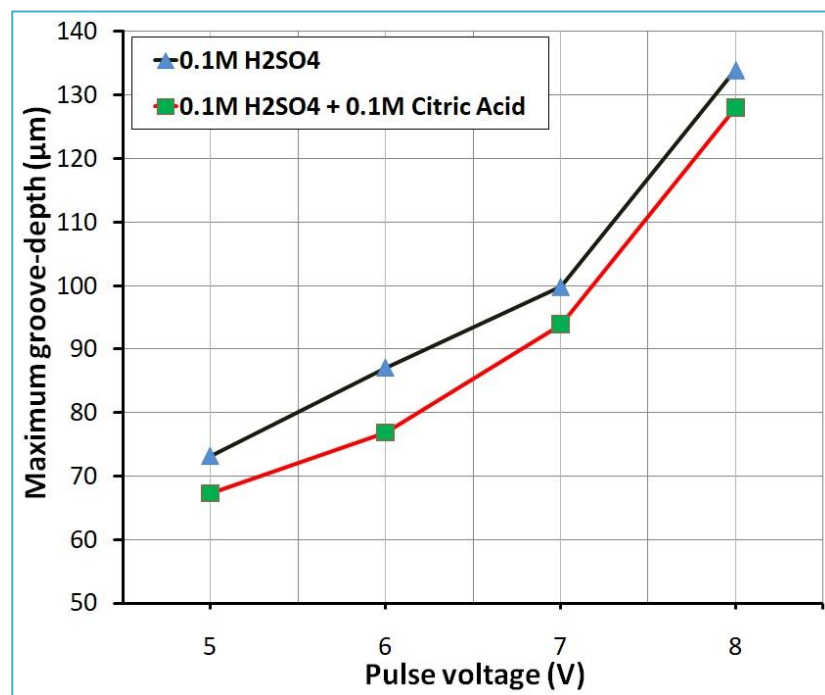
Figure 5.28 Micrograph of maximum groove depth to pulse voltage

It shows how the depth of the groove rises as the pulse voltage increases. According to the aforementioned factor, material removal rate increases as pulse voltage increases, increasing the current density at inter electrode gap near machining zone. The maximum

depth of groove at 5V using 0.1M H_2SO_4 was 73.03 µm which is further increased to 98.9 at 5V pulse voltage as shown in **figure5.29**.
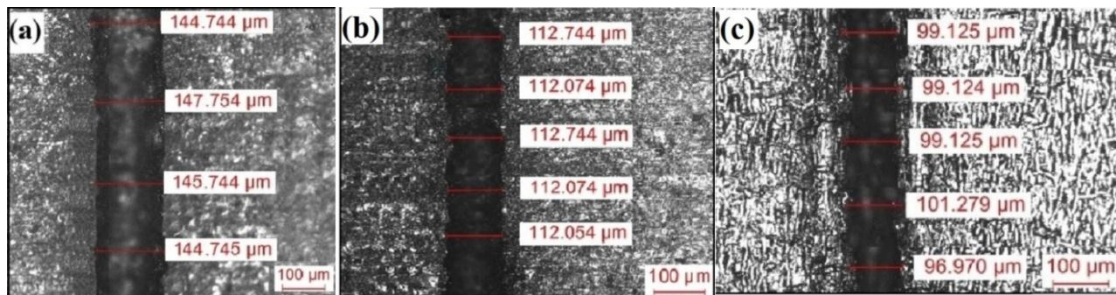

Figure 5.29 Groove depth using 0.1M H2SO4 electrolyte at (a) 7V (b) 6V (c) 5V
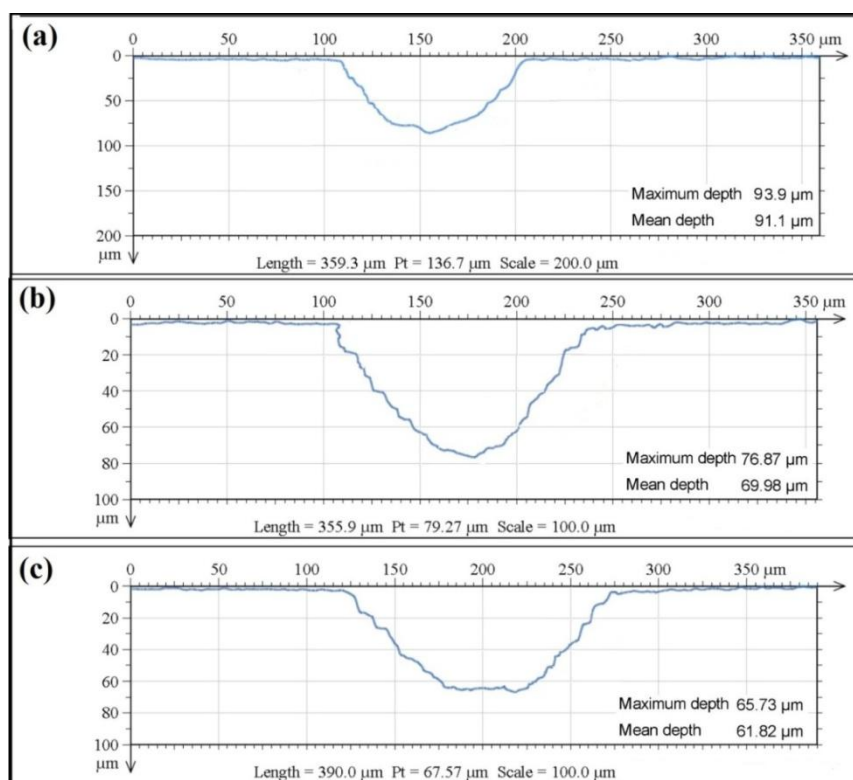
Figure 5.30 Groove depth using 0.1M H_2SO_4 and 0.1M citric acid at (a) 7V (b) 6V (c) 5V

The addition of organic citric acid diluted the concentration of sulphuric acid to some extent with reduction in toxicity by acting as a complexing agent to the electrolyte solution. However, the depth of the grove also reduced to some extent which can be further enhanced by increasing the molar concentration of citric acid in the solution. The deepest machining groove i.e. 93.9µm has been obtained at 7V pulse voltage using mixed 0.1M H_2SO_4 + 0.1M citric acid electrolyte as shown in **figure5.30**. From 5V to 7V pulse voltage at constant wire feed rate, the depth of the groove increases. A parabolic form may have been created because, according to a thorough investigation, the entrance of the groove, where the width is measured, was more susceptible to higher machining times than the groove bottom. However, at low current densities compared to high current densities, the variation in the depth of each groove is greater. The form of the groove reduces the electrode's current focus somewhat, and one of the causes is the electrode's receiving an even distribution of current. Further, experimental results reveal that the de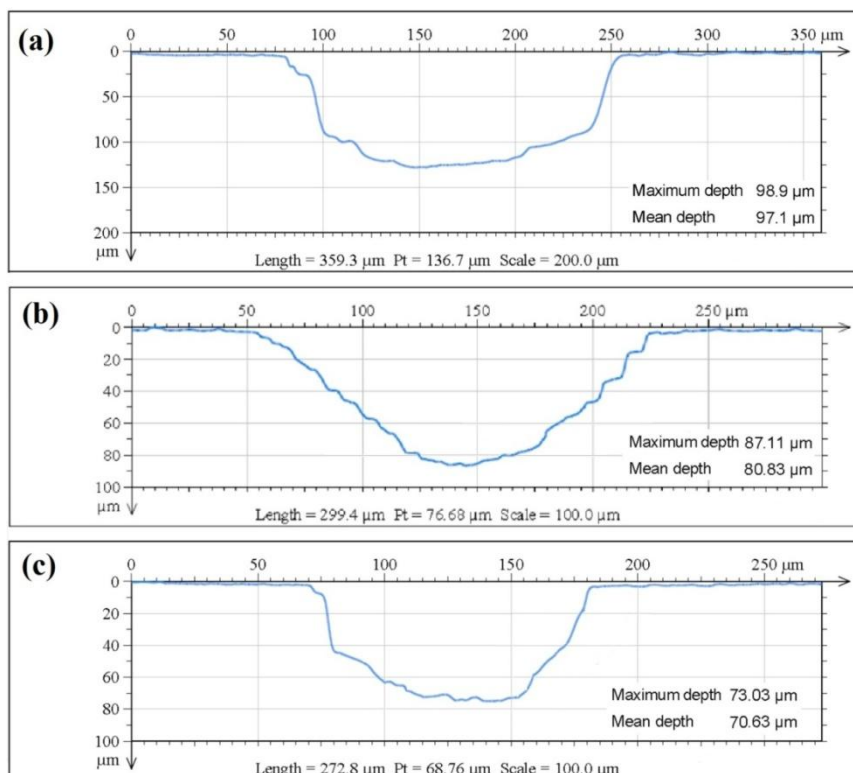pth of groove using 0.1M H_2SO_4 electrolyte was higher as compared to the mixed 0.1M H_2SO_4 +0.1M citric acid solution. It is due to the less current density for machining for same pulse voltage conditions in mixed electrolyte.

5.3.1.4 Effect of electrolytes on Surface Roughness

The surface properties of the various electrolytes employed also vary, which affects how the machining features work. A slight change in potential during the process may result in a decrease in current, which will inevitably cause a drop in current efficiency. The electrolyte with a very low concentration (0.05 M) resulted in poor machined surface. The ability to produce smooth surface micro-features in mixed 0.1M H_2SO_4 + 0.1M citric acid electrolyte solution was particularly useful due to its uniform dissolution in the required concentration. To obtain smooth machined surfaces in WECM, the passive coatings function as insulators to prevent corrosion on the machined surfaces. An acid electrolyte composed of sulfuric acid (0.1M H_2SO_4), citric acid (0.1M), and distilled water (H_2O) was employed to identify a suitable electrolyte for machining Nitinol SMA. Cit3 ion, a polyhydroxy carboxylic acid group ligand that functions as a chelating agent with significant complexing capacity, is present in citric acid. Numerous donor atoms in the ligand are capable of swiftly transferring electrons into the coordination sphere of metal cations. As a result, the link between the metal and oxygen becomes polarized and gradually weakens, allowing metal ions to dissolve.

As a result, in the case of a mixed 0.1M H_2SO_4 + 0.1M citric acid electrolyte, Ni is readily dissolved, leading to a uniform dissolution and a reduction in surface roughness. In

contrast to mixed 0.1M H_2SO_4 + 0.1M citric acid electrolyte solution, the microgroove created while machining nitinol SMA using 0.1M H_2SO_4 electrolyte solution was uneven in shape and had poor surface quality. The surface that was achieved in the 0.1M H_2SO_4 electrolyte was subpar, and the micro grooves that were created had significant electrolytic assault on them in and around the machined surface. Since H_2SO_4 is not environmentally friendly, a mixed electrolyte of H_2SO_4 and citric acid is provided, and its performance is determined to be superior to H_2SO_4. A nitinol sample with an initial surface roughness of 4.076 μm was machined to a roughness of 0.0631 μm using mixed 0.1M H_2SO_4 + 0.1M citric acid at 5V pulse voltage which is lower as compared to 0.09055 μm produced using 0.1M H_2SO_4 electrolyte for these experiments. The effect of pulse voltage on surface roughness using 0.1M H_2SO_4 and mixed 0.1M H_2SO_4 + 0.1M citric acid is shown in **Figure5.31.**
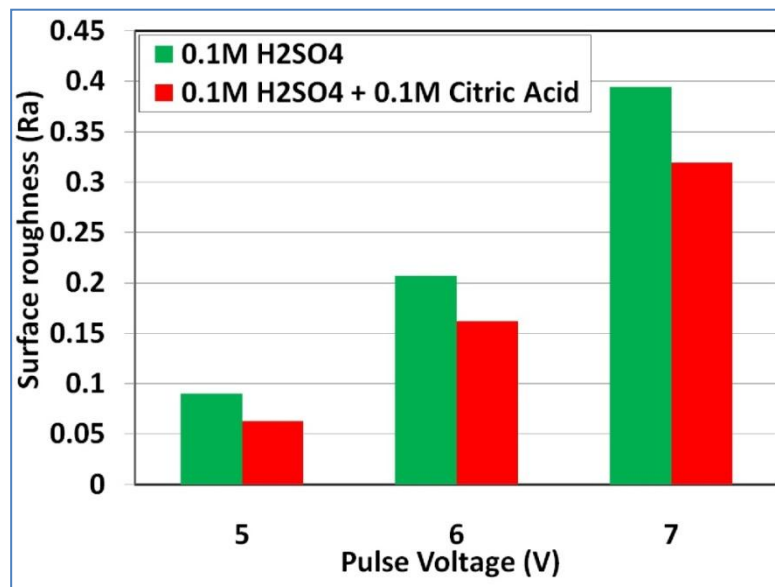
Figure 5.31 surface roughness at different pulse voltages using different electrolytes

Figure5.32 and 5.33 displays the 3D surface view of the microgrooves made using this the 0.1M H_2SO_4 and mixed 0.1M H_2SO_4 + 0.1M citric acid electrolyte. It is observed that the surface roughness increases with increase in pulse voltage. The machining in 0.1M H_2SO_4 electrolyte produces an average surface roughness of 0.3943 μm at 7V and reduced to 0.09055 μm at 5V as shown in **figure5.32.** Because of the poor surface that was formed in the 0.1M H_2SO_4 electrolyte, the surface roughness increased. Due to poor anodic dissolution and etching, the surface roughness of the 0.1M H_2SO_4 electrolyte is increased, and the electrolyte has a high current carrying capacity. When mixed 0.1M H_2SO_4 + 0.1M citric acid electrolyte were used to machine Nitinol SMA, the quality of the microgrooves created with electrolytic attack was superior to that of 0.1M H_2SO_4

electrolyte in terms of surface integrity and **figure5.33** depicts the surface that was produced during the machining of nitinol SMA using mixed 0.1M H_2SO_4 + 0.1M citric acid electrolyte.
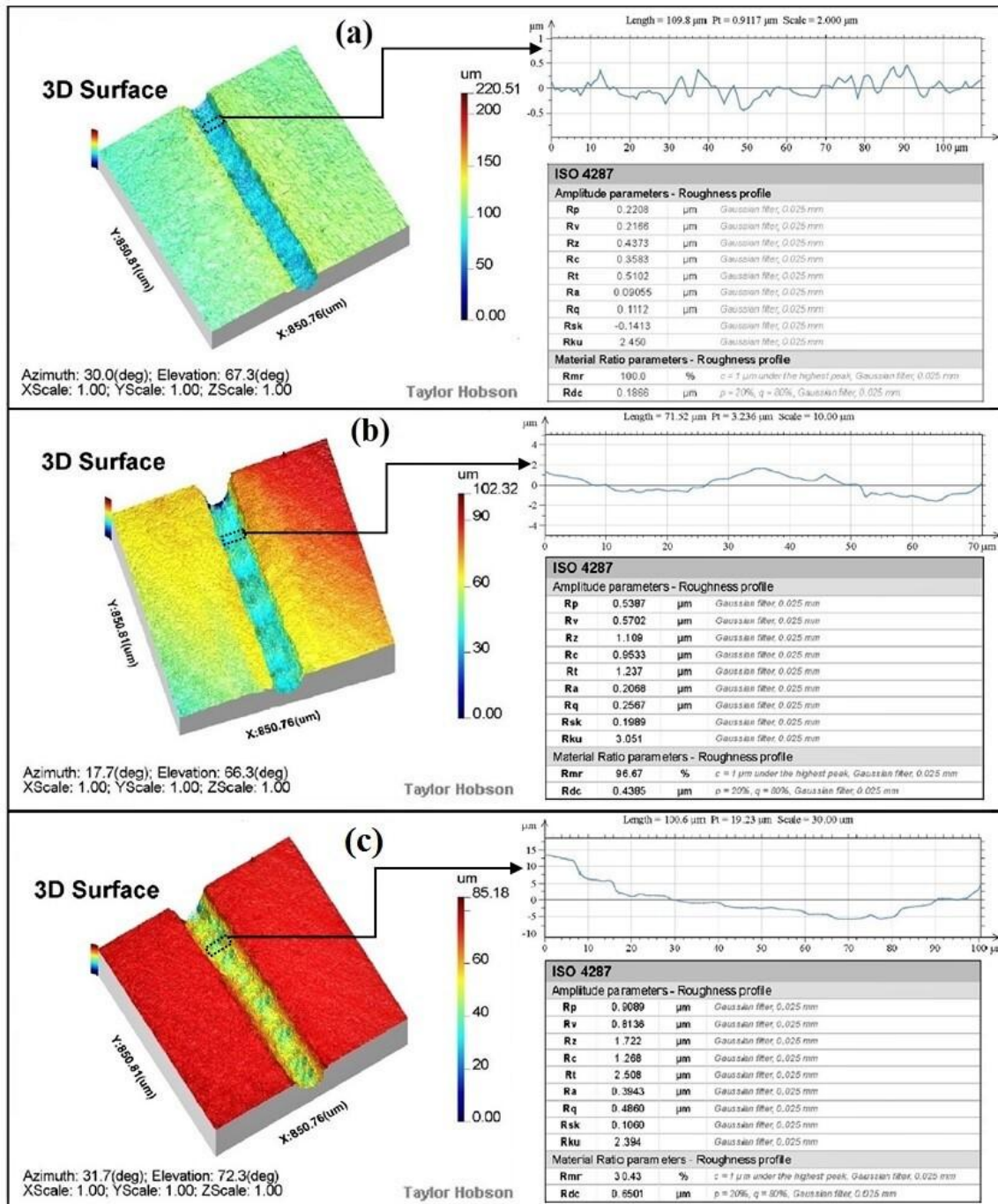
Figure 5.32 3D surface images, surface roughness profiles and amplitude parameters measured using CCI profilometer with 0.1M H_2SO_4 electrolyte at pulse voltage **(a)** 5V **(b)** 6V **(c)** 7V

The micro groove created with 0.1M H_2SO_4 electrolyte mixed with citric acid is better than that of the 0.1M H_2SO_4 electrolyte, and the electrolytic attack is very low (i.e., no

ions are observed impinging), but the machining speed is slower than with 0.1M H_2SO_4 electrolyte.
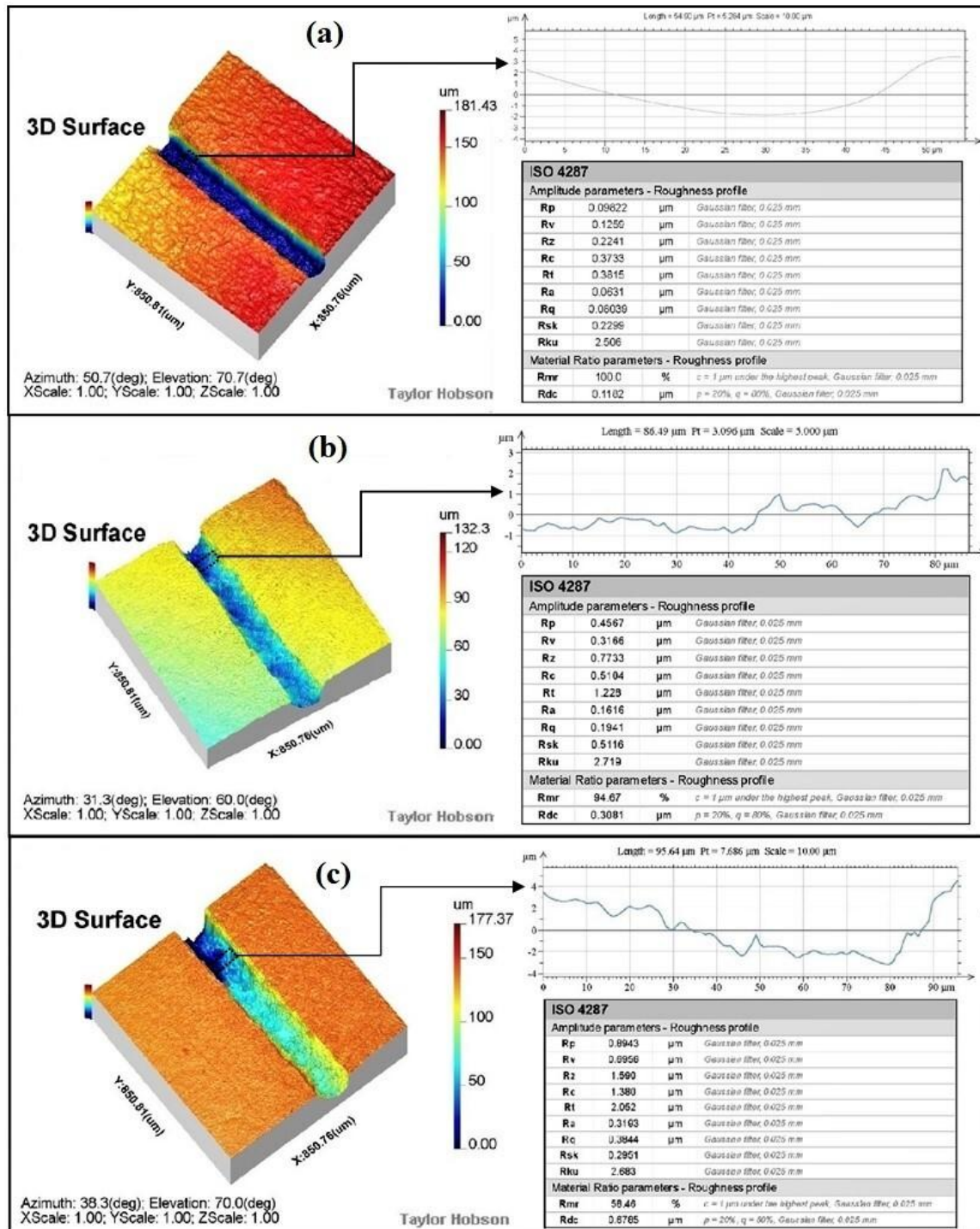
Figure5.33 3D surface images, surface roughness profiles and amplitude parameters measured using CCI profilometer with 0.1M H_2SO_4 + 0.1M citric acid electrolyte at pulse voltage **(a)** 5V **(b)** 6V **(c)** 7V

Smooth dissolving takes place while machining nitinol SMA with mixed 0.1M H_2SO_4 + 0.1M citric acid electrolyte. Ions slowly tear the anodic film, allowing for anodic

disintegration, due to the adsorption of the film. The metal ions instead form oxides, which results in a much slower reaction and longer machining times since they do not produce oxygen vacancies.Due to the presence of passivating ions in the electrolyte, the surface produced in mixed 0.1M H_2SO_4 + 0.1M citric acid electrolyte is comparably excellent. With low current density, the passivating ions firmly migrate towards the surface and subtly damage it. This specific electrolyte produced surfaces with an average surface roughness of 0.3193 μm at 7V and reduced to 0.0631 μm at 5V. The capacity to smoothly and effectively burst the generated anodic film is excellent. Except at higher voltages, mixed 0.1M H_2SO_4 + 0.1M citric acid electrolyte offer the least amount of surface roughness compared to the 0.1M H_2SO_4 electrolyte. Further, it has been observed that the surface roughness was increased with increase in machined groove depth for 0.1M H_2SO_4 electrolyte and mixed 0.1M H_2SO_4 + 0.1M citric acid electrolyte as shown in **figure3.34**.
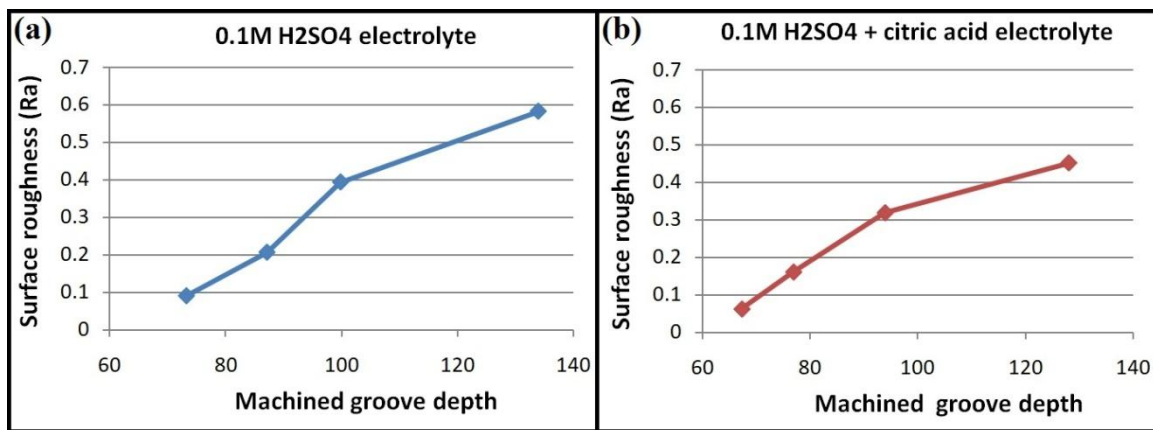
Figure 5.34 Surface roughness relative to machined groove depth with **(a)** 0.1M H_2SO_4 electrolyte **(b)** 0.1M H_2SO_4 + citric acid electrolyte

Further, the micro slit was fabricated at optimized parameter conditions of 5V pulse voltage, 45% duty ratio and 1.4μm/s shown in **figure5.35.**
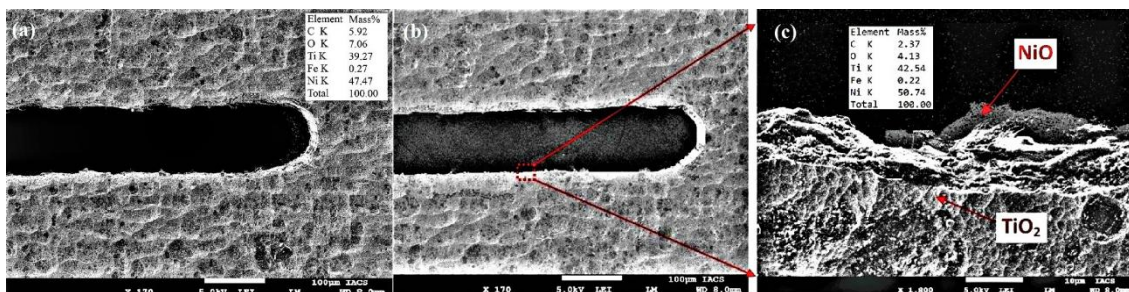
Figure 5.35 SEM of fabricated micro slit using **(a)** 0.1M H_2SO_4 electrolyte **(b)** mixed 0.1M H_2SO_4 + 0.1M citric acid electrolyte **(c)** zoomed view of microslits edge surface

The minimum average slit width of 108.325 µm using 0.1M H_2SO_4 electrolyte with minimum average surface roughness of 0.1217 µm and 92.234 µm using mixed 0.1M H_2SO_4 + 0.1M Citric acid electrolyte with minimum average surface roughness of 0.0691 µm shows the capability of WECM for microfeatures fabrication without affecting original chemical composition of difficult to cut material i.e. nitinol etc.

Although WECM with a neutral electrolyte helped lessen surface roughness, it also made the surface black. However, the mixed 0.1M H_2SO_4 + 0.1M citric acid electrolyte forms thin oxide layer that serves as a layer of corrosion resistance forms with uniform dissolution. Because TiO_2 is formed with a negative enthalpy, nitinol undergoes passivation naturally. During WECM, this oxide layer pushes Ni atoms away from the surface, depleting the surface of Ni and also removing the Ni in the form of nickel oxide (NiO). Due to advancements in corrosion resistance, biocompatibility, and surface quality as compared to conventional surface preparation procedures, mixed 0.1M H_2SO_4 + 0.1M citric acid electrolyte during WECM is appealing for the preparation of nitinol surfaces. The increase of oxygen value 7.06 in 0.1M H_2SO_4 and 4.13 in mixed 0.1M H_2SO_4 + 0.1M citric acid electrolyte shows formation of oxide layer on nitinol surface after machining. The lower of oxygen in mixed 0.1M H_2SO_4 + 0.1M citric acid electrolyte show production of thin oxide layer compared to 0.1M H_2SO_4 electrolyte which has proven to create uniform dissolution and improvement in homogeneity and surface quality of nitinol during WECM.

5.4 Outcomes of experiments

The effects of various neutral aqueous electrolytes i.e. NaBr, NaCl, $NaNO_3$ and EDTA as complexing agent under different mixed and ozonated conditions is a significant contribution for opening new insights for researcher working in the area of WECM during micromachining of nitinol shape memory alloy. Furthermore, dimensional characteristics and surface topography of SMA machined surfaces was performed using FESEM, EDS, and 3D profile surface analysis. Further, the electrochemical characterization of inorganic H_2SO_4 combined with organic eco-friendly complexing agent i.e. citric acid electrolytes that are noble in nature was conducted using potentiodyanamic tests and electrochemical impedance spectroscopy on the corrosion behavior of nitinol SMA followed by subsequent effects of machining parameters on fabricated micro grooves for width and depth overcut as well as surface roughness was studied.

It shows that ozonated mixed NaCl+$NaNO_3$+EDTA electrolyte has been proven as most suitable neutral electrolyte combination to achieve better dimensional characteristics and

surface finish of nitinol during wire electrochemical machining. The EDS findings reveal that oxygen present on the machined surface has lower value, implying that the nitinol surface has no more passivity in the electrolyte solution containing EDTA under ozonated condition as compare to other nonozonated conditions.

The electrochemical characterization of inorganic H_2SO_4 acidic electrolyte combined with organic eco-friendly complexing agent i.e. citric acid electrolyte, that are noble in nature, was conducted using potentiodyanamic tests and electrochemical impedance spectroscopy on the corrosion behavior of nitinol. Further, the subsequent effects of machining parameters on fabricated microgrooves for width and depth overcut as well as surface roughness have been presented and confirmed its suitability for micromachining of nitinol shape memory alloy and proved feasibility of application during WECM. The machining of nitinol with mixed 0.1M H_2SO_4 + 0.1M citric acid electrolyte have obtained reduced surface roughness with better surface integrity. This specific electrolyte produced surfaces with an average surface roughness (Ra) of 0.0631μm and the minimum average machined groove width overcut was 18.10μm in 0.1 M H_2SO_4 + 0.1M citric acid at 5V pulse voltage. According to the EDS data, the oxygen concentration was very less with mixed 0.1M H_2SO_4 + 0.1M citric acid electrolyte. It is clear that the thin oxide layer has been formed on machined surface of nitinol which ultimately helps for uniform dissolution during WECM with improvement in corrosion resistance and biocompatibility of nitinol SMA during WECM.

The scope of this investigation is to know the effect of different ozonated and non ozonated neutral aqueous electrolytes i.e. NaBr, NaCl, NaNO$_3$, and addition of EDTA as a complexing agent are most suitable electrolytes as well as inorganic H_2SO_4 combined with organic eco-friendly complexing agent i.e. citric acid during WECM of nitinol shape memory alloy. The comparison of outcomes using different electrolytes is shown in table5.6. It has been revealed that the better results in terms of overall improvement in dimensional characteristics and surface quality during micromachining of difficult to cut nitinol shape memory alloy using wire electrochemical machining has been obtained with the application of these aqueous electrolytes. However, even though mixing of citric acid with H_2SO_4 obtained best surface quality amongst other combination of neutral electrolytes, the immediate contamination occurred which limited the use of same electrolyte for further machining and creates the requirement of fresh electrolyte for each machining and control of all the influencing parameters during machining of nitinol shape memory alloy.

Table5.6 Comparison in machining at 5V pulse voltage using different electrolytes

Sr. No.	Electrolytes	Concentration of electrolyte (M)	Average groove width(μm)	Mean groove depth (μm)	Average surface roughness (Ra) (μm)
01	NaBr	0.2	No uniform dissolution	20.02	0.5777
02		0.3		8.62	0.8123
03		0.4		10.86	0.9489
04	NaCl	0.2	133.20	168.7	0.3994
05		0.3	155.79	178.7	0.4124
06		0.4	185.77	119.3	0.5653
07	$NaNO_3$	0.2	123.30	179.7	0.3790
08		0.3	137.72	155.7	0.3985
09		0.4	161.51	127.0	0.4295
10	Nacl+ $NaNO_3$	0.2	118.35	188.7	0.3333
11	Nacl+ $NaNO_3$+ EDTA	0.2	188.10	232.9	0.2790
12	Ozonated Nacl+ $NaNO_3$	0.2	115.36	245.9	0.2258
13	Ozonated Nacl+ $NaNO_3$+ EDTA	0.2	105.86	264.6	0.1346
14	H_2SO_4	0.1	99.12	70.63	0.0905
15	H_2SO_4 + Citric acid	0.1	86.63	61.62	0.0631

Hence to achieve the above using most suitable H_2SO_4 electrolyte, further in-depth research may be needed for experimental investigation and characterization of nitinol shape memory alloy for performance enhancement of WECM.

Chapter6: EXPERIMENTAL INVESTIGATION INTO EFFECT OF DIFFERENT INPUT PARAMETERS AND CHARACTERIZATION OF NITINOL SHAPE MEMORY ALLOY EMPLOYING WECM

6.1 Introduction

In this chapter, an investigation into the wire electrochemical machining (WECM) of nitinol SMA at a low concentration of 0.1M H_2SO_4 aqueous acidic electrolyte with effect of small amplitude at low-frequency piezoelectric transducer (PZT) vibration-assisted axial nozzle jet flushing is presented. The variety of input process parameters in the WECM process must be managed to achieve high machining accuracy, surface quality and control the ensuing physical and mechanical properties. The WECM method may be used on any conductive substance despite its hardness. The anodic dissolution is used in the WECM to assist material removal from the workpiece. Hence the present investigation is focused on the impact of different operating machining conditions on slit-width during micromachining of nitinol SMA using WECM. Based on the reviewed literature, machining capabilities and characteristics of nitinol SMA, electrolyte flow rate, and electrolyte temperature with variation in current density, pulse voltage, tool PZT amplitude and frequency, pulse frequency, pulse width and, the wire feed rate were selected as preliminary key input parameters during micromachining of nitinol SMA during WECM as discussed in next experimental planning-I section. Further, this investigation emphasizes the investigation of the influence of energy input parameters i.e. pulse voltage, pulse frequency, and duty ratio on wire feed rate and the machining accuracy and fabricated fine microfeatures as discussed in experimental planning-II in the next section. Also, the present investigation will provide end-users useful information on effect of most prominent process parameters for micromachining of nitinol SMA and characterization nitinol SMA before and after machining using scanning electron microscopy (SEM), surface characteristics and energy-dispersive X-ray (EDX), X-ray diffraction (XRD) tests to get more insight into the benefit of WECM over other non conventional machining processes. Also, dissolution behaviors of nitinol SMA were studied in 0.1M H2SO4 aqueous acidic electrolyte during WECM for getting more insight of the process.

6.2 Experimental planning I: Influence of different input parameters

To conduct preliminary experimental trials for micromachining of nitinol SMA with appropriate process parameter operating conditions, proper schemes and methods have

been planned with the use of in-house newly developed vibration-assisted axial nozzle jet flow WECM experimental setup. Preliminary experiments reveal that the machined slit width decreases as electrolyte concentration decreases. However, very low concentration (0.05M) creates very poor surface quality and high concentrations create more dissolution and also corrode and damage the available experimental setup. Therefore 0.1M H_2SO_4 electrolyte aqueous solution was selected which was prepared from de-ionized water and analytical grade H_2SO_4 (98%). A flushing nozzle is attached to the wire holding tool and the electrolyte is flushed axially along the wire electrode. The electrolyte flow rate was adjusted as per the requirement with the help of the rotameter attachment of the flushing system **[59]**.

The experimental method was created to investigate the effect of variable parameters like electrolyte flow rate, PZT vibration amplitude and frequency, pulse voltage, electrolyte temperature, pulse frequency, pulse width, and wire feed rate while micromachining of nitinol SMA. One factor at a time order for experimental investigation was used to obtain best value for each parameter and its effects was observed for fabricating homogeneous minimum slit width. In this experimental investigation, variable parameters details were recognized to perform experimentations keeping other parameters fixed for all experiments and working ranges were selected based on data given in literature review and trial experiments for micro-slits machining carried out to understand the effect most influencing parameters with vibration-assisted nozzle jet flow WECM. Process parameter machining conditions with their ranges used in experimentations are shown in **Table6.1.**

Table 6.1 Process parameter machining Conditions

Fixed parameters	Values	Variable parameters	Values
Workpiece material	Nitinol SMA	Electrolyte flow rate	5 to 20 Lph
Workpiece thickness	120μm	PZT Tool vibration	0 to 30Hz
Wire electrode material	Tungsten	PZT Tool vibration	0.94 to 32.94
Diameter of a wire	Ø50μm	Electrolyte	20 to 30^0C
Electrolyte solution	0.1M H_2SO_4	pulse voltage	4 to 9V
Nozzle diameter	0.4mm	pulse frequency	250 to 450
Nozzle workpiece distance	5mm	Pulse width	1.7 to 2μs
Initial inter-electrode gap	100μm	Wire feed rate	1.0 to 1.8μm/s
Insulating material for wire	Synthetic enamel		

Each experiment has been conducted and repeated at least for three times with a same parameter set during WECM. Machined slit-width was measured with the help of Olympus STM6 measuring optical microscope and average slit width is calculated from the measured values of slit width of fabricated micro slits. Further, micro structural

analysis of the machined surface was carried out through SEM, EDX, and XRD analysis and surface quality was measured using Taylor Hobson CCI profilometer.

6.2.1 Experimental observations and discussions

After conducting necessary experiments, the machined micro slits have been cautiously observed. To find out the effect of different variable parameters on machined micro slit width accuracy as well as dimensional characteristics and to get further insight; the experimental observations with results and discussions have been given hereunder.

6.2.1.1 The effect of nozzle jet electrolyte flow rate

The effect of flow rate may be simply related to metal removal rate and increased rate of mass transport of dissolved products with electrochemical dissolution process during new developed WECM. As the flow rate is reduced to less than 1lph, the temperature within the inter-electrode gap increases to a maximum value results in an increase in electrolyte temperature leading to the fluctuation of machining current. The effect of electrolyte flow rate for machining of nitinol SMA plays an important role in obtaining minimum slit width with homogeneity for good machining quality. The velocity of electrolyte during WECM has an enormous effect on the fabricated slit width of nitinol SMA. Therefore, the effect of different flow rates on machining of micro slit width of nitinol SMA was investigated in this research work with a different flow rate in the range of 5lph to 20lph during WECM.
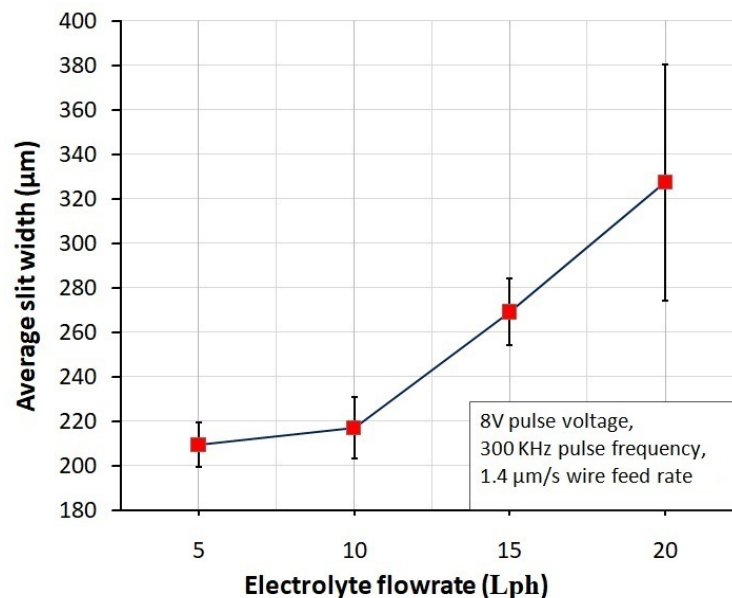

Figure 6.1 Effect of electrolyte flow rate on the average slit width.

All the preliminary experiments were performed at 8V pulse voltage, 300KHz Pulse frequency, and 1.4 μm/s wire feed rate with other constant values of process parameters.

The experiment was performed at 25^0C electrolyte room temperature for understanding the effect of flow rate on machined slit width. The results are depicted by graphical plots in **figure6.1.** When the electrolyte flow rate was 5lph, the machined slit width obtained was minimum with an improvement of homogeneity and machining accuracy but not up to the expectations for micromachining of nitinol SMA. In contrast to that, when the electrolyte flow rate was 20Lph, the machined slit-width has an increase in overcut with no uniformity from the beginning to end. The reason may be that the high flow rate might have caused high flow pressure in the narrow IEG leading to sudden swing and vibration of wire vibration and the diameter of the wire may get deflected and deteriorate due to short-circuit and micro sparks.

The microslits machined under different operating variable conditions of electrolyte flow rate are shown in **figure6.2.** The experiment reveals that minimum slit width of 208 µm was obtained with a 5lph electrolyte flow rate with a quite good homogeneity as compared to the micro slit width obtained at a higher flow rate. Proper flow rate excludes away sludge and dissolved products without affecting electrochemical reactions. If the flow rate is sufficiently high, short-circuit and micro sparks are usually prevented. However, at flow rates below 5lph, the temperature within the gap lowers which decreases current efficiency with large voltage fluctuations. The current density decreases with increasing flow velocity and absolute pressure. Therefore, It also reduced the heat and wash away the gas bubbles generated by the reactions, and helped to manage the electrolyte temperature. This minimum electrolyte flow rate of 5lph is used for further experimentations to investigate the effect of other most influencing process parameters.
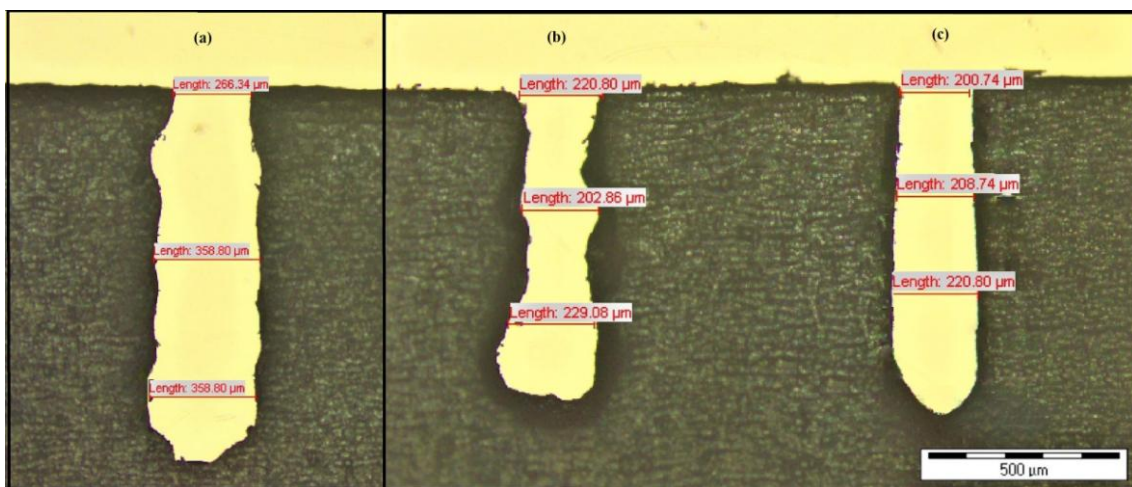

Figure 6.2 Micro slits machined under the following conditions of nozzle jet electrolyte flow rate **(a)** 20lph **(b)**10lph **(c)** 5lph

6.2.1.2 The effect of cathode (wire tool) PZT vibration amplitude

The wire tool PZT vibration amplitude has a considerable effect on slit width during machining nitinol SMA. **Figure6.3** exhibits the effect of PZT vibration amplitude ranging from 0.94 to 34.94µm on slit width. It is observed that slit width increases with amplitude, whereas, when tool PZT vibration amplitude is very low below 0.94µm, short-circuits occurred due to accumulation of sludge and dissolved products in the narrow IEG.
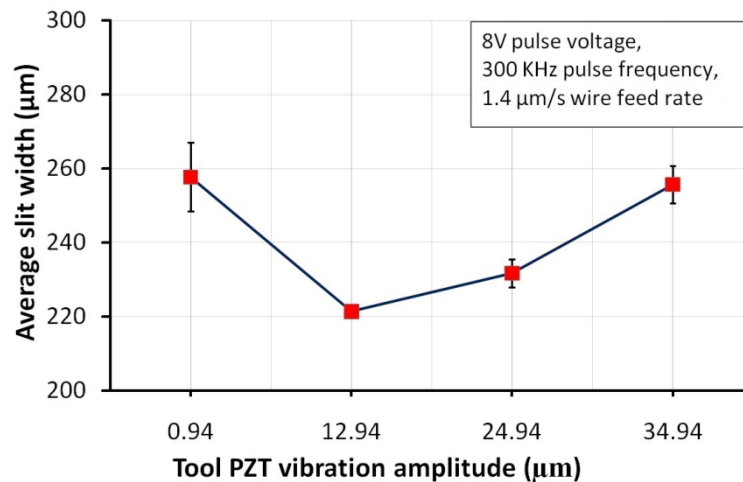

Figure 6.3 Effect of tool PZT vibration amplitude on the average slit width.

The PZT vibration amplitude of 12.94 µm is better for adequate expelling of the sludge and dissolved products out of the narrow IEG results in a hydrodynamic effect on mass transport, which leads to better machining stability. However, the amplitude above 24.94µm is detrimental which adversely affects the dissolution, and results in the radial swing of wire. Also, At very low and too high PZT vibration amplitude, the deviation was quite high and machining accuracy was reduced to a greater extent. Therefore appropriate small amplitude is preferred in the machining of nitinol SMA.

6.2.1.3 The effect of cathode (wire tool) PZT vibration frequency

Although the wire vibration improves the sludge removal, the slit width is not changed to a greater extent at vibration frequency ranges from 10 to 20Hz. However, when wire frequency is very low, sludge and gas bubbles accumulated near the machining zone of workpiece and prevented further dissolution. With increase of frequency above 30Hz, acceleration and inertia forces increases greatly leads to unstable machining conditions during machining of nitinol resulted in poor machining accuracy as shown in **figure6.4.** Therefore appropriate vibration frequency is preferred in the machining of nitinol SMA. It can be further improved with the implementation of proper flushing techniques and controlling the flow and temperature of electrolytes to a greater extent.
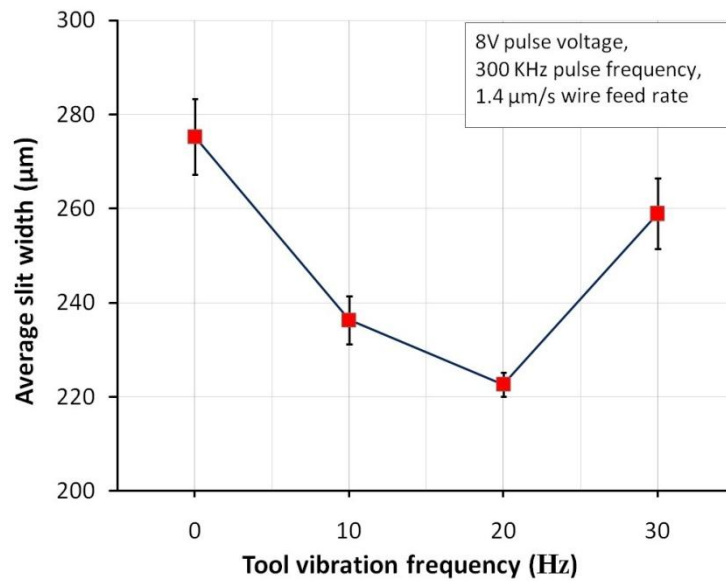
Figure 6.4 Effect of tool PZT vibration frequency on the average slit width.

6.2.1.4 The effect of electrolyte temperature

As nitinol SMA is very sensitive to high temperatures and also tends to form passive oxide layers during the WECM process. The effect of electrolyte temperature plays an important role in obtaining minimum slit width with homogeneity at good machining quality. The generation of heat as a result of the flow of current alters the resistance across the IEG, affecting current flow. A more generated heat may result in a cavitations phenomenon at the IEG. Therefore, it is required to analyze the effect of different electrolyte temperature conditions on machining of micro slits with proper flushing of electrolyte during the machining process to minimize the effect of heat. The experiments were performed under a variation of four different temperatures ranging from 20^0C to 35^0C and electrolyte solution concentrations of 0.1M H2SO4 were subjected to these temperature variations and 8V pulse voltage, 300KHz pulse frequency, and 1.4 µm/s wire feed rate with all other fixed process parameters.

Thus, **figure6.5** shows that a maximum current density of 0.16A was produced at the highest electrolyte temperature of 35^0C used in the experimental investigation and obtained maximum slit width. Experimental results revealed that the temperature of electrolytes influenced electrochemical reactions and increased the chemical activity with an increase in current density during machining. The slit width increased with the increase in electrolyte temperature and the maximum average slit width of 257µm was produced at 35^0C. In contrast, at the low temperature, the current density was lower and a minimum slit width of 190µm was produced at 20^0C at a previously optimized value of 5Lph electrolyte flow rate. This may be due to the increased electrolyte conductivity at

high temperatures. As the electrolyte conductivity increases with temperature, resistance gets reduced due to which current flow increases in the narrow IEG results in overcut during micromachining. The minimum average current density of 0.03A was produced at the lowest electrolyte temperature of 20^0C may be due to the decreased electrolyte conductivity at low temperature. The machined micro-slit width increases with an increase in electrolyte temperature as shown in **figure6.6.** High electrolyte temperature has a predominant effect on the effective conductivity of electrolyte solution and hence the shape of the IEG at micro slit.
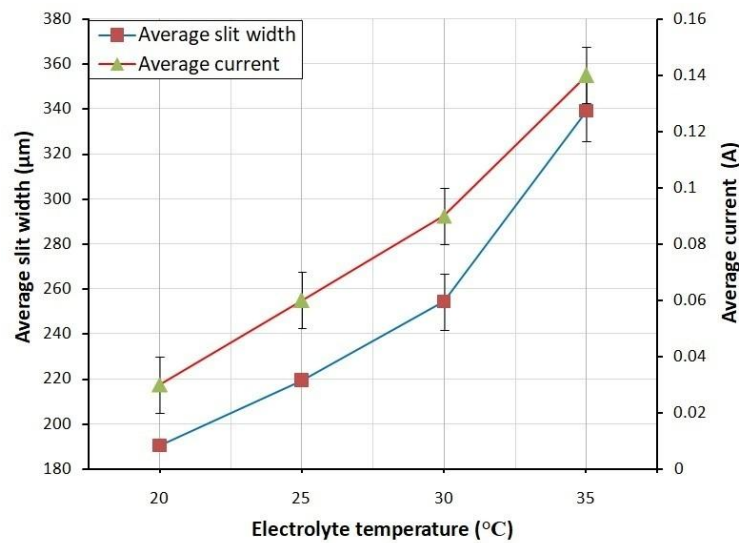

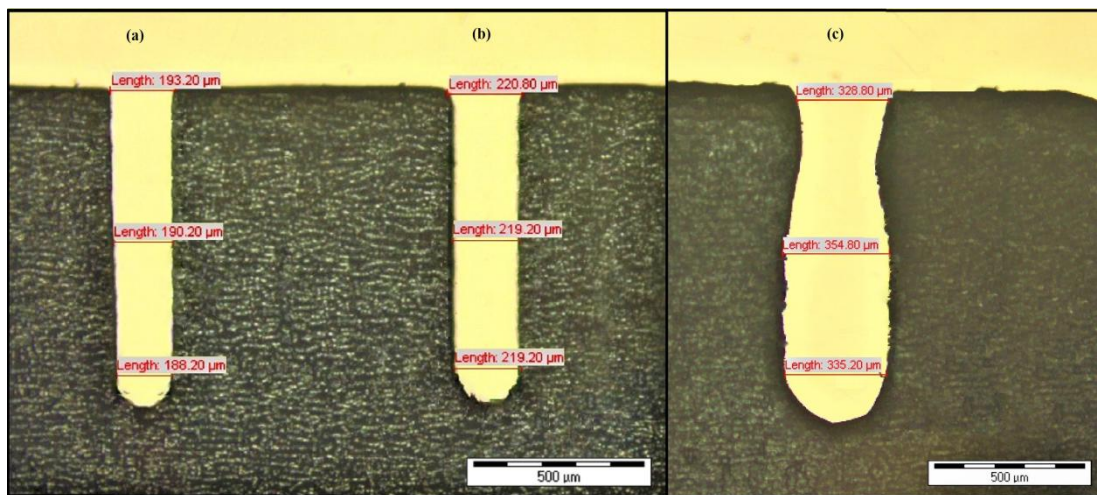**Figure 6.5** Effect of electrolyte temperature on average slit width with variation in average current.

Figure 6.6 Micro slits machined under the following conditions of electrolyte temperature with homogeneous minimum slit width **(a)** 20^0C **(b)** 25^0C **(c)** 35^0C

This may result in more practical difficulties during the machining of complex micro

features using WECM. Thus, finding out the best electrolyte flow rate and temperature operating conditions is much more important in the micromachining of nitinol SMA during WECM for enhancement of overall performance. Further, the micro-slit machining quality and accuracy were improved with tight control of other variable process parameters discussed hereunder keeping 5LPh electrolyte flow rate and maintaining the electrolyte temperature at 25^0C.

6.2.1.5 The effect of pulse voltage

It is found in the previous experimental results that pulse voltage has a great influence during wire electrochemical micromachining. Therefore the selection of proper pulse voltage during WECM plays a very important role. The machining was performed with a previous best value of 5Lph flow rate by maintaining the electrolyte temperature at room temperature of up to a maximum 25^0C , 1.4 µm/s wire feed rate with two different conditions of 300KHz and 400KHz pulse frequency for in-depth analysis for the effect of pulse voltage during machining. The initial IEG was 100µm. The effect of pulse voltage on machined slit width is plotted on a graph as shown in **figure6.7.**
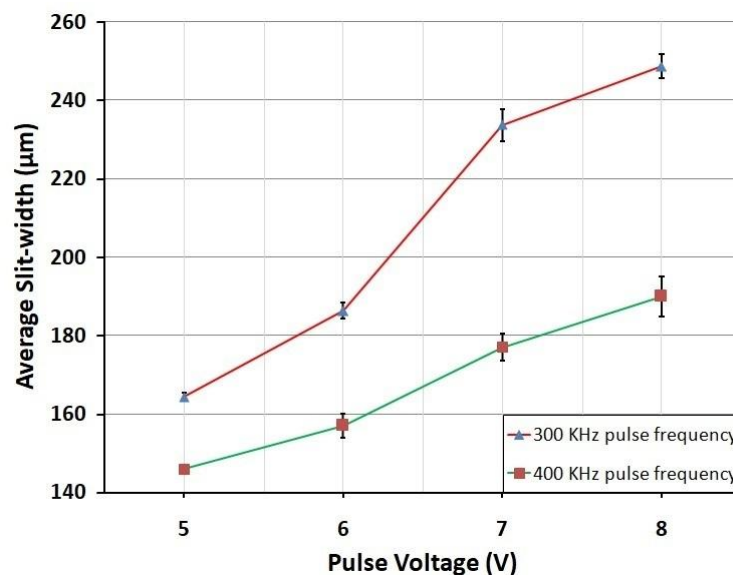
Figure 6.7 Effect of pulse voltage on the average slit width

The maximum slit width of 190 µm at 400 KHz and 227 µm at 300 KHz pulse frequency was obtained during micromachining of nitinol SMA during machining. Therefore, a proper IEG is necessary for successful machining. At selected operating conditions, below 4V pulse voltage with other constant parametric conditions, there is negligible or no machining at all which is seen only continues micro-sparks at the beginning of machining. Experimental results reveal that, at 4V pulse voltage, small micro-pits were obtained with overcut. It was observed that machining depth in this condition was very

poor, therefore, it was not recommended to take pulse voltage below 4V for getting proper machining efficiency during micromachining of nitinol SMA with other parametric conditions used in this investigation. Further, it is observed from the previous results for the effect of flow rate and temperature at 8V pulse voltage, dissolution rate increases drastically due to high current density at narrow IEG results in more material removal rate with overcut in machined slit-width. Therefore, further experimental study reveals that the range of 5V to 8V is suitable with these other operating conditions with the developed experimental setup. It is observed that at 5V pulse voltage, the quite homogeneous average minimum machined slit width of 145 μm at 400 KHz pulse frequency and 164 μm at 300 KHz pulse frequency was obtained during micromachining of nitinol SMA as shown in **figure6.8.** Pulse voltage below 8V shows a decreasing trend of machined slit width and pulse voltage above 8V seen a drastic change of an increase in slit width during machining of nitinol SMA considering tight control of other process parameters.
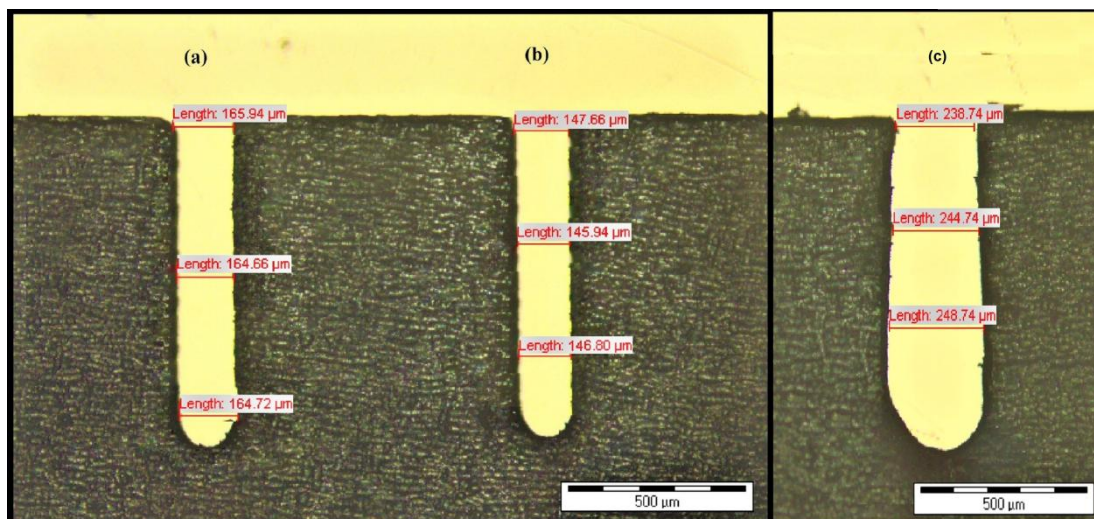
Figure 6.8 Micro slits machined under the following conditions **(a) 5V Pulse voltage,** 300KHz Pulse frequency, 1.2 μm/s wire feed rate **(b) 5V pulse voltage,** 400KHz Pulse frequency, 1.2μm/s wire feed rate **(b) 8V pulse voltage,** 300KHz Pulse frequency, 1.2μm/s wire feed rate

The slit width of nitinol may vary due to uncontrolled machining conditions which leads to unstable processing and homogeneous slit width machining cannot be obtained and worsening the machining quality may be due to the wire deformation at other experimental parameters conditions. Finally, it is observed that 5V pulse voltage in combination with 1.2μm/s wire feed rate and 400 KHz pulse frequency shows the best results produced minimum slit width with proper homogeneity. Again further increase in

pulse voltages below and above the selected range leads to continuous micro sparks and large overcut on the machined slit width. However, the effect of micro sparks and overcut was greatly reduced. It is also observed that newly developed WECM with new flushing method for obtaining less slit width with greater machining accuracy. Further in-depth investigations are required to understand the dissolution mechanism of nitinol shapes memory alloy by experiments with other most influencing parameters i.e. pulse frequency and wire feed rate at a combination of different ranges using the previously best value of electrolyte flow rate, temperature, and this optimized value of 5V pulse voltage for performance enhancement during micromachining employing new flushing method.

6.2.1.6 The effect of pulse frequency

The effect of pulse frequency on the slit width of nitinol SMA was investigated at a value of 5lph electrolyte flow rate at room temperature, 5V pulse voltage. Also, 1.4 μm/s wire feed rate and 1.6 μs pulse width, and 250 KHz to 450 KHz pulse frequency were selected based on the previous experimentations with remaining fixed parameters for machining, and results were plotted graphically as illustrated in **figure6.9.** It is observed that with the increase in pulse frequency, the micro-slit width decreases almost linearly. Moreover, with a further increase in frequency beyond 450 KHz at constant duty ratio, then lesser machined slit length or micro-pit was obtained or no machining will occur with further increase in pulse frequency. It was also observed that the frequency may be up to 200 KHz, generation of more heavy micro sparks and short-circuit occurs and dissolved products will fully clog the narrow IEG which further stop the machining.
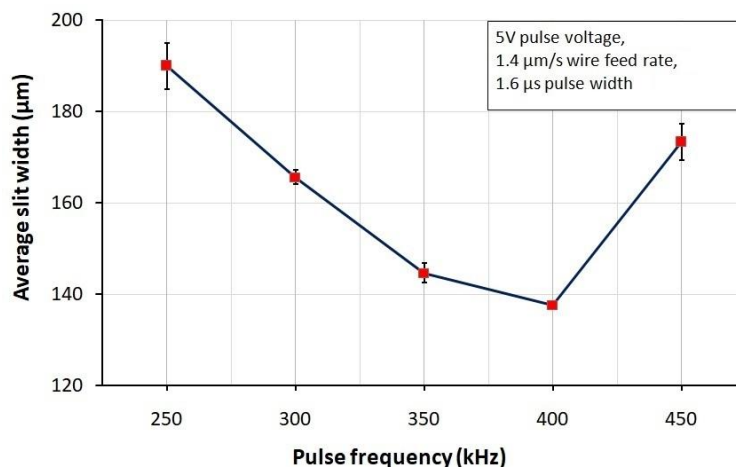

Figure 6.9 Effect of pulse frequency on the average slit width.

A pulse frequency of 400 KHz is best with a minimum slit width of 138 μm which was obtained during machining of nitinol SMA**.** It indicates that for machining of nitinol SMA with low pulse voltage i.e. 5V, high pulse frequency of 400 KHz having pulse period of

2.5 µs with more pulse width of 1.6 µs results in better machining. The pulse period decreases with an increase in pulse frequency which further reduces the effective machining time. Thus, the slit width becomes smaller with the increase in pulse frequency. However, at a high pulse frequency greater than 250KHz, the effect of micros-parks and short-circuit were reduced to a greater extent due to enough flushing and proper removal dissolved products at narrow IEG and machining zone as both vibrations, nozzle jet combined with the axial flow has been utilized at the same time. Slit width has been decreased as sludge and dissolved products are effectively removed during machining. With a pulse frequency above 450 KHz, the tendency of sparking was more common due to a sudden increase in current density distribution at narrow IEG results in poor machining or failure of machining for further increase in pulse frequency. Therefore, this investigation shows that 400 KHz of pulse frequency is optimal under these machining conditions and it is used in the further investigation for the effect of pulse width and wire feed rate on machined slit width of nitinol SMA during WECM discussed hereunder.

6.2.1.7 The effect of pulse width

Pulse width is another important factor during micromachining of nitinol SMA. It plays an important role in the material dissolution process and remaining pulse off time cleaning the sludge and dissolved products in the narrow IEG keeping the machining zone ready for subsequent dissolution. Due to the pulse power supply of the experiment, aside from the working pulse voltage, the pulse width also was proportional to the amount of input energy. To investigate the effective difference between pulse voltage and constant pulse frequency, the pulse width was used in the research. It was observed that low pulse width below 1.5 µs hinders the machining process under a constant duty ratio results in a decrease in dissolution rate to a large extent. Therefore, in this investigation, a fixed-pulse frequency of 400KHz having a pulse period of 2.5 µs was used to investigate the effect of different pulse widths in the range of 1.7 µs to 2.0µs with fixed 5V pulse voltage, 1.4 µm/s wire feed rate on processing characteristics. The results are plotted graphically as illustrated in **figure6.10.** In the fixed-pulse period, the pulse width determined the amount of input energy for which the pulse width could be expected to be proportional to the slit width. The experimental results showed that the relationship between the pulse width and the slit width was proportional, as expected. However, when the pulse width was gradually reduced below 1.6 µs, the processing pulse voltage of 5V could no longer draw enough current to achieve material removal. On the other hand, the pulse width was above 2 µs produced frequent sparking and short-circuits due to the

accumulation of sludge and dissolved products in the narrow IEG. The slit width of 138µm at 1.8 µs and 140 µm at 1.7 µs were produced as shown in **figure6.11.**
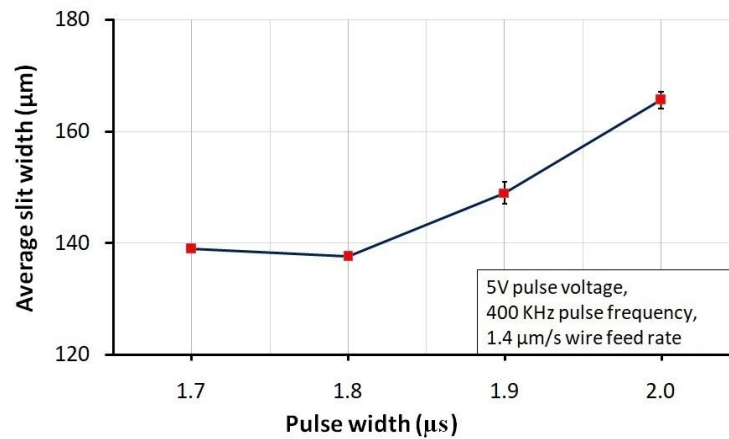
Figure 6.10 Effect of pulse width on the average slit width.
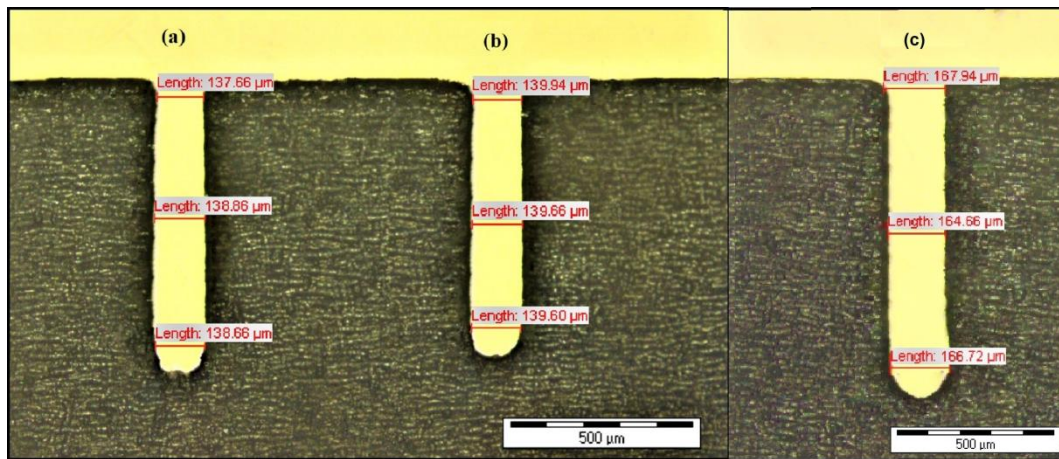
Figure 6.11 Micro slits machined with pulse width **(a)** 1.8 µs **(b)** 1.7 µs **(c)** 2 µs

Therefore, the minimum slit width was with the process parameter combination of 5V pulse voltage,1.4 µm/s wire feed rate, and 400KHz pulse frequency with a pulse width of 1.8 µs obtained is the best value in this combination of machining parameter and which is further used to investigate the effect of wire feed rate hereafter.

6.2.1.8 Maximum wire feed rate condition Test

Figure6.12. depicts the procedure for determining the maximum wire feed rate. The pulse voltage in the range of 5 to 8V was selected keeping the best values of 5Lph electrolyte flow rate maintaining constant electrolyte room temperature, 400 KHz pulse frequency, 1.8 µs pulse width as a constant throughout experimentation. Initially, the microslit was machined at a slow wire feed rate of 1µm/s for the first 5 minutes, then raised by 0.2 µm/s every 5 minutes. During the machining of nitinol SMA micro slit, the fluctuation in current is also monitored in real-time, and short-circuit and micro sparks occurred that leads to sudden rupture and breakage of wire which shows that the tungsten

wire electrode had reached the maximum feed rate for the machining circumstances. When the wire feed rate reached 2.4 µm/s, heavy micro sparks and short-circuit occurred. The results show that the maximum wire feed rate for the machining was below 2.4 µm/s using a maximum pulse voltage of 8V under other stable parametric conditions as shown in **figure6.13.**
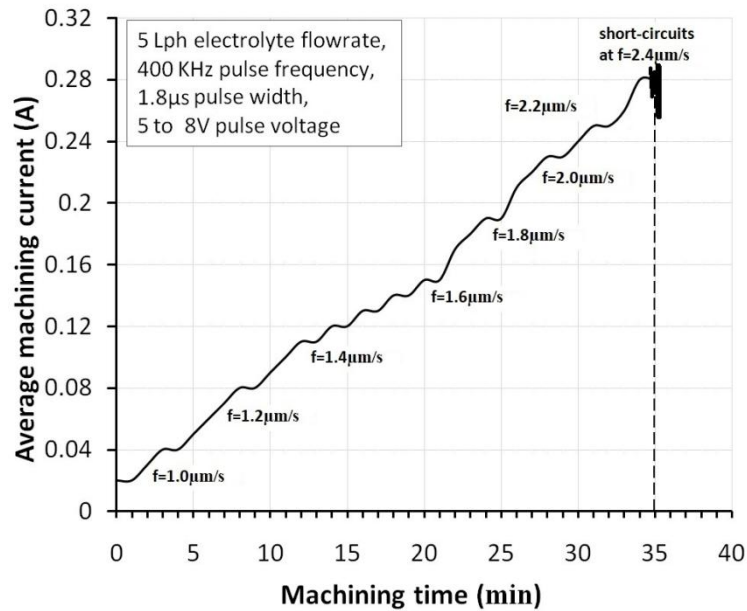
Figure 6.12 Method for maximum wire feed rate condition test
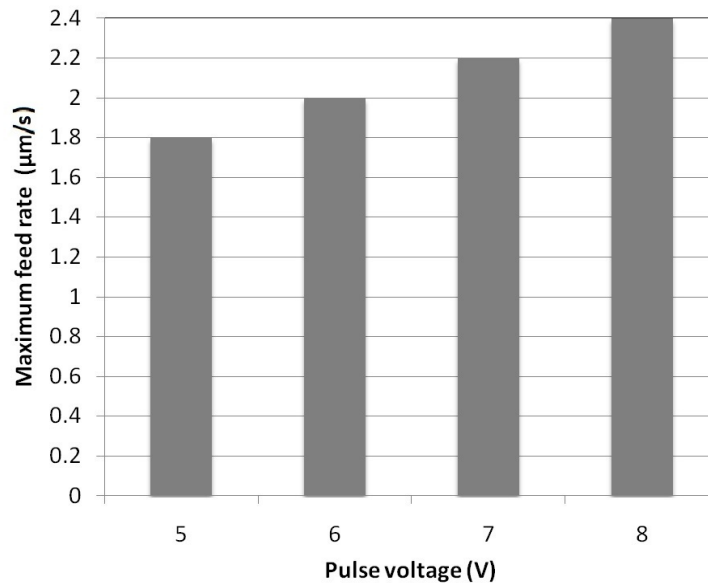
Figure 6.13 The effect of pulse voltage on maximum feed rate

6.2.1.9 The effect of wire feed rate on the slit width

The effect of the wire feed rate on the slit width at nitinol SMA was investigated by using best values of 5lph electrolyte flow rate maintaining constant electrolyte room temperature, 5V pulse voltage, 400KHz pulse frequency, 1.8 µs pulse width. Also,

experiments were conducted at a high pulse voltage of 8V and a low pulse frequency of 300KHz to obtain more insights into the effect of wire feed rate on machined micro slit width. The range of wire feed rate was selected from 1 to 1.8 µm/s based on experimental investigations. The results are represented with graphical plots as illustrated in **figure6.14.** Experimental investigation reveals that the minimum slit width of 110 µm at a wire feed rate of 1.8µm/s and 115 µm at a wire feed rate of 1.6µm/s were obtained using investigated best values of other variable process parameters as shown in **figure6.15.**
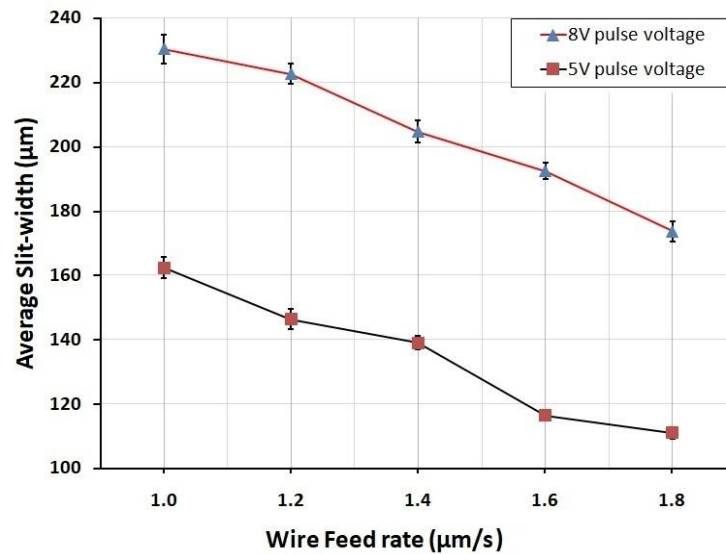
Figure 6.14 Effect of wire feed rate on the average slit width
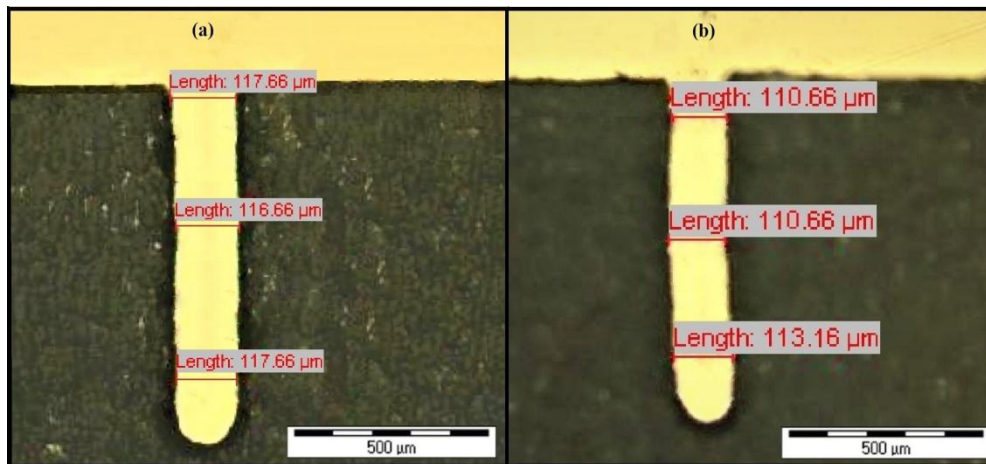
Figure 6.15 Micro slits machined under the following conditions **(a)** 5V Pulse voltage, 400KHz Pulse frequency, **1.6 µm/s wire feed rate** **(b)** 5V pulse voltage, 400KHz Pulse frequency, and **1.8 µm/s wire feed rate**

Wire feed rate below and above this range leads to an increase in slit width. It also reveals that a reduction in the wire feed rate below 1µm/s produces a significant effect for machining which produced micro-pits or no machining on the workpiece. It is observed

that occurrence of less overcut in slit width at high wire feed rate and more overcut at a low wire-feed rate keeping other machining conditions at a constant value. Experimental results reveals that a smaller slit width is obtained at 5V pulse voltage, 400KHz pulse frequency, 1.8μs pulse width with 1.8 μm/s wire feed rate, compared to the use of 8V pulse voltage, 300KHz pulse frequency, 1.8μs pulse width for the same 1.8 μm/s wire feed rate. Also, the machined slit quality at machining of these best values at 1.8 μm/s wire feed rate is smoother and more uniform than any other wire feed rate. Increasing the wire feed rate reduces the side gap. Therefore, for machining of nitinol SMA with WECM, controlled parametric setting of wire feed rate is needed which should not be at the lower or higher side due to reduction in machining accuracy. The wire feed rate range near 1.8 μm/s is found to be best for homogeneous and smooth machining of nitinol SMA utilizing investigated best values of other process parameters.

6.2.2 Characterization of nitinol SMA micro structure

The SEM image of 120 μm thick nitinol SMA before machining and after machining is shown in the **figure6.16.**
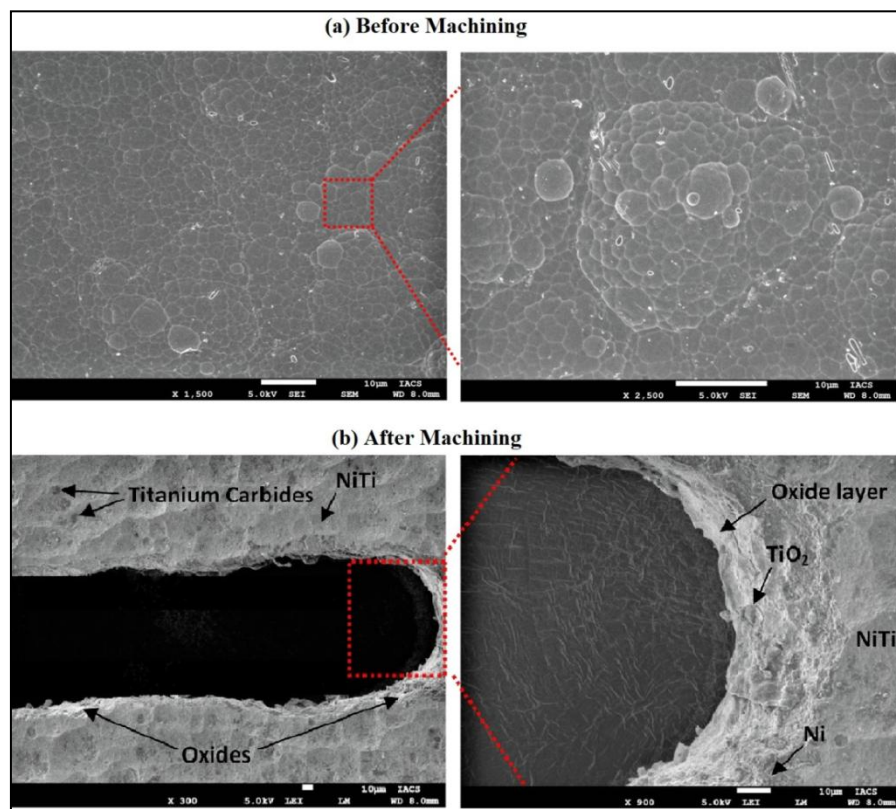
Figure 6.16 SEM images of nitinol surface microstructure (a) Before

machining (b) After machining

It is observed that the thin oxide layer thickness appears to form with oxidation time and temperature. This thermally produced thin oxide layer consists primarily of TiO_2 with a

large number of nickel atoms forming on the surface. However, the formation of passive oxide layer of titanium and electrolysis precipitates TiO_2 and removal of nickel Ni inhibits further material removal of nitinol SMA and deteriorates the surface quality during WECM. The machined micro slits workpiece surface quality was measured using Taylor Hobson CCI profilometer. The surface roughness values (Ra) have been measured. **Figure6.17** shows 3D and 2D profiles and measurements taken on machined surface and the average roughness value, R_a has been observed as 0.108 µm using Gaussian filter.
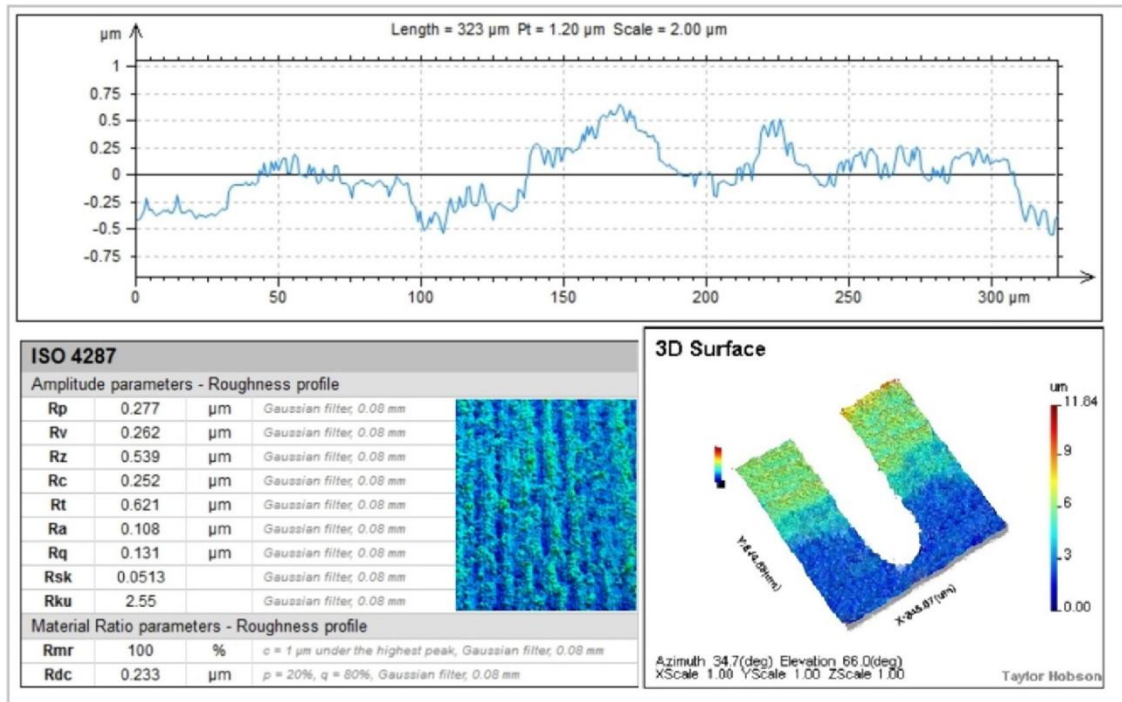
Figure 6.17 Surface characteristics of nitinol SMA

Additional process is needed to achieve smooth surface and form protective layer of TiO_2 in order to remove nickel atoms in the outermost layers which can be further achieved by anodic dissolution during WECM process**.** Also, Titanium carbides were produced during the anodic dissolution process of nitinol SMA. The surface quality of the machined micro-slit has no effect due to the titanium carbide particles, The surface quality has a direct relation with pulse voltage, pulse frequency, and duty cycle keeping electrolyte temperature constant at room temperature with proper flushing and cooling system. The surface quality in WECM is related to the anodic dissolution rate. At higher pulse voltage, the anodic dissolution rate is increased which is directly related to the increase in material removal rate which in turn increases the surface roughness due to increase in electrolyte activity and corrosive action. Further, It is observed that the surface quality at machining zone has no effect of heat affected zone (HAZ), recast layers, strain hardening, and

change in properties during WECM since the principle of process is well known as heat-free and strain-free process.

X-ray diffraction tests are utilized to analyze the crystal structure of nitinol shape memory alloy before and after machining. XRD patterns of nitinol SMA before and after machining are shown in **figure6.18**. Only the diffraction peaks of nickel and titanium crystals are observed, indicating no more electrochemical reaction products, and other dissolved by-products were generated in vibration-assisted axial nozzle jet WECM experiment. Although the crystalline structure of the fresh sample and machined sample are comparable to some extent, there are still substantial variances due to formation of oxide layers near the machining zone. The peak intensities after machining are relatively higher than those in the pattern before machining. The dissolution of surface atoms with low lattice energy is slower than those with high lattice energy on crystal faces, resulting in a built-up of numerous high lattice energy crystal faces throughout the electrochemical reaction. The presence of TiO_2 layer is required for nitinol SMA's corrosion resistance. The oxide surface cracks are visible making it easier for the electrolyte to penetrate the substrate and enhancing the machining rate. The oxide layer mostly composed of TiO_2, and Ni atoms often occurs due to passivation. The formation of thin oxide layer protects the surface against corrosion and removes toxic Ni atoms from the surface of the material.
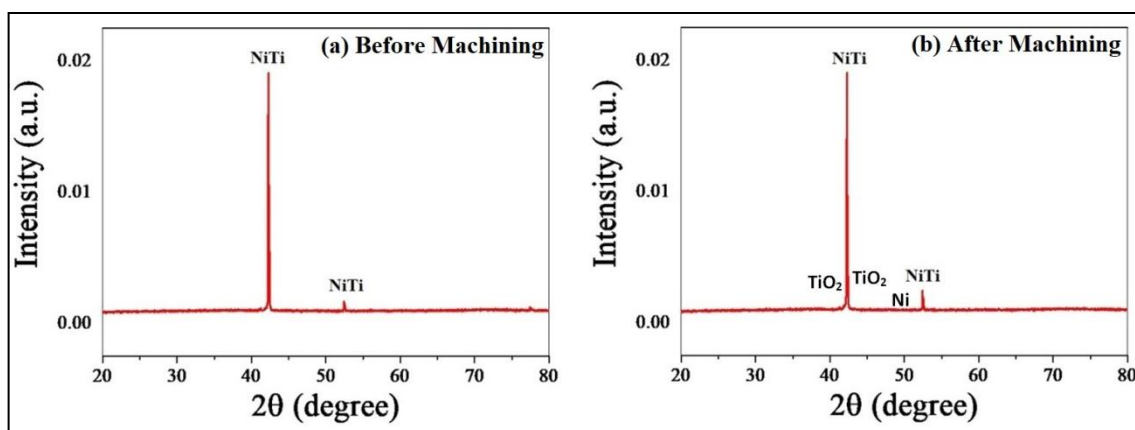
Figure 6.18 XRD pattern of nitinol SMA (a) before machining (b) after machining

To further confirm about any oxides and other dissolved products generated during the process of anodic dissolution in the electrolyte solution and any elements of the electrolyte affected the rim zone, EDX analysis was performed before and after machining to detect the composition of nitinol SMA and the result was shown in the **figure6.19.** The strong signal of Ni (nickel) and titanium (Ti) is shown in the EDX

pattern. However very small signal of carbon (C), oxygen (O) and ferrous (Fe) due to the development of an oxide layer at the machining zone compared to basic microstructure is unlikely, which revealed that the composition of sample surface has no more adverse effect and no influence of the process can be seen at all in each analysis point after wire electrochemical machining.
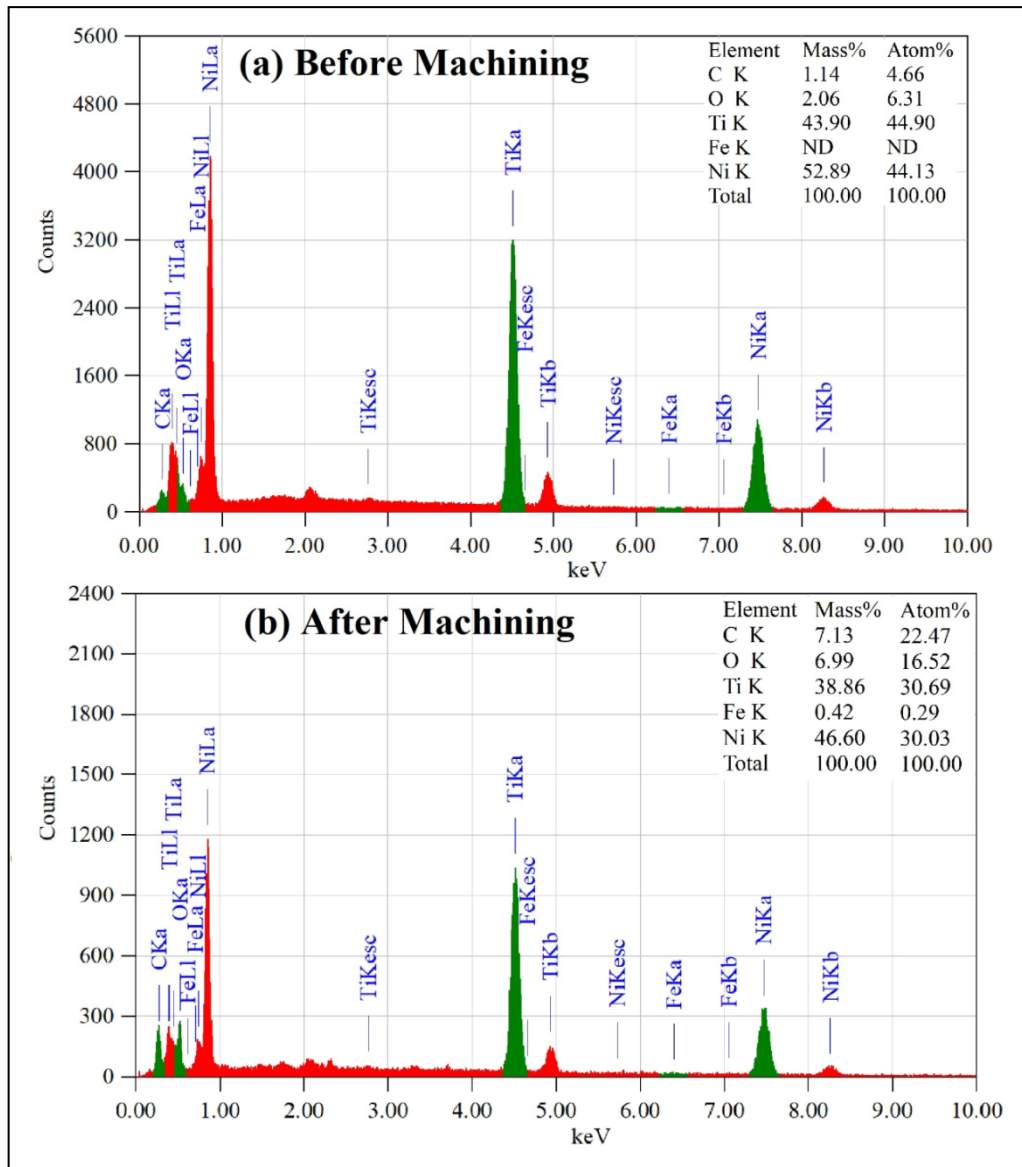
Figure 6.19 Chemical composition of nitinol using EDX analysis (a) Before machining (b) After Machining

The presence of oxygen O is related to O^{2-} anions in the TiO_2 lattice, presence of O^- vacancies in the oxides. The presence of carbon C were related with different chemical bonds of the carbon atoms, the increased value of oxygen were observed near the TiO_2 layer and seen as a bright area. The results of element compositions obtained are represented **in figure6.19.** It is seen that the increase in carbon and oxygen element

composition were detected and attached to the surface of micro slit during the WECM process. The 1.14 carbon and 2.06 oxygen mass % without presence of ferrous was observed before machining which further increases to 7.13 carbon, 6.99 oxygen and 0.42 ferrous mass % after machining. The element composition of titanium were decreases from 43.90 to 38.86 and nickel from 52.89 to 46.60 mass % after machining. According to the results of the analysis, no significant deterioration in nitinol SMA properties has been observed after WECM. The content of the machined workpiece surface was almost identical to the original nitinol SMA content, and the element mapping results showed the same consequence as shown in **figure.6.20.** This shows spatial distribution of elements in textural context showing compositional zones of C, O, Ti, Fe, and Ni of machined nitinol sample. The complete elemental spectrum with relative intensity has been collected associated with all these elements signifying layers and sites of elemental compositional information.
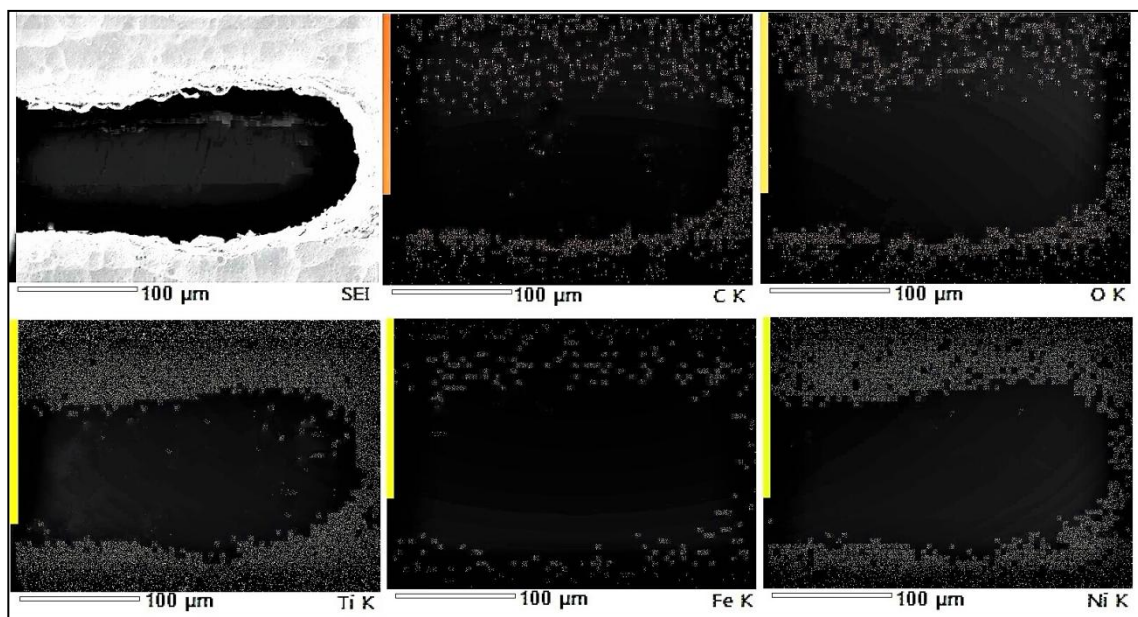
Figure 6.20 Element mapping of nitinol SMA machined surface

6.2.3 Study on anodic dissolution behavior of nitinol SMA in 0.1M H_2SO_4 electrolyte

The electrochemical dissolution behavior has been observed in a 0.1M H_2SO_4 aqueous acidic electrolyte. The experiments were conducted at 5V pulse voltage, 1.8 μm/s wire feed rate and 400KHz pulse frequency , 1.8 pulse width, and 20KHz PZT frequency with 12.94 μm amplitude. The current density distribution in 0.1M H_2SO_4 acidic electrolyte solution was quite uniform with very less passivation effect due to formation of thin titanium oxide layer on the machined surface. It is observed that the surface oxidation of nitinol SMA creates major problem in electrochemical dissolution which form passive

oxide film on the surface of machined workpiece. The electrochemical dissolution of titanium in neutral electrolytes shows change of electrolyte color and formation of black sludge due to local pitting of oxide layer [102]. However, the use of 0.1M H_2SO_4 aqueous acidic electrolyte had produced negligible insoluble products and sludge. Also, anodic oxidation in sulphuric acid (H_2SO_4) significantly increases corrosion resistance and biocompatibility. Although Titania film resulting from anodic oxidation in H2SO4 electrolyte has a porous structure, it can be effectively block-out diffusion of Ni from nitinol SMA.

After machining, the proportion of oxygen evolution found in the EDX measurement was quite low when compared to neutral electrolytes. It indicate that very thin oxide layer were generated in 0.1M H_2SO_4 electrolyte solution resulting controlled dissolution of nitinol SMA and no more pitting corrosion were seen on the machined surface as shown in **figure6.16.** Also, The average surface roughness R_a=0.108 μm was obtained on machined surface which is quite less confirming a uniform dissolution of nitinol during WECM shown in **figure6.17.** Further, in-depth studies on dissolution behavior of nitinol SMA were observed. The potential during the machining process measured with the help of pulse power supply. At narrow IEG in the machining zone, the ensuring current fluctuation owing to electrochemical reaction was observed.

During anodic dissolution, a curve of anodic potential against current density can be explained as outlined in **figure6.21.** It can be shown that at the low potentials, very little current is obtained since no dissolution occurs. The dissolution potential and current density are solely determined by the material, type of electrolyte and its concentration. At higher current densities, the rate of dissolution is faster. On the other hand, high current density also generates a stray current effect in WECM which results in poor machining quality. However, when the potential reaches the dissolution state, there is an abrupt increase in current density and the material begins to dissolve at this potential. In the region of A-B **(Active state),** only metal dissolution suppose to occur. The current density increases rapidly as the potential increases in the region A-B. However, the rate of increase in current density decreases in the region B-C. This may be due to the passivation of working electrode as nitinol SMA forms an oxide layer on the workpiece surface. TiO_2 layer formed due to passivation which becomes firmly attached to the metal forming a barrier between it and electrolyte solution. This passive oxide layer makes nitinol as a a corrosion resistance material. The formed passive protective oxide layer has been confirmed through XRD and EDX analysis of the surface as shown in **figure6.18**

and figure6.19. The current density begins to rise swiftly and linearly again indicating passive oxide layer breakdown and onset of pitting corrosion on the surface. As the current density increased along D-E **(Transpassive state),** the anode potential also increases resulting oxygen formation.
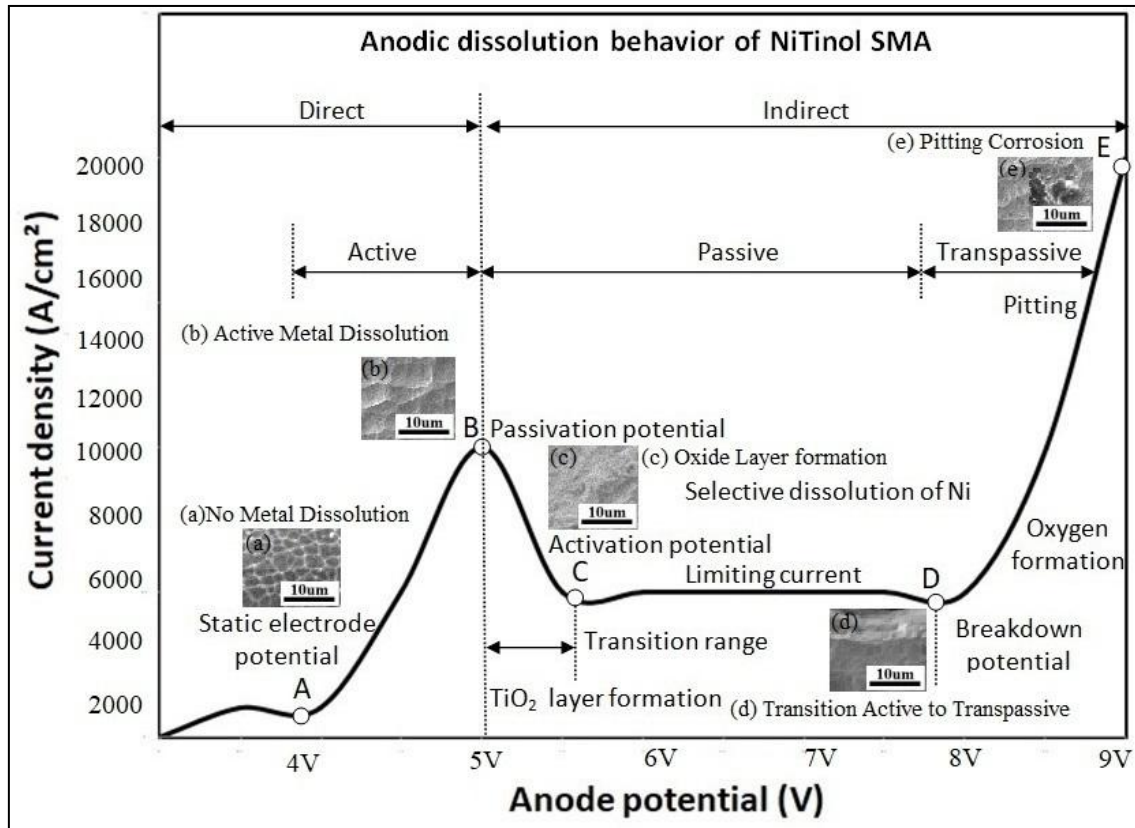
Figure 6.21 Anodic dissolution behavior of nitinol SMA

Also, the rise in current density due to increase in temperature as well as flow rate attributed to an increase in electrochemical reaction and induced rise in electrolyte conductivity which disrupts the material removal and pitting corrosion were observed on the surface of machined workpiece near the edge of micro slits. The higher pulse voltage leading to increase and uneven current density distribution near the machining zone resulting pitting corrosion. Titanium dioxide is formed when titanium is subjected to oxidizing conditions. The oxidation of nitinol SMA occurs as follows **[103]**:

$$NiTi + O_2 \ \rightarrow Ni_4Ti + TiO_2 \ \rightarrow Ni + TiO_2 \tag{6.1}$$
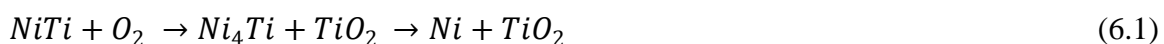
Other anodic and cathodic reactions using 0.1M H_2SO_4 aqueous acidic electrolyte during WECM as follows:

$$TiO_2 \ + \ H_2SO_4 \rightarrow TiOSO_4 + H_2O \tag{6.2}$$

$$Ni + \ H_2SO_4 \ \rightarrow H_2 + \ Ni_2(SO_4)_3 \tag{6.3}$$

$$Ni^{2+} + 2e^- \rightarrow Ni \tag{6.4}$$

$$Ti + O_2 \rightarrow TiO_2 \tag{6.5}$$

$$Ti + C \rightarrow TiC \tag{6.6}$$

$$2H^+ + 2e^- \rightarrow H_2 \tag{6.7}$$
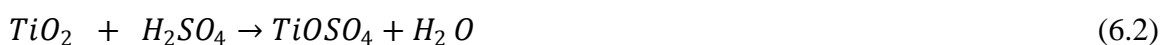
The circumstances at an anode might change from passive to the transpassive, resulting in an increase in current density and hence an increase in anode potential due to TiO_2 layer. Anodic oxidation of oxide layer causes it. At higher current density and after a transition range with active dissolution, the dissolution process switches to transpassive state. The critical current density at which the transformation occurs was increased by increase in electrolyte flow rate and temperature. Increased current density and decreased flow rate shortened the transition period. Ti is passive in nature but Ni is not passive in nature. The presence of Ni in nitinol limits the passivity range while simultaneously considerably increasing the hydrogen evolution resulting in a surface oxide with very different properties from the passive layer of TiO_2. This transpassivity of Ni-Ti was better seen which indicates that at higher potentials, the dissolution of nitinol SMA is controlled by the oxidation of Ni^{2+} cathions in a mixed oxides. It generates stable oxide layer at lower potential. Dissolution at 0.1M H_2SO_4 aqueous acidic electrolyte did not alters Ni-Ti surface chemically and morphologically indicating uniform dissolution of Ni and Ti which has been confirmed through XRD and EDX analysis of workpiece surface before and after machining as shown in **figure6.15 and figure6.19**.

The equiatomic constituent of Ni and Ti in nitinol SMA has distinct electrode potentials. The ones with lowest potential will be dissolved first. At lower current densities, differential dissolution of the Ni and Ti resulting in a difference in surface finish. At high current densities, because the applied potential difference at the anode is higher at high current densities, the influence of discrepancies in Ni and Ti electrodes potential is decreased, and the potentials required for dissolution of the Ni and Ti are more easily obtained. If the grain material's electrode potential is higher, it will not dissolve until the potential at the anode surface meets its electrode potential. The surrounding material will be machined during this period, leaving the grain projecting at the surface. If the grain, on the other hand, has a lower electrode potential, it will dissolve first, leaving a recess on the surface. Ni cations are released slowly in to the electrolyte in a passive region with no Ti dissolution, but Ni and Ti are released at the same rate in the transpassive region. The majority of the current is used for the oxygen evolution and the creation of passive layer at high potential. Ni current density is substantially higher than mean current density in

the passive region. At this position, current is mostly utilized for the selective dissolution of Ni **[103].**

6.3 Experimental planning II: Influence of energy input parameters on feed rate

The nitinol workpiece specimens were 300μm thick sheet (Activation: 45°C +/- 10°C) for investigating energy input parameter effects on wire feed rate and 120μm thick sheet (Activation: 15° +/- 10°C) for fabricating complex curved micro-features to the effect of thickness of material with specimen size of 10mm x 10mm x 0.1mm has been used. All the experiments are planned with equipment and material detailed in **Table6.2** and maintained 50μm initial IEG using a developed vibration-assisted axial nozzle jet flow WECM experimental setup.

Table 6.2 Experimental equipment and materials

Pulse power generator	POA75-4 power supply, Matsusada Precision Inc, Japan
Positioning system and motion controller	MTN100PP XYZ Movement stage, 0.1μm resolution and 100mm travel length for each axis, Newport Corp. USA
Piezoelectric vibration unit	ENV 800 voltage amplifier, PU65 HR Piezo-positioner stage of resolution - 0.13nm and maximum stroke - 65μm, Piezosystem Jena GmBH, Germany
Function generators	Agilent 33250A and U1252A function waveform generator
Oscilloscope	Tektronix's TBS1062
Tool electrode	Tungsten smooth cylindrical wire Diameter – 50 μm with PTFE tube coating
Electrolyte	0.1M H_2SO_4 (98% analytical grade)
Optical microscope	Leica (Germany)
Vision system	Dinolite digital microscope (Taiwan)
Surface Measurement Instrument	CCI noncontact surface profiler mfg. by Taylor Hobson, UK

The experiments were planned to investigate the influence of prominent parameters for energy interaction behavior during the fabrication of micro-slits for better homogeneity, and machining accuracy of nitinol SMA machined micro features during wire

electrochemical machining. **Table6.3** shows the recommended machining conditions chosen as per previous research experiences for the experimentations to fabricate nitinol SMA micro features**.**

Table 6.3 Recommended machining conditions

Electrolyte flow rate	5Lph
PZT Tool vibration	20Hz
PZT Tool vibration	12.94μm
Electrolyte temperature	Room
pulse voltage	6 to 10V
pulse frequency	150 to 400KHz
Duty ratio	20 to 70%
Nozzle diameter	0.4mm
Nozzle workpiece	5mm
Inter-electrode gap	50μm

Each experiment has been conducted a minimum of three times using different ranges of parameters selected from the previous published literature. The machined nitinol micro features dimensions were measured using Leica optical microscope and the Taylor Hobson CCI instrument has been used for surface roughness measurement. Further, micro-structural analysis of the machined surface was conducted through scanning electron microscopy (SEM), and energy-dispersive X-ray spectrum (EDS).

6.3.1 Experimental observations and discussions

To detect the influence of different energy input parameters i.e. pulse voltage, pulse frequency, and duty ratio on wire feed rate, machining accuracy, and surface characteristics, the experimental observations have been discussed hereunder.

6.3.1.1 Influence of pulse voltage on wire feed rate and machining accuracy

The theoretical study from the developed mathematical model predicts that as the wire feed rate increases, the slit width and secondary electrolysis will decrease. However, the wire feed rate has an upper limit in specific conditions during actual machining, because of the restriction of mass transfer **[47].** All the experiments have been carried out using 250 KHz pulse frequency and 50% duty ratio with a wide range of varying pulse voltages from 6 to 10V. It can be seen that the maximum achievable wire feed rate increases with an increase in applied voltage because an increase in applied voltage increases the current in the circuit, the amount of electricity passing through per unit time, the amount of anode material dissolution, and the frontal and side gap. Experiments are designed to investigate the influence of pulse voltage on the maximum achievable feed rate and slit width as shown in **Figure6.22.**
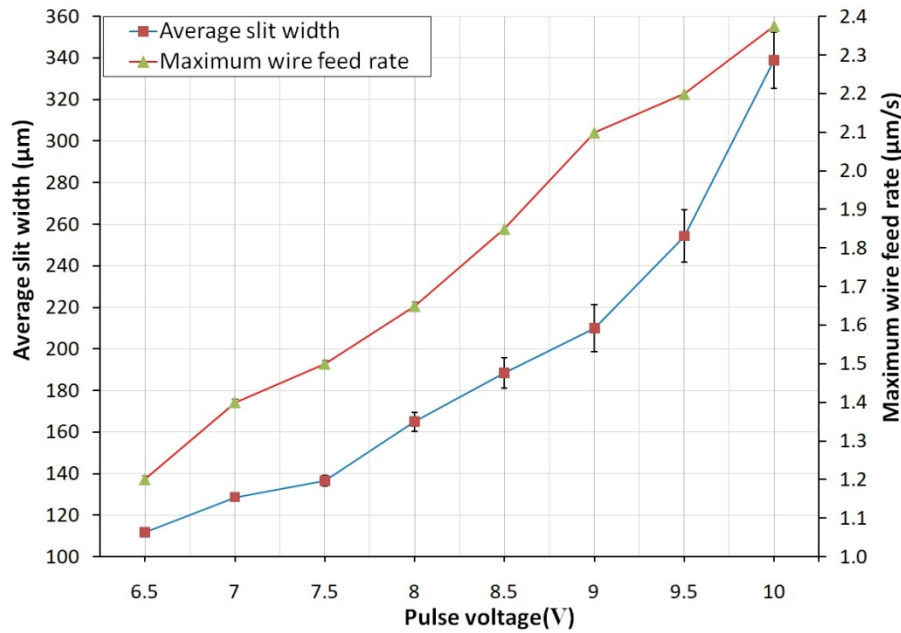
Figure 6.22 Influence of pulse voltage on wire feed rate and slit width

The maximum 2.4μm/s wire feed rate has been achieved at 10V pulse voltage with 342μm average slit-width. It shows that even though the wire feed rate increases with pulse voltage, overcut of the slit width also increased. However, the increase of applied voltage will also increase the electrolysis products produced per unit time, and it leads to a short circuit if the machining gap becomes tiny, which limits the further increase of wire feed rate. For this reason, it can be observed that when the applied voltage increases above 10V, the maximum achievable wire feed rate does not continue to increase at this condition. Although the slit width is the smallest i.e. 111μm when the voltage is 6.5V, the secondary corrosion of the sidewall is serious and the homogeneity of the slit sidewall is poor because the wire feed rate is too small. Therefore, considering the WECM efficiency, localization, homogeneity, and machining accuracy, 7V is selected as the appropriate voltage parameter and the minimum average slit width of 128μm has been fabricated at 1.4μm/s wire feed rate.

6.3.1.2 Influence of pulse frequency on wire feed rate and machining accuracy

The influence of pulse frequency on wire feed rate and slit width in the WECM process has been carried out using 7V pulse voltage and 50% duty ratio with a varying pulse frequency of 150 to 450 KHz and the observed results are graphically represented as shown in **Figure6.23.** It is revealed that the pulse frequency below 200KHz has very poor dissolution rate resulting in poor machining with reduced wire feed rate and higher pulse frequency above 400KHz had higher feed rate resulting in micro sparks during machining due to reduced inter-electrode gap and produces poor machining accuracy.
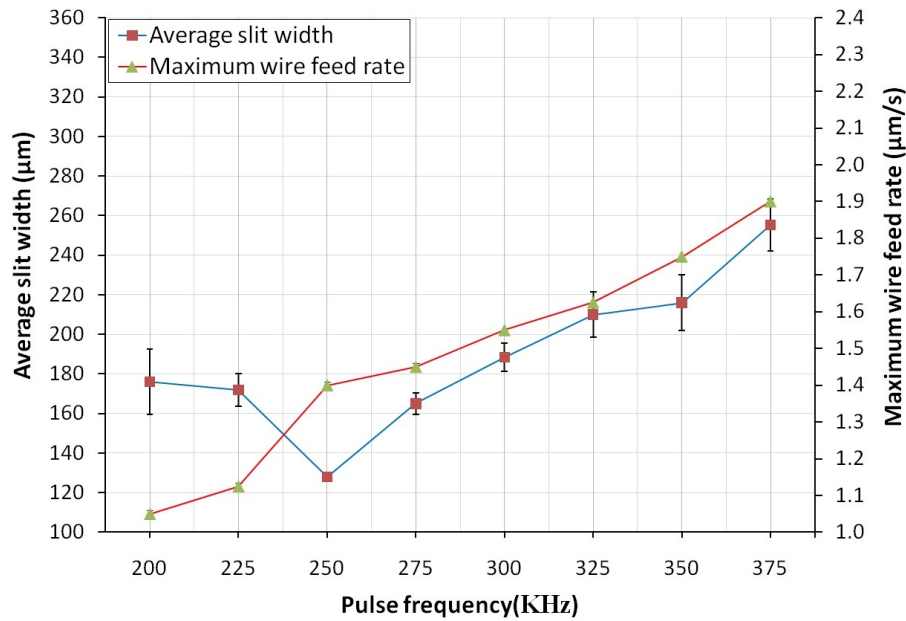
Figure 6.23 Influence of pulse frequency on wire feed rate and slit width

Also, it is observed that the maximum attainable feed rate decreases from 1.4 to 1μm/s with the increase of the pulse frequency from 250 to 200 KHz. This is because the increase in the pulse frequency reduces the pulse period. When the duty cycle is constant, the effective machining time per unit time decreases. Also, it is observed that the pulse frequency from 250 to 375 KHz shows linear increase in wire feed rate. The maximum 1.9μm/s wire feed rate has been achieved at 375 KHz pulse frequency above which no further dissolution takes place and machining of nitinol SMA has been stopped because of short-circuits and heavy micro-sparks due to high wire feed rate and current density in the machining area. The maximum attainable wire feed rate is decreased as a result of less anode material dissolution and smaller machining gap during wire electrochemical machining process for nitinol shape memory alloy.

But when the frequency is too low, the same duty cycle utilized during machining process will result in a more effective machining time per unit time. Although the maximum wire feed rate is now somewhat higher, the increase in wire feed rate is simultaneously constrained by the rise in electrolysis product by the anodic dissolution rate. Therefore, while making sure that the maximum wire feed rate is not drastically decreased, a greater pulse frequency should be chosen taking into account the WECM efficiency, homogeneity, and machining accuracy.

6.3.1.3 Influence of duty ratio on wire feed rate and machining accuracy

The effect of duty ratio on wire feed and slit width using 7V pulse voltage, 250 KHz pulse frequency with 20% to 70% duty ratio in the WECM process is shown in

Figure6.24. It can be observed that the maximum achievable wire feed rate increases with the increase in duty ratio, which is due to the increase in effective machining time, the increase of average machining current, the increase of anode material erosion, and the increase of machining gap, so the maximum achievable wire feed rate increases. Similarly, it can be observed from the curve that the increase rate of wire feed rate increases with the increase in duty ratio, which is opposite to the trend of an increasing rate of slit width. It shows that the increase in duty ratio increases the production of electrolytic products per unit time, which makes machining stability worse and limits the increase of feed rate. From the machining results, it can be observed that under the faster wire feed rate, the slit width is still increased when the duty ratio is 50% to 60%. When the duty ratio is 25% to 40%, the decrease in the etching rate will significantly reduce the maximum achievable wire feed rate and very poor or no dissolution takes place at a 20% duty ratio.
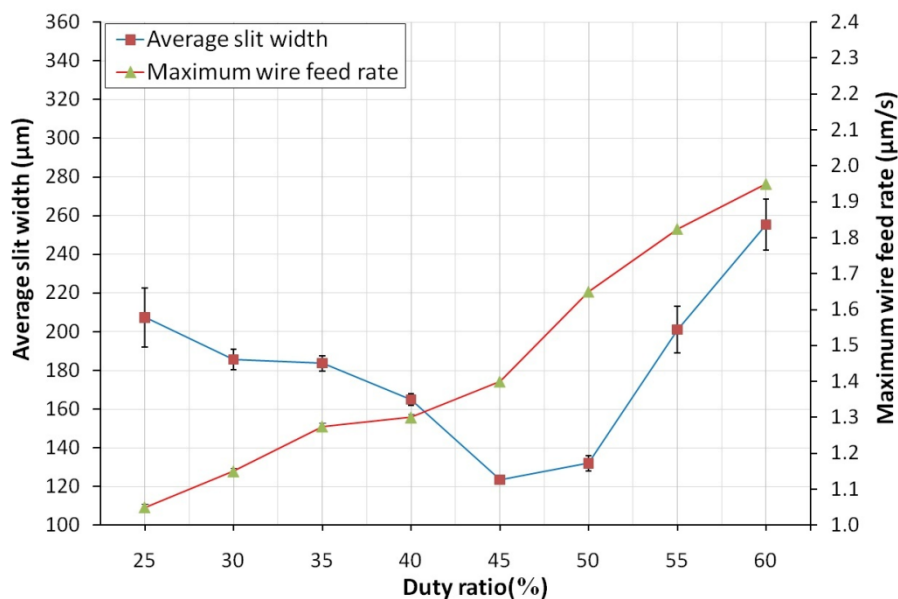
Figure6.24. Influence of duty ratio on wire feed rate and slit width

The average slit width of 207µm at 25% duty ratio and maximum average slit width of 255µm at 60% duty ratio has been obtained. However, the minimum average slit width of 123µm has been obtained at 45% duty ratio. Therefore, considering the WECM efficiency, localization, and slit quality, 45% is selected as the appropriate duty ratio parameter. Nitinol shape memory alloy microslits with different combinations of pulse voltage, pulse frequency, and duty ratio have been shown in **Figure6.25.** It is observed that the micro slit fabricated with a parameter combination of 7V pulse voltage, 250KHz pulse frequency, and, 45% duty ratio achieved better machining accuracy

with minimum slit width as compared to micro slits machined at a combination of 8V, 300KHz, 25%, and 9V, 350KHz, 50%.
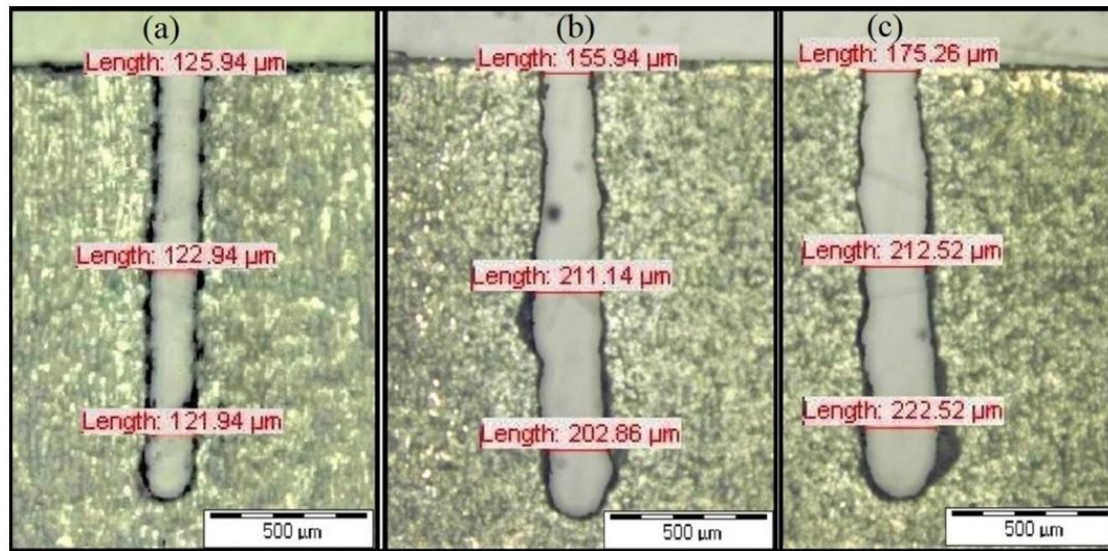
Figure 6.25 Micro-slits at **(a)** 7V, 250KHz, 45% **(b)** 8V, 300KHz, 25% **(c)** 9V, 350KHz, 50%

Further, it has been observed that the slit width has been increased drastically with higher pulse voltage and pulse frequency with poor homogeneity and machining accuracy as shown in **figure6.25(c).** The overcut has been greatly reduced and a straight micro slit has been fabricated at 7V pulse voltage, 250KHz pulse frequency, and 45% duty ratio as shown in **figure6.25 (a).** Also, it is seen that the use of very low duty ratio i.e. 25% affected machining accuracy and homogeneity to a large extent due to the uncontrolled machining process as shown in **figure6.25 (b).**

6.3.1.4 Influence of pulse voltage on surface roughness of nitinol SMA microfeatures

The surface roughness has a direct relation with the pulse voltage. The surface roughness of nitinol SMA at 0.1M H_2SO_4 electrolyte concentration after machining at 250KHz pulse frequency, 45% duty ratio, and different pulse voltages varying from 7 to 10V are shown in **figure6.26.** An increase in pulse voltage applied increases the surface roughness due to a rise in the anodic dissolution rate. At higher pulse voltage coupled with electrolyte concentration, the electrolyte action increases resulting increase in material removal rate (MRR). As the MRR increases, poor surface finish will be obtained in the machining process. The machining accuracy has been greatly improved at 7V with an increase in surface roughness. If the potential difference between the wire and workpiece is very high then poor surface roughness can be achieved from the nitinol SMA.
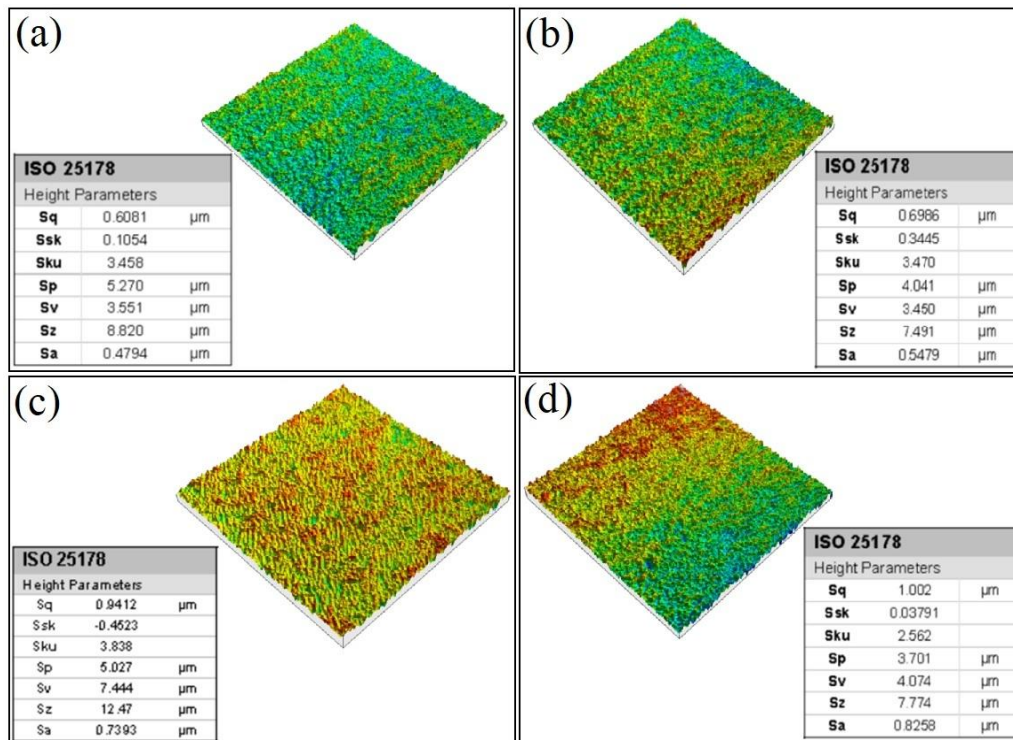
Figure 6.26 Nitinol surface microstructure at pulse voltages **(a)** 7V **(b)** 8V **(c)** 9V **(d)** 10V
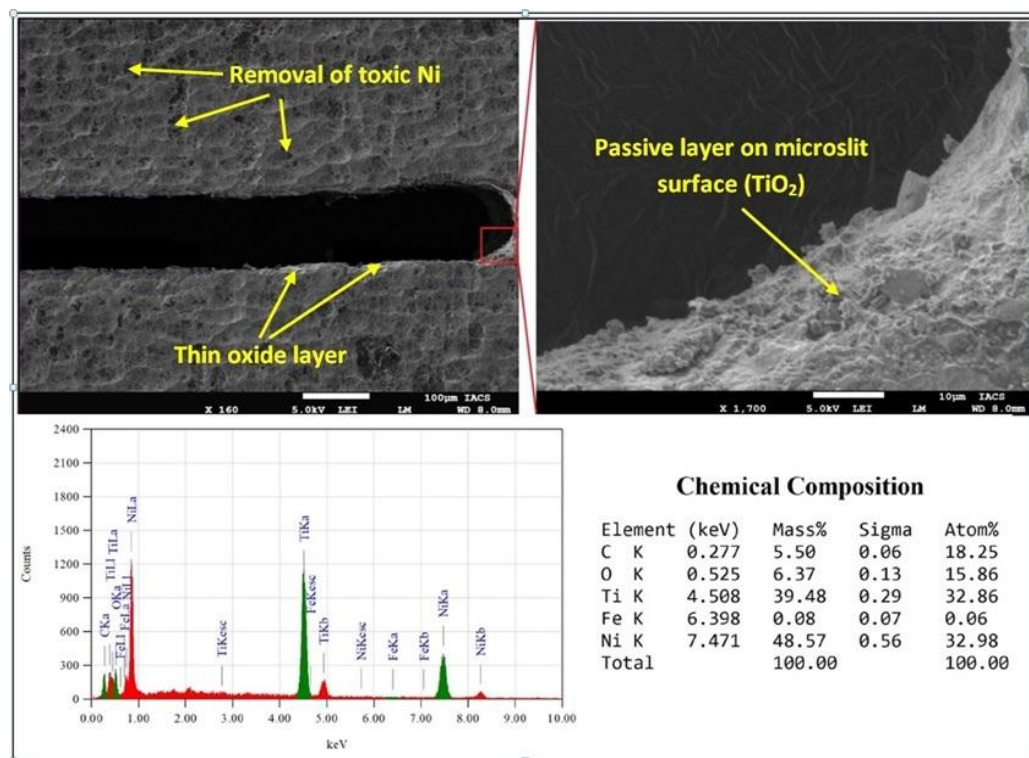
Figure 6.27 SEM and EDS analysis of nitinol SMA microslit

The surface finish was smoothly reduced with the increase in pulse voltage above 8V and finally, poor surface roughness occurred for further increase in pulse voltages up to 10V. The surface roughness at 7V was 0.4797µm which is further increased to 0.8258µm at

maximum pulse voltage level i.e. 10V. The EDS analysis was carried out for the microslit machined at 7V pulse voltage, 250KHz pulse frequency, and 45% duty ratio to identify the composition of nitinol SMA after machining as shown in **figure6.27.** It is seen that the mass of oxygen (O) has been increased to 6.37% after machining which shows the formation of a thin protective passive layer of TiO_2 on the surface of the microslit. Also, the increase in 5.50% mass carbon after machining shows that it oxidizes away the toxic carbon monoxide or carbon dioxide. Further, a decrease in Ni mass from 56% to 48.57% shows the removal of more toxic Ni atoms. The minimum average surface roughness (Ra) of the machined micro-slit has been measured as 0.1076μm as shown in **Figure6.28.** It shows that the WECM is capable of producing complex microfeatures on any difficult-to-cut conductive material with a higher surface finish compared to other nonconventional machining processes.
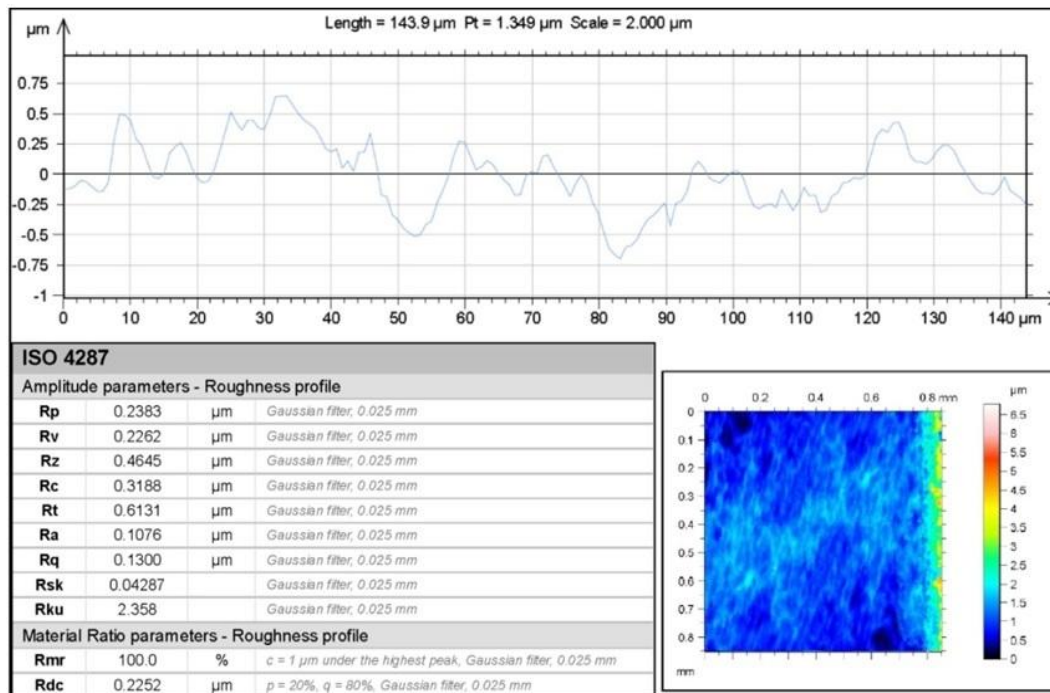
Figure 6.28 Surface roughness of nitinol SMA microslit at 7V Pulse Voltage

6.3.1.5 Fabrication of complex curved micro-feature of nitinol SMA

After successfully identifying the effect of prominent energy input parameters on wire feed rate for obtaining a better machining accuracy and surface quality, 7V pulse voltage, 250 KHz pulse frequency, 1.4μm/s wire feed rate, 45% duty ratio has been used and homogeneous complex curved microfeatures has been successfully fabricated on nitinol SMA as shown in **figure6.29.** This shows the capability and utility of newly developed experimental setup and applicability for fabrication on nitinol SMA nonlinear microfeatures for advanced high potential applications in the biomedical and other

industries. It generates good surface quality and high aspect ratio microfeatures with high productivity which is urgently needed for MEMS applications.
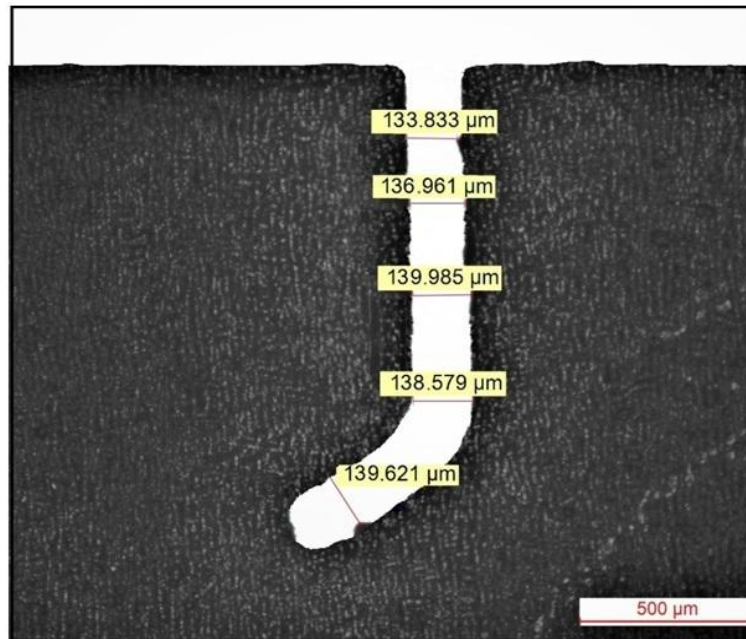
Figure 6.29 Curved complex microfeature of nitinol SMA

The requirement of energy input increase with an increase in workpiece thickness to obtain minimum overcut and better surface quality of fabricated microfeatures during WECM of nitinol SMA.

6.4. Outcomes of Experiments

This chapter deals with the experimental investigation into micromachining of nitinol SMA with 0.1M H_2SO_4 electrolyte concentration which poses significant difficulties by other traditional and nontraditional machining processes due to its material properties. The effect of some of the prominent parameters on the machining of microfeatures was studied which include electrolyte flow rate, electrolyte temperature, cathode PZT amplitude, cathode PZT frequency, pulse voltage, pulse frequency, pulse width, and wire feed rate in one factor at a time order for experimental investigation into wire electrochemical machining of nitinol SMA. Also, the characteristics of nitinol SMA were analyzed before and after machining using SEM, EDX, and XRD tests. Further, this research work presented experimental investigation into the effect of prominent energy input parameters i.e. pulse voltage, pulse frequency, and duty ratio on wire feed rate for homogeneity, machining accuracy, and surface characteristics of nitinol SMA microslits.

Experimental results revealed that the slit width increased with increasing electrolyte flow rate due to high flow pressure and increase with temperature due to an increase in current flow density in the machining zone. Also, Low frequency and small amplitude of

PZT tool vibration during machining reduced slit width to a great extent. Further, it is observed that the slit width increased with increasing input energy, such as pulse voltage, pulse frequency, and pulse width. In addition, the slit width was reduced with increasing wire feed rate due to the appropriate dissolution rate during machining. The results of the experiments with the best combination of machining parameters show homogeneity and uniformity in the machined slit width with better machining accuracy.

SEM analysis and characterization results of nitinol SMA during WECM shows the formation of thin layer of TiO_2 in order to remove nickel atoms in the outermost layers. During XRD analysis, large diffraction peaks of nickel and titanium crystals are observed while titanium dioxide is formed when titanium is subjected to oxidizing conditions and removes toxic Ni atoms from the surface of the material. Also, EDX analysis reveals that the increase in carbon and oxygen element composition were detected from 1.14 carbon and 2.06 oxygen mass % without presence of ferrous to 7.13 carbon, 6.99 oxygen and 0.42 ferrous mass % after machining with decrease in nickel from 52.89 to 46.60 and titanium from 43.90 to 38.86 mass % after machining . According to the results of the analysis, no significant deterioration in nitinol SMA properties has been observed after WECM. During the study on dissolution behavior of nitinol SMA in 0.1M H_2SO_4 electrolyte, no adverse effects were found in the machined surface quality. The surface roughness Ra=0.108 µm was observed on the machined surface which is quite less confirming a uniform dissolution of nitinol during WECM. Also, it is observed that machining of nitinol SMA is active when only metal dissolution to occur and switches to transpassive state for anodic oxidation of TiO_2 layer in H_2SO_4 electrolyte solution.

The experimental analysis drawn from particular experimental setup and conditions highlight the effects of predominant energy input parameters like pulse voltage, pulse frequency and duty ratio on corresponding maximum achievable wire feed rate during microslits machining. Based on the findings major outcomes have been drawn here. The microslits fabricated with different pulse voltage, pulse frequency and duty ratio for different maximum achievable wire feed rate values have showed very good and controlled dissolution where the fabricated microslits are homogeneous with similar width in the desired range. This fact clearly supports the idea of increasing wire feed rate by increasing the corresponding energy input parameters. The release of unpredictable and high pulse energy over the work material and very low and very high wire feed rate reduces the homogeneity and surface quality of the fabricated micro-slits of nitinol SMA. After successfully identifying the best energy input parameter combination amongst

others, a parametric combination of 7V pulse voltage, 250 KHz pulse frequency, 1.4µm/s wire feed rate, 45% duty ratio, and nitinol SMA homogeneous complex curved microfeatures has been successfully fabricated with 137µm average slit width during WECM of 120µm thick nitinol SMA . It shows that the requirement of energy input increases with an increase in workpiece thickness to obtain minimum overcut.

However, to achieve the above, further and immediate actions are required that can increase the lateral dimensions or width of the feature and can provide chance to enhance the feed rate more and precise controlling of operating parameters to fabricate high aspect ratio complex microfeatures of difficult to cut nitinol shape memory alloy. Hence, this research work can be used to understand the effect of different input parameters and influence of energy input parameters for maximum achievable wire feed rate to improve the performance of WECM during machining of nitinol shape memory alloy.

Chapter 7: GENERAL CONCLUSIONS

7.1 General Conclusions

Wire Electrochemical machining (WECM) is a promising method for the fabrication of high aspect ratio complex microfeatures for fulfilling the requirements of micromachining for recent industrial and medical applications without affecting any properties of materials. As a matter of time, there is need to broadening of existing material processing window to understand dissolution mechanisms during WECM for performance enhancement during machining of nitinol SMA by developing novel experimental setups and planning, proper setting of control parameters, and achieving different outcomes. Hence, in this research work, in-depth experimental investigation for performance enhancement of WECM during micromachining of nitinol shape memory alloy has been presented and different novel strategies and methods are developed for fabrication of nitinol shape memory alloy microfeatures giving special attention to machining accuracy, efficiency and surface finish by cautiously addressing the existing knowledge research gaps and may be useful for effective utilization of WECM process for various practical engineering applications. However, after conducting indetails experimental investigations within a constraints and restrictions of in-lab available equipments and resources, and based on the experimental observations and discussions, following conclusions can be drawn:

(i) The development of successful and indigenous vibration assisted axial nozzle jet flow WECM setup has been carried out utilizing various procured, customized and in-lab fabricated components and subsystems containing mechanical units, motion control units, machining and electrolyte chambers, flow control unit and other accessories. Further, the developed setup employed for machining of stainless steel and difficult to cut nitinol SMA microfeatures to justify the uniqueness of the investigation with different flushing approaches for effective analysis of the influences of various process parameters and exploring significant electrochemical phenomena. This is one of the initial unique original contributions of present research work.

(ii) The most unique and novel research finding that has been observed includes investigations on effect of nozzle diameter and workpiece nozzle stand-off distance on different micromachining criteria such as homogeneity and machining accuracy. It has proved feasibility of application during micromachining of stainless steel

SS304 and nitinol SMA which follows the trend of developed mathematical models for slit width calculation and overall improvement in machining quality and accuracy were observed using this novel technique. The overall improvement of 36% microslit width reduction and 75% increase in accuracy compared to axial flow WECM and 23% microslit width reduction and 40% increase in accuracy compared to axial flow with PZT vibration WECM were observed using this novel technique with microslits machined on 100μm thick stainless steel SS304. Finally, the nitinol SMA microslit has been fabricated with better homogeneity and machining accuracy.

(iii)   An economical way of fabrication of microslits over metal surface by WECM for the reduction of micro sparks and overcut has been successfully presented during micromachining of stainless steel SS304. The influence of different input parameters i.e. pulse voltage, pulse frequency, duty ratio, wire feed rate, PZT vibration frequency and amplitude, etc have been analyzed for reduction of micro sparks and overcut which agree well with different machining conditions during micromachining of nitinol SMA employing WECM.

(iv)   The application of various novel wire electrode coating and insulation methods for reduction of stray current attack and overcut of fabricated microfeatures during WECM has significant original research outcomes due to its uniqueness. The effect of various prominent parameters have been investigated for the enhancement of machining accuracy, homogeneity, and surface quality during fabrication of SS304 and nitinol SMA microfeatures with and without coatings is another significant outcome. Also, the use of synthetic enamel and novel PTFE tube insulation method was used to reduce the stray current effect and overcut during WECM and a comparative study has been made with uncoated wire. The PTFE pipe tube wire insulation method has been proved to be the most prominent method with no stray current attack on fabricated microslits. Also, overcut is reduced to a large extent which is below 5 μm and microslit of 100 μm average slit width has been fabricated using PTFE tube insulation method with 180° exposed wire angle and 100 μm insulation distance from workpiece upper surface at 40 μm initial inter-electrode gap. Further, the microslit array of nitinol shape memory alloy has been fabricated and analyzed based on SEM and EDX analysis for understanding effect of PTFE tube wire insulation method during WECM.

(v)   The effects of various neutral aqueous electrolytes i.e. NaBr, NaCl, NaNO$_3$ and EDTA as complexing agent under different mixed and ozonated conditions is a significant contribution for opening new insights for researcher working in the area of WECM during micromachining of nitinol shape memory alloy. Furthermore, dimensional characteristics and surface topography of SMA machined surfaces was performed using FESEM, EDS, and 3D profile surface analysis. It shows that ozonated mixed NaCl+NaNO$_3$+EDTA electrolyte has been proven as most suitable neutral electrolyte combination amongst other to achieve better dimensional characteristics and surface finish of nitinol during wire electrochemical machining. The average groove width of 118.35μm, 115.365μm, 112.68 μm, 105.86μm, mean depth of 188.7μm, 232.9μm, 245.9μm, 264.6μm and the surface roughness (Ra) of the machined surface achieved was 0.3333μm, 0.2790μm, 0.2258μm, and 0.1346μm with 0.2M of mixed NaCl+NaNO$_3$, mixed NaCl+NaNO$_3$+EDTA, ozonated mixed NaCl+NaNO$_3$, ozonated mixed NaCl+NaNO$_3$+EDTA electrolytes respectively.

(vi)   The electrochemical characterization of inorganic H$_2$SO$_4$ acidic electrolyte combined with organic ecofriendly complexing agent i.e. citric acid electrolyte, that are noble in nature, was conducted using potentiodyanamic tests and electrochemical impedance spectroscopy on the corrosion behavior of nitinol. Further, the subsequent effects of machining parameters on fabricated microgrooves for width and depth overcut as well as surface roughness have been presented and confirmed its suitability for micromachining of nitinol shape memory alloy and proved feasibility of application during WECM. The machining of nitinol with mixed 0.1M H$_2$SO$_4$ + 0.1M citric acid electrolyte have obtained reduced surface roughness with better surface integrity compared to combination of neutral electrolytes. However, this mixed electrolyte had immediate contamination which required renewal of fresh electrolyte for each machining. This specific electrolyte produced surfaces with an average surface roughness (Ra) of 0.0631μm and the minimum average machined groove width overcut was 18.10μm in 0.1 M H$_2$SO$_4$ + 0.1M citric acid at 5V pulse voltage. According to the EDS data, the oxygen concentration was very less with mixed 0.1M H$_2$SO$_4$ + 0.1M citric acid electrolyte. The surface roughness (Ra) of 0.108 μm was observed on the machined surface which is quite less confirming a uniform dissolution of nitinol during WECM.

(vii) The study presented in this research work through in-depth experimental investigations and characterization of nitinol SMA during WECM may be useful for effective utilization of this process for various practical engineering applications. In this research work, the investigation into WECM of nitinol SMA at a low concentration of 0.1M H_2SO_4 aqueous acidic electrolyte with effect of small amplitude at low-frequency PZT vibration-assisted axial nozzle jet flushing is presented and the effect of electrolyte flow rate, tool PZT amplitude and frequency, electrolyte temperature, pulse voltage, pulse frequency, pulse width and, the wire feed rate has been investigated during machining on microslits to understand the benefit of WECM on nitinol SMA machining. According to FESEM, XRD and EDX analysis and characterization results of nitinol SMA during WECM had no significant deterioration in nitinol SMA properties. During the study on anodic dissolution behavior of nitinol SMA in 0.1M H_2SO_4 electrolyte, no adverse effects were found in the machined surface quality. The surface roughness (Ra) of 0.108 μm was observed on the machined surface which is quite less confirming a uniform dissolution of nitinol during WECM. One of the unique contributions of this research is the development of polarization graph for different phases of anodic dissolution behaviour of nitinol SMA during WECM.

(viii) This research work presented experimental investigation into the effect of prominent energy input parameters i.e. pulse voltage, pulse frequency, and duty ratio on wire feed rate for homogeneity, machining accuracy, and surface characteristics of nitinol SMA microslits that have been re-established which agreed well the operating parameters and machining conditions. The successful fabrication of complex curved nitinol microfeatures also reveals the fact that by changing the parameter settings, microfeatures with different cross sections for advanced engineering field can be fabricated easily.

The aforementioned conclusions, which were achieved after substantial research, demonstrate its strategy for filling the knowledge gap and, ultimately, creating a solid foundation for this novel anodic dissolution process for nitinol SMA. The modern fabricators from manufacturing and biomedical industries may benefit greatly from the process when it is applied on a wider scale because it is more efficient and applicable not only in micro domains but also in macro regions for hard to machine nitinol shape memory alloy materials. However, individual working conditions, in-house and lab

limitations affect the research effort and the conclusions reached. But even so, a brief summary from the research work of some novel strategies, creative ideas, and successful original finding and major research contributions are briefly concluded as follows:

(i)   The most important research finding includes development of indigenous WECM setup and vibration assisted axial nozzle jet flow system with mathematical model for the performance enhancement of WECM during micromachining of SS304 and difficult to cut nitinol shape memory alloy.

(ii)   Investigations on the influence of different diameter nozzles at varying stand-off distances by studying effect of vibration assisted axial nozzle jet flow for characterization of machining accuracy and surface quality.

(iii)   This research work also presented novel PTFE tube insulation method and considered effect of exposed wire angle and coating distance for reduction of stray current and overcut of fabricated microslits with improved machining accuracy.

(iv)   The use of ozonated mixed aqueous neutral electrolytes (NaBr, NaCl, and NaNO$_3$) and mixed acidic electrolytes (H$_2$SO$_4$) with suitable complexing agents (ex. EDTA, Citric acid) has been presented for improvement in surface quality and homogeneity of fabricated microfeatures of nitinol SMA during WECM.

(v)   The unique original finding and contribution of this research is micromachining and characterization of nitinol SMA considering effects of most of the prominent parameters and investigation on the influence of different energy input parameters for maximum achievable wire feed rate during fabrication of nitinol SMA microslits employing WECM

The researcher has taken genuine efforts to justify the uniqueness of the present research work by exploring the possibilities of fabricating various microfeatures of nitinol shape memory alloy during WECM for effective utilization in advanced industrial and biomedical applications. It can also provide direction for indigenous development of suitable WECM setup for practical industrial applications and the technological guidelines for best parameter settings for fabrication of different useful micro components of nitinol with enhanced machining performance. The research work will provide insight to the researchers, scientists as well as engineers who are working in the area of wire electrochemical machining and fabrication of nitinol SMA. In addition to the aforementioned, certain other research activities are needed for the

benefit of this newly emerging process, which might be considered a viable area for future scope.

7.2 Future scope of research

The present research work exploited wire electrochemical machining for fabricating microfeatures of nitinol shape memory alloy. However, it can be justified from the entire investigations that, at the end, apart from the aforementioned that has been discussed, few issues are worthwhile to mention and need to be taken up as future scope of research on urgent basis at this stage and can be investigated immediately. These are briefly elaborated as follows.

(i)   First and foremost, dedicated flushing need urgent care. This is because the flushing phenomenon substantially alters with cycle time.

(ii)   Investigation on high aspect ratio complex microfeatures of nitinol shape memory alloy is required to be carried out. The various prominent process parameters and their settings in varied machining conditions are also required to be studied.

(iii)   This area of research still requires further investigation for controlling and maintaining inter electrode gap and accurate consistence motion wire electrode to develop efficient feeding systems.

(iv)   Experimental investigation on various optimization aspects of the WECM technique is required during micromachining of nitinol SMA for better machining accuracy, homogeneity and surface integrity.

(v)   However, in order to accomplish this, WECM requires a perfect, stable, commercial, and standard setup suitable for fabricating high aspect ratio complex microfeatures of widely used nitinol shape memory alloy in order to deal with adverse machining conditions and control of online processing etc.

According to the author, the current research makes significant original contributions and will serve as a major catalyst for the efficient and effective application of WECM when creating various shaped microfeatures of nitinol shape memory alloy. The present experimental investigations and the discussions that follow will help scientists, engineers, and researchers who are working on micromachining of nitinol shape memory alloy which have potential uses in MEMS, advanced industrial and biomedical applications using wire electrochemical machining process. It can be concluded that the lab-scale WECM used up till now has a realistic chance of ensuring product quality. As a result, the first essential step is to commercialize WECM and offer a business platform for the process.

BIBLIOGRAPHY

1. B. Bhattacharyya, Electrochemical micromachining for nanofabrication, MEMS and nanotechnology, William Andrew applied science publishers, Imprint of elsevier Inc., Massachusetts, USA, (2015).

2. K. P. Rajurkar, M.M. Sundharam, A.P. Malshe, Review of electrochemical and electrodischarge machining, Procedia CIRP, Vol.6 (2013) pp.13-26.

3. S. Debnath, B. Doloi, B. Bhattacharyya, Review-wire electrochemical machining process: overview and recent advances, J. Electrochem. Soc. 166 (2019) E293–E309.

4. Vyom Sharma, Divyansh Singh Patel, V.K.Jain, J. Rajkumar, Wire electrochemical micromachining: An overview, International Journal of Machine Tools and Manufacture, 155 (2020) 103579.

5. J. A. McGeough, Principles of electrochemical machining, Chapman and Hall, London, (1974)

6. J. Munda, M. Malapati, B. Bhattacharyya, Control of micro-spark and stray-current effect during EMM process, Journal of Materials Processing Technology, 194 (2007) 151–158.

7. B Bhattacharyya, J Munda, M Malapati, Advancement in electrochemical microachining, International Journal of Machine Tools and Manufacture 44 (15) (2004) 1577-1589.

8. B. Bhattacharyya, S. Mitra, AK Boro, Electrochemical machining: new possibilities for micromachining, Robotics and computer integrated manufacturing, 18(3-4) (2002) 283-289.

9. P.K. Kumar and D.C. Lagoudas: Introduction to Shape Memory Alloys, Shape Memory Alloys, Modelling and Engineering Applications, Springer, New York, 2008.

10. A. Rao, A.R. Srinivasa, and J.N. Reddy: Introduction to Shape Memory Alloys, Design of Shape Memory Alloy (SMA) Actuators, Springer, London, UK, 2015.

11. S.A. Oliveira, M.A. Savi, and N. Zouain: A three-dimensional description of shape memory alloy thermomechanical behavior including plasticity. J. Braz. Soc. Mech. Sci. Eng. 38 (2016) 1451.

12. A. Ölander, An electrochemical investigation of solid cadmium-gold alloys. J. Am. Chem. Soc. 54(10) (1932) 3819–3833.

13. J.M. Jani, M. Leary, A. Subic, M.A. Gibson, A review of shape memory alloy research, applications and opportunities. Mater. Des. 56 (2014)1078–1113.

14. P. Lobo, J. Almeida, L. Guerreiro, Shape memory alloys behaviour: A review, Procedia Engineering, 114 (2015) 776-783.

15. A.P. Markopoulos, I.S. Pressas, D.E. Manolakos, Manufacturing processes of shape memory alloys in Materials Forming and Machining (Research and Development) (2016) p. 155.

16. W.J. Buehler, J.V. Gilfrich, R.C.Wiley, Effect of low-temperature phase changes on the mechanical properties of alloys near composition TiNi. J. Appl. Phys. 34(5) (1963) 1475–1477.

17. M.H. Elahinia, M. Hashemi, M. Tabesh, S.B. Bhaduri, Manufacturing and processing of NiTi implants: a review. Prog. Mater Sci. 57(5) (2012) 911–946.

18. Y. Zhou, Micro-welding of shape-memory alloys in Joining and Assembly of Medical Materials and Devices (2013) pp. 133–153.

19. E. Ezugwu, J. Bonney, Y. Yamane, An overview of the machinability of aeroengine alloys, Journal of Materials Processing Technology, 134(2) (2003) 233-253.

20. D. Manolakos, A. Markopoulos, A review on the machining of Nickel-Titanium shape memory alloys, Reviews on Advanced Materials Science, 42(1) (2015) 28-35.

21. K. Zadafiya, Dinbandhu, S. Kumari, S. Chatterjee, A. Kumar. Recent trends in non-traditional machining of shape memory alloys (SMAs): A review. CIRP Journal of Manufacturing Science and Technology, 32 (2021) 217–227.

22. S. Kumari, Dinbandhu, A. Kumar. Study of machinability aspects of shape memory alloys: A critical review. Materials Today: Proceedings, 44 (2021) 1336–1343.

23. B. Dash, M. Das, M. Das, T.Mahapatra, D. Mishra. A concise review on machinability of NiTi shape memory alloys, Materials Today: Proceedings, 18 (2019) 5141–5150.

24. J. Mwangi, L. Nguyen, V. Bui, T. Berger, H. Zeidler, A. Schubert, Nitinol manufacturing and micromachining: A review of processes and their suitability in processing medical-grade Nitinol, Journal of Manufacturing Processes 38 (2019) 355−369.

25. R. Maeda, K. Chikamori, H. Yamamoto, Feed rate of wire electrochemical machining using pulsed current, Precis. Eng. 6 (1984) 193–199, https://doi.org/10.1016/0141-6359(84)90004-7.

26. F. Bejar, M A, Eterovich, Wire-electrochemical cutting with a NaNO3 electrolyte, J. Mater. Process. Tech. 6 (1996) 417–420.

27. D. Zhu, K. Wang, N.S. Qu, Micro wire electrochemical cutting by using in situ fabricated wire electrode, CIRP Ann. - Manuf. Technol. 56 (2007) 241–244, https://doi.org/10.1016/j.cirp.2007.05.057.

28. H.S. Shin, B.H. Kim, C.N. Chu, Analysis of the side gap resulting from micro electrochemical machining with a tungsten wire and ultrashort voltage pulses, J. Micromechanics Microengineering. 18 (2008), 075009, https://doi.org/10.1088/0960-1317/18/7/075009.

29. X.Zou, X.Fang, Y.Zeng, P.Zhang, D. Zhu, In situ fabrication of ribbed wire electrodes for wire electrochemical micromachining, Int. J. Electrochem. Sci., Vol.11 (2016) pp. 2335 – 2344.

30. X. Gao, W. Hu and Y. Gao, Preparation of ultrafine tungsten wire via electrochemical method in an ionic liquid, Fusion Engineering and Design, Vol. 88 (2013) pp. 23– 27.

31. X.L. Fang, X.H. Zou, M. Chen, D. Zhu, Study on wire electrochemical machining assisted with large-amplitude vibrations of ribbed wire electrodes, CIRP Annals – Manufacturing Technology, Vol. 66 (2017) pp. 205–208.

32. X. Fang, X.Zou, P. Zhang, Y.Zheng, N.Qu, Improving machining accuracy in wire electrochemical micromachining using a rotary helical electrode. Int J Adv Manuf Technol. Vol. 84 (2016) pp. 929–939.

33. H. He, Y. B. Zeng, and N. S. Qu, An investigation into wire electrochemical micro machining of pure tungsten. Precision Engineering, Vol. 45 (2016) pp. 285–291.

34. L. Meng, Y. B. Zeng, and D. Zhu, Investigation on wire electrochemical micro machining of Ni-based metallic glass. Electrochimica Acta, Vol. 233 (2017) pp. 274–283.

35. L.Meng, Y.B. Zeng, X.Fang and D. Zhu, Micropatterning of Ni-based metallic glass by pulsed wire electrochemical micro machining. Intermetallics, Vol. 81 (2017) pp. 16-25.

36. L. Meng, Y. Zeng, X. Fang, & D. Zhu, Wire electrochemical micromachining of metallic glass using a carbon nanotube fibre electrode. Journal of Alloys and Compounds, 709 (2017) 760-771.

37. F. Klocke, T. Herrig, M. Zeis and A. Klink. (2018), Experimental Investigations of Cutting Rates and Surface Integrity in Wire Electrochemical Machining with Rotating Electrode, Procedia CIRP, 68 (2018) pp.725–730.

38. C. Gao, N. Qu, H. He, L. Meng, Double-pulsed wire electrochemical micro-machining of type-304 stainless steel, J. Mater. Process. Technol. 266 (2019) 381–387.

39. V. Volgin, V. Do, A. Davydov, Modeling of wire electrochemical machining. Chemical engineering transactions, vol. 41 (2014), https://doi.org/10.1016/j.procir.2015.08.098.

40. Y. Zeng, H. Ji, X. Fang, Y. Wang, Q. Ningsong, Analysis and reduction of stray-current attack in reciprocated traveling wire electrochemical machining, Hindawi Publishing Corporation, Advances in Mech. Engg. 6 (2014) 505932.

41. X Wang, X. Fang, Y.Zheng, and N. Qu, Fabrication of Micro Annular Grooves on a Cylindrical Surface in Aluminum Alloys by Wire Electrochemical Micromachining. Int. J. Electrochem. Sci., Vol.11 (2016) pp. 7216 – 7229.

42. He H, Zeng Y, Yao Y, Ningsong Q, Improving machining efficiency in wire electrochemical micromachining of array microstructures using axial vibration-assisted multi-wire electrodes. J. Manuf. Process. 25 (2017) 452–460. http://dx.doi.org/10.1016/j.jmapro.2017.01.004.

43. H. D. He, N. S. Qu, Y. B. Zeng, band P. Z. Tonga, Improvement of hydrogen bubbles detaching from the tool surface in micro wire electrochemical machining by applying surface microstructures, Journal of The Electrochemical Society, 164 (9) (2017) pp. E248-E259.

44. F.Xu, L.Meng, Y.Wang and N.Qu, In situ fabrication of a microwire electrode using dynamic liquid membrane electrochemical etching," Journal of Engineering Manufacture. Proc IMechE Part B: J Engineering Manufacture, Vol.233 (2019) pp. 381–387.

45. H. He, X. Zhang, N. Qu, Y. Zeng, B. Zhong, Wire electrochemical micro machining assisted with coupling axial and intermittent feed-direction vibrations", Journal of the electrochemical society, 166(6) (2019) E165-E180.

46. T. Yang, Y. Zeng, Y. Hang, Workpiece reciprocating movement aided wire electrochemical machining using a tube electrode with an array of holes, Journal of Materials Processing Tech. 271 (2019) pp. 634-644.

47. S. Debnath, J. Kundu, B. Bhattacharyya, Modeling and influence of voltage and duty ratio on wire feed in WECM: possible alternative of WEDM, J. Electrochemical Soc. 165 (2018) E35–E44.

48. S. Debnath, J. Kundu, B. Bhattacharyya, Influence of high duty ratio and frequency in WECM employing in situ fabricated wire electrode. Journal of micro-and nano-manufacturing, Transactions of ASME, Vol.5 (2017) pp.041005-1–9. https://doi.org/10.1115/1.4037768.

49. Q. Jing, P. Li, Y. Zhang, J. Li, J. Fang, Micro machining by wire-preposed Jet electrochemical machining", Procedia CIRP 95 (2020) 809–814.

50. C. L. Lee, Y. Kanda, S. Ikeda, and M. Mastumura, Electrochemical method for slicing Si blocks into wafers using platinum wire electrodes. . Solar Energy Materials & SolarCells, Vol. 95 (2011) pp. 716-720.

51. Z.Liu, Y.B. Zeng, and W. Zhang, Fabrication of metal microtool applying wire electrochemical machining. Advances in Mechanical Engineering, Vol.6 (2014) pp.1-7.

52. K. Xu, Y.B. Zheng, P.Li, X.L.Fang, and D.Zhu, Experimental research on multiple wire electrodes electrochemical micro machining. Int. J. Electrochem. Sci., Vol. 11 (2016) pp. 5403 – 5415.

53. Kun Xu, Yongbin Zeng, Peng Li, Di Zhu,Vibration assisted wire electrochemical micro machining of array micro tools, Precision Engineering 47 (2017) pp. 487-497.

54. X.Wu & S. Li & W. Zhao, L. Tang & Z. Li. Experiment investigation of using wire electrochemical machining in deionized water to reduce the wire electrical discharge machining surface roughness, The International Journal of Advanced Manufacturing Technology, 102 (2019) pp.343–353.

55. X. Bi, Y. Zeng, N. Qu, Wire electrochemical micromachining of high-quality pure-nickel microstructures focusing on different machining indicators, Precision Engineering 61 (2020) pp.14–22.

56. A. Tyagi, V. Sharma, V.K. Jain, J. Ramkumar, Investigations into side gap in wire electrochemical micromachining (wire-ECMM), Int. J. Adv. Manuf. Technol. (2017) 1–10.

57. K. Rajkumar, N. A. Thushal, A. Gnanavelbabu, P. Sabarinathan, Experimental investigations on the wire electrochemical micro machining (WECM) integrity of AA6061-TiB$_2$ composite", Materials Today: Proceedings 5 (2018) pp.6990–6998.

58. S. Debnath, J. Kundu, B. Bhattacharyya, Influence of wire electrochemical

machining parameters during fabrication of micro features, Int. J. Precision Technology, Vol.7 (2017) Nos.2/3/4.

59. S. Debnath, J. Kundu and B. Bhattacharyya, Influence of wire feed rate on microslit width fabricated by wire ECM process, Int. J. Precision Technology, Vol.8 (2019) Nos. 2/3/4.

60. Y. B. Zeng, Q. Yu, S. Wang, D. Zhu, Enhancement of mass transport in micro wire electrochemical machining, CIRP Ann. – Manuf. Technol. 61 (2012) 195–198.

61. S. Wang, Y. Zeng, Y. Liu, D. Zhu, Micro wire electrochemical machining with an axial electrolyte flow, Int. J. Adv. Manuf. Technol. 63 (2012) 25–32.

62. N. Qu, X. Fang, W. Li, Y. Zeng, D. Zhu, Wire electrochemical machining with axial electrolyte flushing for titanium alloy, Chinese J. Aeronaut. 26 (2013) 224–229.

63. N.S. Qu, K. Xu, Y.B. Zeng, Qia Yu, Enhancement of the homogeneity of micro slits prepared by wire electrochemical micromachining", Int. J. Electrochem. Sci., 8 (2013) 12163 - 12171.

64. N. S.Qu, H. J. Ji, and Y. B. Zeng, Wire electrochemical machining using reciprocated traveling wire. Int J Adv Manuf Technol., Vol. 72 (2014) pp. 677–683.

65. Y. Zeng, Q. Yu, X. Fang, K. Xu, H. Li, N. Qu, Wire electrochemical machining with monodirectional traveling wire, Int. J. Adv. Manuf. Technol. Vol.78, (2015) pp.1251-1257.

66. K. Xu, Y. Zeng, P. Li, D. Zhu, Study of surface roughness in wire electrochemical micro machining, J. Mater. Process. Tech. 222 (2015) 103–109.

67. K. Xu, Y. Zeng, P. Li, X. Fang, D. Zhu, Effect of wire cathode surface hydrophilia when using a travelling wire in wire electrochemical micro machining, J. Mater. Process. Technol. 235 (2016) 68–74.

68. M. Kalaimathi, G. Venkatachalam, M. Sivakumar, S. Ayyappan, Experimental investigation on the suitability of ozonated electrolyte in travelling-wire electrochemical machining, J Braz. Soc. Mech. Sci. Eng. 39 (2017) 4589–4599.

69. N. Qu, and C. Gao, Improving surface processing quality in wire electrochemical micromachining by gas bubble chain, Journal of Materials Processing Tech. 294 (2021) 117136.

70. K. Jiang & X. Wu, J. Lei, Z.Wu, W. Wu, W. Li & D. Diao, Vibration-assisted wire electrochemical micromachining with a suspension of B_4C particles in the electrolyte, The International Journal of Advanced Manufacturing Technology, 97,(2018) pp. 3565-3574.

71. S. Li, Y. Zeng, Y. Hang, and T. Yang, Improving surface quality and machining efficiency of microgrooves by WECMM in H_3PO_4-C_2H_5OH solution, Journal of The Electrochemical Society, 166 (16) (2019) E584-E593.

72. M. Tak, V. Reddy, A. Mishra and R. Mote, Investigation of pulsed electrochemical micro-drilling on titanium alloy in the presence of complexing agent in electrolyte, Journal of Micromanufacturing 1(2) (2018)142–153.

73. S. Maity, S. Debnath, B. Bhattacharyya, Modeling and investigation on multi-wire electrochemical machining (MWECM) assisted with different flushing strategies, Journal of Manufacturing Processes 57 (2020) pp. 857-870.

74. Shi Hyoung Ryu, Eco-friendly ECM in citric acid electrolyte with microwire and microfoil electrodes, International Journal of Precision Engineering and Manufacturing vol. 16, No. 2 (2015) pp. 233-239.

75. Z. Zhou, X. Fang, Y. Zeng, D. Zhu, Generating micro grooves with a semicircular cross-section using wire electrochemical micromachining, The International Journal of Advanced Manufacturing Technology 110 (2020) 2929–2940.

76. N. Qu, and C. Gao, Fabrication of microstructures with mirror surfaces by wire electrochemical micromachining of stainless steel 304 using $NaNO_3$-ethylene glycol, The International Journal of Advanced Manufacturing Technology 112 (2021) 261–272.

77. A. Sethi, B. R. Acharya, and P. Saha, Electrochemical dissolution of WC-Co micro-tool in micro-WECM using an eco-friendly citric acid mixed $NaNO_3$ electrolyte", Journal of The Electrochemical Society, 169 (2022) 033503.

78. R. Kedare, V. Nanavare, S. Sharma, A.Midathad, U. Ravell, Review on WEDM of shape memory alloy", Materials Today: Proceedings 5 (2018) 28313–28319.

79. C.L Chu, R.M. Wang , L.H. Yin , Y.P. Pu, P.H. Lin, Y.S. Dong, C.Y. Chung, K.W.K. Yeung, P.K. Chu, Effects of anodic oxidation in H2SO4 electrolyte on the biocompatibility of NiTi shape memory alloy, Materials Letters 62 (2008) 3512–3514.

80. E. Lee, T. Shin, An evaluation of the machinability of nitinol shape memory alloy by electrochemical polishing, Journal of Mechanical Science and Technology, 25(4) (2011) 963–969.

81. M. Frensemeier, D. Schirra, M. Weinmann, O. Weber, E. Kroner, Shape-memory topographies on nickel–titanium alloys trained by embossing and pulse

electrochemical machining, Advanced Engineering Materials, 18(8) (2016) 1388-1395.

82. S. Ao, K. Li, W. Liu, X.Qin, T. Wang, and Y. Dai, Electrochemical micromachining of NiTi shape memory alloy with ethylene glycol–NaCl electrolyte containing ethanol. Journal of Manufacturing Processes, 53 (2020) 223–228.

83. E. Lee, T. Shin, B. Kim and S. Baek, Investigation of short pulse electrochemical machining for groove process on Ni-Ti shape memory alloy, International journal of precision engineering and manufacturing, Vol. 11, No. 1 (2010) pp. 113-118.

84. X. Ma, L. Zhang, G. Cao, Y. Lin, J. Tang, Electrochemical micromachining of nitinol by confined-etchant-layer technique, Electrochimica Acta 52 (2007) 4191–4196.

85. T. Mineta, Pulse electrochemical etching of NiTi shape memory alloy in LiCl-ethanol electrolyte." Journal of the Surface Finishing Society of Japan, 54 (2003) 693–7.

86. B. Mouliprasanth and P. Hariharan, Evaluation of 3D surface roughness in electrochemical micromachining of nitinol, Surf. Topogr. Metrol. Prop. 9 (2021) 045012.

87. J. Hung and P. Yang, Electrochemical microslot machining by ultrasonic-vibration-aided electrolyte on nitinol wire. Processes, 9 (2021) 1752. https://doi.org/10.3390/pr9101752.

88. V.K. Jain, and A. K. Chouksey, A comprehensive analysis of three-phase electrolyte conductivity during electrochemical micromachining/micromachining. Proc Inst Mech Eng Part B J Eng Manuf. 232 (2018) 2449–2461.

89. S. Wang, Y. Zeng, Y. Liu, Microwire electrochemical machining with an axial electrolyte flow. Int J Adv Manuf Technol. 63 (2011) 25–32.

90. S. Ahn, S.Ryu, D. Choi, and C. Chu, Electrochemical micro drilling using ultra short pulses. Precision Engineering, Vol. 28, issue2, 2004, p. 129-134

91. R. Sueptitz, S. Horn, M. Stoica, M. Ulhemann, and A. Gebert, Electrochemical micromachining of passive electrodes-application to bulk metallic glasses. J. Mater. Process. Tech., Vol. 219 (2015) pp. 193-198.

92. Ding R, Shang JX, Wang FH, Chen Y, Electrochemical pourbaix diagrams of Ni–Ti alloys from first- principles calculations and experimental aqueous states. Comput Mater Sci 143 (2018) 431–438. https:// doi. org/ 10. 1016/j. comma tsci. 2017. 11. 033.

93. Davydov AD, Kabanova TB, Volgin VM, Electrochemical machining of titanium. Review Russ J Electrochem 53 (2017) 941– 965. https:// doi. org/ 10. 1134/ S1023 19351 70900 4X.

94. Munoz-Portero MJ, Garcia-Anton J, Guinon JL, Perez-Herranz JL, Pourbaix diagrams for nickel in concentrated aqueous lithium bromide solutions at 25 °C. Corrosion 63 (2007) 625– 34. https:// doi. org/ 10. 5006/1. 32784 12.

95. A. Sethi, B.R. Acharya, P. Saha, Study of the electrochemical dissolution behavior of Nitinol shape memory alloy in different electrolytes for micro-ECM process, Int. J. Adv. Manuf. Technol. 121 (2022) 7019–7035. https://doi.org/10.1007/s00170-022-09802-z.8

96. Zarubitskii OG, Dmitruk BF, Zakharchenko NF Titanium interaction with hydroxide-salt melts. Prot Met 43 (2007) 483– 486. https:// doi. org/ 10. 1134/ S0033 17320 70501 16.

97. Sreekumar NV, Bhat NG, Narayana B, et al. Selective complex- ometric determination of titanium(IV) using sodium potassium tartrate or ascorbic acid as masking agent. Mikrochim Acta, 141 (2003) 29–33.

98. Linder HJ, Ufer PP, Heck K, Schmoger G, Method and apparatus for electro chemical machining. (1985) US Patent 4504370.

99. Tomiyasu, H., Fukutomi, H., Gordon, G., Kinetics and mechanism of ozone decomposition in basic aqueous solution. Inorg. Chem. 24 (1985) 2962–2966.

100. Buxton, G.V., Greenstock, C.L., Helman, W.P., Ross, A.B., Critical review of rate constants for reactions of hydrated electrons, hydrogen atoms and hydroxyl radicals (*OH/*O⁻) in aqueous solution. J. Phys. Chem. Ref. Data 17 (2) (1988) 513–886.

101. Chelkowska, K., Grasso, D., Fa´bia´n, I., Gordon, G., Numerical simulations of aqueous ozone decomposition. Ozone: Sci. Eng. 14 (1992) 33–49.

102. S. Anasane, B.Bhattacharyya Experimental investigation on suitability of electrolytes for electrochemical micromachining of titanium. Int J Adv Manuf Technol. 86(2016) 2147–60.

103. D.A.Dalla Corte, L.F.P.Dick, Selective dissolution of Ni from nitinol for increasing the biocompatibility. ECS Transactions, 11 (21) (2008) 29-38.

Vibration-Assisted Axial Nozzle Jet Flow Wire Electrochemical Machining for Micromachining

Naresh Besekar[1]
Production Engineering Department,
Jadavpur University,
Kolkata 700032, India
e-mail: nareshwbesekar@gmail.com

B. Bhattacharyya
Professor
Production Engineering Department,
Jadavpur University,
Kolkata 700032, India
e-mail: bb13@rediffmail.com

Wire electrochemical machining (WECM) has the capability to produce metal microcomponents with high aspect ratios. However, because interelectrode gap mass transportation of electrolyte is not homogeneous due to inappropriate and insufficient flushing, novel vibration-assisted axial nozzle jet flow WECM is introduced, and a unique experimental setup and tool are created. A comparison of the axial flow system, axial flow with PZT vibration with this newly developed flushing strategy was made. The effect of the most influencing parameters, i.e., pulse voltage, wire feed rate, and duty ratio, on the machining results of each flushing strategy being analyzed. The improvement of 36% slit width reduction and 75% increase in machining accuracy compared to axial flow WECM and 23% slit width reduction and 40% increase in machining accuracy compared to axial flow with PZT vibration WECM was observed using this novel technique with microslits machined on 100 μm thick stainless steel SS304. The effect of nozzle diameter and workpiece nozzle stand-off distances on slit width machining results has been investigated. The average slit width is 115 μm at 0.4 mm nozzle diameter, and it rises to 143 μm at 1 mm nozzle diameter. The average slit width is 110 μm at a 5 mm workpiece nozzle stand-off distance, and it rises to 145 μm at a 20 mm workpiece nozzle stand-off distance. This research report also discusses microslit machining of NiTinol shape memory alloy for improving WECM performance.
[DOI: 10.1115/1.4053747]

Keywords: wire electrochemical machining, WECM, micromachining, microfeature, axial flow, nozzle

1 Introduction

The fabrication of advanced difficult-to-cut metallic complex microstructures with better machining quality has to turn into a key issue in today's manufacturing industries. Wire electrochemical machining (WECM) is an electrochemical anodic dissolution process that can be applicable for machining difficult-to-cut metallic structures despite the other material properties. According to Bhattacharyya, continuous removal of sludge and dissolved products, and replenishment of clean electrolytes becomes difficult in the narrow IEG, resulting in unsteadiness and repeated microsparks during micromachining [1]. Qu et al. used an innovative gas bubble chain to release sludge and dissolved products

outside IEG, resulting in a significant improvement in surface processing quality [2]. Jing et al. presented wire-preposed jet electrochemical machining based on jet ECM of microstructure [3]. Debnath et al. reviewed the particulars of different flushing strategies to provide an understandable representation of the WECM [4]. Sharma et al. has proven WECM as a promising technology for micromachining with tungsten is the most commonly utilized of the numerous tool materials owing to its enormous chemical stability and tensile strength [5]. Ghosal et al. used vibration-assisted electrochemical micromachining to produce high aspect-ratio microfeatures due to adequate sludge disposal during machining [6]. He et al. presented the experimental analysis of Ti-Al alloy machining using axial electrolyte flow WECM [7]. He et al. investigated WECM assisted by combined axial with intermittent feed-direction vibrations to improve electrolyte replenishment in the tiny IEG [8]. Debnath et al. experimental analysis highlight the importance of adding axial electrolyte flow combined with small vibrations by PZT for producing regulated and homogeneous machining [9]. Zeng et al. found that enhanced mass transport techniques can considerably improve machining stability, and quality for micro-WECM [10]. Qu et al. used WECM to explore the process of machining titanium alloy microfeatures [11]. Xu et al. adopted low-frequency workpiece vibration and cathode wire movement in the axial path [12]. Wang et al. investigated that the small amplitude with low-frequency vibration greatly increases machining stability, slit-width, machining accuracy [13]. Debnath et al. investigated that an electrolyte flow system with proper selection of process parameters can be used to achieve higher wire feed-rate machining [14].

According to a review of research, improved machining accuracy, homogeneity, and surface quality require improved mass transport owing to adequate flushing. Electrolyte flushing with a vibration-assisted axial nozzle jet flow system has yet to be implemented. As a result, in this investigation, attempts are made to improve mass transport by using vibration-assisted axial nozzle jet flow to improve WECM performance. A comparison of axial flow, axial flow with PZT, and novel vibration-assisted axial nozzle jet flow WECM has been made, with the effect of the most influencing parameters, such as pulse voltage, feed rate, and duty ratio, on the machining results of each flushing strategy being examined. The impact of nozzle diameter and workpiece nozzle stand-off distances on slit width machining results has been investigated. There has been no research into the anodic dissolving mechanisms for NiTinol shape memory alloy during WECM investigated in the literature to date. As a result, this study report also discusses microslit machining of NiTinol shape memory alloy for improving WECM performance.

2 Principle of Vibration-Assisted Axial Nozzle Jet Flow Wire Electrochemical Machining

The principle of vibration-assisted axial nozzle jet flow WECM is depicted in Fig. 1(a). The pulse generator is used to dissolve metal by electrochemical reactions between the cathode wire and anode workpiece soaked in an appropriate electrolyte solution separated by a tiny IEG during micromachining for renewal of fresh electrolyte in the narrow IEG to avoid any microsparks and short-circuit for stable machining conditions. The tool is fed toward the workpiece in a predetermined trajectory for anodic dissolution with a given feed travel length to machine the workpiece with a small diameter nozzle jet flow electrolyte at a specific workpiece nozzle stand-off distance coaxial with a wire electrode along with small amplitude and low-frequency PZT vibration. The electrolyte in the narrow IEG can be effectively renewed by this process. A comprehensive sketch of the side gap in the WECM process, which is used to assess the homogeneity and machining accuracy of WECM shown in the Fig. 1(b) and can be expressed mathematically as follows:

$$\text{Slit width} = d_w + 2\Delta s = d_w + 2\Delta b\sqrt{\frac{2d_w}{\Delta b} + 1} \qquad (1)$$

Experimental investigation and characterization of NiTinol shape memory alloy during wire electrochemical machining

Naresh Besekar [a,b,*], B. Bhattacharyya [a,b]

[a] Jadavpur University, Kolkata 700032, India
[b] Production Engineering Department, Jadavpur University, Kolkata 700032, India

ABSTRACT

NiTinol-based microstructures have piqued interest in a variety of industrial applications. Nonetheless, due to material features and characteristics, micromachining of NiTinol shape memory alloy (SMA) offers a significant problem due to a detrimental combination of shape memory effect and super-elasticity. In this paper, an investigation into the wire electrochemical machining (WECM) of NiTinol SMA at a low concentration of 0.1 M H_2SO_4 aqueous acidic electrolyte with effect of small amplitude at low-frequency PZT vibration-assisted axial nozzle jet flushing is presented. During the machining process, initially, the effect of most influencing WECM process parameters i.e. electrolyte flow rate, tool PZT amplitude and frequency, electrolyte temperature during micromachining of NiTinol SMA was studied on machining characteristics for microslit fabrication. Additionally, the effect of pulse voltage, pulse frequency, pulse width and, the wire feed rate was also investigated during machining on micro slit width to understand the benefit of WECM on NiTinol SMA machining in sequential order. Furthermore, after several experiments for controlled machining conditions, finally, NiTinol SMA - based homogeneous minimum slit width of 110 μm with 0.57 μm standard deviation were obtained with 120 μm thick NiTinol sheet at a 100 μm initial inter-electrode gap. The characteristics of NiTinol SMA were analyzed before and after machining using scanning electron microscopy (SEM), and energy-dispersive X-ray (EDX), X-ray diffraction (XRD) tests. Also, dissolution behavior of NiTinol SMA in 0.1 M H_2SO_4 aqueous acidic electrolyte was studied. The surface roughness R_a was observed as 0.108 μm on the machined surface confirming a uniform dissolution during WECM.

1. Introduction

NiTinol alloy composed of nearly equal atomic percent composition of nickel (Ni) and titanium (Ti) in terms of its invention at the Naval Ordnance Laboratory is one of the shape memory alloys (SMAs). Because of their remarkable overall capacity to memorize or restore their original shape from a plastically distorted state by heating, magnetic or mechanical loading, NiTinol shape memory alloys have begun to gain popularity. NiTinol is extensively utilized in micro-electromechanical system (MEMS) devices, and a variety of other advanced applications in the robotics, electronics, aerospace, biomedical, automotive areas, among others. However, it is a hard-to-cut metal because of its diverse particular features and properties. There are numerous obstacles to machining NiTinol SMA with traditional machining. Noncontact operation between the wire electrode (cathode) and workpiece (anode) of the wire electrochemical machining (WECM) process removes many of

the issues associated with traditional machining techniques. Further, the working principle of WECM is well known for the outstanding property of an unaffected rim in terms of residual stresses and HAZ. The variety of input process parameters in the WECM process must be managed to achieve high machining accuracy, surface quality and control the ensuing physical and mechanical properties [1]. In today's competitive manufacturing market, new technology adoption is essential to meet the overall requirement of products without any environmental effect. Aside from these standard challenges, the fabrication of newly developed smart materials necessitates the use of intelligent machining techniques. WECM is a type of nontraditional machining technology that is better at overcoming these challenges. The WECM method may be used on any conductive substance despite its hardness. The anodic dissolution is used in the WECM to assist material removal from the workpiece.

Soni Kumari et al. (2021) reviewed that the excellent features of NiTinol SMA make them a well-suited material for several industrial

ORIGINAL ARTICLE

Wire electrode insulation method for stray current and overcut reduction during WECM—a novel approach

Naresh Besekar[1] · Bijoy Bhattacharyya[1]

Abstract

Wire electrochemical machining (WECM) is a transport-limited dissolving process. The application of various wire electrode coating and insulation methods and the effect of various prominent parameters for reduction of stray current attack and overcut play a more important role in the enhancement of machining accuracy, homogeneity, and surface quality during the fabrication of microfeatures. Therefore, the characteristics of the stray-current attack in WECM were identified through simulation for electrolyte potential, and current density distribution at narrow IEG in the machining zone and overcut model is presented in this paper. Also, the use of synthetic enamel and novel PTFE (polytetrafluoroethylene) tube insulation method was used to reduce the stray current effect and overcut during WECM, and a comparative study has been made with uncoated wire. The stray-current attack and overcut have been greatly reduced by the proposed insulating methods under different parametric conditions. The PTFE pipe tube wire insulation method is proved to be the most prominent method with no stray current attack on fabricated microslits. Also, overcut is reduced to a large extent which is below 5 μm, and a microslit of 100.61 μm average slit width has been fabricated using PTFE tube insulation method with 180° exposed wire angle and 100 μm insulation distance from workpiece upper surface at 40 μm initial interelectrode gap. Further, NiTinol shape memory alloy microslit array was fabricated and analyzed based on SEM and EDX analysis for understanding the effect of PTFE tube wire insulation method during WECM.

Keywords Wire electrochemical machining · WECM · Synthetic enamel coating · PTFE tube insulation · Stray current effects · Overcut

1 Introduction

WECM has enormous potential for the fabrication of high aspect ratios and complex microfeatures of any conducting materials with better surface quality. However, the reduction of stray current attack and overcut during machining plays important role to achieve improved surface quality using different insulation methods related to recent development of WECM.

1.1 Stray current reduction in WECM

When a typical pulse or DC is used for machining, the stray current attack degrades the accuracy and surface quality. The electric field is dispersed far away from the wire electrode, allowing a stray current attack on the workpiece to occur due to current flux passing through the machining zone. Many attempts have been made to mitigate the stray current attack in the ECM process. The key to solving this problem is to pinpoint the electric field-affected zone which is usually reduced by using electrode coating and insulation. However, WECM is still under investigation, and the effect of stray current deteriorates, degrades, and distorted homogeneity and stability of the process as well as dimensional characteristics of generated microfeatures leading to overcut. The elimination of stray current during WECM is needed in practice for effective utilization of this process in the area of microfabrication.

✉ Naresh Besekar
nareshwbesekar@gmail.com

Bijoy Bhattacharyya
bb13@rediffmail.com

[1] Production Engineering Department, Jadavpur University, Kolkata, India 700032

Influence of energy input parameters on wire feed rate and surface characteristics during WECM of Nitinol SMA

Naresh Besekar[1] [ID] and B. Bhattacharyya[1]

Abstract

Nitinol shape memory alloy (SMA) has outstanding chemical and mechanical properties which make the machining of Nitinol SMA more difficult than other materials due to super-elasticity and multiphase transformation. Wire electrochemical machining (WECM) is a nontraditional process, which removes conductive material through anodic dissolution despite of material's properties. In this paper, the mathematical model is presented for slit width calculation for the influence of different parameters using vibration-assisted nozzle jet flushing. In this experimental investigation, the effect of prominent energy input parameters on wire feed rate to achieve better homogeneity, machining accuracy, and surface quality with a 300 µm thick sheet of Nitinol SMA micro-slits has been presented using an in-house developed WECM set-up. Experimental results revealed that the wire feed rate and surface roughness drastically increases with an increase in the most influencing energy input parameter, that is, pulse voltage with minimum average surface roughness (Ra) of 0.1076 µm and 123.60 µm average slit width at 7 V pulse voltage. Finally, the curved complex micro-feature of a 120 µm thick sheet of Nitinol SMA was fabricated successfully with a 137.795 µm average slit width under the controlled process parameter combination using WECM.

Keywords

WECM, Nitinol SMA, micro features, machining accuracy, surface characteristics

Received 23 September 2022; **revised** 17 October 2022; **accepted** 01 November 2022

Introduction

The prerequisite behind reducing the size of components is motivated by the objective of saving resources in terms of energy, material, and space. In the modern era, this objective is being highly prioritized by industrialists, academicians, and researchers from a development and application point of view. The increasing use of these micro-sized products has resulted in the evolution of new machining methods. The micro-machining describes as one of the machining methods where an unwanted material is removed in micro-dimensions from the work material to obtain the microfeatures. However, the parallel development of new materials is also a challenge for micro-machining processes to produce precise components. In this context, several developments in the machining processes have come into existence over the different phases in the last few years. The micro-structures after the wire electrochemical machining (WECM) operation were free from recast layers, craters, and micro-pores. The formation of an oxide layer on a machined conventional ECM process limits the current flow across the circuit. Consequently, no further electrolytic dissolution of material takes place. Thus, there is a need to remove this oxide layer for maintaining the process continuity

At present, the factor restricting WECM is the machining instability caused by dissolved electrolysis products and sludge removal on the surface near the machining zone. According to Bhattacharyya, high machining accuracy and surface quality can be obtained by optimizing and managing input process parameters during WECM.[1] Zadafiya et al. studied that the use of SMA's is restricted due to several unusual thermal effects.[2] Sharma et al. reviewed and concluded that WECM is established to be a feasible process for difficult-to-cut conductive material machining.[3] The experimental investigation of the TiAl alloy machining utilizing axial electrolyte flow WECM is presented by He et al.[4] The influence on the side gap of the vibrating workpiece with traveling wire parameters and uniformity of micro-slits during WECM was examined by Qu et al.[5] To expedite mass movement and improve dissolution localization, Xianghe et al. employed a vibratory ribbed instrument. When a ribbed tool was used instead of a smooth wire tool, the width of the machined incision was lowered.[6] To increase machining efficiency, He et al. used multi-wire electrodes assisted with vibration and high traveling speed, which they tested using produced microstructures.[7] Zeng et al. increased machining precision

[1] Production Engineering Department, Jadavpur University, Kolkata, India

Corresponding author:
Naresh Besekar, Production Engineering Department, Jadavpur University, Kolkata 700032, India.
E-mail: nareshwbesekar@gmail.com

Investigation into energy interaction behavior of nitinol SMA during WECM

Naresh Besekar[*], B. Bhattacharyya

Jadavpur University, Kolkata, India

ABSTRACT

KEYWORDS

WECM,
Wire Electrochemical
 Machining,
Micromachining,
Shape Memory Alloy,
Nitinol.

Wire Electrochemical Machining (WECM) combines the advantages of electrochemical machining working principle with the kinematic of wire EDM which is properly applied for fabrication of micro-features. WECM utilizes the advantages of these processes to enhance machining quality. Exceptional features of shape memory alloys (SMA) make them encouraging for widely advanced industrial applications. These difficult-to-cut materials micromachining without affecting original properties plays crucial role. Through this paper, an attempt has been made for the improvement of WECM during micromachining of nitinol SMA and explains the fundamentals of WECM process. This paper discusses various elements of developed WECM system. The paper also includes some experimental results of micro-slit machining by utilizing developed WECM setup and energy interaction behavior during fabrication of microslits of nitinol SMA. The homogeneous microslit with average slit width 111 µm with 1.68 µm standard deviation has been fabricated at 5V pulse voltage and 1.4 µm/s wire feed rate.

1. Introduction

In today's scenario of ultra-precise, advanced equipment, manufacturing industries have no option but to opt for automation and miniaturization to produce sophisticated products. WECM is one of the most appealing and promising technology in the area of micro-part manufacturing where machining is carried out with an anodic dissolution process without HAZ and change in properties of the material. This technique can be employed for the fabrication of complex 3D micro-features of any electrically conductive material. Shape memory alloy i.e. nitinol is very difficult-to-cut material as its super-elastic properties. Reviews of different research activities conducted in the area of WECM in the past as well as the basic nitinol micro-machining processes involved are presented herewith. Bisaria & Shandilya (2018) used the EDM process for nitinol SMA by taking into account different input process variables parameters during machining. Debnath et al. (2017) in-situ fabricated wire electrode and

*Corresponding author E-mail: nareshwbesekar@gmail.com

investigated the effect of high frequency and duty ratio during WECM. Sharma et al. (2018) observed that traditional machining of nitinol decreases its properties and releases Ni+ ions. Sharma et al. (2020) reviewed the entire WECM process and its application in fabricating complex micro-features using different work materials. Vakharia et al. (2022) found that the surge in T_{off} decreases the discharge and thermal energy obtaining a tiny crater with better smooth surface after machining. Wang et al. (2020) revealed that the requirement for shape memory alloy was improved fast subsequent to realizing their capability to preserve original shape after the deformation stage at plasticity. Woo et al. (2019) revealed that the thermal deformation and residual stresses problems of shape memory alloys can be solved using electrochemical machining processes.

This paper, therefore, emphasizes the improvement of WECM during micromachining of nitinol shape memory alloy by investigating input energy interaction behavior and its effects during the fabrication of micro slits in different zones through redox reaction considering different levels of pulse voltages and wire feed rate.

Electrochemical Characterization and Micromachining of Nitinol SMA by WECM Using Citric Acid Mixed H₂SO₄ Electrolyte

Naresh Besekar[z] and B. Bhattacharyya[z]

Production Engineering Department, Jadavpur University, Kolkata, 700032, India

Nitinol shape memory alloy (SMA) is a tough material to machine because it is difficult to cut. The results of the current research work demonstrate how two different electrolytes affect the electrochemical behavior in relation to electrochemical machining performance of nitinol. Potentiodynamic polarisation (PDP) and electrochemical impedance spectroscopy (EIS) tests have been conducted using 0.1 M H_2SO_4 and mixed 0.1 M H_2SO_4 + 0.1 M citric acid electrolyte. Further, the experimental investigation on the machining characteristics of nitinol during wire electrochemical machining (WECM) has been conducted. It is revealed that the grooves width and depth increase with increase in applied pulse voltage and surface roughness increase with increase in groove depth. The minimum width overcut of machined groove was 18.10 μm in 0.1 M H_2SO_4 + 0.1 M citric acid at 5 V pulse voltage which is less compared to width overcut of 24.85 μm produced in 0.1 M H_2SO_4 electrolyte for same parametric machining condition. This specific mixed electrolyte produced average surface roughness (Ra) of 0.0631 μm at 5 V which is lower compared to 0.09055 μm produced using 0.1 M H_2SO_4 electrolyte. The fabrication of homogeneous average slit width of 92.234 μm using citric acid mixed H_2SO_4 electrolyte with minimum average surface roughness (Ra) of 0.0691 μm shows the capability of WECM.

Nitinol, which gets its name from the two main metals that make up the material—nickel (Ni) and titanium (Ti)—was first discovered at the Naval Ordinance Laboratory (NAL). It has many advantages, including high strength, excellent damping properties, good biocompatibility, low density, high corrosion resistance, and the unique characteristics of thermally and mechanically induced superelasticity and shape memory effect. Nitinol is a smart material of choice for making biomedical devices like cardiovascular stents, catheter tubes, needles, guide wires, filters, dental files, and arch wires as well as other surgical instruments, aerospace and automotive industry applications. Nitinol is an intermetallic compound that, when nickel and titanium combined in equiatomic proportion, speeds up the transition between the martensite and austenite phases. The performance of nitinol micro-features that have been manufactured is mostly dependent on the surface state which is caused by surface reconstruction of the local crystal due to surface tension, surface defects and passivating molecules. Currently, the complicated biomedical components are often manufactured using laser machining or WEDM for micromachining of nitinol. However, these machining procedures result in heat damage to machined microfeatures' surfaces, generating HAZ and recast layers, which results in poor surface quality and lowers the functionality of the microfeature. Therefore, the surface quality improvement plays very important role for maintaining the properties of machined microfeatures for biomedical applications. As is well known, electrically conductive materials are typically machined using the WECM method. It is discovered that because of the special material qualities, machining nitinol without altering original properties is a bit challenging.

The acidic H_2SO_4 electrolyte performed the best among the investigated electrolytes in terms of a larger MRR and a lower surface roughness. However, it is an extremely corrosive acid that, even at modest concentrations, can result in secondary burns and serious chemical burns. Long-term inhalation of low amounts of substances can have harmful consequences on human health. A complex machining chamber and an electrolyte filtering unit are necessary to contain H_2SO_4 toxicity during the WECM process, which will ultimately increase the cost of the machining. The researchers have investigated methods that involve adding an additive to a primary electrolyte. Hence, citric acid working as

complexing agent mixed with the H_2SO_4 electrolyte to reduce the challenges and other harmful consequences of using H_2SO_4 electrolyte. This method entirely eliminates the sludge while also reducing the creation of thick oxide layers. Because they create soluble complex products with metal ions, these additives are known as complexing agents.

Rakesh Chaudhari et al. (2020) investigated the surface integrity of a sample achieved by WEDM of nitinol at optimal parameter values.[1] Kishan Zadafiya et al. (2021) presented that the characterization of high-temperature SMA's has received comparatively little attention. Due to different unpredicted phenomena, including the appearance of residual stresses, elevated temperatures during machining, and the production of the recast layer, the uses of SMAs are restricted.[2] James Wamai Mwangia et al. (2019) has reviewed on production and fabrication of micro features of nitinol for medical use.[3] For the purpose of researching the impacts of pulse voltage on the fundamental properties, nitinol was processed in a LiCl-ethanol solution. Wide etching patterns were seen, with typically rough surfaces.[4] For investigating nitinol machinability characteristics, electrochemical (EC) polishing was carried out using aqueous electrolytes prepared of 17.8 M of H_3PO_4, 14.6 M of H_2SO_4, and neutral electrolytes prepared of 1.5 M of $NaNO_2$ and 0.1 M of $Na_2C_4H_4O$.[5] The microstructures were created in NiTi alloys using ethanol as the water-free electrolyte to minimize the production of $TiCl_4$ oxide layer. However, if too much ethanol was injected, it had an impact on the surface quality and precision of the machining.[6] Rutvij Kulkarni et al. (2021) studied the impact of constrained groove pressing which causes an increase in shear and deformation bands, grain boundaries and deteriorates nitinol corrosion resistance.[7] Yuebin Guo et al. (2013) focused on surface characteristics in EDM of nitinol and compared with milling. When milling at a high feed rate, large burrs occur, whereas EDM creates surfaces without burrs but resulted in thick white layers due to heat which can be reduced using an EDM finish trim cut.[8] G. Ebenezer et al. (2021) studied electrochemical behavior of machined $Ni_{55}Ti_{45}$ alloy by wire electro spark erosion techniques by considering different process parameters and the surface of the corroded specimens considering NaCl as a electrolyte solution.[9]

Xin-Zhou Maa et al. (2013) fabricated 3D microstructures using confined layer technique on Nitinol by HF and HNO_3 electromagnetic etching and NaOH scavenger by optimizing the electrolyte composition.[10] Natalia Isabel de Azevedo Lopes et al. (2017) studied different parameters for electrolytic polishing of nitinol wire in both

[z]E-mail: nareshwbesekar@gmail.com; bb13@rediffmail.com

ORIGINAL PAPER

Wire electrochemical micromachining of nitinol shape memory alloy using different electrolytes

Naresh Besekar[1] · B. Bhattacharyya[1]

Abstract

Nitinol shape memory alloy (SMA) is one of the toughest and difficult to cut advanced smart material. Also, the properties of the material should not be affected during machining operations. Wire electrochemical machining (WECM) was created to address these issues as a result of technological innovation and the necessity for high aspect ratio products. This paper explains the effect of different aqueous solution of electrolytes, i.e., NaBr, NaCl, and $NaNO_3$ on nitinol dimensional and surface characteristics by microgroove fabrications during WECM. Further, in order to improve machining performance, the machining has been carried out with mixed and ozonated mixed conditions of $NaCl + NaNO_3$ electrolytes, and the quality of machined microgrooves is examined for surface topography, dimensional precision, and homogeneity. The best electrolyte, i.e., $NaCl + NaNO_3$ has been further used in combination with EDTA (ethylenedinitrilotetraacetic acid disodium salt dehydrate) complexing agent under non-ozonated and ozonated conditions and resulted in improved surface finish and dimensional features of the microfeatures by expeditiously removing sludge and dissolved products and increasing the efficacy of dissolution than other electrolytic conditions. The average groove width of 105.86 μm, mean depth of 264.6 μm, average surface roughness of 0.1346 μm, homogeneous microslit of average width of 106.40 μm, and average surface roughness (Ra) of 0.1261 μm have been obtained at 5 V pulse voltage and 1.4 μm/s wire feed rate with ozonated aqueous 0.2 M $NaCl + 0.2$ M $NaNO_3$ mixed with 0.2 M EDTA.

Keywords Wire electrochemical machining · Electrolytes · Micromachining · Nitinol · Shape memory alloy

Introduction

Electrochemical micromachining (EMM) has made a remarkable impact in the area of advanced micro manufacturing through fabrication of various microproducts that are successfully utilized in various micro engineering applications. EMM has diversified, and their operational capability has been increased by the introduction of different features to exploit its potential in the area of submicron and nano range fabrication. Wire electrochemical machining (WECM) is a relatively recent technique that can effortlessly produce complex 3D high aspect ratio microfeatures on a variety of tough to process materials without experiencing any heat stress, burr formation, or tool wear [1]. Nitinol is a special material that can change shape when heated; as a result, it is referred to as a shape memory alloy. However, nitinol's beneficial properties, such its high ductility, work hardening, and temperature sensitivity, can make it challenging to use in conventional fabrication techniques. Among these challenges include tool wear, the development of many burrs, and micro cracks. Furthermore, the material's shape memory effect may be reduced or eliminated by the mechanical and thermal stresses. These difficulties make it challenging to machine nitinol, severely restricting its use in a variety of sectors. Alternative machining procedures were investigated in an effort to overcome the difficulties nitinol presented during standard machining techniques. These include, among others, water jet machining, electrical discharge machining, and laser machining. But these unconventional methods frequently have unwanted effects, like the development of a recast layer, an increase in residual stress, and higher machining temperatures [2]. High corrosion resistance, biocompatibility, elasticity, resilience, and

✉ Naresh Besekar
  nareshwbesekar@gmail.com

  B. Bhattacharyya
  bb13@rediffmail.com

[1] Production Engineering Department, Jadavpur University, Kolkata 700032, India

Ⓐ Springer

Experimental Investigation into Wire Electrochemical Micro-Machining for Reduction of MicroSparks and Overcut

Naresh Besekar and Bijoy Bhattacharyya

1 Introduction

Wire electrochemical micromachining (WECMM) is such an advanced machining process that dissolves material by required electrochemical reactions between cathode wire and anode workpiece dipped inside suitable electrolyte solution separated by a narrow inter-electrode gap (IEG). The WECMM is a transport-limited electrochemical dissolution process. The continuous removal of dissolved products and sludge becomes more difficult in the tiny IEG due to frequent microsparks and unstable machining [1]. Moreover, of the several research works for investigating the influence of various process parameters, no effort has been focused to control the effect of microsparks and reduction in overcut on wire electrochemical microma-chining process considering most of the influencing parameters which is a primary requirement during machining. During the process, there may be a possibility of unusual sludge and dissolved products in narrow IEG causing microsparks which in turn reduces homogeneity and machining stability. Feed rate of tool wire has a great influence on corresponding micromachining criteria [2]. The machining stability and slot profile investigated with DP-WECMM are considerably better than those with traditional WECMM where frequent microsparks occur [3]. A proper combination of voltage and pulse period and pulse duration results in outstanding machining accuracy for a thick workpiece [4]. The axial and intermittent feed-direction vibrations combination are capable of improving the maximum feed rate [5]. A lower initial IEG can decrease the stray current results in a better entrance shape [6]. Proper feed rate leads to a small machined roughness surface without any microsparks [7]. High precision micro features can be achieved with the vibration of cathode wire [8]. Low frequency and small amplitude improve machining stability, accuracy, and

N. Besekar (✉) · B. Bhattacharyya
Department of Production Engineering, Jadavpur University, Kolkata 700032, India
e-mail: nareshwbesekar@gmail.com